Mechanisms of epigenetic regulation in epidermal keratinocytes during skin development

Role of p63 transcription factor in the establishment of lineage-specific gene expression programs in keratinocytes via regulation of nuclear envelope-associated genes and Polycomb chromatin remodelling factors

Valentina Rapisarda

Submitted for the degree of Doctor of Philosophy

Centre for Skin Sciences
Division of Biomedical Sciences
School of Life Sciences
University of Bradford

2014

Abstract

During tissues development multipotent progenitor cells establish tissue-specific gene expression programmes, leading to differentiation into specialized cell types. It has been previously shown that the transcription factor p63, a master regulator of skin development, controls the expression of adhesion molecules and essential cytoskeleton components. It has also been shown that p63 plays an important role in establishing distinct three-dimensional conformations in the Epidermal Differentiation Complex (EDC) locus (Fessing et al., 2011). Here we show that in p63-null mice about 32% of keratinocytes showed altered nuclear morphology. Alterations in the nuclear shape were accompanied by decreased expression of nuclear lamins (Lamin A/C and Lamin B1), proteins of the LINC complex (Sun-1, nesprin-2/3) and Plectin. Plectin links components of the nuclear envelope (nesprin-3) with cytoskeleton and ChIP-qPCR assay with adult epidermal keratinocytes showed p63 binding to the consensus binding sequences on *Plectin 1c*, *Sun-1* and *Nesprin-3* promoters.

As a possible consequence of the altered expression of nuclear lamins and nuclear envelope-associated proteins, changes in heterochromatin distribution as well as decrease of the expression of several polycomb proteins (Ezh2, Ring1B, Cbx4) has been observed in p63-null keratinocytes. Moreover, recent data in our lab have showed that p63 directly regulates Cbx4, a component of the polycomb PRC1 complex.
Here we show that mice lacking Cbx4 displayed a skin phenotype, which partially resembles the one observed in p63-null mice with reduced epidermal thickness and keratinocyte proliferation.

All together these data demonstrate that p63-regulated gene expression program in epidermal keratinocytes includes not only genes encoding adhesion molecules, cytoskeleton proteins (cytokeratins) and chromatin remodelling factors (Satb1, Brg1), but also polycomb proteins and components of the nuclear envelope, suggesting the existence of a functional link between cytoskeleton, nuclear architecture and three dimensional nuclear organization.

Other proteins important for proper epidermal development and stratification, are cytokeratins. Here, we show that keratin genes play an essential role in spatial organization of other lineage-specific genes in keratinocytes during epidermal development. In fact, ablation of keratin type II locus from chromosome 15 in epidermal keratinocytes led to changes in the genomic organization with increased distance between the *Loricrin* gene located on chromosome 3 as well as between *Satb1* gene located on chromosome 17 and keratin type II locus, resulting in a more peripheral localization of these genes in the nucleus. As a possible consequence of their peripheral localization, reduced expression of Loricrin and Satb1 has also been observed in keratins type II-deficient mice. These findings together with recent circularized chromosome conformation capture (4C) data, strongly suggest that *keratin 5*, *Loricrin* and *Satb1* are part of the same interactome, which is required for the proper expression of these genes and proper epidermal development and epidermal barrier formation.

Taken together these data suggest that higher order chromatin remodelling and spatial organization of genes in the nucleus are important for the establishment of lineage-specific differentiation programs in epidermal progenitor cells. These data provide an important background for further analyses of nuclear architecture in the alterations of epidermal differentiation, seen in pathological conditions, such as psoriasis and epithelial skin cancers.

Acknowledgements

I would like to greatly thank my Principal Supervisor Prof. Vladimir Botchkarev for having given me the possibility to work in his lab as a part of this wonderful project and for all the support and suggestions he has given me during these three years of my PhD studies.

I would like also to thank my Second Supervisor Dr. Michael Fessing for his support and always useful suggestions.

To conclude I would like to greatly thanks Dr. Andrei Mardaryev for having thought me a lot of experimental techniques extremely useful for the progress of this project and for having shared and supported my ideas.

A special thanks to all my family for all the support they gave me during these three years.

Contents:

Figures

Tables:

Abbreviations:

AC= astrocyte
ADP= adenosine diphosphate
ATP= adenosine triphosphate
BAC= bacterial artificial chromosome
BCP= bromo 3-chloropropane
BLAST= basic local alignment search tool
BMP= bone morphogenetic protein
BrdU= bromodeoxyuridine
BSA= bovine albumine serum
cDNA= coding DNA
ChIP= chromatin immunoprecipitation
CT= chromosome territory
CTD= C-terminal domain
DAPI= 4'6-diamidine 2-phenylndole
DBD= DNA binding domain
DIG= digoxigenin
DMSO= dimethylsulphoxyde
DNA= deoxyribonucleic acid
DOP-PCR= degenerate oligonucleotide primers polymerase chain reaction
DPE= downstream promoter element
ECM= extracellular matrix
EDC= epidermal differentiation complex
EDTA= ethylenediaminetetraacetic
ESC= embryonic stem cell
EtOH= ethanol
FAT= factor acetyl transferase
FE= fold enrichment
FGF= fibroblasts growth factor
FISH= fluorescence in situ hybridization
FITC= fluorescein isothiocyanate
GNAT= Gcn5 related N-acetyltransferase

GTF= general transcription factor

HAT= histone acetyl transferase

HDAC= histone deacetylase

HEPES= 4-2-hydroxyethyl-1 piperazineethanesulfonic

HF= hair follicle

HKMT= histone lysine methyl transferase

HP1= heterochromatin protein 1

IC= interchromosome compartment

ICN= interchromatin network

IF= intermediate filament

IHC= immunohistochemestry

INM= inner nuclear membrane

KO= knock-out

LCE= late cornified envelope

LINE= long interspersed element

LRC= label retaining cell

MPF= mouse primary fibroblast

NAD= nicotinammide adenine dinucleotide

NAR= nucleoporin associated region

NCBI= national centre for biotechnology information

NE= nuclear envelope

NL= nuclear lamina

NLS= nuclear localization signal

NPC= nuclear pore complex

ON= overnight

ONM= outer nuclear membrane

PBS= phosphate saline buffer

PCR= polymerase chain reaction

PF= perichromatin fibril

PIC= pre-initiation complex

PR= perichromatin region

PRC= polycomb repressor complex

RNA= ribonucleic acid

RT= room temperature

SAM= sterile α motif domain

SC= stem cell

SINE= short interspersed element

siRNA= small interference RNA

SPRR= small proline rich region

SSC= saline sodium citrate

SYBR Green= Syber Green

TF= transcription factor

TID= transcriptional inhibitory domain

TSS= transcription start site

WT= wild-type

Chapter 1

Introduction

1. INTRODUCTION

1.1. Skin development

Skin is the largest organ of the body and, together with its appendages, it ensures a number of critical functions, necessary for animal survival. In fact, the skin is able to protect animals from water loss, temperature change, radiation, trauma and infections and it allows animals to perceive their environment through tactile sense (Blanpain and Fuchs, 2006).

Adult skin is composed of different organized arrays of cells emanating from different embryonic origins. In mammals, shortly after gastrulation, the neuroectodermal cells, remaining at the embryo surface, follow an epidermal fate and form a single layer of unspecified progenitor cells. During further development, this layer of cells forms a stratified epidermis, the hair follicles (HFs), sebaceous glands, and, in non-haired skin, the apocrine (sweet) glands (Blanpain and Fuchs, 2009). Keratinocytes are the major cell types within the epidermis and they constitute the 95% of cells of the epidermis. Merkel cells, melanocytes and Langerhans cells are also present in the epidermis. Merkel cells are specialized receptor cells and they are associated with the sense of light touch discrimination of texture and shape (Halata et al., 2003; Morrison et al., 2009). Melanocytes are melanin-producing cells, the pigment primarily responsible for skin colour and protection against UV-light; Langerhans cells are dendritic cells (antigen-presenting cells) and play an essential role during skin infections (Barden and Levine, 1983; Chomiczewska et al., 2009).

The epidermis is separated from the underlying dermis by a basement membrane, which helps in controlling the traffic of molecules between the dermis and the epidermis. In addition, the basement membrane plays an

important role in the control of physiological remodelling and in repair processes (Iozzo, 2005).

Mesoderm-derived cells contribute to the collagen-secreting fibroblasts of the dermis, the dermal vasculature that supplies nutrients to skin, aerector pili muscles that attach to each HF, the subcutaneous fat cells, and the immune cells that infiltrate and reside in the skin.

Also, neural crest-derived progenitor cells contribute to development of skin pigmentory system, innervation and the dermis (Figure 1).

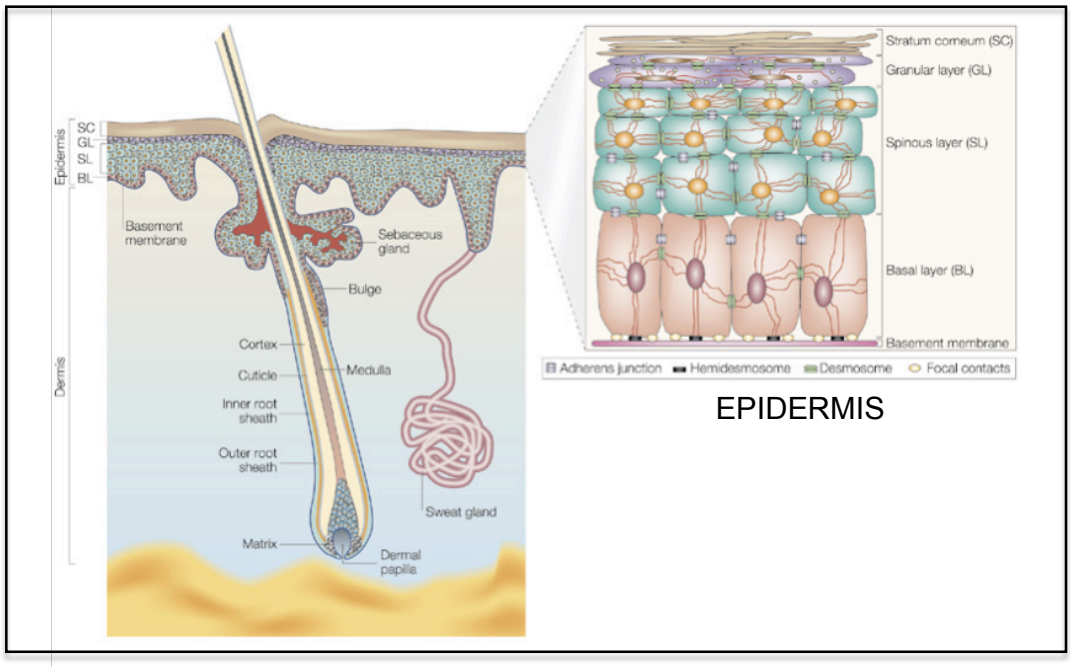

Figure 1: Schematic representation of the structure of skin and epidermis.

modified from (Fuchs and Raghavan, 2002).

1.1.1. Skin epithelial Stem Cells

Self-renewing tissues, such as epidermis and HF, continuously generate new cells, that form epidermal barrier or hair shaft due to their capacity to generate terminally differentiated cells in adult tissues (Cotsarelis, 2006).

With respect to the epidermis, it has been known that cells are generated through proliferation that occurs only in the basal layer; therefore, stem cells must be located there (Cotsarelis, 2006).

In the 1980s, the first model of skin epithelium maintenance has been generated. According to it, the slow cycling stem cells in the basal layer are able to give rise to a proliferating cell population, referred to as *transient amplifying cells*, which populate most of the basal layer and, following their proliferation, give rise to differentiated mature epidermal cells (Alonso and Fuchs, 2003).

In the 1990s, researchers, using the ^{3}H thymidine method to evaluate label retention in haired murine skin, discovered that the majority of LRCs were located in a region of the HF, called “bulge” (Cotsarelis et al., 1990) cit. in (Alonso and Fuchs, 2003).

Each HF undergoes regeneration to produce a new hair shaft through a process called hair cycle, which is divided into four different stages (anagen, catagen, telogen, exogen). By consequence, the hair cycle might be considered as a very useful model to study stem cells properties. According to the “bulge activation hypothesis”, bulge stem cells are stimulated to divide and to produce a new germinative hair matrix only after receiving signals from specialized hair follicle mesenchymal cells (Cotsarelis et al., 1990) (Figure 2).

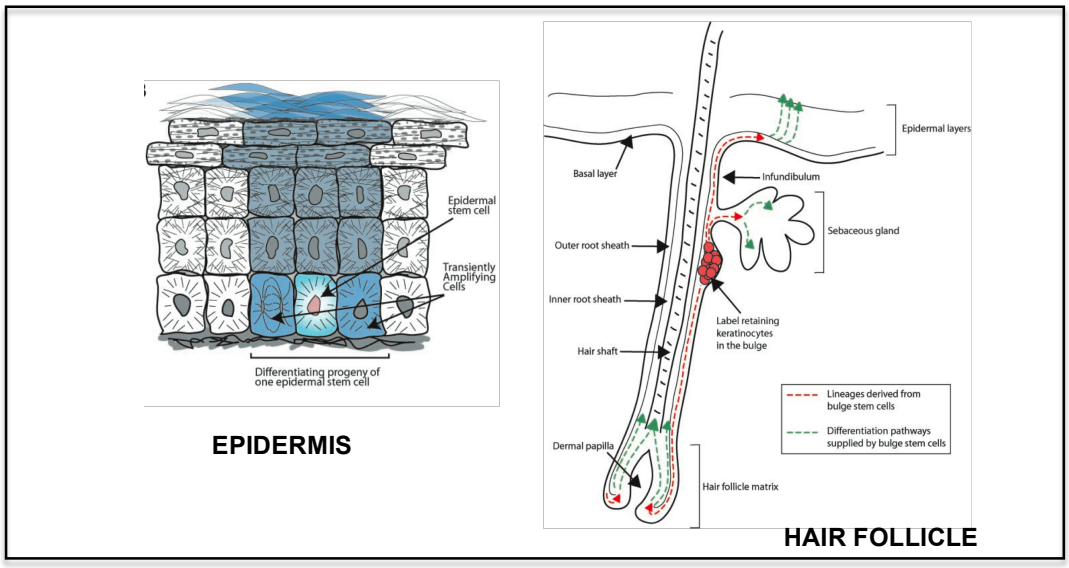

Figure 2: Schematic representation of the epidermis and hair follicle with their respective proliferative units.

(A) Schematic representation of the epidermal proliferative unit. The putative basal stem cell is a slow-cycling cell and gives rise to a stem cell daughter and to a transient amplifying cell, which is able to dived up to four times, giving rise to a progeny that leave the basal layer and execute a program of epidermal differentiation. (B) Schematic representation of the hair follicle and cell lineages supplied by epidermal stem cells, which are found in the bulge. (modified from (Alonso and Fuchs, 2003))

Other type of stem cells, such as mesenchymal stem cells can be characterized and detected by the presence of specific cell surface markers (Sasaki et al., 2008), able to identify every cell types, starting with stem cells and extending through the most differentiated forms of the progeny types (Alonso and Fuchs, 2003). It has been shown that mesenchymal stem cells, which reside in the dermis, play an important role in wound healing as well as in the differentiation of different skin cell types (Sasaki et al., 2008).

With respect to the epidermal stem cells, one class of possible markers belongs to the integrins family of transmembrane receptors, important for the attachment of the basal layer of the epidermis to its underlying substratum, the basement membrane (Watt, 1998).

Integrin α6 is present in both epidermal stem cells and transient amplifying cells while β1 integrin is present only in stem cells. By consequence it is possible that stem cells require strong adherence to the basement membrane to maintain their stemness or their position within the *"stem cell niche"* (Tani et al., 2000).

Another surface marker, which showed different expression between stem cells and transient amplifying cells is the transferrin receptor (CD71) (Tani et al., 2000). It has been shown that stem cells had a lower expression of this receptor compared to transient amplifying cells and, sorting of primary skin cells, using antibodies against integrin α6 and CD71, identified that LRCs were enriched in α6-high, CD71 low population, whereas actively dividing cells were enriched in the α6 high and transferrin receptor high population (Tani et al., 2000).

With respect to the hair follicle, Trempus et al. (Trempus et al., 2003) firstly identified CD34 as the best marker for mouse hair follicle bulge stem cells. Although this cell surface marker is also present in dermal cells, it is largely used to collect viable bulge cells by fluorescent activated cell sorting (Trempus et al., 2003; Tumbar et al., 2004).

Two different type of stem cell divisions during tissue homeostasis have been described in the skin epidermis (Blanpain and Fuchs, 2009): an asymmetric division, where one daughter cell remains a stem cell throughout self-renewal while the other daughter cell becomes committed to enter a programme of terminal differentiation. This type of division can be achieved or by segregation of cell fate determinants, like specific proteins and/or RNAs, or by positioning of one of the two daughter cells away from the "stem cells niche" (Blanpain and Fuchs, 2009; Gonczy, 2008; Knoblich, 2008; Morrison and Kimble, 2006).

The other type of division is a symmetric division, according to which both daughter cells adopt the same fate, which in the case of stem cells would result in the generation of two identical stem cells (a process called symmetric self-renewal) or of two differentiated cells (a process called symmetric differentiation).

The two different type of stem cells divisions occur at different time points of epidermal development (Blanpain and Fuchs, 2009): during early stages of embryonic development, most cell divisions are symmetric, ensuring the growth of the surface of the developing embryo and the maintenance of the epithelium as a single layer. During epidermal stratification, 70% of cell divisions are asymmetric, allowing the development of suprabasal cells and the establishment of a terminally differentiated functional epidermal barrier (Blanpain, 2010; Blanpain and Fuchs, 2009).

1.1.2. Formation and stratification of the epidermis

The epidermis is a stratified squamous epithelium, which represents the outermost layer of the skin surface.

Within the epidermis the only mitotically active layer is the basal layer, which produces, secretes and assembles an extracellular matrix (ECM). The ECM constitutes much of the underlying basement membrane that separates the epidermis from the dermis.

In mice the program of epidermal differentiation begins at about embryonic day 12.5 (E12.5). The spinous and granular layers appear at about E16.5, followed by the establishment of a functional epidermal barrier at E18.5 (Blanpain and Fuchs, 2009; Fuchs, 2007; Koster and Roop, 2007).

After gastrulation, the embryo's surface is composed of single layer of neuroectoderm, which will at the end specify the nervous system and the skin epithelium.

Several different signalling pathways play an important role in epidermal commitment and stratification as well as in the acquisition of a functional skin barrier. Among these, the Wnt signalling pathway plays an important role in the commitment of the ectoderm to an epidermal fate as it blocks the ability of the ectoderm to respond to fibroblast growth factors (FGFs). In turn, cells, lacking the FGF signalling, express bone morphogenetic proteins (BMPs) and become committed to develop into epidermis. In contrast, the acquisition of neural fate arises in the absence of the Wnt signalling, which allows the ectoderm to receive and translate the FGFs signal, which then attenuates the BMP signalling (Stern, 2005).

The resulting embryonic epidermis is a single layer of multipotent epithelial cells. It is covered by a transient protective layer of tightly connected squamous endodermis-like cells, known as periderm, which are shed once the epidermis has stratified and differentiated (Fuchs, 2007). Once cells have reached the last stage of differentiation, they die generating dead flattened cells of the cornified layer. However, inner cells moving outward continually replace them (Fuchs, 2007).

Keratinocytes of different layers express different markers, which can be used to discriminate between different stages of epidermal differentiation.

The major components and markers of epidermis are keratins, which generate a network of 10-nm keratin intermediate filaments (IFs). They are able to connect to $\alpha 6\beta 4$-integrin-containing hemidesmosomes that anchor the base of

epidermis to the lamin 5-rich assembled ECM. Keratins are also able to connect intercellular junctions such as desmosomes, which are characterized by the presence of a core of desmosomal cadherins (Blanpain and Fuchs, 2006).

Based on size, charge and gene structure, keratin genes are located on two different clusters on mouse chromosome 11 (keratins type I) and chromosome 15 (keratins type II) and are co-ordinately transcribed to allow the formation of keratins filaments from heterodimers of a type I and a type II protein (Herrmann et al., 2003; Kurokawa et al., 2011). Type I keratins (K10, K11, K12, K13, K14, K15, K16, K17, K18, K19) have acidic properties, while type II keratins (K1, K2, K3, K4, K5, K6, K7, K8) have basic properties.

Keratins are differentially expressed in different types of epithelia: K1, K2, K5, K10 and K14 are expressed in normal epidermis; K3 and K12 in the cornea; K4, K13 and K15 are expressed in the oesophagus and other non-keratinizing epithelia; K8 and K18 are expressed in simple epithelia; K19 is expressed in the periderm; K9 is expressed in palmar and plantar tissues; K6, K16 and K17 are expressed mainly in the epidermis under pathological stresses (Blumenberg, 1993; Sato et al., 1999).

Keratins are also serve as important markers of epidermal differentiation. In fact, the different epidermal layers express different types of keratins, depending on the stage of epidermal differentiation. In the basal layer, the expression of K5 and K14 (also K15 in the embryo) has been shown, while in the intermediate suprabasal (spinous) layer K1 and K10 are expressed. The difference in the expression of different types of keratins is responsible for different networks of connections. In fact, basal cells use a more dynamic cytoskeletal network of microtubules and actin filaments compared to

suprabasal cells, that interface through β-and-α-catenins to E-cadherin-mediated cell-cell (adherens) junctions, in addition to the αβ-integrin-mediated cell ECM junctions (Perez-Moreno et al., 2003) cit. in (Blanpain and Fuchs, 2006).

Mutations and/or depletion of keratin genes have been associated with keratinocytes fragility as demonstrated in K5 and K14 knock-out mice, which displayed basal keratinocytes fragility. With respect to suprabasal keratins, depletion of K10 resulted in very limited tissue damages, possibly due to the compensatory expression of K14, raising the issue of isotype-specificity of keratins. By contrast K1-/- mice developed an impaired inside-out barrier resulting in a 2-fold increase in trans-epidermal water loss while the outside barrier was undisrupted (Roth et al., 2012).

Once cells leave the basal layer and move towards the skin surface, they exit the cell cycle, switch off the integrin and laminin expressions, and undergo a terminal differentiation program, generating the three different epidermal layers: spinous layer, granular layer and the stratum corneum (Blanpain and Fuchs, 2006). This program is characterized by the presence of numerous proteins, including filaggrin, loricrin and involucrin, whose expression appears in the granular layer.

Several groups of regulators, including transcription factors, chromatin remodelling proteins and signalling pathways, play an essential role in the control of epidermal stratification process.

Among these, the canonical Notch pathway plays an important role in the commitment of basal cells to a spinous fate (Blanpain et al., 2006; Watt et al.,

2008). Ablation of RPBJ, a DNA binding protein, which forms a bipartite transcription factor with Notch intracellular domain, led to a failure in spinous layer formation (Blanpain et al., 2006). Furthermore, loss of *Hes1*, one of the main Notch target genes in skin epidermis and responsible for the timing of stem cells differentiation, led to altered specification of the spinous layer (Moriyama et al., 2008). By contrast, enhancement of the Notch pathway led to a precocious conversion of basal cells to spinous cells (Blanpain et al., 2006). It has been suggested that the Notch signalling acts in part by influencing the expression of C/EBP DNA-binding proteins, which work in concert with AP-2 family of transcription factors to regulate the commitment to a terminally differentiated epidermis (Wang et al., 2008).

Other important factors involved in epidermal stratification process are microRNAs (miRNAs) (Yi et al., 2008). In fact, precocious expression of miR-203, usually expressed suprabasally at the same time as epidermal stratification and differentiation, induced a premature differentiation of basal cells and an alteration of their proliferative potential (Yi et al., 2008).

The outermost epidermal layer is the cornified envelope (or stratum corneum), which has the important function of protecting from external insults and providing a barrier against the excessive loss of fluids from the body (Candi et al., 2005; Fuchs, 1995) cit. in (Blanpain and Fuchs, 2006). The cornified envelope is mainly characterized by cells, which have lost their internal organelles, forming a thickened intracellular cell envelope and an intercellular lipid multilamellar structure before desquamation as corneocytes (DiSepio et al., 1995).

Loricrin and filaggrin are considered important late differentiation markers in the epidermis. In murine epidermis, loricrin is first a small, non-membrane granules called L-granules and it is released from the granules, deposited and cross-linked by transglutaminases as a dense marginal band on the internal part of the corneocytes membrane (DiSepio et al., 1995).

Although the regulatory mechanism of loricrin expression remains unknown, it has been hypothesised that calcium concentration may play an important role during epidermal differentiation and in the regulation of loricrin expression. In fact, several *in vitro* experiments have shown an induction of epidermal differentiation markers, like loricrin, filaggrin, K1 and K10, after increased calcium concentrations (Menon et al., 1985).

Most of the genes implicated in terminal keratinocyte differentiation are located within the Epidermal Differentiation Complex (EDC), which consists of 1.6 Mbs mapped on human chromosome 1q21 (mouse 3q). Four clusters of tandem gene families have been identified: Filaggrin (FLG)-like, Late Cornified Envelope (LCE), Small Proline Rich Region (SPRR) and the S100 genes (Volz et al., 1993) cit. in (de Guzman Strong et al., 2010). The first three clusters of gene families encode proteins, which are cross-linked together and essential for skin barrier formation; the fourth cluster of genes, S100 genes, encode chemoattractant proteins expressed once the skin barrier is impaired.

In mice the majority of the genes (44/61) within the EDC start to be expressed at the onset of the epidermal stratification at E15.5. Additional genes, most notably the LCE genes as well as increased expression of other EDC genes, are induced at E16.5 (de Guzman Strong et al., 2010).

The spatial and temporal expression of several genes within the EDC during development and differentiation of epidermis and their dense tandem genomic organization, suggest the existence of genomic regulatory mechanisms to coordinate their expression. In addition, the conservation of the EDC throughout different mammalian genomes suggests the existence of a genetic mechanism able to maintain the EDC as a regulatory block. In fact *in vitro* experiments on cultured terminally differentiated keratinocytes, allowed the identification of *cis*-regulatory elements within the EDC, which may have enhancer or repressor activity, regulating the differentiation program (30%) or the proliferation (20%). However, also involvement of *trans* interactions with regulatory elements located on different chromosomes in the control of coordinated expression of epidermal genes should not be excluded (de Guzman Strong et al., 2010).

1.1.2.1. p63: a major regulator of epidermal development and stratification

Increasing evidence suggests that the transcription factor p63 is one of the key elements in the epidermal differentiation process. P63 is one of the members of the p53 family, which includes the transcription factors p53, p63 and p73 (Mills et al., 1999), as mice lacking p63 are characterised by an early block in epidermal stratification, as well as, by the development of truncated limbs, craniofacial malformations, abnormalities in epidermal appendages and the absence of normal stratified epithelia, including epidermis and all related appendages (hair follicles, vibrissae and tooth primordial) (Mills et al., 1999; Yang et al., 1999). The defects related to epidermal development are confirmed by lack of typical characteristics of the basal, suprabasal and cornified layers, causing dehydration and early death of p63-deficient mice; embryos and new-

borns, lacking p63, retained isolated patches of disorganized epithelial cells along the exposed epidermis (Mills et al., 1999) (Figure 3).

Tissues derived from the same stem cells that give rise to the epidermis, including mammary, sebaceous, lacrymal and salivary glands, are also absent in p63 knock-out mice (Yang et al., 1999). The same defects are also observed in the tongue epithelium, the oesophagus and proximal portion of the stomach. Also the epithelium of the urinary bladder is thinner than normal, confirming an important role of p63 in stratified squamous epithelia development (Yang et al., 1999).

p63-null mice are characterised by the lack of keratin 5 expression, one of the markers of the basal and progenitor cells of stratified squamous epithelia and by a re-induction of the expression of keratins 8 and 18, usually associated with a simple epithelium (Truong et al., 2006; Yang et al., 1999). These results suggest possible defects in the commitment of stem cells to squamous epithelial lineages or in the maintenance of the progenitor stem cell population, which is required for proper epidermal development and whose loss results in a reversion to a simple epithelial phenotype (Truong et al., 2006; Yang et al., 1999).

Since the generation of two independent p63-deficient mouse models, the role of p63 in epidermal development has been controversial. Both models lack epidermal appendages, have severe defects limb and craniofacial and epidermal development, and die soon after birth. However, subtle differences between them led to strikingly different hypothesis about the role of p63 in epidermal development (Vanbokhoven et al., 2011). The mouse model generated in the McKeon laboratory displayed different patches of differentiated

keratinocytes, that express epidermal terminal differentiation markers, such as loricrin, filaggrin and involucrin. These patches were interpreted as as remnats of an initially developing epidermis that could not be maintenained during embryogenesis. Therefore, the defects in these mice might be the result of the loss of the regenerative population of cells involving p63, which might be related to the identity or renewal capacity of epithelial stem cells ("stem cell self-renewal" model) (Yang et al., 1999).

On the other side, the mouse model generated in Bradley laboratory showed a failure of the surface ectoderm to commit to an epidermal lineage with absence of the expression of epidermal differentiation markers, suggesting that p63 is required for simple epithelial cells to commit to a stratified epithelial lineage during development ("commitment model"). This observation was also confirmed by the very low level of keratin 14, marker usually expressed in proliferating keratinocytes, and by the absence of keratin 1, early marker of epidermal differentiation (Mills et al., 1999).

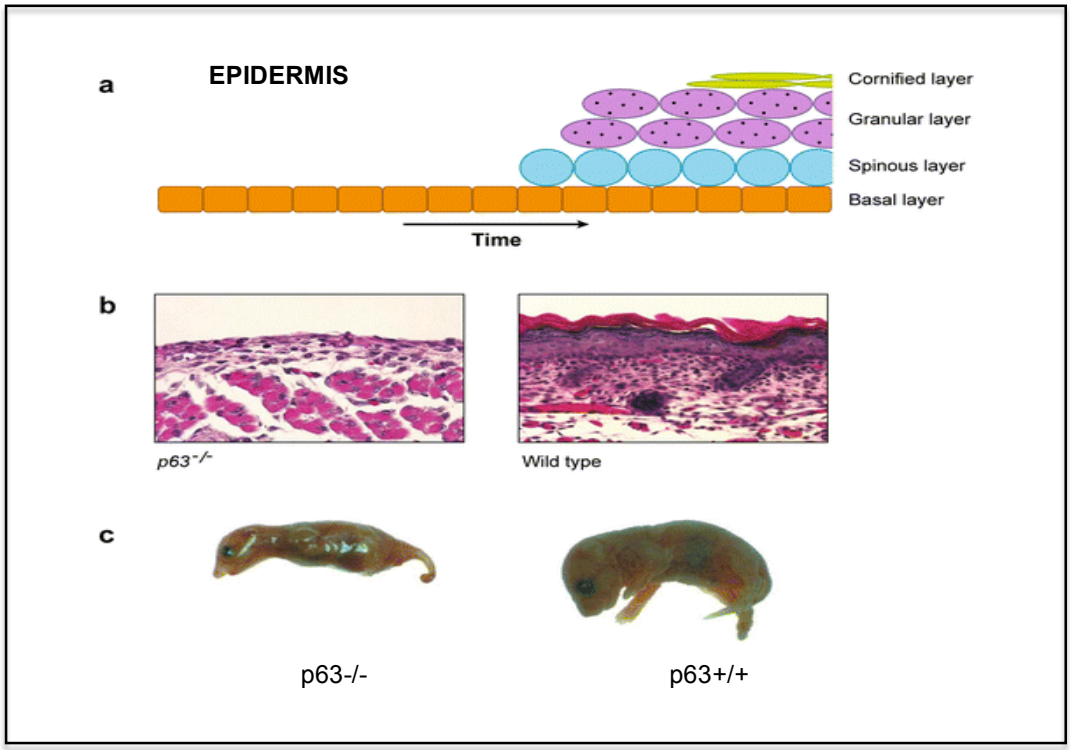

Figure 3: Schematic illustration of murine epidermis morphogenesis.

(A) Schematic illustration of epidermis morphogenesis. During epidermal stratification a first single basal layer.Once cells leave the basal layer and move outward toward the skin surface, they exit the cell cycle, switch off integrins and laminins expression, and undergo a terminal differentiation program, generating the three different epidermal layers: spinous layer, granular layer and the stratum corneum. **(B)** The epidermal stratification program begins in mice at E 14.5 and it is completed at E 18.5. In the wild-type mice (right) the epidermal development is completed by birth, while in $p63^{-/-}$ mice (left) a lack of epidermal stratification is observed. As a consequence $p63^{-/-}$ mice die immediately after birth as they are characterised by a single layer of ectodermal cells, which does not protect and prevent newborns from dehydration. **(C)** Images of $p63^{-/-}$ and wild-type mice. (modified from (Mills et al., 1999))

Six isoforms of p63 protein have been identified as the results of multiple splice variants, whose differences are localised at the 5'-end, by utilization of alternative promoters, and at the 3'-end with splice variants (α, β, γ) (McDade and McCance, 2010; Murray-Zmijewski et al., 2006). They all maintain the basic structure of the p53 family members, which is characterised by a highly conserved core DBD (DNA-binding domain), which recognizes all transcription binding sites. In addition to it the TA isoforms contain an N-terminal TA domain

with a high degree of homology to p53 and they are able to bind to p53-responsive elements through their DBD to activate p53 target genes, such as *p21*, *Bax* and *Mdm2* (murine double minute 2). In addition to p53 direct targets, p63 is also able to bind to its own transcription sites, modulating the transcription of a unique subset of genes (Perez et al., 2007) cit. in (McDade and McCance, 2010).

In the ΔN variants, the TA domain is omitted. These variants act as negative inhibitors of transcriptional activation by TA isoforms. Additionally, because of the presence of a TA2 domain at the C-terminal end, the ΔNp63α, ΔNp63β and ΔNp63δ isoforms are also able to activate the transcription of a subset of genes (Ghioni et al., 2002). Furthermore, only ΔNp63α isoform contains a SAM domain (sterile α motif domain), which is thought to be involved in protein-protein interactions (Ghioni et al., 2002) and a TID (transcriptional inhibitory domain). This domain can auto-inhibit the transcriptional activity of TA and ΔNp63α or inhibit heterocomplexes with other transactivating p63 or family members isoforms (Kim and Bowie, 2003) cit. in (McDade and McCance, 2010) (Figure 4).

Both TAp63 and ΔNp63 RNA transcripts are present in mouse embryos and in postdevelopmental cells and tissues, but ΔNp63 is more abundant than TAp63 at the proteins level (Mikkola, 2007). ΔNp63α is expressed in the basal layer and it is reduced in suprabasal keratinocytes.

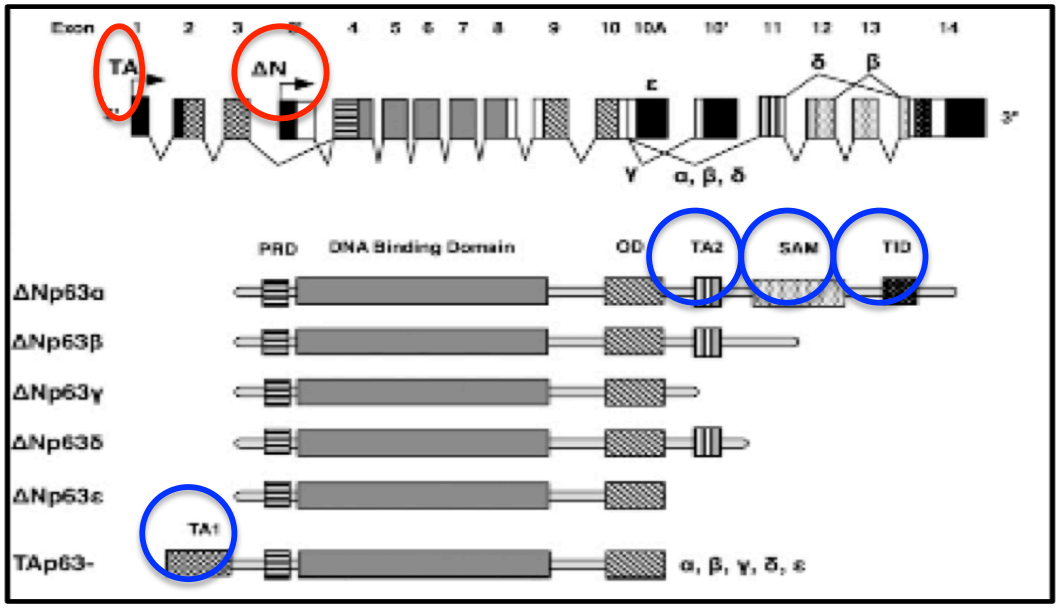

Figure 4: Schematic representation of the different p63 isoforms.

Modified from (McDade and McCance, 2010)

According to RNA interference studies, it has been shown that the knock-down of TAp63 isoforms caused no detectable effects on keratinocytes proliferation and only few abnormalities in differentiation, like incomplete development of granular layer and stratum corneum. In contrast the knock-down of ΔNp63 isoforms caused dramatic reduction of cell proliferation, as the majority of cells were arrested in G1 phase with a consistent reduction of cells in S phase and G2/M phases (Truong et al., 2006). Furthermore, no expression of differentiation markers and an induction of keratin 8 expression have been observed, suggesting a dominant role of ΔNp63 isoforms both in epidermal proliferation and differentiation (Truong et al., 2006), while TAp63 isoforms may play a role in the induction of epidermal stratification (Koster et al., 2004). Consistent with this hypothesis, ΔNp63 isoforms expression has been first detected at E9.5, after the developing epidermis has committed to stratification, but prior to terminal differentiation. In contrast, TAp63 isoforms have been

detected earlier than E7.5, before the commitment to stratification has occurred (Koster et al., 2004). In addition transfection experiments with different TAp63 and ΔNp63 isoforms confirmed this hypothesis, as only TAp63 isoforms transfected keratinocytes were able to induce the expression of K14 (Koster et al., 2004). These data suggest that TAp63, in particular the isoform TAp63α, is the key regulator of the initiation of epithelial stratification program and execution of this program requires a shift in the balance between TAp63α and ΔNp63α isoforms, which are able to respond to signals required for keratinocytes proliferation and differentiation, through the regulation of Notch and IKKα signalling pathways and through the inhibition of p21 (inhibitor of the cell cycle) (Koster et al., 2004; Nguyen et al., 2006).

While down-regulated by Notch activation, p63 in turn, counteracts the ability of Notch to restrict growth and promote differentiation, with antagonistic effects on Notch-responsive genes. Therefore, the p63-Notch cross-talk acts through a p63 selective modulation by Notch1-dependent transcription, with the *Hes-1* gene as one of its negative targets, and with other genes, including K1 marker, being induced rather than suppressed, through a mechanism dependent on *Hes-1* down-modulation, occurring at very early stages of epidermal differentiation. Increased Notch signalling at later stages, down-modulates p63 expression, and, synergized by other pathways and factors, leads to the expression of markers of later stages of epidermal development (Nguyen et al., 2006).

With respect to IKKα, its direct regulation by ΔNp63 led to epidermal terminal differentiation as mice lacking IKKα displayed defects similar to those observed in p63-null mice with absence of the spinous layer, although skin and

appendages development arrested at later stages in IKK$\alpha^{-/-}$ mice than in p63 $^{-/-}$ mice (Koster et al., 2007).

Differently from p63-null mice, IKKα -/- mice normally expressed genes required for epidermal differentiation, including K1, suggesting that additional genes, essential for the formation of the spinous layer, might be under ΔNp63 control (Koster et al., 2007).

p63-null mice not only fail to develop a terminally differentiated epidermis, but they also fail to establish a functional basement membrane, suggesting that ΔNp63 might control the expression of genes responsible for basement membrane formation. In line with this hypothesis, microarray analysis and ChIP-qPCR assay showed that ΔNp63 was able to directly regulate the expression of *Fras1*, important for basement membrane formation and skin integrity (Koster et al., 2007).

ΔNp63 isoforms are also able to regulate cell proliferation by inhibiting p53 functions (Lee and Kimelman, 2002). Double transfection of keratinocytes with siRNAs directed against both p63 and p53 inhibited the up-regulation of p21, that was seen with p63 knockdown alone (Truong et al., 2006), suggesting that cell proliferation defects in p63 knock-out mice might require p53 (Truong et al., 2006). However, the knockdown of p53 in a p63 knockdown environment is not able to rescue epidermal differentiation as the expression of differentiation markers remains absent (Truong et al., 2006), suggesting the involvement of additional factors and mechanisms in this process.

In addition to *p21*, *Fras1*, Notch and IKKα signalling pathways, p63 regulates a large number of other genes in keratinocytes, including transcription factors, cell cycle-associated proteins, as well as tissue-specific proteins, such

as keratins 1 and 10. p63 regulates keratins expression through indirect mechanism, which requires not only p63 but also the cooperative function of additional transcription factors, including AP-1, AP-2 (Koster and Roop, 2007). In addition it regulates the expression of involucrin, loricrin, corneodesmin, desmoglein-1 and desmocollin-1, as well as enzymes, such as transglutaminase-1 andlipoxygenase-3. Furthermore, different studies provide evidence of a role of p63 in regulating the expression of proteins involved in cellular adhesion (Carroll et al., 2006), like desmosomal proteins. In fact, it has been shown a direct binding of p63 to the desmosomal protein *Perp* and absence of this protein caused severe embryonic blistering, resulting in early neonatal death because of dehydration (Koster and Roop, 2007).

Knockdown experiments showed that ΔNp63 isoforms regulate 218 genes, which are mainly involved in desmosomes assembly, formation of the stratum corneum and regeneration of skin barrier, while TAp63 isoforms knockdown only affected 39 genes. These findings confirm that ΔNp63 isoforms play a dominant role in the epidermal differentiation program differently from the Tap63 isoforms, which might be involved mainly in ectoderm commitment to an epidermal fate and in the maintenance of epidermal stem cells (Truong et al., 2006), and that TAp63 and ΔNp63 isoforms may not have opposing actions in regulating differentiation, but may instead cooperate to carry out the epidermal program of stratification and differentiation (Truong et al., 2006).

1.1.2.2. p63 and its role in limb and craniofacial development

In addition to its major role in epidermal development, it has been demonstrated that p63 also plays an important role in limb and craniofacial development (Mills et al., 1999; Yang et al., 1999).

With respect to limb development, several studies showed severe defects in p63-mutant mice. In fact p63 homozygous mutant mice displayed truncated forelimbs and complete absence of hindlimbs at birth with absence of distal skeletal elements. Phalanges and carpals were absent in all of p63-homozygous mutant forelimbs skeletal preparations analysed, whereas more proximal forelimb structures were slightly heterogeneous in the extent of truncation. For example, the radius was not present in any of the mutants analysed and the ulna was present in 37.5% of the limbs. The humerus, although present, was usually truncated, deformed and smaller than that one of wild-types. The femur and all distal skeletal elements were absent in all of p63-homozygous mutant limbs (Figure 5) (Mills et al., 1999).

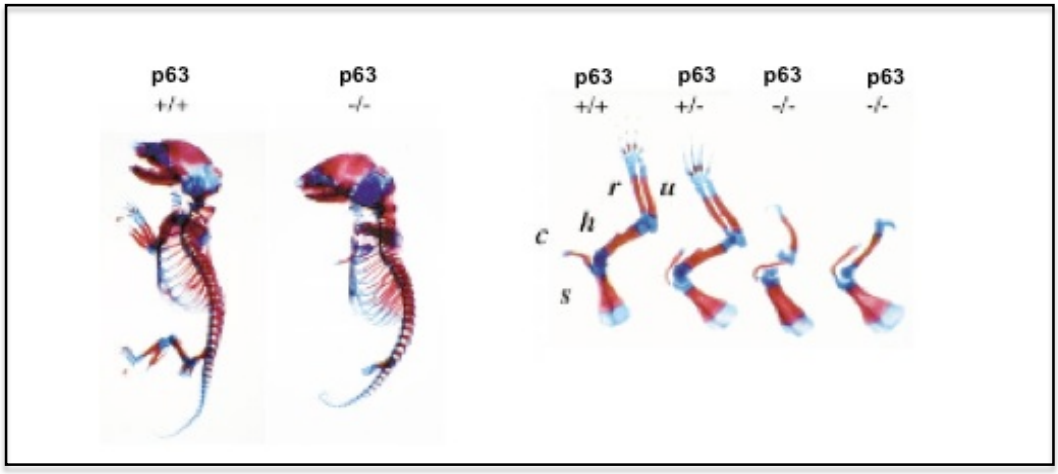

Figure 5: Skeletons of wild-type, p63 heterozygous and p63 homozygous mutant animals.

In p63-/- mice forelimbs are truncated with complete absence of phalanges, radius and ulna and deformed humerus. Abbreviations:c, cavicle; h, humerus; r, radius; s, scapula; u, ulna. modified from (Mills et al., 1999).

Additional molecular studies revealed that alterations in ectoderm-mesenchyme signalling were responsible for the observed limb defects in p63-null animals.

Ectoderm-mesenchyme signalling is crucial for the proper development of the apical ectodermal ridge (AER), a structure required for limb outgrowth along the proximal-distal axis, absent in p63-null mice (Mills et al., 1999), and it is regulated by several transcription factors, including Msx-1 and Msx-2. Expression of Msx-1 in the mesenchyme depends on ectodermal signal, whereas expression of Msx-2 is independent of signalling from the ectoderm (Wang and Sassoon, 1995). p63-homozygous mutant limb buds expressed Msx-2 in a pattern similar to wild-type mice, while on the contrary Msx-1 was not expressed in the mesenchyme of p63-deficient limbs, suggesting that the ectoderm-mesenchyme signalling was perturbed (Mills et al., 1999). Furthermore, the analysis of other structures that require ectodermal-mesenchyme interaction during morphogenesis were examined in p63-deficient mice, using expression of Lef-1 as a marker. Lef-1 is normally expressed within the ectoderm of hair placodes and within mammary buds before morphogenesis, providing a cue for the underlying mesenchyme to initiate development of the appropriate structure (Zhou et al., 1995). In p63-deficient mice, Lef-1 is not expressed within the ectoderm overlying the site at which follicles and mammary buds normally form, additionally suggesting alterations in ectodermal-mesenchyme signalling (Mills et al., 1999).

1.2. Gene expression regulation within the eukaryotic nucleus

1.2.1. Transcriptional regulation

The transcriptional process represents the first step in eukaryotic gene expression and could be divided into three different main steps: initiation, elongation and termination (LewinB, 2003).

During the initiation step the RNA Polymerase, the enzyme that catalyzes the synthesis of RNA, is recruited to a promoter region by different proteins, which first recognize promoters, causing the assembly of a large complex containing Pol II and multiple general transcription factors (GTFs) on the promoter, which include TFIIB, TFIID (contains the TATA-binding protein TBP), TFIIE, TFIIF and TFIIH. The recruitment of Pol II to the promoter region is also influenced by the presence of DNA-binding transcription activators and different nucleosome remodelling and modifying enzymes (Li et al., 2007), as it will be discussed.

The promoter region is characterized by the presence of specific sequences such as the TATA box, the Initiator or Downstream Promoter Element (DPE), which influences the specific binding of the GTFs to the promoter followed by the Pol II recruitement. The local melting of DNA around the transcription start site (TSS) and the formation of the first few phosphodiester bonds of mRNA, follow the polymerase recruitment.

Once Polymerase II is recruited to the promoter, it is phosphorylated within the C-terminal domain (CTD) of its largest subunit. The CTD contains multiple hepto-repeats with a consensus sequence YSPTSPS, that can be phosphorylated at several sites (Phatnani and Greenleaf, 2006) (cit. in (Nechaev and Adelman, 2011). The CTD remains usually unphosphorylated

during the initiation step, as it is very important to favour its interaction with factors that stabilize the pre-initiation complex (PIC), such as Mediator complex, and it is phosphorylated at Serine-5 by the Cdk7 subunit of TFIIH at early elongation step. This phosphorilation favours the destabilization of the interactions between Pol II and promoter bound factors, facilitating promoter escape. A second phosphorylation occurs at Serine-2 residues and it is catalyzed by the Positive Transcription Elongation Factor b (P-TEFb) kinase, favouring the transition into productive elongation. This Serine-2 phosphorylation changes the entourage of Pol II-associated factors to favour processive transcription through chromatin and RNA processing (Peterlin and Price, 2006) cit. in (Nechaev and Adelman, 2011). In addition, another Serine-2 phosphorylation is catalyzed by a kinase, comprised of Cyclin K and Cdk12 or Cdk13, increasing CTD phosphorylation levels towards the 3'-end of genes. The Serine-2 phosphorylation provides a platform for the assembly of different complexes which travel with the Polymerase into the gene, including those one that regulate transcription elongation, RNA processing and termination (Peterlin and Price, 2006) cit. in (Nechaev and Adelman, 2011), as well as the chromatin remodelling factors (Li et al., 2007).

Different pathways are crucial for the termination of the transcriptional process. The most of Pol II transcripts terminate using cleavage and poly-adenilation machinery, while several shorter transcripts, resulting from premature pauses of Pol II during the elongation process, use distinct poly-A independent pathways (Steinmetz et al., 2006). Once the cleavage and termination of full-length transcripts have occurred, Pol II is released from the template DNA. In many cases, the Pol II may be recycled back to the promoter

region of those genes, which have multiple rounds of transcription (Yao et al., 2007) cit. in (Nechaev and Adelman, 2011).

As previously reported, the role of chromatin structure and chromatin remodelling factors also play an important role in the transcriptional outcome. Previous genome-wide studies showed that there was a lower density of nucleosomes at promoter regions of actively transcribed and "paused" genes compared to their coding regions (Bernstein et al., 2004; Li et al., 2007) and that TFs are able to bind to nucleosome DNA in a cooperative manner: once the activators bind to the promoters, they recruit co-activators, such as chromatin remodelling complexes, histone-modification enzymes and components of mediator, which are able to organize chromatin structure at the promoter regions, facilitating the binding of the activators to DNA and making nucleosomal DNA elements more accessible to GTFs. In addition an increase in histones acetylation at the promoter region has been shown. In fact, the histone acetyl transferases (HATs) Gcn5 and Esa1 are recruited to promoters genome-wide, resulting in an increased mobility of nucleosomes (Li et al., 2007).

Two different models have been proposed to explain how chromatin is regulated during transcription initiation. In one model, a combination of acetylation and chromatin remodelling directly results in a loss of the histone variant H2A.Z containing nucleosome, which is preferentially enriched at the promoters (Li et al., 2005). The loss of Htz1 is required for efficient transcription and by consequence exposes the entire promoter to the GTFs and Pol II. Subsequently SAGA, co-activators and mediators, facilitates PIC formation through direct interactions (Li et al., 2007).

With respect to the second model, partial PIC could be assembled on the promoter without the loss of Htz1. Only once Pol II and TFIIH bind to the promoter, Htz1-containing nucleosome is displayed, favouring the full assembly of the PIC.

(Figure 6)

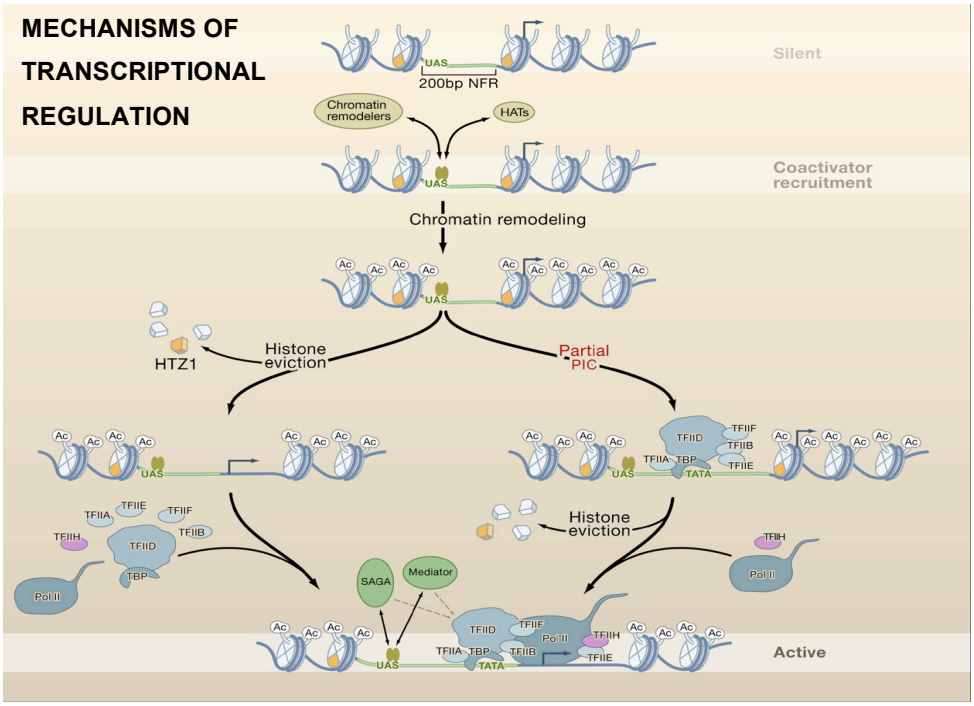

Figure 6: Schematic representation of the two models of chromatin regulation during transcriptional initiation process.

The first model (left) a combination of acetylation and chromatin remodelling directly results in the loss of Htz1-containing nucleosomes, exposing the entire core promoter to the GTFs and Pol II. SAGA and mediator then facilitate PIC formation through direct interactions. In the second model (right) partial PIC could be assembled at the core promoter without loss of Htz1. It is the binding of Pol II and TFIIH that causes the displacement of Htz1 containing nucleosomes and the full assembly of PIC. Taken from (Li et al., 2007).

Different factors and chromatin remodelling complexes control chromatin architecture also during the elongation step of transcription. Interestingly the factors required at the beginning of the elongation process are different from those required at the end, increasing the efficiency in RNA synthesis and

ensuring the integrity of chromatin structure while Pol II travels through the body of the gene (Li et al., 2007).

The role of chromatin remodelling complexes during elongation is strictly associated with phosphorylation, which occurs at the Pol II CTD. PAF/RTF, which is a multisubunit complex (Ctr9, Cdc73, Leo1 and Rtf1) and the first complex involved in elongation, recognizes the Serine-5 phosphorylated CTD, facilitating the binding of FACT, COMPASS and Rad6/Bre1 to the Serine-5 phosphorylated CTD (Li et al., 2007). This binding is followed by the H2B ubiquitination and accumulation of trimethylation of H3K4 at the 5'-end of Open Reading Frame (ORF). Although H2B monoubiquitination by Rad6/Bre1 is required for K4 methylation, in particular di-and-tri-methylation, PAF appears to directly regulate both H2B ubiquitination and K4 methylation. In addition another factor, Set2, interacts directly with Serine-2 phosphorylated CTD, methylating H3K36 at the 3'-part of actively transcribed genes (Li et al., 2007).

1.2.2. Chromatin organization within the eukaryotic nucleus

The DNA within the eukaryotic nucleus is complexed with histone and non-histone proteins into a chromatin fiber. The tightly-packed and organized structure of the chromatin fiber serves two essential cellular functions: it condenses meters-long genomic DNA by several orders of magnitude to enable its packaging into micrometer-sized cell nucleus and it regulates the template-directed transcription of genes through local unfolding of chromatin (Felsenfeld and Groudine, 2003; Horn and Peterson, 2002).

In dividing cells, the chromatin complex of DNA and proteins can be seen as individual compact chromosomes while in non-dividing cells, chromatin appears to be distributed throughout the nucleus and organized into

"condensed" (heterochromatin) and decondensed regions (euchromatin) (Felsenfeld and Groudine, 2003), which play an essential role in gene expression regulation (Figure 7).

The fundamental subunit of chromatin is the "nucleosome", composed of approximately 147 base pairs (bp) of DNA wrapped 1.65 turns around the histone proteins octamer and there are 14 contact points between the DNA and histones (Luger et al., 1997). The histones octamer core contains two copies of each histone H2A, H2B, H3 and H4 (Luger, 2003). This results in the formation of a structure called "beads on a string" and in a five to ten fold compaction of the DNA (Kornberg, 1974) cit. in (Felsenfeld and Groudine, 2003). Each nucleosome is connected with its neighbours by a short segment of DNA linker (~10-80 bp in length), which is folded into a compact fiber with a diameter of 30 nm, producing a compaction of roughly 50-fold. This structure is stabilized by the binding of a fifth histone, H1, to each nucleosome and its DNA linker (Felsenfeld and Groudine, 2003) (Figure 7).

It has also been reported the existence of histone variants, such as H2AX, H3.3 and H2A.Z (Htz1).

H2AX is distributed throughout the genome and it is a target of phosphorylation accompanying repair of DNA breakage (Redon et al., 2002). In addition it seems to be also involved in the *V(D)J* recombination events, which occur before the assembly of immunoglobulins and T-cell receptor genes.

The H3.3 histone variant can be incorporated into chromatin of non-dividing cells, and seems to be associated with transcriptionally active genes (Ahmad and Henikoff, 2002) cit. in (Felsenfeld and Groudine, 2003).

With respect to H2A.Z (or Htz1), it has been related to both activation and repression of transcriptional process. In fact, it has been shown that H2A.Z functions as anti-silencing factor, able to antagonize the spread of heterochromatin to euchromatic regions (Meneghini et al., 2003). However, H2A.Z is also able to negatively regulate transcription through heterochromatic silencing (Dhillon and Kamakaka, 2000; Swaminathan et al., 2005) and nucleosomes containing Htz1 are relatively immobile and refractory to chromatin remodelling (Li et al., 2005) as a consequence of the increased intramolecular compaction of nucleosomal arrays (Fan et al., 2002).

The typical distance between nucleosomes varies, depending on the organism and cell type, between 10 and 50 bp. However, the spacing and positioning of nucleosomes at critical *cis*-acting control regions (i.e., promoters) are tailored for the proper regulation of the locus (Clapier and Cairns, 2009). Remodelers are needed to fully package the genome, to specialize chromatin regions, and to provide regulated DNA accessibility in pack- aged regions. Below, as a broad preview, we list the challenges chromosomes present, and how specialized remodelers have evolved to help provide solutions. Thus, remodelers are needed for nucleosome dynamics to move, eject, or restructure the composition of nucleosomes. Certain remodelers promote dense nucleosome packaging genome wide, with regions directly upstream of transcription start sites excepted. However, other specialized remodelers move and eject nucleosomes to help transcription factors to access DNA sequences in a regulated manner (Clapier and Cairns, 2009).

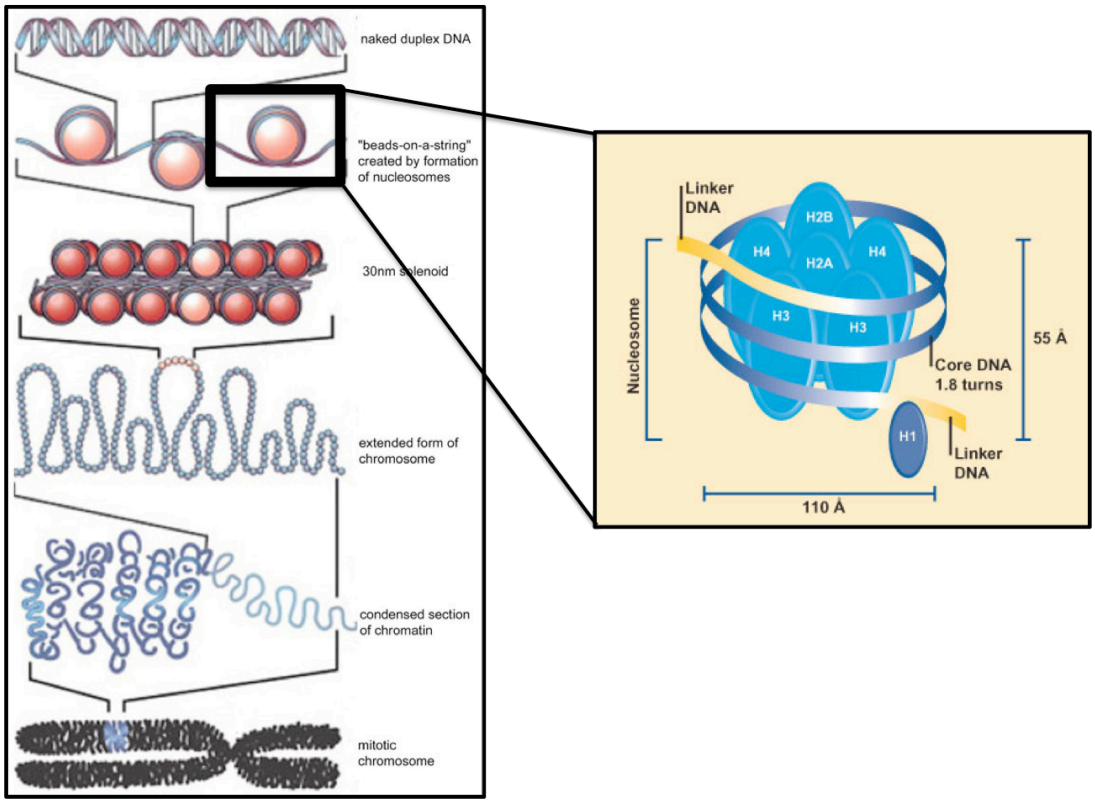

Figure 7: Chromatin organization within the eukaryotic nucleus (left) and nucleosome structure (right).

Modified from Abcam.com

ATP-dependent chromatin remodelling complexes use the energy derived from ATP hydrolysis to alter the histone-DNA-contacts. Many of these complexes are members of the so-called SWI/SNF superfamily, which includes SWI/SNF in budding yeast and human, RSC in yeast and Brahma in *Drosophila*. Another SWI/SNF subfamily is based on the helicase-domain protein ISWI, which combines with other proteins forming the complexes NURF, CHRAC and ACF in *Drosophila*, and RSF in human. A third subfamily is based on the helicase motif protein Mi-2 (Felsenfeld and Groudine, 2003).

The consequences of remodelling include transient unwrapping of the end DNA from histone octamers, forming the DNA loop or moving nucleosomes to

different translational positions (sliding), influencing the accessibility of nucleosomal DNA to transcription factors (Li et al., 2007).

1.2.2.1. DNA methylation and histone modifications

DNA methylation plays an important role in gene regulation in vertebrates.

In vertebrates DNA methylation is a post-replication epigenetic modification, characterized by the addition of a methyl group in C5 position of cytosine, generating the 5-methylcytosine and it mainly occurs at CpG dinucleotides (Feng et al., 2010). In the mammalian genome around 60-70% of CpG sites are methylated in a cell-specific and developmental-specific manner (Feng et al., 2010). The majority of CpG sites are located in gene regulatory regions, beyond proximal promoters, approximately 2 kb from the transcription start site or even further (Feng et al., 2010).

DNA methylation is usually associated with transcriptional silencing and it acts through the inhibition of the binding of transcription factors to DNA or via interaction with methyl-DNA binding proteins that target repressive chromatin remodelling complexes to the methylated regions of the genome (Feng et al., 2010; Reik, 2007).

However, DNA methylation might also be associated with transcriptional activation. For example, it is required for the induction of C/EBPα target genes through the creation of new binding sites from half-CRE sequences for this transcription factor (Rishi et al., 2010) cit. in (Botchkarev et al., 2012).

The enzymes involved in DNA methylation are the DNA-methyltransferases (DNMTs), which include DNMT1, DNMT2 and DNMT3A/B. DNMT1 is responsible for the maintenance of the methylation status of the

genome via methylation of cytosine within hemimethylated CpG sites after DNA replication. By contrast DNMT3A and DNMT3B are responsible for the *de novo* methylation of DNA (Feng et al., 2010).

DNA methylation pattern constantly changes during early distinct developmental stages (in germ-cells and pre-implantation embryos), as well as during somatic cell differentiation, thus representing important epigenetic mechanisms in establishing cell type-specific programs of gene expression, controlling tissues development and homeostasis (Feng et al., 2010).

Histone post-translational modifications, including acetylation, phosphorylation, methylation, demethylation, ubiquitination, sumoylation, ADP-ribosylation, glycosylation, biotynilation and carbonylation (Margueron et al., 2005), also play an important role in gene regulation in vertebrates and they occur at the amino-terminal tails as well as globular domains of histone proteins. In particular, methylation occurs on arginine (R) and lysines (K) residues, while acetylation, ubiquitination, ADP-ribolsylation and sumolation occur only on lysines (K) residues.

The combination of different histones modifications constitutes the “histone code” (Jenuwein and Allis, 2001), which is fundamental in the regulation of gene expression as combinatorial or sequential histones modifications on one or multiple tails, are important for the recruitment of specific regulatory proteins, which regulate the transcriptional state of a specific gene (Strahl and Allis, 2000). Modifications associated with activation of transcription are usually acetylation of lysines on histone 3 and histone 4 (H3 and H4) or di-or-trimethylation (me2/me3) of H3K4 and H3K36 and they are commonly referred to as euchromatic modifications. It has been proposed that distinct patterns of

lysines acetylation on histones are important for the regulation of co-expressed genes (Kurdistani et al., 2004) cit. in (Li et al., 2007). Another view proposes that the biological function of histones acetylation relies primarily on the number of lysines modifications (e.g. cumulative effect) with the one known exception of H4K16Ac (Dion et al., 2005) cit. in (Li et al., 2007).

By contrast, inactivation of transcription is usually determined by methylation of H3K9 and H3K27, which are often termed as heterochromatic modifications (Li et al., 2007).

The histones modifications are catalyzed by a subset of different enzymes, which covalently modify the N-terminal tail of core histones (Fischle et al., 2003).

The acetylation is the best characterized histones modification and it is dynamically regulated by the opposing action of two families of enzymes, histone acetyl-transferases (HATs) and histone deacetylases (HDACs).

HATs are enzymes that transfer an acetyl-group from acetyl-CoA to the ε-amino group of conserved lysines located at the N-terminal tails of histones. By consequence, a neutralization of the charge occurs, resulting in a weakening of the interactions of histones with DNA and/or neighbouring nuclesomes and consequently a change in chromatin structure (Berger, 2002; Strahl and Allis, 2000).

In addition, HATs are able to acetylate lysines of transcription factors and regulatory proteins, regulating their activity. In this case HATs are often referred to as FAT (factor acetyl-transferase) or LAT (lysine acetyl transferase) (Roth et al., 2001; Yang, 2004).

There are two major classes of HATs: type-A and type-B. The type-B HATs are predominantly cytoplasmic, acetylating free histones but not those already deposited into chromatin. This class of HATs is highly conserved and all type-B HATs share sequence homology with scHat1, the founding member of this type of HAT. Type-B HATs acetylate newly synthesized histone H4 at K5 and K12 (as well as certain sites within H3), and this pattern of acetylation is important for deposition of the histones, after which the marks are removed (Parthun, 2007).

The type-A HATs are a more diverse family of enzymes than the type-Bs. Nevertheless, they can be classified into at least three separate groups depending on ami- no-acid sequence homology and conformational structure: GNAT, MYST and CBP/p300 families (Hodawadekar and Marmorstein, 2007). Broadly speaking, each of these enzymes modifies multiple sites within the histone N-terminal tails. Indeed, their ability to neutralize positive charges, thereby disrupting the stabilizing influence of electrostatic interactions, correlates well with this class of enzyme functioning in numerous transcriptional coactivators (Yang and Seto, 2007).

HDAC enzymes oppose the effects of HATs and reverse lysine acetylation, an action that restores the positive charge of the lysine. This potentially stabilizes the local chromatin architecture and is consistent with HDACs being predominantly transcriptional repressors. There are four classes of HDAC (Yang and Seto, 2007): classes I and II contain enzymes that are most closely related to yeast scRpd3 and scHda1, respectively, class IV has only a single member, HDAC11, while class III (referred to as sirtuins) are homologous to yeast scSir2.

However, it is not just the histone tails that are involved in the acetylation process, but there are additional sites of acetylation present within the globular histone core, such as H3K56 (Tjeertes et al., 2009) cit. in (Bannister and Kouzarides, 2011). The H3K56 side chain points towards the DNA major groove, suggesting that acetyla- tion would affect histone/DNA interaction, a situation reminiscent of the proposed effects of acetylating the histone N-terminal tail lysines.

Unlike histone acetylation, the methylation of histones does not affect the charge of the amino acid side-chain and by consequence it does not have a single effect on transcriptional activity. On the contrary, depending on which amino acid and which site is methylated, methylation can be related to both activation and repression of transcription. Arginine methylation of H3 and H4 is associated with transcriptional activation, while lysine methylation of histones may have positive or negative effects on transcription, depending on the methylation site: methylation of K9 and K27 in H3 is generally associated with repression, whereas H3K4, K36 and K79 methylation has been associated with active transcription (Li et al., 2007). Lysines methylation is catalysed by enzymes, called histone lysine methyltransferases (HKMTs), because of their conserved methyltransferase domain termed SET domain, while arginine methylation is catalysed by members of the protein arginine methyltrasnferase (PRMT). For many years histone methylation was considered a stable, static modification. However, in 2004 the first histone demethylase was identified (Shi et al., 2004). It was found to utilize FAD as co-factor, and it was termed as lysine-specific demethylase 1 (LSD1). The demethylation reaction requires a protonated nitrogen and it is therefore only compatible with mono- and di-

methylated lysine substrates. In 2006, another class of lysine demethylase was discovered (Tsukada et al., 2006). Importantly, certain enzymes in this class were capable of demethylating tri-methylated lysines (Whetstine et al., 2006). They employ a distinct catalytic mechanism from that used by LSD1, using Fe(II) and α-ketoglutarate as co-factors, and a radical attack mechanism. The first enzyme identified as a tri-methyl lysine demethylase was JMJD2 that demethylates H3K9me3 and H3K36me3 (Whetstine et al., 2006). The enzymatic activity of JMJD2 resides within a JmjC jumonji domain.

Ubiquitination is another post-translation modification, characterized by the covalently linkage of the 76 amino-acid polypeptide ubiquitin (Ub) to lyisine residues on acceptor proteins. The histone H2A has been the first protein identified to be ubiquitinated. However, ubiquitination of H1, H2B and H3 has also been reported.

H2AK119ub1 is involved in gene silencing (Wang et al., 2004), whereas H2BK123ub1 plays an important role in transcriptional initiation and elongation (Lee et al., 2007).

Similar to ubiquitination, another histone modification, termed sumoylation, involving attachment of a small Ub-like modifier SUMO, has been identified. The sumoylation has an effect on chromatin structure, recruiting HDAC1 and HP1 (Heterochromatin protein 1) to the sumoylated histones and consequently inducing transcriptional repression (Shiio and Eisenman, 2003).

1.2.3. Polycomb Repressive Complexes

Essential proteins, which have been recognized to have a role in transcriptional repression, are the Polycomb Group (PcG) proteins. They were originally identified in the fruit fly *Drosophila Melanogaster* as repressors of *Hox*

genes, thereby preserving body pattern along the anterior-posterior axis (Sparmann and van Lohuizen, 2006). In mammals, they also influence cell cycle control, cancer and stem cell self-renewal (Valk-Lingbeek et al., 2004). PcG proteins exert a transcriptional repressive function through chromatin structure modulation and covalent histone post-translational modifications (Muller and Verrijzer, 2009)

PcG proteins are classified into two groups on the basis of their association with different classes of multimeric complexes termed Polycomb Repressive Complexes (PRCs).

In *Drosophila,* the first group, PRC2, is formed by Enhancer of Zeste (E(z)), Suppressor of Zeste (S(z)), sex comb extra (Sce) and extra sex comb like proteins; the second one, PRC1, consists of polycomb (Pc), polyhomeotic (Ph), posterior sex comb (Psc) and posterior sex comb extra proteins.

In mammals homologues of *Drosophila Melanogaster* Enhancer of zeste homolog 2 (Ezh2), Suppressor of Zeste 12 homolog (SUZ12), extra sex comb and extra sex comb like (EED and EED variants), form the core of the PRC2 complex; the second complex, PRC1, comprises in mammals the core components Polycomb homologues (CBX2, CBX4, CBX6, CBX7 and CBX8), the polyhomeotic homologues (PH1 and PH2), Posterior sex comb homologues (BMI1, PCGF1 and PCGF2) and Posterior sex comb extra homologues (RING1 and RING1B) (Simon and Kingston, 2009).

Polycomb repressive complexes assemble at specific regulatory elements called Polycomb Responsive Elements (PREs) in *Drosophila* (Muller and Kassis, 2006) cit. in (Muller and Verrijzer, 2009) and several studies have shown that the proteins Pho and Pho-like in *Drosophila* are essential for

anchoring the PcG protein complexes PRC1 and PRC2 at PRE DNA (Muller and Kassis, 2006). Pho is not a component of either PRC1 or PRC2 but exists in a distinct complex called PhoRC and it seems to be required for anchoring PRC1 and/or PRC2 at a large number of target genes in *Drosophila* (Klymenko et al., 2006).

In mammals, it has been shown that sequences enriched in CpG dinucleotides (CpG sites) play a potential widespread role in recruiting PcG complexes on the DNA. These sequences were implicated through genome-wide analyses in mouse embryonic stem cells, that correlated CpG-rich DNA with H3K27me3 (Ku et al., 2008) cit. in (Simon and Kingston, 2013). Moreover, bacterial artificial chromosome (BAC) constructs containing mouse-derived CpG sites can recruit PRC2 components following their integration into mouse genomic sites (Mendenhall et al., 2010) cit. in (Simon and Kingston, 2013).

However, not all CpG sites can recruit PRC2 and the incapable ones tend to include binding sites for transcriptional activators and/or methylation of CpGs. Indeed, several data have suggested that CpG sites that are unmethylated and devoid of bound activators are able to recruit PRC2. One possibility is that PRC2 subunits or associated proteins bear affinity for unmethylated CpGs. Indeed, depletion of a PRC2 cohort, PCL3, impacts PRC2 binding to CpG sites (Hunkapiller et al., 2012), although it is still not clear whether PCL directly binds to CpG sites. Another possibility is that DNA methylation regulates PRC2 binding to DNA and Tet-1 might involved in PRC2 recruitment on CpG sites, due to its ability to modify methylated DNA by converting the DNA modified base 5-methylcytosine to 5-hydroxymethylcytosine (Tahiliani et al., 2009). Indeed, it has been shown that Tet-1 activity was needed for full recruitment of

PRC2 to target sites in mouse embryonic stem cells (Wu et al., 2011) cit. in (Simon and Kingston, 2013).

Similar to Drosophila PREs, two elements have been identified in mammals: a 3kb element termed PRE-kr, shown to be able to repress a reporter gene in mice as well as in Drosophila and the silencing was dependend upon PcG proteins recruitment on PRE-kr (Sing et al., 2009). Another element from the human HOX cluster between HOXD11 and HOXD12, called D11.12, also recruits PcG proteins and represses reporter expression in a PcGs-dependent manner (Woo et al., 2010).

Besides CpG sites and PREs, other mechanisms are involved in PcGs targeting, including binding of PcGs components to transcription factors (Yu et al., 2012) as well as PRC2 recruitment by lncRNAs (Zhao et al., 2008) cit. in (Simon and Kingston, 2013).

In mammals, once PRC2 binds to its target genes, it is involved in the initiation of the transcriptional repression process through the mammalian protein Ezh2, which is able to trimethylate lysine 27 and to a less extent lysine 9 on histone H3 (Sparmann and van Lohuizen, 2006). However, more recent studies provide biochemical and functional evidence that Ezh2 methylase activity is regulated and enhanced by the PcG protein Polycomb-like (Pcl), homologues PHF1 (Pcl1) and Mtf2 (Pcl2) in mammals, which interact with PRC2, as confirmed by co-immunoprecipitation experiments (O'Connell et al., 2001) cit. in (Muller and Verrijzer, 2009).

In accordance with these findings, biochemical purifications from *Drosophila* embryos and larvae identified a distinct form of PRC2, called Pcl-PRC2, containing the Pcl protein (Nekrasov et al., 2007). Depletion of Pcl in *Drosophila*

embryos and larvae caused a reduction of the repressive histone modification H3K27me3 at target genes (Nekrasov et al., 2007), confirming that Pcl is specifically required for anchoring PRC2 at PREs and to allow the complex to generate high levels of H3K27me3, essential for subsequent PcG repression of target genes.

In addition to H3K27me3 modification, *in vitro* studies have demonstrated that PRC2 also exhibits methyltransferase activity towards lysine 26 of the linker histone H1. This modification can recruit HP1 to chromatin, influencing higher order chromatin structure, thus contributing to the silencing process (Daujat et al., 2005) cit. in (Sparmann and van Lohuizen, 2006).

Interestingly, experiments with HeLa cell line, showed that PRC2 is also able to regulate the CpG methylation pattern through direct binding of Ezh2 to DNA methyltransferases, as demonstrated by GST-Pull down and co-immunoprecipitation experiments (Vire et al., 2006). Ezh2 is also able to recruit DNA methyltransferases to its target genes, as demonstrated by chromatin immunoprecipitation experiments (Vire et al., 2006) and overexpression of Ezh2 mutants lacking the SET domain, failed to induce DNA methylation (Vire et al., 2006).

The histone mark H3K27me3 is important but not essential for the recruitment of PRC1, which is able to recognize the H3K27me3 epigenetic mark via the chromodomain of the mammalian CBX proteins repressing transcription through several possible mechanisms (Sparmann and van Lohuizen, 2006).

Recent studies showed the existence of different functional PRC1 variants during murine embryonic stem cells differentiation, with the incorporation of different Cbx proteins (Morey et al., 2012). In pluripotent cells the most

represented Cbx protein of PRC1 is Cbx7, which is able to maintain the repressive state of differentiation markers, while during differentiation process Cbx2 and Cbx4 proteins are incorporated into PRC1, exerting a non-overlapping repressive function through the repression of mesodermal/endodermal and ectodermal genes respectively (Morey et al., 2012).

Additional studies showed that the recruitment of Cbx proteins to their target genes was strickly dependent on a functional PRC2 and on the chromatin associated mark H3K27me3 (Morey et al., 2012). However, contrasting studies in *Drosophila* demonstrated that PRC1 binding was not directly dependent on H3K27 tri-methylation by PRC2. Absence of PRC2 component Ezh2 and reduced levels of H3K27me3, did not affect the binding of PRC1 components (Ohno et al., 2008) cit. in (Muller and Verrijzer, 2009). Furthermore, binding of PhoRC and PRC1 at PREs is undiminished in Pcl mutant *Drosophila* embryos, even though H3K27me3 levels at target genes are significantly reduced (Nekrasov et al., 2007), suggesting that loss of PRC1 binding, after prolonged depletion of PRC2 component Ezh2, might be due to an indirect effect or to a PRC2 function that is independent of its HMTase activity (Muller and Verrijzer, 2009; Ohno et al., 2008).

Although the silencing mechanisms of PRC1 are not well understood, several possible scenarios have been proposed.

One of these is chromatin compaction, which acts through the compaction of nucleosomal arrays by PRC1, making them refractory to SWI/SNF-class-ATP-dependent chromatin remodelers (Francis et al., 2004; Shao et al., 1999). According to these studies the core PcG components of PRC1 generate

chromatin compaction through interaction with nucleosomes rather than with the DNA linker by a mechanism that does not require histone tails (Francis et al., 2004). In particular the C-terminal end of the PRC1 subunit posterior sex comb, plays an essential role in nucleosomes compaction (Francis et al., 2004). Considering that PREs are nucleosomes depleted and nuclease hypersensitive (Mohd-Sarip et al., 2006) cit. in (Muller and Verrijzer, 2009), it has been suggested that PRC1 chromatin compaction activity acts in the PRE flanking chromatin regions to generate a less accessible chromatin structure for transcription factors at the promoter or in the coding regions of target genes (Muller and Verrijzer, 2009), blocking, therefore, transcriptional initiation and/or elongation.

Another possible mechanism of gene silencing by Polycomb repressive complexes is the ubiquitynation of lysine 119 on histone H2A (H2AK119ub), performed by the mammalian homologues Ring1B and Bmi-1 (Buchwald et al., 2006; Wang et al., 2004) due to their RING finger motif, which has been demonstrated to contain the ubiquitin ligase activity (Wang et al., 2004) (Figure 8). However, recent studies showed that the re-induction of Ring 1B expression in Ring $1B^{-/-}$ embryonic stem cells of a mutant Ring 1B that in vitro lacks the E3 ubiquitinase activity, does not restore H2AK119ub but is nonetheless able to restore chromatin compaction at Hox loci, suggesting that Ring 1B acts to compact higher order chromatin structure independent of its known histone-modifying activity (Eskeland et al., 2010).

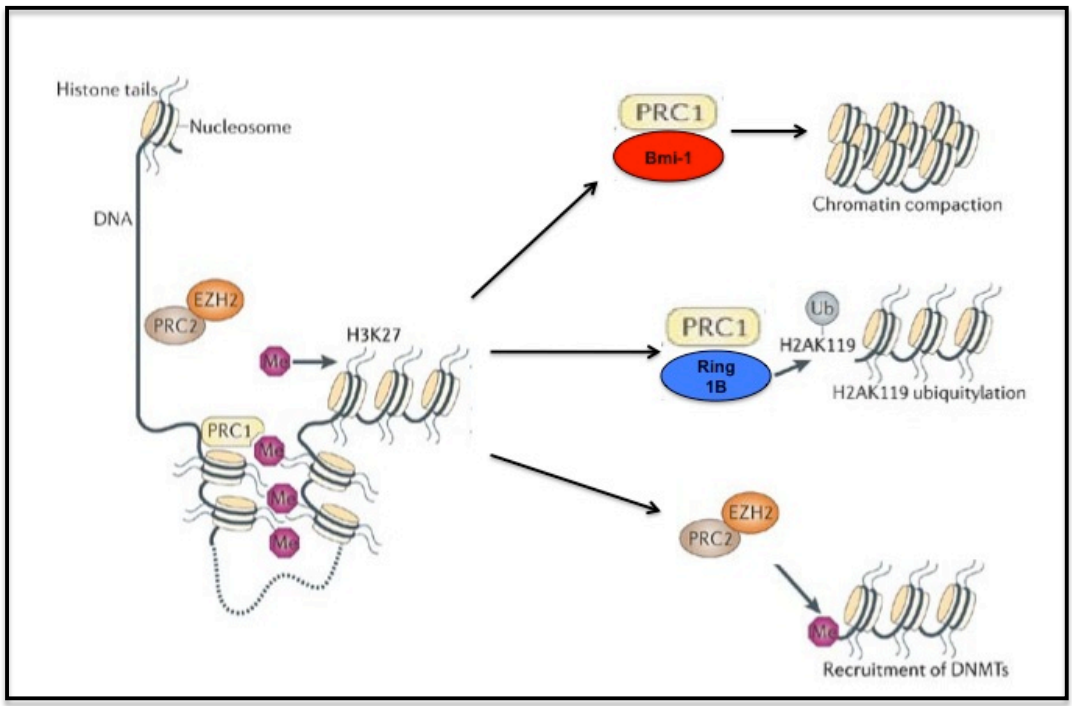

Figure 8: Mechanisms of silencing by Polycomb Repressive Complexes.

PRC2 component Ezh2 tri-methylate lysine 27 on histone 3 (H3K27me3) and this epigenetic modification is recognized by PRC1 components Cbx proteins through their chromodomain. Several possible mechanisms of Polycomb-mediated silencing have been suggested: PRC1 component Bmi-1-mediated chromatin compaction; PRC1 component Ring1B-mediated ubiquitylation of lysine 119 on histone 2A (H2AK119ub); DNMTs recruitment by PRC2 component Ezh2. Modified from (Sparmann and van Lohuizen, 2006)

Different studies performed in *Drosophila,* identified a new complex, called dRAF, containing the ubiquitylase activity (Lagarou et al., 2008). dRAF lacks Polyhomeotic and Polycomb subunits but contains other subunits instead. One of these is dKDM2, which greatly enhances the H2A ubiquitylase activity on nucleosomes, as *in vitro* and depletion of this subunit showed reduced H2A ubiquitynation, suggesting that dRAF rather than PRC1 is the major responsible for H2A ubiquitylation in *Drosophila* (Lagarou et al., 2008).

Another potential mechanism of PcG repression is direct interaction with the general transcription machinery to inhibit function. On transgenes bearing a Drosophila PRE and hsp26 promoter, PcG components blocked transcription

prior to initiation (Dellino et al., 2004). This finding is supported by different studies, showing elevated levels of promoter-associated RNA Pol II observed in a fly PRC2 mutant (Chopra et al., 2011) cit. in (Simon and Kingston, 2013). Furthermore, PcG target genes in ESCs with bound PRC1 have much lower levels of promoter-associated Pol II than target genes lacking PRC1, consistent with an initiation block at these promoters (Min et al., 2011). Moreover, recombinant PRC1 inhibited binding of the Mediator Complex but had little impact on the binding of the general transcription factor TFIID, suggesting that PRC1 gene silencing correlates with a Mediator block but tolerates bound of TFIID (Simon and Kingston, 2013).

1.2.3.1. Polycomb bodies

Polycomb repressive complexes are not randomly distributed within the nucleus. They have been found aggregated in nuclear foci called Polycomb bodies (Hernandez-Munoz et al., 2005; Saurin et al., 1998) cit. in (Pirrotta and Li, 2012). The number and size of these bodies is different in different cell types: they are fewer and larger in embryonic stem cells and they become smaller and more numerous in differentiated cells (Ren et al., 2008).

Several different hypotesis of Polycomb bodies formation have been suggested and one of these is that their formation does not rely on the PcG complexes properties but it is related to the genomic distribution of their target genes (Pirrotta and Li, 2012). PcG target genes have been found to be physically adjacent in the linear genomic map (Kharchenko et al., 2011) cit. in (Pirrotta and Li, 2012) and recent genome-wide chromatin conformation capture techniques and related approaches, using PcG target sites as bait, showed that the most frequent partners were other PcG sites on the same chromosome arm

but long-range contacts with non-PcG sites were rare (Tolhuis et al., 2011). By contrast, when non-PcG targets were used as bait, interactions were also found on the same chromosome but they were generally with non-PcG targets (Tolhuis et al., 2011), suggesting that PcG proteins and their targets might play an important role in the formation of these interactions and polycomb bodies.

However, different studies showed that insulator elements rather than PcG proteins might be important for the formation of the interactions between PcG target genes. 3C experiments using transgenes of PRE regions containing insulators such as *Fab-7* and *Mcp,* can often functionally interact with each other as well as with endogenous elements. In contrast the same PREs alone without any insulator elements did not show such interactions (Muller et al., 1999). However, considering that there are hundreds of insulator protein binding sites per chromosome arm and considering that most of the interactions between PcG targets are found on the same chromosome arms (Tolhuis et al., 2011), the insulator-mediated interactions cannot be considered specific. It is possible, therefore, that both PcG proteins and insulator elements might contribute together to these interactions (Pirrotta and Li, 2012). In line with this observation, it has been suggested that PcG proteins might contribute to these associations through post-translational modifications of the insulator proteins, like the insulator-binding protein CTCF (Pirrotta and Li, 2012). Supporting this idea it has been found that CTCF is sumoylated, possibly through the sumoylation activity of the mammalian SUMO E3 ligase CBX4 protein, also consistent with previous data, showing close association between CTCF, Polycomb bodies and CBX4 protein (MacPherson et al., 2009).

However, still a lot of studies need to be performed to better understand the molecular mechanisms of PcG proteins interactions with their target genes and how there are able to modify the flanking chromatin regions.

Furthermore, with respect to their biological function, future studies will focus on the mechanisms by which PcG proteins control target genes and how this is modulated by cell signalling.

1.2.3.2. Role of PcG proteins in stem cells maintenance and cancer

Several studies demonstrated that PcG proteins play an important role in embryonic stem cells maintenance, as demonstrated by knock-down experiments, which showed that absence of PRC2 members, like Ezh2 or Eed, or PRC1 members, like Ring 1B, results in early embryonic lethality (O'Carroll et al., 2001; Voncken et al., 2003) cit. in (Sparmann and van Lohuizen, 2006). Furthermore, it has been found in both human and mouse ESCs that PcGs directly repress a prominent group of developmental regulators, including transcription factors of the Dlx, Irx, Lhx, Pax, Fox, Sox, Gata and Tbx gene families, whose activation would otherwise promote differentiation (Boyer et al., 2006; Lee et al., 2006). All these genes are involved in a variety of developmental processes, including neurogenesis, haematopoiesis and axial patterning (Sparmann and van Lohuizen, 2006).

Several signalling pathways, including transforming growth factor-β (TGFβ), bone morphogenic protein (BMP), Sonic Hedgehog (Shh), Wnt and fibroblasts growth factor (FGF), required for gastrulation and lineage differentiation in the embryo, are also regulated by PcG complexes (Loebel et al., 2003) cit. in (Sparmann and van Lohuizen, 2006), suggesting that stem cell fate is determined by the suppression of specific differentiation genes possibly

through the suppression of related signalling pathways, as demonstrated in a model of Bmi-1 knock-out mice, according to which Bmi-1 absence was responsible for the reduced level of neural stem cells (NSCs) after birth, due to an incapacity of these cells to efficiently respond to Shh signalling pathway (Leung et al., 2004).

Different studies showed that PcGs pluripotency target genes are co-occupied by the transcription factors OCT4, SOX2 and NANOG, required for the maintenance of the stem cell identity. It is possible therefore that these transcription factors could partially maintain stem cell self-renewal by recruiting PcGs to repress differentiation-promoting genes (Nichols et al., 1998). This hypothesis is consistent with OCT4 knock-down experiments, showing a loss of the PRC2 component Suz12 from its target gene promoters (Squazzo et al., 2006).

Commitment of stem cells to lineage-specific differentiated cells is followed by de-repression of the subset of cell type-specific genes and related signalling pathways. Studies performed in a neural model of differentiation showed that in undifferentiated cells, genes specifying the neuronal cell fate are repressed by PcG complexes and, in response to the induction of differentiation, they become activated through displacement of PcGs from their promoter sequences (Bracken et al., 2006). These results are consistent with previous experiments, showing similar results in muscle and germ-lines terminal differentiation processes (Caretti et al., 2004) cit. in (Sparmann and van Lohuizen, 2006).

All these findings together suggest the existence of dynamic mechanisms, which are essential for de-repressing PcGs target genes, firstly repressed

through the repressive histone modification H3K27me3, implying that this epigenetic modification is reversible.

However, it has been shown that only a relative small fraction of PcG target genes become activated after depletion of PcGs in human embryonic fibroblasts (Bracken et al., 2006), suggesting that some of these genes might stay permanently repressed by additional silencing mechanisms. Considering that PRC2 component Ezh2 is able to recruit DNMTs to its target genes (Vire et al., 2006), it is possible that DNA methylation might provide the second epigenetic mark, required to irreversibly lock some PcGs target genes in the repressed transcriptional state in committed cells.

Beside PcGs role in transcriptional repression, it has been found that some actively transcribed cells are bound by PcG proteins in undifferentiated cells (Bracken et al., 2006), suggesting the existence of additional mechanisms required for PcGs repressive function, possibly through specific developmental signals that are able to induce PcGs-mediated silencing by recruiting or displacing auxiliary regulators at the complexes or by post-translationally modifying PcG core components (Sparmann and van Lohuizen, 2006). Consistent with this hypothesis, recent ChIP-seq data in pluripotent cells, showed enrichment of PRC1 component Ring1B on OCT4, SOX2 and NANOG promoter regions (Morey et al., 2012), suggesting that in pluripotent cells, PcGs might be inactive on the promoter regions of these transcription factors, therefore maintaining the pluripotency of stem cells. Once the differentiation program has started, additional factors might contribute to PcGs activation with consequently repression of OCT4, SOX2 and NANOG and exit of the cells from the pluripotent state.

PcG complexes also play an important role in adult stem cells maintenance, as demonstrated in Bmi-1 knock-down experiments, where Bmi-1 deficient mice display posterior transformation, acute neurological disorders and severe proliferative defects during haematopoiesis (van der Lugt et al., 1994) cit. in (Sparmann and van Lohuizen, 2006). Furthermore, Ezh2 knock-out mice display an increase in epidermal thickness as well as in increased expression markers of late epidermal differentiation during embryogenesis (Ezhkova et al., 2009). On the contrary Ezh2 overexpression prevents haematopoietic stem cells exhaustion and leads to a block of muscle myoblasts differentiation (Caretti et al., 2004; Kamminga et al., 2006) cit. in (Sparmann and van Lohuizen, 2006).

The maintenance of the self-renewal capacity of stem cells is possible due to the direct regulation by PcGs of genes involved in cell-cycle control, including the tumor suppressor locus Ink4a/Arf in neural and haematopoietic stem cells, which has been shown to be negatively regulated by Bmi-1. Lack of Bmi-1 led to increased expression of p16 and p19, genes encoded by the Ink4a/Arf locus (Molofsky et al., 2003; Park et al., 2003) cit. in (Valk-Lingbeek et al., 2004). p16 overexpression, in turn, affected the retinoblastoma protein Rb phosphorylation, thus inhibiting the cyclin D-Cdk4/6 kinase complexes and the hypophosphorylated form of Rb, which sequestered the transcription factors E2F, thus repressing their target genes with consequent cell-cycle arrest, senescence or apoptosis (Valk-Lingbeek et al., 2004). p19 overexpression led to increased binding to MDM2, thus inhibiting the degradation of p53 transcription factor, inhibitor of the cell-cycle. This resulted in the activation of

p53 direct targets, leading to cell-cycle arrest and apoptosis (Valk-Lingbeek et al., 2004).

According to all these considerations, Ink4a/Arf locus plays an important role in restricting the potential dangerous self-renewal division of stem cells and Bmi-1 together with other PcG members, such as Mel-18 and Cbx7 (Jacobs et al., 1999a), might control and maintain the stem cells self-renewal capacity by counterbalancing Ink4a/Arf expression (Valk-Lingbeek et al., 2004), thus generating a controlled mechanism of self-renewal in embryonic and adult stem cells.

All these findings also suggest a possible connection between PcGs and cancer development. Indeed, it has been shown that Bmi-1 is able to inhibit MYC-induced apoptosis through repression of the Ink4a/Arf locus in B and T-cell lymphomas (Jacobs et al., 1999b) cit. in (Sparmann and van Lohuizen, 2006).

Although Bmi-1 is the PcG protein most strongly associated with neoplastic development, several other PcG members are also linked to tumorigenesis. One example is Suz12, which has been found to be overexpressed in both colon and breast cancer (Kirmizis et al., 2003) cit. in (Sparmann and van Lohuizen, 2006). Furthermore, the PRC2 member Ezh2 was found to be overexpressed in several human tumors, such as multiple types of lymphoma, prostate and breast cancer (Varambally et al., 2002) cit. in (Sparmann and van Lohuizen, 2006). According to recent studies, Ezh2 might exert its function in cancer development by influencing cell adhesion and migration, contributing to the metastatic capacity of tumoral cells. Indeed, it has been described a cytoplasmic role of an Ezh2-associated methyltransferase complex, which is able to control actin polymerization (Su et al., 2005)

In addition several promoter regions of PcGs target genes are methylated in several human tumors, suggesting that aberrant expression of PcG members might be responsible for the repression of tumor-supressor genes through DNA methylation, promoting therefore tumorigenesis (Bracken et al., 2006) cit. in (Sparmann and van Lohuizen, 2006).

Besides the silencing of tumor-suppressor genes, PcGs might influence tumor development through a misspecification of cells towards a stem cell fate, considering that PcGs repress genes necessary for the differentiation of stem cells into various tissue types thus maintaining stem cell self-renewal capacity (Bracken et al., 2006). Consistent with this view stem cells can be considered as the main driving force behind tumor proliferation and progression ("cancer stem-cell" hypothesis), as the extensive proliferative potential of cancer cells resembles to some extent the self-renewal of stem cells (Pardal et al., 2003) cit. in (Sparmann and van Lohuizen, 2006).

1.2.4. 3D organization of the eukaryotic nucleus

1.2.4.1. Chromosome territories

Eukaryotics interphase nuclei are characterised by a non-random tri-dimensional chromosomes organization, where chromosomes occupy distinct positions termed chromosome territories (Cremer and Cremer, 2010).

Since the late 19th century an uncounted number of microscopic studies and experiments have appeared on numerous aspects of nuclear structure and on the observation of mitotic chromosomes. The non-random organization of chromatin inside the nucleus was first suggested by Carl Rabl (Rabl 1885), but it was Theodor Boveri who first introduced the term chromosome territories (CTs) in his seminal studies of blastomere stages of the horse roundworm

Parascaris equorum (Boveri 1909). Boveri discovered that each chromosome maintained its individuality during interphase and occupies distinct part of the nuclear space. As a consequence of his first observations, Boveri suggested three conclusions: (I) CT order is stably maintained during interphase; (II) Chromosome neighbourhood patterns change from prophase to metaphase and (III) new chromosome neighbourhood arrangements established in metaphase were conserved during anaphase and telophase, resulting in symmetrical arrangements of CTs in the two daughter nuclei (Cremer and Cremer, 2010).

However, although important evidences in favour of chromosome territories were provided, other experiments carried out with electron microscope did not observe the presence of an organized nuclear architecture and the concept of chromosome territories was considered to be experimentally disproved (Cremer and Cremer, 2010).

It was in 1970s that the researchers Stephen M. Stack, David B. Brown and William C. Dewey, who still believed to the chromosome territories concept, performed an important experiment, which was fundamental for the establishment of the evidence of the presence of chromosome territories within the nuclear space (Cremer and Cremer, 2010).

The experimental procedure was based on UV-induced damage of DNA, using a laser microbeam, which was then labelled with ^{3}H-thymidine and detected either by autoradiography or it was visualized by immunostaining using antibodies against UV-damaged DNA. Depending on the localization of damages, either on single or multiple chromosomes, it was possible to assume

the organization of chromosomes within the nuclear space (Cremer et al., 1982) (cit. in (Cremer and Cremer, 2010).

According to the experiment results, it was provided the first, although still indirect, evidence for the existence of chromosome territories.

Within the nuclear space, between CTs, interchromosomal compartments (ICs) have also been found. This model of nuclear architecture is referred to as "CT-IC model". The width of the IC spaces is highly variable depending on Brownian movements of chromatin domains and they occupy a 60% of the nuclear space, allowing transient contacts between the surfaces of in *cis* and in *trans* domains. The ICs contain the transcription factories, which include elements such as nuclear splicing speckles and a variety of other non-chromatin bodies, which are preferentially located in the interior of the expanded ICs (Albiez et al., 2006). Plasmids, encoding a common origin of replication but different transcription units, have been transfected into cells, where they were assembled into minichromosomes, that the cellular machinery replicated and transcribed (Xu and Cook, 2008). According to these experiments, genes, transcribed by the same promoters, tend to co-localize within the same transcription factories. In addition the number and composition of these transcription factories vary and depend on the cell type (Xu and Cook, 2008). Some of them are enriched for splicing factors, such as SC35 and the localization of genomic regions within the transcriptional factories depends on gene structure, as plasmids containing genes with introns tended to accumulate in SC35 rich factories, whereas plasmids with intronless genes preferentially localized closed to factories lacking SC35 (Xu and Cook, 2008).

ICs also contain several transcription factors (TFs), which according to several studies, tend to be co-localized in specific nuclear compartments. There are not as many TFs identical as the target genes they regulate and one single TF is able to regulate a subset of different target genes. Therefore, the co-localization of TFs in specific nuclear compartments results in a tighter transcriptional co-regulation of their target genes. Furthermore, it has been shown that target genes of other trans regulators, including chromatin remodelers and histone-modifier enzymes, also tend to be co-localized in the nuclear space (Dai and Dai, 2011). However, different studies showed that there was a remarkably little relationship between transcription sites and the distribution of many specific transcription factors (such as OCT1, E2F1 or glucocorticoid receptor) as they were found to be homogeneously distributed throughout the nucleoplasm occupying numerous small domains (Grande et al., 1997). Similarly, although the haematopoietic transcription factors GATA1, 2 and 3 colocalized in foci in erythroid cells, these sites do not correspond to sites of transcription and they do not localize with the β-globin genes (Elefanty et al., 1996) cit. in (Sutherland and Bickmore, 2009).

According to the “IC-CT model”, during the transcriptional process, genes are at least partially decondensed into the perichromatic region (PR), located at the domain periphery, and each perichromatin fibrils (PFs), which are generated on the domain periphery, carries a nascent transcript from a different gene. Splicing speckles located in the IC provide then splicing factors to perichromatin fibrils, which also represent the structure in which the different splicing reactions occur (Cremer and Cremer, 2010) (Figure 9**a/b**).

A second proposed model is the "interchromatin network model" (ICN) according to which intermingling chromatin loops from the same CT, as well as from neighbouring CTs, are able to make contact in *cis* or in *trans* (about 46% of each chromosome is intermingled with the rest of the genome) and there is a correlation between the extent of intermingling and the translocation frequency (Branco and Pombo, 2006) (Figure 9**c**). Furthemore, the intermingling of different CTs is dependent on the activation of transcription. After the treatment of human activated lymphocytes with α-amanitin, which is able to inhibit PolII-driven transcription, a significantly decrease in intermingling has been observed, suggesting that transcription influences chromosomes interactions, determining specific intermingling "partners" according to cell's repertoire of active genes (Branco and Pombo, 2006).

Active genes on decondensed chromatin loops, which are localized outside CTs, are able to co-localized in *cis*-domain in so-called hubs or be transcribed at preassembled transcription factories. This third model focuses the attention on giants loops, which are able to carry genes from a remote part of the nuclear space in an expression hub or, on the contrary, genes may be transported to a remote repressive nuclear compartment to be silenced (Kosak and Groudine, 2004) cit. in (Cremer and Cremer, 2010) (Figure 9**d**).

However, none of these models is fully supported by experimental evidences.

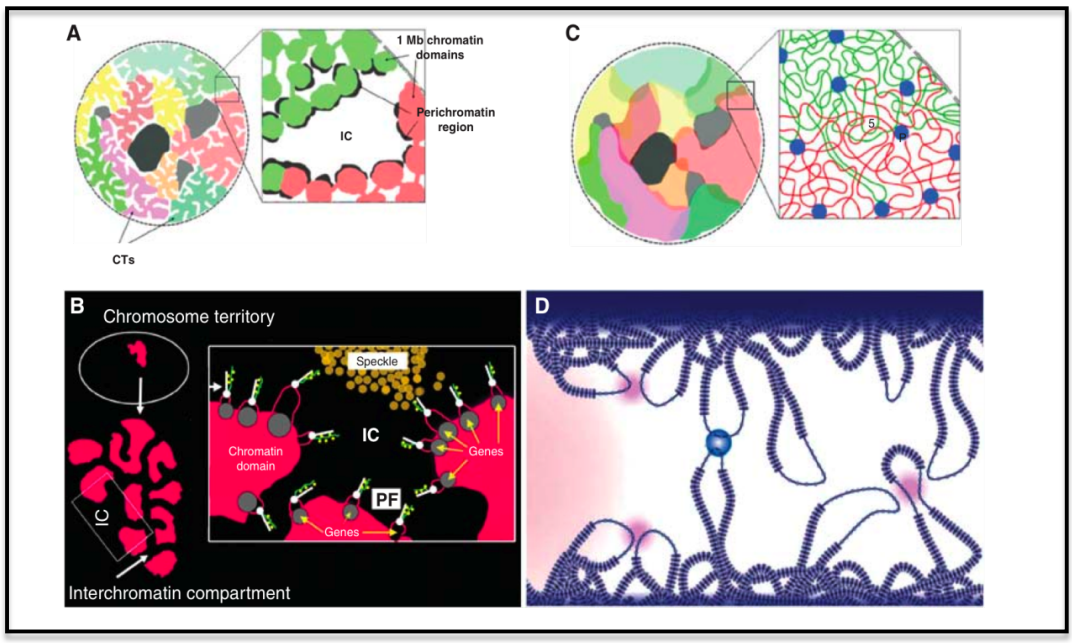

Figure 9: Schematic representation of the "IC-CT" and "interchromatin network model" (ICN).

(A-B) Schematic representation of the "IC-CT model", according to which during the transcriptional process genes are at least partially decondensed into the perichromatin region (PR) located at the domain periphery and each perichromatin fibrils, which are generated on the domain periphery, carries a nascent transcript from a different gene. Splicing speckles located in the IC provide then splicing factors to PFs, which also represent the structure in which the different splicing reactions occur (cit. in (Cremer and Cremer, 2010). **(C)** Schematic representation of the "interchromatin network model" (ICN) according to which intermingling chromatin loops from the same CT, as well as from neighbouring CTs, are able to make contact in *cis* or in *trans*. (D) Model suggested by Fraser and Bickmore (Fraser and Buckmore, 2007). According to the authors transcription factories (dark pink) can recruit genes in *cis* and in *trans* located on decondensed chromatin loops that extend outside chromosome territories. Taken from (Cremer and Cremer, 2010).

1.2.4.2. Enhancer-promoter long-distance interactions

As previously mentioned, different genomic regions can interact with each other *in cis* (on the same chromosome) or *in trans* (on different chromosomes), stimulating transcription by recruiting tissue-specific transcritption factors, RNA Polymerase II and other co-factors involved in transcriptional regulation (Marsman and Horsfield, 2012). Enhancers and the genes they regulate can be as far as 2 or 3 Mbp distant from each other (Krivega and Dean, 2012).

The favoured model for enhancer-mediated activation of gene transcription is that enhancer are brought into proximity with promoters by a chromatin loop, and that this interaction is necessary for recruiting the transcriptional machinery. Since the advent of 3C and related methods, that detect interactions between spatially separated regions of chromosome in *cis* or in *trans*, enhancer-promoter interactions have been found in different loci. Among these, the *β-globin* locus, in which the locus control regions (LCR) contains multiple enhancer, was found to interact with distinct downstream *β-globin* genes at the same time at which they are expressed (Tolhuis et al., 2002). Subsequently, other loci have been investigated including *H19/Igf2* and the *Myb* proto-oncogene (Stadhouders et al., 2012) cit. in (Marsman and Horsfield, 2012). All these studies supported the hypothesis that distant enhancers stimulate transcription by long-range interactions with promoters. However, this does not rule out the possibility that enhancer can influence gene transcription without interacting with promoters; e.g. the production of antisense RNAs from enhancers may influences gene isoform specificity (Onodera et al., 2012) cit. in (Marsman and Horsfield, 2012).

A genome-wide map of intra-chromosomal enhancer-promoter interactions revealed that most promoters associate with a single enhancer, but around 25% associated with two or more enhancers. Genes interacting with multiple enhancers are more highly expressed than those that interact with a single enhancer, suggesting that amplitude of gene expression is positively correlated with the number of interacting enhancers (Chepelev et al., 2012).

In eukaryotic cells transcriptional activation usually correlates with movement of the majority but not of all genes from the nuclear periphery

towards the nuclear interior. In accordance with this view recent studies showed that the Eμ enhancer is required for the movement of the IgH locus to the nuclear interior (Guo et al., 2011) without recombination or transcriptional activation of the target gene, suggesting that loop formation might occur before migration and transcription.

By contrast, other studies showed that intra-nuclear migration during transcriptional activation correlates with entry into a transcription factory (Osborne et al., 2004), suggesting that looping formation might occur after association with a transcription factory, possibly as a result of transcription.

Several different proteins are involved in long range enhancer-promoter interactions, including the chromatin remodeler Satb1, which has been shown to bind to the BCL2 gene promoter and its enhancer to form close contacts between them and Satb1 reduction compromised loop formation and transcription (Gong et al., 2011). The transcription factor GATA-1 can recruit the chromatin remodeler BRG1, which also contributes to loop formation (Kim et al., 2009). BRG1 might facilitate looping directly, but it is also possible that it promotes the binding of other factors that induce looping (Marsman and Horsfield, 2012).

Insulator associated proteins are also involved in long range chromatin associations within the nucleus. One of these proteins is CTCF, which has been shown to mediate interactions between thousand of loci and to organize the genome into different compartments. CTCF insulator-associated protein can mediate these interactions through several different mechanisms, which are strictly dependent on the locus (Krivega and Dean, 2012).

CTCF can interact with another CTCF protein thus mediating the interaction between two insulators, which in turn can positively influence enhancer-promoter interaction (β-globin and APO locus); CTCF can interact with an enhancer and target promoter directly participating in long-range interaction and transcriptional activation; CTCF can interact with an insulator and provide then interaction with a promoter sequence via binding with a specific transcriptional factor, which in turn activates transcription (INFG and MHC class II loci); CTCF provides the interaction with an enhancer which in turn interacts with a target promoter (IgH locus) (Krivega and Dean, 2012).

However, despite this important role of CTCF and other proteins in mediating long-range interactions, further studies will be necessary to better understand the mechanisms underlying the establishment of enhancer-promoter connections, how they move within the nucleus and how the transcription output is influenced by all these events.

On the other side, TFs can also inhibit loop formation by preventing the binding of factors that promote loop formation. For example, at the HoxA locus, OCT4 inhibits loop formation by antagonizing cohesin binding (Kim et al., 2011) cit. in (Marsman and Horsfield, 2012). Cohesin is a complex that has previously been found to participate in chromatin looping.

1.2.5. The nuclear envelope and its role in gene expression regulation

1.2.5.1. The nuclear lamina and the LINC complex

Over many years new experimental technologies, such as 3D in situ hybridization (3D FISH) and chromatin conformation capture technique (3C) have been developed, allowing new discoveries in the field of nuclear organization, such as the relationship between the nuclear organization and the

regulation of gene expression. According to previous studies, gene poor CTs and silenced genes are frequently found in association with the nuclear periphery (Boyle et al., 2001), in particular they have been found to be associated with the nuclear envelope (NE) (Wilson and Berk, 2010), whilst the majority, although not all, gene-rich CTs and active genes are mainly mapped to the nuclear interior.

Strong relationship between nuclear organization and gene expression regulation has been shown during development, as changes in global chromatin structure, that include large-scale compaction of genomic domains, have been observed (Meshorer and Misteli, 2006).

The nuclear envelope consists of the nuclear pore complex, the outer and the inner membranes separated by a luminal space, and the nuclear lamina, a network of different proteins, which is associated with the inner nuclear membrane through different protein-protein interactions (Broers et al., 2006).

The major components of the nuclear lamina are lamins type A, type B and type C, which exist as coiled-coil dimers and are associated in “head to tail” polymers. Lamin A and C derive from the same gene (*Lmna*) as a result of alternative splicing (Lin and Worman, 1993) cit. in (Dechat et al., 2010). Two major lamins type B have been identified: Lamin B1 and Lamin B2, which are encoded by *Lmnb1* and *Lmnb2* genes respectively (Peter et al., 1989) (cit. in (Dechat et al., 2010).

While all cells express B-type lamins during development, A-type lamins expression is finely regulated during developmental process. The expression of both Lamin A and Lamin C is initiated at 10-12 days of mouse embryogenesis and found only in primordial muscle cells. At day E15.0 their expression has

also been found in the epidermis. After birth, their expression is extended to the rest of the organs (Rober et al., 1989). The different expression of Lamins A/C and Lamins type B has also been demonstrated during stem cells differentiation in culture: undifferentiated human and mouse stem cells express Lamins B1 and B2 but not Lamins A/C (Constantinescu et al., 2006).

All lamin proteins have a common structure characterized by a α-helic central rod domain flanked by a short globular amino-terminal "head" domain and a longer carboxy-terminal "tail" domain (Parry et al., 1986), which is similar to the immunoglobulin fold (Ig-fold). Between the carboxy-terminal end of the central rod domain and the Ig-fold, there is a nuclear localization signal (NLS), which is important for the transport of all lamins into the nucleus (Loewinger and McKeon, 1988) (Figure 10).

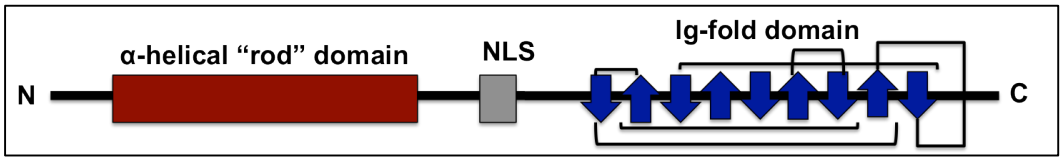

Figure 10: Schematic representation of nuclear lamin structure.

Lamins A, B1 and B2 are firstly expressed as pre-lamins and their maturation require different post-translational modifications of their carboxy-terminal-CAAX box. The first one of these modifications is farnesylation of the cysteine residue by a farnesyltransferase. This modification initiates a sequence of processing steps beginning with the removal of the –AAX by a CAXX prenyl protease, followed by a carboxymethylation of the carboxy-terminal cysteine by isoprenylcisteine carboxy methyltransferase (Icmt) (Winter-Vann and Casey,

2005) cit. in (Dechat et al., 2010). The type-B lamins remain permanently farnesylated and carboxymethylated, while the A-type lamin undergoes an additional modification, which consists of the removal of 15 amino acids from the carboxyl terminus of farnesylated/carboxymethylated prelamin A, resulting in the production of a mature Lamin A. Because Lamin C is 74 residues shorter than mature lamin A, it does not possess a –CAAX box and therefore does not undergo farnesylation or carboxymethylation (Dechat et al., 2010).

Other post-translational modifications, such as phosphorilation, occur in both A and B-type lamins and play a role in the disassemblation of lamins at the onset of mitotis (Fields and Thompson, 1995). In contrast de-phosphorilation is able to incorporate lamins into newly forming daughter cell nuclei during telophase/G1 and, while B-type lamins relocalize exclusively to the periphery of reassembling daughter nuclei, A-type lamins accumulate in the nucleoplasm at the end of mitotis and in early G1. The Lamin A/C structures in the nucleoplasm appear to be more dynamic compared to those one associated with the nuclear lamina. By contrast, B-type lamins in the nucleoplasm seem to form more stable structure compared to A-type lamins (Broers et al., 1999; Moir et al., 2000) cit. in (Dechat et al., 2008).

The nuclear lamina also plays an essential role in the maintenance of nuclear shape, cellular integrity and stability, as cells lacking Lamin A/C displayed impaired mechanical transduction, decreased mechanical stiffness and defective cell migration (Houben et al., 2007).

The maintenance of the proper nuclear shape and nuclear positioning within cells acts through proper connections between the nuclear lamina and cytoskeleton components via the LINC complex (Crisp et al., 2006).

The LINC complex is primarily composed of Suns and Nesprins (also called synes) but other nuclear envelope components such as emerin, might also be components of this complex (Crisp et al., 2006).

Suns (Sun-1 and Sun-2) are type II integral proteins of the inner nuclear membrane (INM) and they directly interact with nuclear lamins. Co-immnoprecipitation and GST-pull down experiments showed that Sun-1 had a very high binding affinity for lamin A but not for B-type lamins. Moreover, it was shown that Sun-1 interacted with pre-lamin A, thus suggesting that Sun-1 might be important for the targeting and assembly of newly synthesized lamin A (Crisp et al., 2006; Haque et al., 2006). However, Sun-1 was properly localized on the INM in LmnA-null mouse embryonic fibroblasts (MEFs), suggesting that Sun-1 localization is not entirely dependent on A-type lamins in mammalian cells (Crisp et al., 2006; Haque et al., 2006; Padmakumar et al., 2005). By contrast Sun-2 was partially displaced in the absence of LmnA, even if lamin A and/or lamin C expression were not able to rescue this displacement, thus suggesting that other factors might be involved in Suns localization on the INM (Crisp et al., 2006).

Suns contain a nucleoplasmic N-terminal domain, responsible for the binding with lamin A, followed by a transmembrane domain and a conserved C-terminal luminal domain, called SUN domain, essential for the anchorage of Nesprins on the outer nuclear membrane (ONM) (Crisp et al., 2006; Padmakumar et al., 2005). It has been demonstrated that depletion of Sun-1, and in particular the SUN domain deletion, led to a displacement of Nesprins from the nuclear envelope (Padmakumar et al., 2005).

In addition to Sun-1 and Sun-2, two other proteins, containing a Sun-protein structure, Sun-3 and Spag4, have been identified. While Sun-1 and Sun-2 are widely expressed in a variety of tissues (Wang et al., 2006) cit. in (Ostlund et al., 2009), Sun-3 and Spag4 expression levels and distribution are much more restricted (Stewart-Hutchinson et al., 2008) cit. in (Ostlund et al., 2009).

Although the precise functions of Sun proteins still remain poorly understood, it was demonstrated that Suns are involved in chromatin nuclear positioning, centromere localization and apotosis (Tzur et al., 2006). Furthermore, Sun-1 has been implicated in the formation of synaptic nuclei in muscle cells, thus suggesting a role of this protein in cellular integrity maintenance during development (Lei et al., 2009).

In contrast to Suns, Nesprins functions have been better defined. In fact, deficiency of nesprin proteins has been associated with abnormal size and morphology of keratinocytes and deficiency in migration and cell polarity of fibroblasts from *SYNE2* knock-out mice. Furthermore, mutations and/or polymorphisms in the genes encoding for nesprins have been associated with several human diseases, including recessive cerebellar ataxia and Emery-Dreifuss muscular dystrophy or similar phenotypes (Gros-Louis et al., 2007; Zhang et al., 2007) cit. in (Ostlund et al., 2009).

Nesprins are integral proteins of the ONM, which interact with Suns within the lumen and cytoskeletal components with their N-terminus domain. Nesprins have multiple spectrin repeats in their nucleo-cytoplasmic N-terminal regions, followed by a conserved KASH domain, consisting of a transmembrane segment and approximately 30 lumenal amino acids (Starr and Fischer, 2005) cit. in (Ostlund et al., 2009).

Four different genes, encoding for different nesprin proteins have been identified in mammals: *SYNE1* and *SYNE2* each one encoding different isoforms of varying molecular masses, some being very large including nesprin-2 giant (796 kDa); nesprin-3 and nesprin-4 are lower molecular mass proteins, encoded by two different genes, which bind to plectin and kinesin-1 respectively, but lack the actin-binding domain, which is present in nesprin-1 and nesprin-2 proteins (Wilhelmsen et al., 2005).

As a result of alternative mRNA splicing and, in the case of mouse, of the use of an alternative transcription start site, nesprin-3 gene encodes two different isoforms: nesprin-3α and nesprin-3β. Nesprin-3α consists of eight spectrin repeats, which are absent in nesprin-3β. Furthermore, it has been found that nesprin-3α, but not nesprin-3β is able to bind the actin binding domain of several plectin isoforms including plectin 1A and plectin 1C, establishing therefore the connection between the nucleoskleton and the cytoskeleton (Kelly et al., 2008; Ketema and Sonnenberg, 2011; Wilhelmsen et al., 2005). Depletion of nesprin-3 led to a partial loss of the association of keratin filaments with the nuclear perimeter in epidermal cells (Postel et al., 2011) and alteration in endothelial cell morphology (Morgan et al., 2011) (Figure 11).

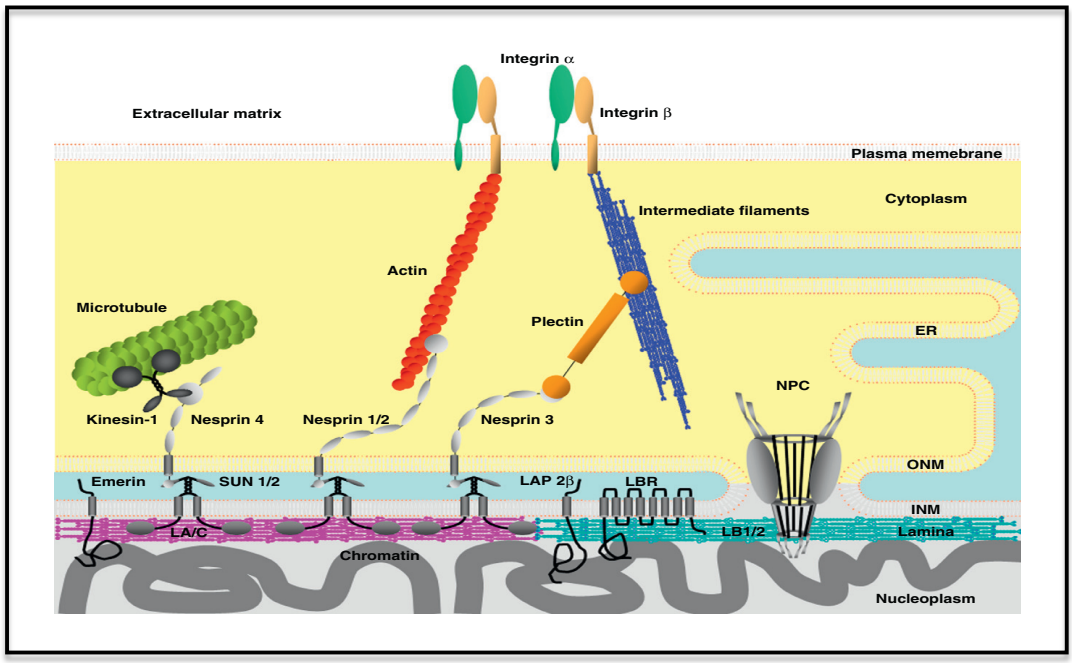

Figure 11: Schematic representation of the cross-talk between the nuclear envelope and cytoskeleton.

The nuclear envelope is characterised by the inner nuclear membrane (INM) and the outer nuclear membrane (ONM). The nuclear lamins A/C contact both the INM and the chromatin. The SUN-1/2, which are integral proteins of the INM, are able to interact with Nesprin proteins, located on the ONM, in the luminal space. These proteins in turn are able to interact with components of the cytoskeleton: Nesprin-4 interacts with microtubules via Kinesin-1 protein, while Nesprin 1/2 interact with actin filaments; Nesprin-3 is able to interact with intermediate filaments through the binding with Plectin. Taken from (Shimi et al., 2011b)

Plectin is a multimodular cytolinker protein with several dozen of interacting partners. It is characterized by two globular multi-interactive end domains separated by an α-helical sequence that dimerizes with another molecule to form a 190 nm-long coiled-coil rod domain.

A special peculiarity about plectin is its isoforms diversity based on the different splicing reactions of over a dozen alternative first exons into a common exon 2 and on different promoters, generating a variety of transcripts that encode different isoforms just varying in short N-terminal sequences (Fuchs et al., 1999; Wiche and Winter, 2011). Because of these differences, plectin isoforms

are able to bind different cellular structures, including hemidesmosomes. It has been found that Plectin is able to associate with hemidesmosomes and cytokeratin filaments in the basal layer of epidermis (Andra et al., 2003), suggesting an important role of the protein in epithelial tissues. Furthermore, plectin deficient mice die 1-3 days after birth, exhibiting severe skin fragility, focal skin barrier defects and growth retardation, although maintaining a normal stratified organization of the epidermis and correct expression patterns of differentiation markers in addition to normal keratinocytes proliferation and survival (Ackerl et al., 2007).

Focal adhesion as well as plectin direct interaction with the nuclear lamina have also been observed (Wiche and Winter, 2011). Plectin interacts with the nuclear lamina acts through the binding to Lamin B1 but not to Lamin A and C (Foisner et al., 1991), possibly as a consequence of the different expression pattern of these lamins during development (Dechat et al., 2008; Rober et al., 1989). According to these studies the binding of plectin to Lamin B1 was possible only after dephosphorylation, while phosphorylation of both binding partners by proteinase A or proteinase C inhibited the binding (Foisner et al., 1991), consistent with the fact that the phosphorylation and dephosphorylation are associated with disassembly and assembly of the nuclear lamina respectively (Dechat et al., 2008).

1.2.5.2. Lamina Associated Domains (LADs) and gene expression regulation at the nuclear lamina

As previously suggested, chromatin is able to contact the nuclear lamina (Wilson and Berk, 2010) and these genomic sites are referred to as lamina-associated domains (LADs). LADs size ranges from 40 kilobases to 15

megabases (Peric-Hupkes et al., 2010) and they are usually poor of genes and most of them lack RNA polymerase II (Pol II) and the histone mark H3K4me2, predominantly present on active genes, suggesting a repressive role of the nuclear lamina in gene transcription regulation (Peric-Hupkes et al., 2010; Zullo et al., 2012).

In support to this theory, recent studies, performed during differentiation of mouse embryonic stem cells (ESCs) via lineage-committed neural precursor cells into terminally differentiated astrocytes (ACs), showed changes in the nuclear lamina-DNA contacts, leading to detachment of repressed genes from the nuclear lamina with subsequently gene activation (Peric-Hupkes et al., 2010). The genes involved in astrocytes differentiation reflect the cell-type lineage, suggesting that the nuclear lamina (NL) may play an important role in transcriptional regulation during differentiation (Peric-Hupkes et al., 2010). Genes that detach from the NL in ESCs are more likely to become activated in ACs in comparison to silent genes with unaltered NL interactions. In contrast, genes with increased NL interactions have a reduce probability to become activated in ACs. All together these data suggest that silent genes that move away from the NL tend to become “unlocked” for expression at a next differentiation step, and, by contrast, silent genes with increased NL interactions tend to become “locked” in their repressed state (Peric-Hupkes et al., 2010). Consistent with these findings, it has been recently shown that nuclear lamins and nuclear lamins-associated proteins, including Lamin B receptor (LBR), are important for the maintenance of peripheral heterochromatin and depletion of both LBR and Lamin A/C caused movement of heterochromatin from the

nuclear periphery to the nuclear interior in all differentiated cell types in new-born mice (Solovei et al., 2013).

NL interactions involve both individual genes, confined to the transcription unit as well as larger regions, that include multiple genes together with the intergenic DNA, that separates these genes (Peric-Hupkes et al., 2010). Different studies, based on the insertion of transgenes into different chromatin environments at the nuclear periphery, have shown that promoter properties as well as genomic environment, such as gene density, gene activity and epigenetic marks also influence NL interactions, contributing to the transcriptional outcome (Geyer et al., 2011).

Recently, it has been reported that LADs contain conserved sequences called lamina associated sequences (LASs), characterized by the occurrence of a GAGA motif (Zullo et al., 2012). According to this model the GAGA motifs are recognized by cKrox, the vertebrate ortholog of the GAGA factor (Matharu et al., 2010) cit. in (Zullo et al., 2012), which interacts with HDAC3 and the INM protein Lap2β. HDAC3 in turn has been proposed to function both as an adaptor for lamina association as well as a transcriptional co-repressor due to its histone de-acetylase activity, creating a transcriptional repressive environment (Zullo et al., 2012).

The role of the nuclear lamina in the repression of transcription has been also observed after lamin B1 knock-down experiments. Previous experiments showed that Lamin B1 knock-down caused an increase in acetylated histone H3, a mark of transcriptionally active euchromatin, as well as an increase in the hyperphosphorylated form of RNA polymerase II, the transcriptional active form of the enzyme (Shimi et al., 2008).

However, a role of the nuclear lamina in the activation of transcription has also been proposed, as demonstrated in experiments performed in yeast. In fact, certain genes located proximal to the nuclear lamina are optimally activated at the periphery, due to the recruitment of transcription factors to these sites (Taddei et al., 2006). The ability of the nuclear lamina to activate and repress genes may in part be due to the interactions with insulator DNA sequences, which are able to protect genes flanked by these sequences from the effects of nearby silencing or activating marks on chromatin (Ishii et al., 2002) cit. in (Schirmer, 2008). This effect is also known as “boundary activity”.

However, whether LADs localization is a cause or consequence of transcription and whether the transcription of LADs is local remain still poorly understood and further studies will be necessary to better understand these mechanisms.

In addition to the nuclear lamina other components such as the components of the nuclear pore, referred to as nuclear pore complex (NPC), contribute to the regulation of gene expression. Several studies in *Drosophila* have demonstrated the presence of specific DNA regions, known as Nucleoporin Associated Regions (NARs), which range in size from 5-kb to 500-kb and constitute a 25% of the whole genome (Vaquerizas et al., 2009). Many of the NARs contain active genes, which are important for development. Furthermore, additional studies in *S.Cerevisiae* have shown the presence of specific sequences, termed “Zip codes”, located in the promoter regions of genes activated by nutrient availability and localized to the nuclear periphery. All these factors together permit the interactions of genes with the nuclear pore proteins (Brickner et al., 2007; Light et al., 2010).

Together with its role in gene expression regulation, the nuclear lamina also plays an important role in DNA replication, as suggested in 3T3 cells, where lamin B1 has been found to be associated with the replication factor proliferating cellular antigen (PCNA) in replication factories during late S phase (Moir et al., 2000). In experiments conducted in *Xaenopus Laevis* eggs, an inhibition of the DNA replication process has been observed after the immunodepletion of the major lamin or the addition of a dominant negative N-terminally deleted mutant lamin (Newport et al., 1990) cit. in (Dechat et al., 2008), suggesting that nuclear lamins play a role in organizing a nucleoplasmic scaffold, necessary for the elongation phase of replication.

1.3. Epigenetic Control of Skin Development and Differentiation

In addition to the transcription factor p63 in epidermal terminal differentiation, different studies identified DNA and chromatin remodelling factors as other key elements in the regulation of epidermal differentiation program.

It has been shown that HDACs play an important role in differentiation and stratification of the epidermis (LeBoeuf et al., 2010). HDACs are able to associate directly with different DNA binding factors or indirectly by incorporation into large multifunctional repressor complexes. They are also able to direct bind and de-acetylate several transcription factors like p53. Several studies have shown a role of histone deacetylation in epidermal development, as HDAC1 and HDAC2 are able to associate with the chromatin remodeler BRG1, which is required for keratinocytes terminal differentiation (Indra et al., 2005; LeBoeuf et al., 2010).

Epidermis specific double knock-out of both HDAC1 and HDAC2 resultes in thin, smooth skin lacking expression of keratin 10, a marker of the suprabasal layer, and loricrin, marker of a terminally differentiated epidermis in embryos. However, no expression of keratin 18, which is usually associated with a simple epithelium, was detected, suggesting that the basal epidermal development is initiated and maintained in the double knock-out embryos, but differentiation and stratification failed (LeBoeuf et al., 2010). The absence of both HDACs caused a marked increase in the expression of ΔNp63 repression targets, like p21 and 14-3-3σ, without affecting p63 expression. Additionally, high levels of acetylated p53 have been observed, causing upregulation of cell-cycle inhibitory genes, accompanied by decreased cell proliferation, which might be

responsible for the defects observed in HDAC1/2 null epidermis (LeBoeuf et al., 2010).

Different studies showed that epidermal specific deletion of Mi-2β, an ATP-dependent chromatin-remodelling enzyme associated with HDAC1 and HDAC2, resulted in a gradual loss of basal epidermal progenitor cells associated with a progressive reduction of suprabasal layer expressing K1, observed from E16.5 to P1. However, the expression of loricrin, was not affected by Mi-2β depletion in the ventral epidermis, suggesting that Mi-2β deletion is mainly related to defects in the ability of epidermal stem cells to renew themselves or to continue to generate their more differentiated progeny (Kashiwagi et al., 2007).

In addition to HDACs and Mi-2β, PcG proteins have been shown to play an important role in epidermal development.

In the epidermis Ezh2 is highly expressed in the basal epidermal layer during skin morphogenesis and its expression is decreased during calcium-induced keratinocytes differentiation in culture. The conditional *K14-Cre/Ezh2fl/fl* knock-out mice, revealed decreased proliferation as well as development of an hyperthickened stratum corneum and pronounced granular layer accompanied by increased expression of markers of terminal differentiation, such as loricrin and filaggrin at E16.5 in embryonic skin (Ezhkova et al., 2009).

These data suggest that PcGs are responsible for the silencing of genes related to differentiation in the basal layer of epidermis, favouring the maintenance of epidermal progenitor cells. Once the differentiation program has started, the down-regulation of polycomb proteins allows the activation of genes related to epidermal differentiation.

Despite the apparent loss of H3K27me3 marks in embryonic basal cells, other skin epithelial cells appeared oblivious to EZH2 loss, displaying what appeared to be a full complement of H3K27me3 marks. Moreover, by birth, this histone mark reappeared in the basal cells (Ezhkova et al., 2009). The incomplete loss of H3K27me3, coupled with the relatively mild defects in tissues lacking EZH2, raises the possibility of redundancy. Indeed, mice targeted for the conditional double *K14-Cre/Ezh1/2* knock-out in the basal epidermal layer, completely lost H3K27me3 modification, showing postnatal phenotypes. They were born alive but they were unable to eat, and died within 24 hours after birth (Ezhkova et al., 2011). However, the skin showed normal morphology and normal expression of epidermal differentiation markers, suggesting that the early post-natal lethality in these mice was most likely attributable to the activity of the K14 promoter in the oral and some other internal stratified epithelia. By contrast, hair follicles morphogenesis was impaired and hair follicles degenerated due to defective proliferation and increased apoptosis in these mice (Ezhkova et al., 2011).

All together these findings underscore functional redundancy between Ezh1 and Ezh2 in controlling skin homeostastis.

In addition to PRC2 components, recent studies discovered an important contribution of PRC1 component Cbx4 in epidermal stem cells maintenance and epidermal development and homeostasis (Luis et al., 2011). The analysis of Cbx4 transcript in human epidermal keratinocytes at different stages of epidermal development, revealed a significant lower level of Cbx4 in differentiated compared to undifferentiated cells. Consistent with this observation, Cbx4 knock-down in human keratinocytes resulted in colonies with

terminally differentiated-like morphology, while Cbx4 overexpression led predominantly to a reduction in number and size of the colonies (Luis et al., 2011). All these results are strictly dependent on Cbx4 alone, as overexpression of other Cbx proteins, like Cbx6, Cbx7 and Cbx8, did not lead to a reduction in number and size of the colonies and Cbx4 chromodomain seemed to be crucial for the regulation of human epidermal stem cells proliferation, as demonstrated by the severe reduction of the size of the colonies after overexpression of inducible chromodomain mutants (Luis et al., 2011). Furthermore, Cbx4 depletion led to an increase of the transcript and protein level of the genes in the Cdkn2a/p16 locus as well as the activity of the senescence-associated β-galactosidase, confirming the already suggested role of PcG proteins in senescence repression (Jacobs et al., 1999a).

In addition to the increased expression of genes within the Cdkn2a/p16 locus, the transcriptome analysis after Cbx4 depletion, revealed an increase in the expression of genes related to epidermal terminal differentiation, suggesting a role of Cbx4 in the maintenance of the stem cell population within the human epidermis by promoting a slow cycling state and by preventing differentiation and senescence. In accordance with this hypothesis the transplantation of human epidermal stem cells, depleted of Cbx4, onto immune-deficient mice, were not able to reconstitute a homeostatic epidermis, as demonstrated by the lack of a human stratified epidermis and by the absence of the expression of human involucrin (Luis et al., 2011).

In contrast to Polycomb proteins, the histone demethylase JMJD3, enzyme capable of demethylating promoters marked by H3K27me3, was showed, in mammalian cells and in live zebrafish, to be important in

antagonizing Polycomb protein complexes mediated gene silencing by modifying chromatin to permit gene transcription (Sen et al., 2008). A decrease in H3K27me3 modification on the promoters of genes involved in terminal differentiation, including *K1* and *S100A8* has been observed upon calcium-induced differentiation (Sen et al., 2008). On the contrary, depletion of JMJD3 blocked induction of these genes. However, no effect was seen in the absence of JMJD3 on the expression of *involucrin* gene, which represents another important marker of epidermis terminal differentiation, suggesting that *involucrin* may be regulated through passive loss of methylation due to reduced SUZ12 binding or due to the action of an unidentified demethylase. Moreover, JMJD3 and SUZ12 protein levels remained constant during calcium-induced differentiation, implying that selective targeting rather than relative expression levels of these proteins was responsible for changes in H3K27me3 on differentiation genes promoters (Sen et al., 2008).

Changes in the position of distinct chromosomes during skin development have also been observed (Marella et al., 2009). In this study, two different chromosomal territories, 18 and 19, have been analysed, because of their different replication and acetylation patterns, as well as, because of different genes density (5.7/Mb and 26.5/Mb respectively). According to this study it has been reported that both chromosome 18 and 19 occupied an overall interior position within the cell nucleus. However, in undifferentiated keratinocytes, chromosome 18 was found in a more peripheral position compared to chromosome 19, while a complete switching of this positioning was detected in the early stage of differentiation, where chromosome 18 was preferentially positioned more internally compared to chromosome 19. This was followed by

another switch in relative positioning in the middle stage of differentiation, as both chromosomes were located in a more internal region of the nucleus. This positioning was maintained throughout later stages of differentiation (Marella et al., 2009). In addition, a close association between the two chromosomes during keratinocytes differentiation has been observed (Marella et al., 2009). In summary these data suggest the important role of the changes in chromosomes positioning during keratinocytes differentiation, in the regulation of transcriptional activity, according to previous studies showing that repressed genes were mostly found in association with the nuclear periphery, while activated genes occupied a more internal position (Boyle et al., 2001). Furthermore, these data suggest an important role of the interchromosomal associations for transcriptional activation of genes during skin development and keratinocytes differentiation by the formation of transcriptional factories where genes from distal genomic regions can assemble to coordinate transcriptional regulation. It is very interesting that the observed changes in the volume of both chromosomes 18 and 19 during keratinocytes differentiation (Marella et al., 2009), are not related to their genes density, suggesting that this process is independent from the type of chromosome as well as from the observed increase in the nuclear volume during keratinocytes differentiation (Elder and Zhao, 2002; Marella et al., 2009).

Different studies showed that the Epidermal Differentiation Complex (EDC) also undergoes changes in its positioning during skin development as well as changes in its methylation status (Elder and Zhao, 2002). As different studies suggested the existence of a strong correlation between the CpG methylation and “closed” chromatin, this finding indicates that chromatin

structural alterations also participate in the control of genes located within the EDC during epidermal development.

In line with all these findings, recent studies uncovered an interesting new correlation between epigenetic regulation within the EDC and p63, master regulator of epidermal development and differentiation, during skin development (Fessing et al., 2011). Co-expression of p63 and the adenine and thymine-rich binding protein Satb1 in the epidermis basal cells of embryonic and post-natal mouse skin has been observed (Fessing et al., 2011). Satb1 is a chromatin organizer, which targets chromatin-remodelling enzymes and transcription factors to specific chromatic regions, establishing region-specific epigenetic patterns, and which plays an important role in tissue-specific gene expression programs (Yasui et al., 2002) cit. in (Fessing et al., 2011). The knock-down of p63 by using siRNA experiments, caused a marked decrease of Satb1 expression. ChIP-qPCR assay as well as luciferase gene reporter assay with ΔNp63 isoform showed direct transcriptional regulation of *Satb1* by p63 (Fessing et al., 2011).

As Satb1 knock-out mice showed several epidermal defects reminescent to those observed in p63-null mice, including significant decrease in epidermal thickness, a thinning of the granular layer as well as a significantly decrease in keratinocytes proliferation, it has been suggested that p63 gene expression program in epidermal keratinocytes might act via Satb1 direct regulation, leading to chromatin remodelling within the EDC locus. In support to this hypothesis, 3D FISH analysis of the conformation of the 5Mbp chromatin domain of mouse chromosome 3, which contains the tissue-specific EDC gene locus in Satb1$^{-/-}$ mice, showed an increase in the distances between *Loricrin*,

gene located in the central part of the locus, and the EDC flanking regions containing the *Ribosomal protein S27* (*Rps27*) and *GA-binding protein subunit beta-1* (*Gabpb2*) genes, suggesting a role of Satb1 in regulating chromatin conformation within the EDC locus (Fessing et al., 2011). In particular it was observed an expansion of the central domain of the EDC as well as an overall expansion in the length of the whole locus was observed in Satb1-deficient epidermal keratinocytes, suggesting that Satb1 compresses the chromatin conformation of the EDC locus, including the regions enriched in genes activated during terminal keratinocytes differentiation (Fessing et al., 2011). Therefore it is possible that this Satb1-mediated compression leads to the formation of dense chromatin loops within the EDC central domain and flanking regions, facilitating the accessibility of protein complexes to target genes as well as interactions between proximal and distal gene regulatory regions. Moreover, based on these results, once Satb1 is induced by p63, it is able to establish its own regulatory network, binding to different targets and controlling the expression of 2,500 genes, including those not epidermal-lineage specific, like cell-cycle controlling genes, based on Satb1 role in promoting cell proliferation in the developing epidermis (Fessing et al., 2011).

In addition to *Satb1*, recent data have demonstrated that p63 is also able to regulate the gene expression of epidermal-specific genes within the EDC via direct regulation of the ATP-dependent chromatin remodeler *Brg1* (Mardaryev et al., 2013). Brg1 is an ATPase part of a chromatin remodelling SWI/SNF complex, able to promote nucleosomes sliding and/or changes in nucleosome conformation using ATP hydrolysis as a source of energy for this process (Eberharter et al., 2004).

Previous studies showed an important role of Brg1 in epidermal stratification and skin barrier formation. In particular, it has been shown that Brg1 absence did not affect keratinocytes proliferation at early embryonic stages (E10-E12.5), but skin barrier formation instead (Indra et al., 2005), suggesting its requirement for epidermal stratification process at later embryonic stages. Consistent with these findings, recent data showed that Brg1 absence led to alterations in the radial position of the EDC as well as in chromatin conformation within the EDC in basal keratinocytes with increased distance between *loricrin* and the EDC flanking regions, containing *Rps27* gene (Mardaryev et al., 2013). While in WT controls the EDC tended to shift from a more peripheral position at early stages of epidermal development (E11.5) to a more internal one at later stages of epidermal development (E16.5), in Brg1-null basal keratinocytes as well as in p63-null keratinocytes, the EDC was mainly found at the nuclear periphery.

All together these findings suggest that EDC repositioning from the nuclear periphery to the nuclear interior at E16.5, together with its association with SC35 positive nuclear speckles and changes in chromatin conformation (Mardaryev et al., 2013), are essential requirements for the proper expression of epidermal-specific genes within the EDC, required for proper epidermal barrier formation and that p63 transcription factor plays an essential role in these processes by regulating the EDC conformation and movements via direct regulation of the chromatin remodelers Satb1 and Brg1.

1.4. Aims of the Study

p63 is one of the major key factors involved in the control of epidermal development and stratification program, through regulation of a subset of genes related to cell proliferation and differentiation (Mills et al., 1999; Truong et al., 2006; Yang et al., 1999). It acts through direct binding to the promoter regions of its target genes as well as through epigenetic regulation of the spatial organization of Epidermal Differentiation Complex via direct regulation of the chromatin remodelers Satb1 and Brg1 (Fessing et al., 2011) (Mardaryev et al., 2013).

Together with epigenetic mechanisms, cellular and nuclear architecture also play an essential role in tissues development, as they are involved in cell proliferation, mechanical stiffness, cell migration and gene expression regulation (Houben et al., 2007).

The aims of this work are:

1) Investigate whether alterations in the nuclear architecture, including alterations in the nuclear shape might contribute to the epidermal defects observed in p63-null mice. For this purpose, basal epidermal keratinocytes of p63 KO mice have been analysed for their nuclear morphology and for the expression of proteins (Lamin A/C, Lamin B1, Sun-1, Nesprin-3, Plectin) involved in the cross-talk between the nucleus and cytoskeleton, which are important for nuclear shape maintenance.

2) Investigate whether alterations in the nuclear shape affect heterochromatin organization and distribution of repressive histone modifications, H3K27me3 and H3K9me3 in p63-null keratinocytes.

3) Analyse the role of polycomb proteins in the execution of p63-dependent developmental program in epidermal keratinocytes by analysing the expression of several PRC1 and PRC2 components in p63-null epidermis and by comparing the epidermal phenotype observed in Cbx4-deficient mice with the one observed p63-null mice.

4) Investigate the role played by keratin type II locus in the organization of the nuclear positioning and in regulating gene expression within the EDC locus in epidermal keratinocytes by using a mouse model where keratin type II locus has been ablated specifically in basal epidermal keratinocytes. For this purpose, 3D FISH experiments have been performed and nuclear positioning have been assessed in the absence of keratin type II locus and compared with the corresponding WT controls.

Chapter 2

Materials and Methods

2. MATHERIALS AND METHODS

1.5. Immuno-fluorescence experiments on p63$^{-/-}$ and WT embryos

Quick frozen embryos samples have been pre-prepared by Dr. Andrei Mardaryev (University of Bradford, United Kingdom) and stored at -80°C. Cryosections of WT, p63-/- and Cbx4-/- embryos were cut (thickness 10 μm) using a cryostat (Microm HM550, Thermo Scientific) at a temperature of -22°C.

Slides with cryosections were left drying for 10 minutes at Room Temperature (RT) and fixed 15 minutes in 4% Paraformaldehyde diluted in 1X Phosphate Saline Buffer (PBS) at RT. The fixation process helps preserving the mechanical characteristics of the tissue, preventing the osmotic shock and maintaining the chemical reactivity as well as the antigenic characteristics of the molecules in the tissue. In addition the fixative is able to create strong bindings between several cellular components and make the tissue able to resist to strong chemical and physical treatments (e.g. high temperatures and microwave), which may have dangerous effects on fresh tissues.

Slides were then washed 5 minutes at RT with 1X PBS/0.05% Triton X-100. The process was repeated three times. Triton X-100 is a detergent able to permeabilize the cellular and nuclear membranes, increasing antibodies penetration.

Slides were then blocked with 5% Albumin Bovine Serum (BSA) 1 hour at RT, which is able to block non-specific protein-protein interactions reducing staining background. Alternatively, 10% goat normal serum or donkey normal serum, depending on the species where the secondary antibody has been raised, were used as blocking solution.

After the blocking step, primary antibodies (Table 1), diluted in 1xPBS/0.5%BSA/0.01% Tritons X-100, were applied and sections were incubated over-night at 4 °C.

The next day, slides were washed in 1X PBS. Secondary antibodies were diluted 1:200 in 1%BSA/PBS or 1% Donkey Normal Serum/PBS. Slides were then incubated 1 hour at 37°C.

After the incubation slides were washed 3X5 minutes with 1X PBS at RT. At the end the VECTASHIELD Hard Set Mounting Medium with 4',6-diamidino-2-phenylindole (DAPI, blue nuclear counter stain) (Vector Laboratories Inc., Burlingame, CA, USA) was applied on the slides, subsequently covered with 22X22 cm, 0.17mm thick coverslips and sealed with nail polish. The Mounting Medium is able to protect and preserve the fluorescence signal over time.

Primary antibody	Dilution	Secondary antibody
goat polyclonal Anti-LaminB1	1:500	Donkey anti-goat-Alexa 488 (Invitrogen)
Goat polyclonal Anti- Plectin	1:100	Donkey anti-goat-Cy3 (Invitrogen)
Rat polyclonal Anti-CD104 (BD Biosciences)	1:100	Goat anti-rat-Alexa 488 (Invitrogen)
Rabbit polyclonal Anti- Lamin A/C (Santa-Cruz Biotechnology)	1:200	Goat anti-rabbit- Alexa 488 (Invitrogen)
Rabbit polyclonal Anti-Ezh2 (Abcam)	1:100	Donkey anti-rabbit-Cy3 (Invitrogen)
Rabbit polyclonal Anti-H3K27me3 (Abcam)	1:100	Donkey anti-rabbit-Alexa 488 (Invitrogen)
Rabbit polyclonal Anti-H3K9me3 (Abcam)	1:100	Donkey anti-rabbit-Cy3 (Invitrogen)
Rabbit polyclonal Anti-Sun1 (Santa-Cruz Biotechnologies)	1:100	Donkey anti-rabbit-Alexa 488 (Invitrogen)
Rabbit polyclonal Anti-Hp1α (Abcam)	1:100	Donkey anti-rabbit-Alexa 488 (Invitrogen)
Rabbit polyclonal Anti-Nesprin-3 (Santa-Cruz Biotechnologies)	1:100	Donkey anti-rabbit-Cy3 (Invitrogen)
Rabbit polyclonal Anti-Caspase-3 (Abcam)	1:100	Donkey anti-rabbit-Cy3 (Invitrogen)
Rabbit polyclonal Anti-Ki67 (Abcam)	1:100	Donkey anti-rabbit-Cy3 (Invitrogen)
Rabbit Polyclonal Anti-H2AK119ub (Active Motif)	1:100	Donkey anti-rabbit-Cy3 (Invitrogen)
Rabbit polyclonal Anti-Ring1B (Active Motif)	1:100	Donkey anti-rabbit-Alexa 488 (Invitrogen)
Mouse monoclonal Anti-Bmi-1 (BD Biosciences)	1:100	Goat anti mouse-Cy3 (Invitrogen)
Rabbit polyclonal Anti-Cbx4 (Abcam)	1:100	Donkey anti-rabbit-Cy3 (Invitrogen)
Rabbit polyclonal anti-Nefl1	1:100	Donkey anti-rabbit-Cy3 (Invitrogen

Table 1: List of Primary and secondary antibodies used for immuno-fluorescence experiments with the corresponding dilutions.

1.5.1. Fluorescence Microscopy

In conventional fluorescence microscopy the sample is illuminated by a light source of an appropriate wavelength and an image is formed from the resulting fluorescent light. The fluorescence is a characteristic of some molecules, known as fluorophores, which are able to absorb the light at one specific wavelength and then emit light of a different wavelength. At ordinary temperatures most molecules are in their lowest energy state, the ground state (Semwogerere D. and Weeks E.R., 2005). However, they may absorb a photon of light, increasing their energy, causing the jump of an electron to a discrete singlet excited state (Guibault., 1990). The molecule usually dissipates some of the absorbed energy through collision with surrounding molecules, causing a light emission of a longer wavelength. The wavelength of the excitation light and the colour of the emitted light are material dependent.

The fluorescence microscope uses a dichroic mirror, which is able to reflect light of shorter wavelength and transmits light of longer wavelength. By consequence, the light source is reflected by the mirror and passes through the objective and then direct to the sample, while the longer wavelength light, which comes from the sample, passes through both the objective and the dichroic mirror (Semwogerere D. and Weeks E.R., 2005) (Figure 12).

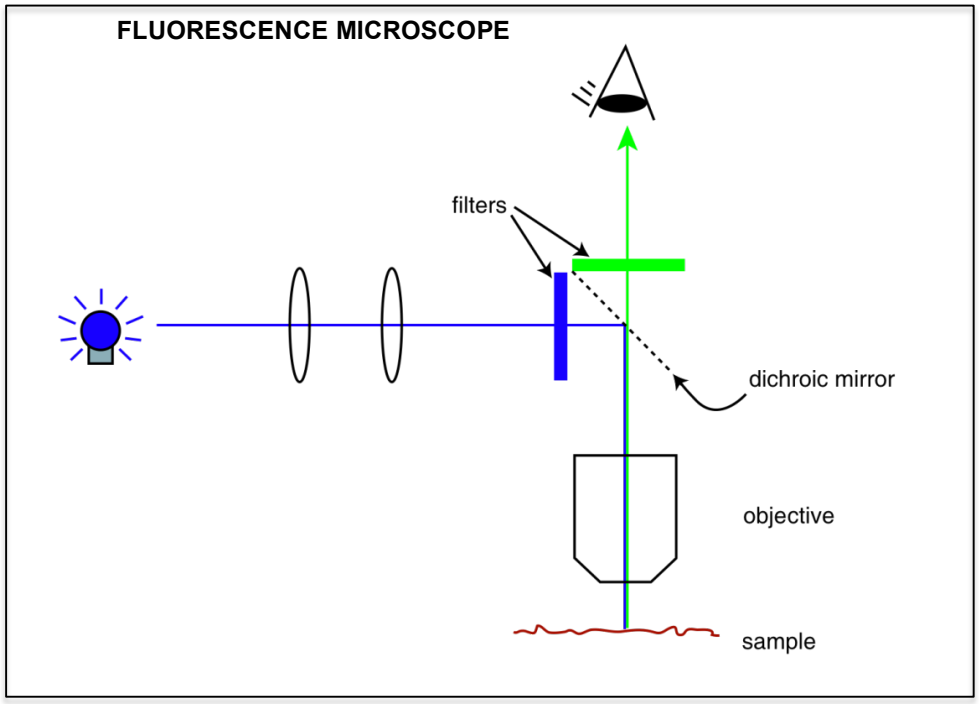

Figure 12: Schematic illustration of the working mechanism of the fluorescence microscope

Working mechanism of the fluorescence microscope: the dichroic mirror is able to reflect the light source of lower wavelength (blu light) directly to the sample, while the light of higher wavelength (green light) coming from the fluorescent sample passes through the dichroic mirror Modified from (Semwogerere D. and Weeks E.R., 2005).

1.5.1.1. Image processing

Microscope slides were analyzed using a Fluorescence Microscope *Eclipse 50i* (Nikon) and images were recorded in separate channels responding to their respective flurophores.

Three different fluorophores with emission peaks far enough to be distinguished from each other and excited efficiently with available filters, were used: 4',6-diamidino-2-phenylindole (DAPI, blue nuclear counter stain), Fluorescein isothiocyanate (FITC, green) and Indocarbocyanine (Cy3, red).

Images were acquired using 40X/0.75 plan fluor objective and were processed with the *ImagePro Express 6.3* software.

1.5.2. Confocal Microscopy

The Confocal microscopy was firstly performed by Marvin Minsky in 1995. His invention was to use a point-by-point image construction by focusing a point of light sequentially across a specimen and then collecting some of the returning light. By consequence most of the unwanted scattered light, that obscures the image when the entire specimen is illuminated at the same time, as in the conventional fluorescence microscopy, was avoided. Furthermore, a second pinhole aperture, which would reject rays that were not directly from the focal point, was added. Consequently only few “desiderable” rays would then be collected by a photomultiplier. The detector is connected to a computer, which built up the image one pixel at a time. The image created by the confocal microscope is of a thin planar region of the specimen referred to as *optical sectioning*.

The creation of a point-by-point image increased the time needed. The solution was to use a light source of very high intensity and in the modern confocal microscopes a laser light source is used, which has the additional benefit to provide a wide range of wavelengths. The laser provides the intense excitation light at a particular wavelength. The light reflects off a dichroic mirror, to an assembly of vertically and horizontally scanning mirrors. These motor-driven mirrors scan the laser across the specimen (Semwogerere D. and Weeks E.R., 2005) (Figure 13).

As a consequence of the presence of these scanning mirrors, the confocal microscope is able to build up a three-dimensional (3D) reconstructions of a volume of specimen by assembling a series of thin slices taken along the vertical axis.

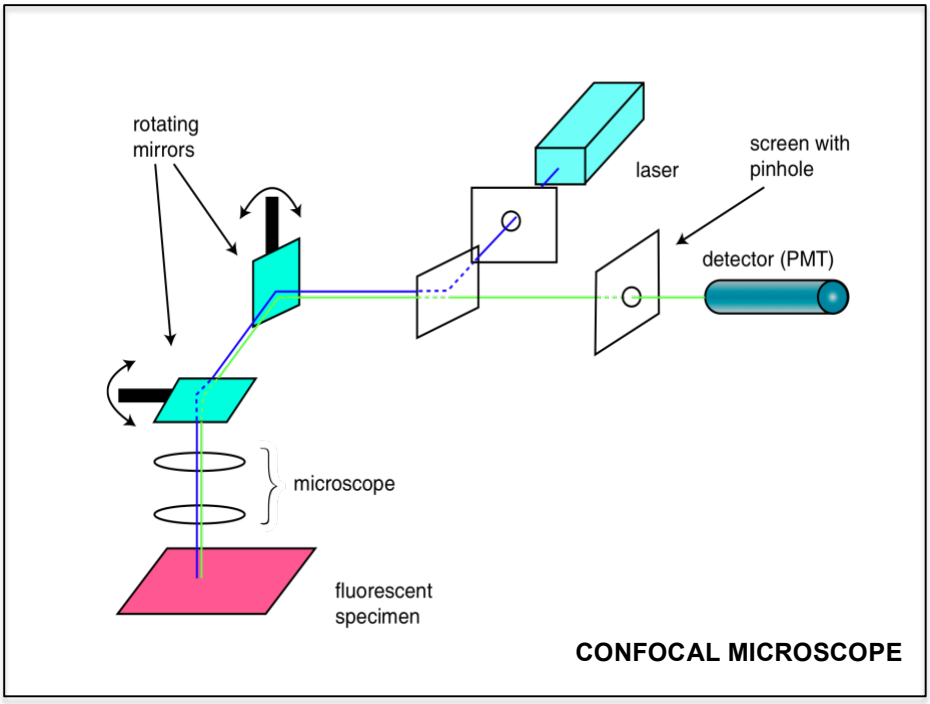

Figure 13: Schematic illustration of the working mechanism of the confocal microscope

Light from the laser is scanned across the specimen by the scanning mirrors. Optical sectioning occurs as the light passes through a pinhole on its way to the detector.

1.5.2.1. Image processing

Microscope slides were scanned using confocal laser scanning microscope *LSM 510 Meta* (Carl Zeiss) equipped with UV laser (Enterprise, emitting light of 351nm, 364 nm wavelengths) and VIS lasers: Argon (458 nm, 477 nm, 488 nm, 514 nm), HeNe1 (543 nm) and HeNe2 (633nm). Z-Stacks of confocal images of voxel size of 100nm x 100 nm x 200 nm were acquired with a 63x/1.4 plan-apochromat oil objective.

Three different fluorophores with emission peaks far enough to be distinguished from each other and excited efficiently with available lasers were used for labelling: 4',6-diamidino-2-phenylindole (DAPI, blue nuclear counter stain), Fluorescein isothiocyanate (FITC, green) and Indocarbocyanine (Cy3,

red).

Images were recorded in separate channels corresponding to respective flurophores (filter settings; (Hernandez-Munoz, Taghavi et al. 2005).

1.5.2.2. Analysis of the nuclear shape in p63-/- and WT mice

Images were analysed using the ImageJ software. In total 135 nuclei for the WT and 123 nuclei for $p63^{-/-}$ embryos were counted. Only basal keratinocytes were analyzed and to do so the CD104 (also known as β4 integrin) marker was used. This protein is normally expressed on the cell surface of basal keratinocytes and it is very important for cell attachment to the basement membrane.

Alterations in the nuclear morphology have been calculated using ImageJ plugin "circularity" (circularity = 4pi(area/perimeter^2)) after selection of the nucleus of interest. Only nuclei with a circularity value <0.80 have been considered abnormal and used for further analyses.

Data were then exported in Excel and percentages were calculated and statistically analysed.

1.5.2.3. Statistical analysis

As the aim of this part of study was not only to analyze the nuclear shape but also to compare these results between the WT sample and the $p63^{-/-}$ sample, statistical analysis by means of Chi-square test (X_2) of "r x k contingency tables'' sets was performed.

"r x k contingency table" contains specifically ordered data where "r"stands for raw data record consisting of the nuclear shape, which was divided into "normal nuclear shape" and "altered nuclear shape", and "k" means column, represented the two groups, WT and $p63^{-/-}$embryos, which were analysed in this

study.

Null hypothesis (H0) on equality of each pair of data sets (data of the nuclear shape in one particular sample) were tested separately assuming probability of wrongly rejection of the H0 (Type I error) below 0.05.

The Chi square test (X^2) was calculated using the following formula:

$$X^2 = \sum \frac{(O - E)^2}{E}$$

X^2-chi-square statistic
O – observed frequency
E- expected frequency

Values of the expected frequency were derived each time from the "r x k contingency" tables:

$$E = \frac{(Raw\ total) * (Column\ total)}{Grand\ Total}$$

E- expected frequency

Finally, values of Chi-square statistic were compared with the critical

values for the Chi-square test with 1 degrees of freedom (df) and the level of significance α=0.05.

$$df= (r-1)(k-1)$$

df- degrees of freedom
r - raw
k - column

1.5.2.4. Analysis of H3K27me3 and H3K9me3 distribution

40±5 basal keratinocytes nuclei have been considered for this analysis in both WT and p63-/- embryos and each single nucleus has been analysed for the distribution of the fluorescence signal using imageJ plugin “plot profile”, which measures the distribution of fluorescence in each separate channel and provides a graph and values of the fluorescence intensity along a line defined by the user.

For this analysis, the nuclear geometric centre has been calculated by collecting in imageJ few hundreds random coordinates throughout the nuclear surface depicted by DAPI staining and by averaging them.

Next, eight single lines starting from the nuclear geometric centre to the nuclear border have been drawn on the entire nuclear surface and values of fluorescence intensity in each channel (DAPI, FITC/Cy3) have been collected in imageJ and exported in Excel.

Each line has been subsequently divided into four different shells and values in each shell have been averaged and normalized to the mean percentage of DAPI signal in that shell.

1.6. p63 knock-down in Primary Mouse Keratinocytes using small interfering RNAs

1.6.1. Primary mouse keratinocytes isolation and culture

New-born mice have been sacrificed and washed twice in sterile PBS. Next, sterilization process was performed in a 50 ml Falcon tube (Falcon) by rinsing mice twice in 70% Ethanol for few minutes. Mice were rinsed once in PBS and kept in PBS on ice until processed.

Skin removal has been performed in a sterile environment and one by one the carcasses were placed on a sterile 60 mm culture dish with few drops of PBS to not let the skin dry.

First, tail, genitals and limbs have been carefully removed and, using a sterile scalpel, a longitudinal incision from tail to snout has been perfomed and, using sterile curved forceps, the skin has been carefully peeled off from the carcass and placed dermis facing down on a new sterile 100 mm culture dish. Next, 0.25% Trypsin (Life Technologies, Carlsbad, CA, USA) was added to the culture dish containing the skin, making sure to not cover the epidermis. Skin has been then incubated overnight at $4^{o}C$.

The next day, each skin was transferred to a new dry sterile culture dish with the epidermis facing down and, using sterile forceps, the dermis was pulled off from the epidermis and discarded. The epidermis was placed in a new sterile Falcon tube (Falcon) containing primary mouse keratinocytes growth medium: EMEM Ca^{++} free supplemented with 4% chelated FBS (Life Technologies,

Carlsbad, CA, USA), 0.05 mM $CaCl_2$, 0.4 ug/ml hydrocortisone (Sigma-Aldrich), 5 ug/ml insulin (Sigma-Aldrich), 10 ng/ml epidermal growth factor (EGF) (Life Technologies, Carlsbad, CA, USA), 10^{-10} M cholera toxin (ICN), $2x10^{-9}$ M T3 (Sigma-Aldrich), 100 units/ml penicillin and 100µg/ml streptomycin (Life Technologies, Carlsbad, CA, USA), 2 mM L-Glutamine (Life Technologies, Carlsbad, CA, USA).

After pipetting up and down for 5-10 minutes to release keratinocytes from the epidermis, the suspension has been passed through a sterile 70 um nylon filter (Becton Dickinson) into a fresh 50 ml Falcon tube.

For RNA interfering experiments one skin/6-wells plate previously coated with collagen has been used.

To coat plates with collagen, a stock solution containing 3 mg/ml of Vitrogen, HBSS, 5% BSA, 1M HEPES, has been prepared and 1 ml has been added into the first well making sure to cover the entire surface for 30-60 seconds before being aspirated and added to the second well. Once all the wells have been properly coated with collagen, the plate has been left drying for at least 30 minutes up to overnight in a sterile environment.

1.6.2. PMKs transfection with p63 siRNA and control siRNA

PMKs have been plated on a previously collagen-coated coverslips in a 6-well plate and left growing at 33°C with 8% CO_2 until they reached 80% confluence. Medium has been changed every day.

Transfection with p63 siRNA and control siRNA at 50 nM and 100 nM final concentration with Lipofectamine RNAiMax (Life Technologies, Carlsbad, CA, USA) was performed and the complex siRNAs-Lipofectamine was added to each well and PMKs have been incubated at 33°C and 8% CO_2 for 6-8 hours.

The DNA-containing liposomes (with positive charge on their surfaces) can fuse with the negatively charged plasma membrane of living cells, due to the neutral co-lipid mediating fusion of the liposome with the cell membrane, allowing nucleic acid to cross into the cytoplasm and contents to be available to the cell.

After 6-8 hours incubation fresh complete EMEM medium containing 4% FBS and antibiotics was added to each well and cells have been incubated for additional 24-48 hours.

At the end of the incubation period, cells were gently washed twice with sterile PBS and coverslips with PMKs were placed on microscope slides and fixed in 4% Paraformaldehyde. The immuno-fluorescence with Lamin B1 and Lamin A/C-specific antibodies was perfomed according to ***Paragraph 2.1***. Alternatively, PMKs were washed twice with sterile PBS and detached from the well surface using a scraper and TRI Reagent (Ambion, Life Technologies, Carlsbad, CA, USA) and processed for RNA isolation (see ***Paragraph 2.3.1***).

1.7. Relative expression of nuclear envelope proteins in p63$^{-/-}$ and WT embryos

1.7.1. RNA Extraction and Reverse Transcription

Quick frozen cryosections (approximately 50 per each sample) for WT, p63$^{-/-}$ and Cbx4$^{-/-}$ embryos were cut (thickness 10 μm) using a cryostat (Microm HM550, Thermo Scientific) and collected in 1.5 ml eppendorf tubes with 1 ml of TRI Reagent Solution (Ambion, Life Technologies, Carlsbad, CA, USA).

TRI Reagent solution works by maintaining RNA integrity during tissue homogenization, while at the same time disrupting and breaking down cells and cell components.

RNA extraction was performed according to the manufacturer's protocol (TRI Reagent Solution, Applied Biosystems, Life Technologies, Carlsbad, CA, USA). In brief, tissues were homogenized, using standard homogenization procedures, and left 5 minutes at RT. Samples were centrifuged at 12,000 x g for 10 minutes and the supernatant transferred to a fresh tube; 100 μl of 1-Bromo 3-chloropropane (BCP) per 1 ml TRI Reagent Solution were added to the samples, allowing the separation of RNA/DNA from proteins and other organic components. Samples were then mixed vigorously and incubated 15 minutes at RT.

Samples were centrifuged at 12,000 x g for 15 minutes at 4°C (centrifugation at temperatures >8°C may cause some DNA partition in the aqueous phase) and the aqueous phase, containing the RNA, was transferred to a fresh tube, where 500 μl of isopropanol per 1 ml of TRI Reagent Solution were added to precipitate RNA. Samples were vortexed for 5-10 seconds and incubated at RT for 10 minutes.

Next, samples were centrifuged at 12,000 x g for 8 minutes at 4-25°C and the supernatant was discarded. Subsequently, the pellet was washed in 1 ml of cold 75% Ethanol and centrifuged 5 minutes at 7,500 x g at 4-25°C.

The supernatant was discarded and left few minutes at RT to dry. At the end the RNA pellet was resuspended in TE Buffer (10 mM Tris HCl pH 7.6; 1 mM EDTA pH 8.0). The final volume of TE Buffer was chosen based on the pellet size.

The RNA concentration was measured using the Spectrophotometer (SmartSpec Plus, Bio-Rad) at 260 nm wavelength and a conversion factor of 40 μg/m; RNA purity was checked using the ratio 260/280nm.

10 μg of RNA were used for DNase treatment, which was performed according to the manufacturer's protocol TURBO DNA-free Kit (Applied Biosystems, Life Technologies, Carlsbad, CA, USA). In brief, for 10 μg of RNA, 1 μl of TURBO DNase (2U) was used in 50 μl final reaction volume and samples were incubated 30 minutes at 37°C. The enzyme was then inactivated using 5 μl of DNase Inactivation Reagent and samples were incubated 5 minutes at RT with occasionally mixing.

Samples were then centrifuged at 10,000 xg for 1.5 minutes and the RNA was transferred to a fresh tube. 1 μg of RNA DNase treated was used for reverse transcription reaction.

The reverse transcription reaction was performed using Random Primers according to the manufacturer's protocol (Reverse Transcription System, Promega, CA, USA) and the PCR program was run as follows: RNA denaturation at 70°C for 10 minutes, followed by annealing of Random Primers

at 25°C for 10 minutes. The elongation step was performed at 42°C for 30 minutes followed by additional 10 minutes at 95°C for enzyme inactivation.

1.7.2. qRT-PCR for nuclear lamins and nuclear envelope-associated components

qRT-PCR reaction was performed using the StepOne Plus Real-Time PCR System (Applied Biosystems, Life Technologies, Carlsbad, CA, USA). 0.5 μM primers (Sigma-Aldrich) for *Lamin B1, Plectin, Lamin A/C, Nesprin-3, Sun-1*, (see **Table 2** for primers sequences) were used to amplify 50ng cDNA using Syber Green master mix (Applied Biosystems, Life Technologies, Carlsbad, CA, USA) in 10 μl of final reaction volume. Each PCR reaction was run in duplicate and *Gapdh* gene was used as normalizer.

Primers were designed using the *Beacon Designer Software 7* (see ***Paragraph 3.2.2.1***) and the specific annealing temperature for each pair primers was chosen after prior optimization at four different temperatures (57°C, 59°C, 61°C, 63°C)(see Table 2 for primers sequence, PCR programs and annealing temperatures for each pair-primer).

Gene Symbol	Accession number	Oligo Sequence	PCR program
Lmnb1	**NM_010721.2**	GAGGAGGAGGAGGAG CAAGTTCACATAATGCCACAG	95°C 20 sec 95°C 3 sec 61°C 30 sec x 40 cycles
Plec	**NM_201389.2**	CGCCATTACCAGCAGTTAC GCACAGTCCGAGTCTCAC	95°C 20 sec 95°C 3 sec 62°C 30 sec x 40 cycles
LmnA	**NM_001002011.3**	CCACTCATCCCAGTCTCAG CTTCCTCTACCGCCACAC	95°C 20 sec 95°C 3 sec 61°C 30 sec x 40 cycles
Syne3	**NM_001042699.1**	AGACAGCCACAGAGGATG TTCTTCAGTTGAGTTTGTAACC	95°C 20 sec 95°C 3 sec 61°C 30 sec x 40 cycles
Sun1	**NM_001256115.1**	TACTCGTCGGATGCTCTG CCTGCTGGTGCTAATGTG	95°C 20 sec 95°C 3 sec 61°C 30 sec x 40 cycles

Table 2: List of primers used in the qRT-PCR reactions with the corresponding PCR programs and annealing temperatures.

The PCR program was then followed by a metling curve stage, which included one cycle of 95°C for 15 seconds, followed by gradual increase from 65°C to 90°C.SYBR Green normally detects any double stranded DNA including primers dimers, contaminating DNA, and PCR products from misannealed primers. Consequently, the melting curve is essential as it gives indication if the desired amplicon was specifically amplified.

1.7.3. qRT-PCR for Polycomb Complexes components

qRT-PCR reaction was performed as described in ***paragraph 2.3.2*** using primers for *Ezh2, Ring 1B, Cbx4, Cbx6, Cbx7, Cbx8, Pcgf1, Phc1* (see Table 3 for primers sequences, PCR programs and annealing temperatures).

Gene Symbol	Accession number	Oligo Sequence	PCR program
Ezh2	**NM_007971.2**	TGATGATGATGATGACGATGATGG TCCGAGGTGGGCAAGTTTC	95°C 20 sec 95°C 3 sec 61°C 30 sec x 40 cycles
Rnf2	**NM_011277.2**	TGTGCAGACAAATGGAACTC TCTTTGTTGCCACTTCTAAGG	95°C 20 sec 95°C 3 sec 63°C 30 sec x 40 cycles
Cbx4	**NM_007625.2**	AGTGGAGTATCTGGTGAAATGGA TCCTGCCTTTCCCTGTTCTG	95°C 20 sec 95°C 3 sec 63°C 30 sec x 40 cycles
Cbx6	**NM_028763.3**	CGATCAAGTACAGCATTGG GACAGAGAAATGCACATCAC	95°C 20 sec 95°C 3 sec 61°C 30 sec x 40 cycles
Cbx7	**NM_144811.3**	CTACGAGGAGAAGGAGGAGAF CACGGTAACTTCACTTGAGG	95°C 20 sec 95°C 3 sec 63°C 30 sec x 40 cycles
Cbx8	**NM_013926.1**	ATCTCGTGAAATGGAAGGGC CTTGAGAAGGAAGGTTTTAGGC	95°C 20 sec 95°C 3 sec 63°C 30 sec x 40 cycles
Pcgf1	**NM_197992.1**	GCAACATCAAGATCCAC CGTTTCTCTTCACTGTCTTTGC	95°C 20 sec 95°C 3 sec 63°C 30 sec x 40 cycles
Phc1	**NM_001042623.2**	CTCACGCACATCATTGA TCTTCTCTAACTCTACAGAGGG	95°C 20 sec 95°C 3 sec 63°C 30 sec x 40 cycles

Table 3: List of primers used in the qRT-PCR reactions with the corresponding PCR programs and annealing temperatures.

1.7.4. qRT PCR analysis for neural genes

qRT-PCR reaction was performed as described in ***paragraph 2.3.2*** using primers for *Nefl-1, Nrn-1 and Scn3b* (see Table 4 for primers sequences, PCR programs and annealing temperatures).

Gene Symbol	Accession number	Oligo Sequence	PCR program
Nefl	**NM_010910.1**	CGCCATGCAGGACACAATCA GAGTAGCCGCTGGTTATGCT	95°C 20 sec 95°C 3 sec 61°C 30 sec x 40 cycles
Nrn-1	**NM_153529.2**	CGGTGCAAATAGCTTACCTG GTTTATCCCACATATCTTTCGC	95°C 20 sec 95°C 3 sec 63°C 30 sec x 40 cycles
Scn3b	**NM_001083917.1**	TGAAGACCACAAGACTAATAACC GTAGTCAGACGCATTTTCCTG	95°C 20 sec 95°C 3 sec 63°C 30 sec x 40 cycles

Table 4: List of primers used in the qRT-PCR reactions with the corresponding PCR programs and annealing temperatures.

1.7.4.1. Primer design

Primers were designed using the *Beacon Designer Software*. A search for the mRNA sequence for each gene was performed on NCBI website and the sequence was then opened with the *Beacon Designer Software*. Firstly, each sequence was scanned for the presence of template structures, avoided in the following primers design, and the best pair primers for each sequence was chosen.

Several parameters were considered in the choice of the best pair primers, including GC content, melting temperature, primers length and PCR product length as well as the formation of cross-dimers between primers and secondary structures (short hairpin, self dimers). Ideally, primers should have a GC content of 50%, a melting temperature between 58-65°C, a length between 18-24 nucleotides and the final PCR product should have an ideal size of 100-200 bp. Additionally ideal primers should not form cross-dimers or secondary structures.

Finally, an *in silico PCR* was performed to check primers specificity with the sequence of interest (**www.premierbiosoft.com**).

1.7.4.2. qRT-PCR data analysis

The data were exported in *Excel* and analysed according to the ΔΔCt method. Firstly, C_t values of each sample replicates were normalized using *Gapdh* as reference gene:

$$\Delta \mathbf{C_t}\ \textbf{[normalized samples]} = (C_t\,[\text{target}] - C_t\,[\textit{Gapdh}])$$

ΔCt values have been averaged and ΔΔCt has then been calculated:

$$\Delta\Delta \mathbf{C_t} = (\Delta C_t\,[\text{target sample}] - \Delta C_t\,[\text{control}])$$

Next, the linear conversion of the normalized samples ΔΔCt was calculated ($2^{(-_{\Delta\Delta}Ct)}$) and standard deviation and Standard Error (SEM), were then calculated.

1.8. Laser Capture Microdissection (LCM) and RNA amplification

1.8.1. Sample preparation and processing

Quick frozen cryosections of E16.5 WT and E 16.5 p63-/- embryos or E18.5 WT and E18.5 Cbx4-/- embryos were cut (thickness 8 μm) with the cryostat (Microm HM550, Thermo Scientific) and placed on the RNase free membrane of an alluminium slide (Molecular Machines and Industries) and stored at -80^{o}C or on dry ice until processed.

The staining procedure of samples was performed using the Arcturus LCM staining kit (Applied Biosystems, Life Technologies, Carlsbad, CA, USA) according to the manufacturer's protocol. In brief, slides were thawed for no more than 30 seconds and placed in a plastic jar containing 75% ethanol for 30 seconds; slides were then placed in another plastic jar and rinsed in distilled water for 30 seconds. Using an RNase-free pipette, the tissue sections were stained with the HistoGene Staining Solution (Arcturus LCM staining kit, Applied Biosystems, Life Technologies, Carlsbad, CA, USA) for 20 seconds and then rinsed in distilled water for 30 seconds. HistoGene staining solution is a fast penetrating stain which provides good contrast by differential staining of nuclei (purple) and cytoplasm (light pink). By minimizing the exposure of tissues to water where nucleases may be activated, the Histogene process helps to preserve RNA integrity that may be otherwise compromised when using longer staining protocols.

Next, slides were dehydrated by incubating them in several different alcohol graded solutions (75%, 95% and 100% ethanol) for 30 seconds each, followed by a final incubation in xylene solution for 5 minutes.

Slides were left drying for few minutes before proceeding with the laser capture microdissection procedure.

For the microdissection procedure a laser dissection microscope *Nikon TR2000* was used and the epidermis was cut off from the embryo and collected on a thermoplastic film covering a cap of 0.5 ml tube.

An area of interest (epidermis) was identified under the microscope and a cutting line was drawn using the software (name). A laser beam by passing through a cap of a 0.5ml tube and by following the line, was able to cut off the outlined cells allowing them to adhere to the cap.

1.8.2. RNA isolation and amplification

For RNA isolation after laser capture microdissection, using ReliaPrep RNA Cell Miniprep System (Promega, CA, USA) was used and RNA was isolated according to the manufacturer's protocol. In brief, cells were lysed and RNA was precipitated with 100% isopropanol. The cell lysate was then collected in a ReliaPrep minicolumn (Promega, CA, USA), centrifuged for 30 seconds at RT and the flow-through was discarded. This step was followed by one washing with RNA Wash Solution and by DNase I (Promega, CA, USA) treatment. After 15 minutes incubation at RT with DNase I, the column was washed with Column Wash Solution and centrifuged at maximum speed for 30 seconds. After a final washing in RNA Wash Solution, RNA was eluted with 12 µl of RNase free water.

RNA amplification was performed according to the Arcturus RiboAmp HS Plus RNA Amplification kit's protocol (Applied Biosystems, Life Technologies, Carlsbad, CA, USA). In brief, in the first step the first cDNA strand was synthesized with the incorporation of a T7 promoter sequence, followed by the

synthesis of a second strand of cDNA using exogenous primers. cDNA has been purified using specifically designed MiraCol purification columns (Applied Biosystems, Life Technologies, Carlsbad, CA, USA). The purified cDNA was then used for the *in vitro* transcription reaction, which utilized the T7 RNA polymerase to generate antisense RNA (aRNA). aRNA was then purified with MiraCol columns (Applied Biosystems, Life Technologies, Carlsbad, CA, USA). This process was repeated twice (2 rounds of amplification). The RNA concentration was measured with the spectrophotometer (SmartSpec Plus, Bio-Rad) at a wavelength of 260 nm and a conversion factor of 40 µg/ml (Figure 14). The final RNA product was then used for reverse transcription (see ***Paragraph 2.3.1***).

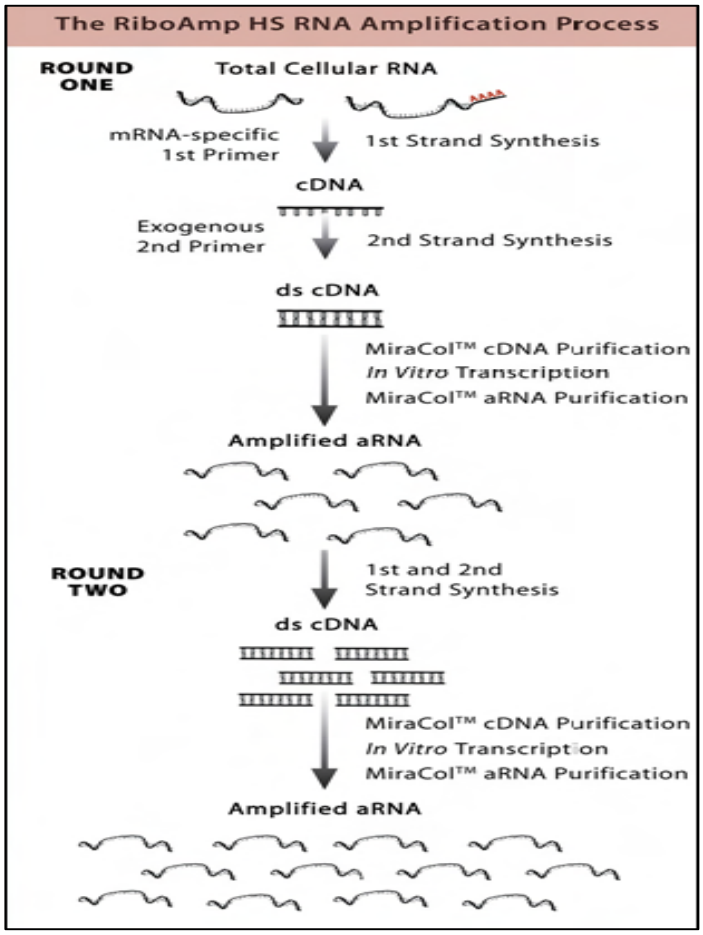

Figure 14: Overview of the RiboAmp HS Plus RNA kit amplification process (Applied Biosystems).

1.9. Chromatin Immunoprecipitation Assay (ChIP)

Chromatin Immunoprecipitation assay is a type of immuno-precipitation experimental technique used to investigate the interaction between proteins and DNA within cells. It aims to determine whether specific proteins are associated with specific genomic regions, such as transcription factors on promoters or other DNA binding sites. ChIP also aims to determine specific locations in the genome that are associated with various histone modifications and histone modifiers.

Chromatin Immunoprecipitation assay includes different steps: cell lysis, fixation, sonication, immuno-precipitation, de-crosslinking, DNA purification and precipitation. The data analysis can be performed using different approaches like PCR, qPCR, Microarrays or DNA sequencing (Figure 15**a**).

Firstly, $5X10^6$ adult primary mouse keratinocytes were fixed in 1% Formaldehyde, to favour the cross-linking of proteins to their binding sequences, for 15 minutes at RT. Next, they were resuspended in *Lysis Buffer* (2.5% Glycerol; 50mM HEPES pH 8.0; 140mM NaCl; 0.5% IGEPAL; 0.25% Triton X-100; 1X Proteinase Inhibitors cocktail; 1mM EDTA pH 8.0) and centrifuged at 2,000 rpm for 8 minutes at 4°C. Supernatant was then discarded and cells were resuspended in *Buffer A* (10mM Tris HCl pH 8.0; 0.2M NaCl; 1X Proteinase Inhibitors cocktail; 1mM EDTA pH 8.0) and left for 15 minutes at RT, followed by a centrifugation step at 2,000 rpm for 8 minutes at 4°C.

The second main step, sonication, was then performed. Cells were resuspended in 1ml *Sonication Buffer* (10mM HEPES pH 8.0; 0.5% SDS; 1X Proteinase Inhibitors cocktail; 1mM EDTA pH 8.0) and sonicated for 8 minutes at 30% amplitude, using the Digital Sonifier 450 (Branson). This step allows the fragmentation of chromatin and it is very crucial as the length of the DNA

products may interfere with the following immuno-precipitation reaction and the final PCR amplification. Ideally, DNA fragments should have a size comprised between 200 bp and 600 bp (Figure 15**b**). To check the sonication efficiency 50 µl of the sample were de-crosslinked for 2 hours at 65°C after the addition of 0.2 M NaCl and 100 µg/ml of Proteinase K (New England Biolabs). This step was then followed by DNA purification with Phenol/Chlorophorm and by DNA precipitation. For DNA precipitation 3 volume of 100% EtOH and 1/10 volume of Sodium Acetate (NaAc) were added and samples were precipitated 1 hour at -80°C.

The pellet was then resuspended in TE Buffer and 15 µl were mixed together with 10X Loading Buffer (Promega), loaded onto a 1% Agarose gel in 1X Tris-Acetate-EDTA (TAE) Buffer pH 8.5, and run at 100 V for 30 minutes.

Meanwhile, the sonicated sample was centrifuged at 14,000 rpm for 5 minutes at 4°C, allowing the elimination of cellular debris and big chromatin fragments, which may not be amplified in the final PCR reaction (pre-clearing step).

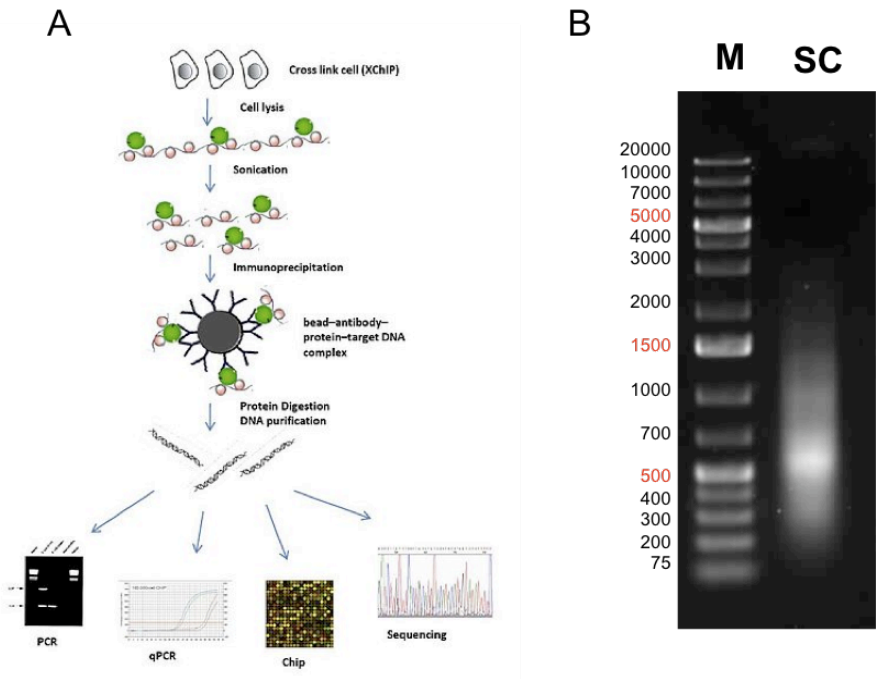

Figure 15: Schematic representation of the main steps of ChIP technique and the Sonication check run on 1% Agarose gel in 1X TAE Buffer.

(A) Schematic representation of Chromatin Immunoprecipitation (ChIP) technique. It is divided into five main steps: cell lysis, sonication, immunoprecipitation, magnetic beads binding with the protein-target DNA complex and de-crosslinking followed by DNA extraction and purification. Different methods are available for the check of the final result like PCR, qPCR, Microarray or Sequencing. **(B)** 15ul of sonicated sample were run on a 1% Agarose gel in 1X TAE Buffer using the 1 kb Plus Ladder (Fermentas) as marker: the smear represents the fragmented DNA of different size with an enrichment in 500 bp DNA fragments. The ideal size of the sonicated fragments should be between 400 bp and 600 bp.

Next, 400μl/IP reactions were taken from the sonicated sample and the remaining amount (~100μl), named “INPUT”, was collected and stored at -20°C. The INPUT is the total sonicated and non-immunoprecipitated chromatin, which is used as normaliser in the final qPCR reaction.

Each IP sample was then diluted by adding *Dilution Buffer* (50mM Tris HCl pH 8.0; 168mM NaCl; 1% Triton X-100; 0.1% SDS; 1X Proteinase Inhibitors Cocktail; 1mM EDTA pH 8.0) and samples were incubated for 15 minutes at RT.

Next, antibodies were added to each IP reaction: 5 μg of Ab α-p63 (Mouse Polyclonal 200μg/ml, Santa-Cruz Biotechnology) and 5 μg of Mouse IgG (Mouse polyclonal 1mg/ml, Active Motif), negative control for the immuno-precipitation step. Samples were then incubated o.n. at 4°C with constant rotation.

In the meantime magnetic beads, used for capturing antibodies, were first washed twice with *Dilution Buffer* and then pre-blocked overnight at 4°C in *Blocking Buffer* (15 μg/μl Glycogen Blue; 2.5% BSA; 5 mg/ml yeast tRNA in Delution Buffer up to 1ml) with constant rotation. Protein G beads (Millipore) were used due to their high specificity for Mouse IgG.

The following day, beads were washed with *Dilution Buffer* for 2 minutes at 4°C. This step was repeated twice and then beads were resuspended in *Dilution Buffer* and added to each sample. Samples were incubated 1 hour at 4°C with constant rotation.

Washings with different *Washing Buffers* followed this step. Firstly, beads were washed for 5 minutes at 4 °C with *Washing Buffer I* and the same process was repeated with *Washing Buffer II* and *Washing Buffer III* (for Washing Buffers composition see Table 5).

After washing, TE Buffer was added to each sample, which were then incubated for 2 minutes at 4°C at constantly rotation. The step was repeated twice.

Next, the supernatant was aspirated and 200 μl of *Elution Buffer* (100 mM $NaHCO_3$; 1% SDS), pre-heated at 65°C, were added to each sample, including the INPUT. The de-crosslinking step was then performed after the addition of

0.2 M NaCl and 100 μg/ml of Proteinase K (New England Biolabs) to each sample including the INPUT.

Samples were then incubated at 65 °C for 4 hours. During this step the digestion of proteins by proteinase K allows to release the DNA fragments, that were bound to proteins and immuoprecipitated.

	Washing Buffer I	**Washing Buffer II**	**Washing Buffer III**
5 M NaCl	150 μl	500 μl	-
1 M Tris HCl pH 8.0	100 μl	100 μl	50 μl
2.5 M LiCl	-	-	500 μl
0.5 M EDTA pH 8.0	20 μl	20 μl	10 μl
10% SDS	50 μl	50 μl	50 μl
10% Triton X-100	500 μl	500 μl	-
10% IGEPAL	-	-	500 μl
H_2O	4180 μl	3830 μl	3890 μl

Table 5: Composition of the three different washing buffers, used for washings after ChIP immuno-precipitation step.

Next, DNA was purified with Phenol/Chlorophorm and precipitated o.n. at -80 °C with 3 volumes of 100% Ethanol and 1/10 volume of NaAc.

The next day samples were centrifuged a 14,000 rpm for 30 minutes at 4°C and the pellet was then washed once with 70% EtOH and centrifuged for 5 minutes at 14,000 rpm at 4°C to eliminate salts.

Finally, DNA pellets were resuspended in Tris HCl pH 7.6.

1.9.1. ChIP-qPCR

qPCR reaction was performed using the StepOne Plus Real-Time PCR System (Applied Biosystems) and 0.5 μM of primers (Sigma) to specific regions in the promoter of selected genes (*Plectin 1c* -3.7 kb, *Sun-1* -3.7kb, *Nesprin-3* -0.9kb) were used together with 2X Syber Green Master Mix (Applied

Biosystem) in 20 μl final reaction volume. 5 μl for each ChIP-DNA sample, mouse IgG control, mouse IgG anti-p63 and INPUT, were used. Each PCR reaction was run in triplicate and the INPUT was used to normalize the results (for primers sequences, PCR programs and annealing temperatures see **Table 6**).

Primers were designed using the *Beacon Designer Software* (for primer design refer to ***paragraph 2.3.1.1***) and the specific annealing temperature for each pair primers was chosen after prior optimization at four different temperatures (57°C, 59°C, 61°C, 63°C). For the PCR programs refer to Table 6.

Gene alias	Primers sequence	PCR Program	bp
Plectin 1c promoter **(chr15:76232952-76233245)**	F:TCTGGTTCCCTGCTCTACAAAGTC R:CCCCACTCCCCAAACAGGTC	95 °C 20 sec 95 °C 3 sec 61 °C 30 sec x 40 cycles	24 bp 20 bp
Syne3 promoter **(chr12:105010406-105010569)**	F:GAGAGGAGATGGACATTCTTGG R:GAGCGACACAGGCAACAG	95 °C 20 sec 95 °C 3 sec 61 °C 30 sec x 40 cycles	22 bp 18 bp
Sun1 promoter **(chr5:139196701-139196830)**	F:ACTCTGCCTGCCATCTTCTTCTG R:TTGTTGTTGTGGTCATCGG	95 °C 20 sec 95 °C 3 sec 61 °C 30 sec x 40 cycles	23 bp 19 bp
Claudin1 promoter **(chr16:26372802-26373008)**	F:TGGAAGCATCCCTTGTTTTC R:TTGCTGTCCTCTCTGGGTCT	95 °C 20 sec 95 °C 3 sec 61 °C 30 sec x 40 cycles	20 bp 20 bp
Intergenic regions **(chr8:73659729-73659868)**	F: AAGGGGCCTCTGCTTAAAAA R: AGAGCTCCATGGCAGGTAGA	95 °C 20 sec 95 °C 3 sec 61 °C 30 sec x 40 cycles	20 bp 20 bp

Table 6: List of primers used in the ChIP-qPCR reaction with their corresponding PCR programs and annealing temperatures.

1.9.1.1. Primer design

Primers were designed using the *Beacon Designer Software*. Firstly, a search for the genomic sequence of the gene of interest was performed using

Ensembl genome browser and *Plectin1c, Sun-1* and *Nesprin-3* promoter regions were found. The first exon of the gene and the start codon were found and the region upstream of it was considered as the promoter region. 10 kb of this region were used for the search of the known consensus binding sites of the transcription factor p63.

Regions surrounding p63 consensus binding sites were exported in the *Beacon Designer Software* and primers were designed within these regions, considering the parameters mentioned in ***paragraph 3.2.2.1***.

Finally an *in silico PCR* was performed to check primers specificity with the sequence of interest.

1.9.1.2. ChIP-qPCR data analysis

The ChIP data of the Real-Time PCR were calculated using the "ΔΔ Ct method".

Firstly, the starting INPUT fraction was adjusted to 100%. If, for example, the starting INPUT fraction was 1%, then a fold dilution of 100 (DF) or 6.644 cycles (log2 of 100) were subtracted from the Ct value of the diluted INPUT. Secondly, each ChIP DNA fraction Ct value, including the mock IgG fraction Ct value, was normalized to the Input DNA fraction Ct value for the same qPCR Assay (ΔC_t) to account for chromatin sample preparation differences:

ΔCt [normalized ChIP] = (Ct [ChIP] - (Ct [Input] - Log2 (Input Dilution Factor))

Where, Input Dilution Factor = (fraction of the input chromatin saved)

The average of the replicates of each normalized ChIP sample was then

calculated.

Next, the % Input was calculated for each ChIP fraction (Linear conversion of the normalized ChIP ΔCt):

% Input = $2^{(-\Delta Ct\ [normalized\ ChIP])}$

After, the normalized ChIP fraction Ct value is adjusted to the normalized background (mock IgG) fraction Ct value (ΔΔCt):

ΔΔCt = ΔCt [normalized ChIP] - ΔCt [normalized IgG mock]

Finally, the *Assay Site IP Fold Enrichment* was calculated above the sample specific background (Linear conversion of the normalized ChIP ΔΔCt):

Fold Enrichment = $2^{(-\Delta\Delta Ct)}$

1.10. Alkaline Phosphatase staining of WT and Cbx4-/- embryos and measurements of epidermal thickness

1.10.1. AP staining

Alkaline Phosphatase is a hydrolase enzyme responsible for removing phosphate groups from several molecules, including nucleotides, proteins and alkaloids and the enzyme is most effective in an alkaline environments. Alkaline phosphatase is abundant in undifferentiated cells, suggesting it as a good tool to detect and stain embryonic stem cells. With respect to the skin, alkaline phosphatase is abundantly expressed in the dermal papilla and, after the addition of naphthol AS-Bi-Phosphate, the enzyme is able to hydrolyse it in the presence of a chromogen, like New Fuchsin, and produce a red precipitate.
The additional hematoxylin staining allows the analysis of epidermal morphology and thickness.

In brief, WT and Cbx4-/- embryos from different stages of embryonic development (E14.5, E16.5 and E18.5) have been cut with the cryostat (thickness 10 µm) (Microm HM550, Thermo Scientific) and slides were left drying for 15 minutes at RT and fixed in cold acetone at -20^{o}C for 10 minutes. Next, slides were washed in 1X PBS (pH 7.5). In the meantime, the developing solutions were prepared as follows: solution A (40 mM Tris Base, 10mM Tris HCl, 150 mM NaCl), solution B (4 mM Na-Nitrite, 30% New Fuchsin diluted in 750 µl of distilled H_2O), solution C (1.6 mM Naphthol AS-Bi-Phosphate diluted in 900 µl of dimethylformamide).
Solution B was added to the solution A and mixed. Solution C was then added to the mix and mixed again. Slides were then incubated in this solution for 15 minutes at RT.

Next, slides were washed twice in 1X PBS and stained with hematoxylin for 30 seconds.

Finally, slides were washed in running water and cover slips were mounted on the slides with Polyvinylpirrolidone mounting medium (60 mM Polyvinylpyrrolidone, 4% glycerol, one small crystal of Thymol).

1.10.2. Images acquisition and analysis of epidermal thickness

Images from different embryos of different embryonic developmental stages were acquired using Nikon *Eclipse 50i* light microscope at a magnification of 20X. Additional images from a calibration slide, containing beads of known size, were also acquired at the same magnification.

Images were then opened in imageJ and the appropriate scale bar was set by using the calibration slide. These settings were applied to all images analysed and 100 measurements of the thickness of the epidermis were acquired for each sample.

Next, the data were exported in excel, averaged and analysed statistically using the Peterson's Chi-square test.

1.11. Fluorescence in situ hybridization (FISH)

1.11.1. Bacterial artificial chromosomes (BACs) Mini-Preps preparation and isolation

Bacteria plates were prepared with 20 ml/plate of LB Agar pH 7.0 (1% Bacto-tryptone; 0.5% yeast extract; 1% NaCl; Agar) with the addition of 12.5 μg/ml of antibiotic Chloramphenicol for bacteria selection. The agar was left solidifying for 30 minutes at RT.

Different bacteria clones containing Bacterial Artificial Chromosomes (BACs) with the sequence of interest, taken from the previously prepared glycerol stock by Dr Andrei Mardaryev and Dr Michael Fessing (University of Bradford, United Kingdom), were used for FISH experiments (see Table 7).

Clone name	Covered Sequences	Position
RP23-473O22	*Keratin 5*	Chr15: 101,662,665-101,838,778
RP24-352C4	*Satb1*	Chr17: 51,729,136-51,884,712
RP24-171O2	*Acvr1b*	Chr15:101,113,201-101,277,439
RP24-177N5	*Eif4b*	Chr15:101,934,357- 102,133,113
RP23-66A15	*Rps27*	Chr3: 91.327.318-91.564.141
RP24-61G19	*Loricrin*	Chr3: 91,716,002-91,899,804
RP23-480F10	*Dnn4b/Gata2b*	Chr3: 89.997.746-90.169.775
RP24-248L10	*Sprr2j/Sprr3/Sprr1a*	Ch3: 92.215.201-92.392.463
RP24-75K3	EDC	Chr3: 92.583.402-92.766.349
RP23-425P7	*Tchh/S100a11/S100a10*	Chr3: 93.215.624-93.411.886

Table 7: List of BAC probes used for 3D Fluorescence in situ hybridization experiments.

Each bacteria clone was then plated on different LB Agar plates in a way which allowed the growth of single colonies and bacteria were left growing o.n. at 37°C.

The following day, using pipette tips, a single isolated bacterial colony was selected from each plate and inoculated into different 15 ml conical tubes with

LB media supplemented with 12.5 μg/ml of Chloramphenicol. Bacteria were left growing up to 16 hours, shaking at 225-300 rpm at 37°C.

Bacteria mini-preps were then transferred to 1.5 ml tubes (Eppendorf) and centrifuged at 3,000 rpm for 10 minutes. Temperature is not critical at this stage. Supernatants were discarded and each pellet was resuspended, by gently mixing, in P1 Resuspension Buffer (50mM Tris Cl pH 8.0; 10mM EDTA; 100μg/ml RNase A). To lyse bacteria P2 Lysis Buffer (0.2N NaOH; 1% SDS) was then added and each tube was gently shaked to mix the content. Tubes were then incubated for 5 minutes at RT. After incubation P3 Neutralization Buffer pH 5.5 (3M KoAc) was added to each tubes, which were gently shaked during addition, and placed on ice for 5 minutes. A white precipitate of proteins and *E.Coli* DNA formed.

Next, tubes were centrifuged at 10,000 rpm for 10 minutes at 4°C and the supernatants were transferred, avoiding any white precipitate material, to fresh 1.5 ml tubes (Eppendorf) containing cold isopropanol, used for BACs precipitation. Tubes were left on ice for 5 minutes and then centrifuged in cold microfuge for 15 minutes at 14,000 rpm. Pellets were then washed by adding 70% EtOH to each tube, mixed and centrifuged in cold microfuge for 5 minutes. This step was repeated twice.

After the removal of 70% EtOH, pellets were left drying at RT until they turned from white to translucent in appearance, and resuspended in TE Buffer (10mM Tris HCl pH 7.5; 1 mM EDTA pH 8.0).

Once the pellets were completely dissolved, BACs concentration was measured using the spectrophotometer (SmartSpec Plus, Bio-Rad) at a

wavelength of 260 nm and a conversion factor of 50 µg/ml. DNA purity was checked using the ratio 260/280 nm.

BACs amplification was then performed using *illustra GenomiPhi V2 DNA Amplification Kit* (GE Healthcare) according to the manufacturer's protocol and 10 ng of each BAC were used for the reaction. The PCR program was run as follows: denaturation at 95 °C for 3 minutes; 1 hour and 30 minutes at 30 °C followed by a final step at 65 °C for 10 minutes.

The amplified samples were run at 100 V on a 1% Agarose gel in 1X Tris-Acetate-EDTA (TAE) Buffer (Tris, Glacial acetic acid, 0.5M EDTA) to check the reaction result (Figure 16**a**).

1.11.2. Probe preparation and labelling

1.11.2.1. Nick Translation (NT)

Each BAC was labelled by the Nick Translation Reaction. According to this reaction, a low concentrated DNase I (1:200) creates several single-stranded "nicks" on the DNA sequence, subsequently repaired by a DNA Polymerase I. This enzymes, thanks to its 5'-3' exonuclease activity, is able to elongate the 3' hydroxyl terminus by removing nucleotides and by replacing them with labelled dUTPs. dUTPs can be radiolabelled or labelled with fluorophores (Indocarbocyanine, Fluorescein Isothyocianate) or with antigens for immunodetection (Digoxigenin).

For the preparation of the EDC pool, equimolar amount of BACs RP23-66A15, RP24-75K3, RP23-425P7, RP23-480F10, RP24-248L10, amplified separately by GenomiPhi, were pooled together and labelled with biotin.

To label the dUTPs with Cy3, 20 mM of Cy3 (Amersham/Pharmacia) were dissolved in Dimethyl Sulphoxide (DMSO) and mixed together with 20 mM

aminoallyl dUTPs, H_2O and 0.2 M Bicarbonate Buffer. After 4 hours incubation at RT, 2 M glycine pH 8.0 and 1 M Tris HCl pH 7.75 were added to stop the reaction and to stabilize the nucleotides respectively (pre-prepared by Dr Michael Fessing, University of Bradford).

To label dUTPs with biotin (pre-prepared by Dr Mohammed Ahmed, University of Bradford), 40 mM Biotin (Molecular Probes) were dissolved in DMSO and mixed together with 20 mM aminoallyl dUTPs, H_2O and 0.2 M Bicarbonate Buffer. After 4 hours incubation at RT, the reaction was stopped by adding 2 M glycine pH 8.0 and the nucleotides were stabilized after the addition of 1 M Tris HCl pH 7.75.

The Digoxigenin-labelled dUTPs were prepared by dissolving 40 mM of Digoxigenin (Molecular Probes) with DMSO and by mixing them together with 20 mM aminoallyl dUTPs, H_2O, 0.2 M Bicarbonate Buffer and DMSO. They were then incubated 4 hours at RT and after incubation, 2 M glycine pH 8.0 and 1 M Tris HCl pH 7.75 were added (pre-prepared by Dr Michael Fessing, University of Bradford).

The Nick Translation Master Mix, which included 0.1M Mercaptethanol, 10X NT Buffer (0.5 M Tris HCl pH 7.5; 50 mM $MgCl_2$; 0.05% BSA) and 2mM dNTPs mix (Promega) was then prepared and aliquoted into different 0.2 ml tubes; BAC, labelled dUTPs, diluted DNase I (Promega) and DNA Polymerase I (Promega) were then added to each tube and incubated for 1 hour and 30 minutes at 15°C.

10 μl of the Nick Translation reaction were mixed together with 10X Loading Buffer (Promega) and run at 100 V on a 1% Agarose gel in 1X TAE Buffer (Figure 16**b**).

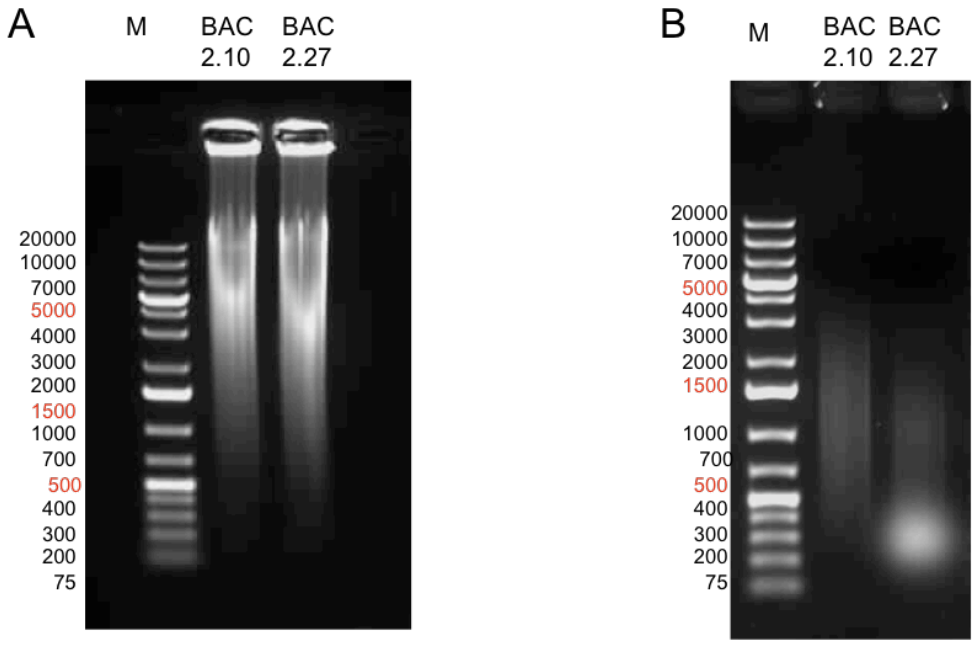

Figure 16: Representative images of GenomiPhi and Nick Translation check run on a 1% Agarose gel in 1X TAE Buffer.

(A) GenomiPHI amplification check of BAC 2.10 and BAC 2.27 using 1 kb Plus Ladder (Fermentas). Two smears with a size around 5000 bp were observed as a result of the amplification of products of different size. **(B)** Nick Translation check of BAC 2.10 and BAC 2.27 using 1 kb Plus Ladder (Fermentas). Two smears with a size between 1000 bp and 1500 bp were observed as a result of the amplification of products of different size. The DNase I treatment in the Nick Translation reaction was responsible for the products size reduction compared to the GenomipHI reaction. This was also an indication of the Nick Translation efficiency and by consequence the products were likely to have correctly incorporated the respective labelled dUTPs.

1.11.2.2. DOP-PCR Amplification and DOP-PCR Labelling

In addition to BACs probes, which hybridize with specific DNA sequences, the Whole Chromosome Paint three (MMU3) was used. It consists of several probes mixed together, which are able to bind the whole chromosome three, characterising the Chromosome Territory three.

To amplify the Whole Chromosome Paint three, a special PCR reaction named Degenerate Oligonucleotide Primers Polymerase Chain Reaction (DOP-PCR) was used, allowing the random amplification of DNA from any source. This reaction is generally used when there is not a specific sequence to amplify. In

fact the DOP-PCR primer consists of three regions: the 5′-end carries a recognition sequence for *Xho*I (C·TCGAG), a restriction endonuclease that cuts rarely within the genome; the sequence is then followed by a middle portion containing six nucleotides of degenerate sequence (*NNNNNN*, where *N* = A, C, G, or T in approximately equal proportions) and a 3′-end sequence containing six specific bases (ATGTGG), which binds the DNA approximately every 4 kb. Normally, the reaction is based on two different steps: at the beginning a low annealing temperature is used for the binding of the central degenerate sequence to DNA to initiate the PCR reaction; an increase in the annealing temperature increases the stringency, allowing the binding of the 3' end specific sequence (Telenius et al., 1992). Different DNA sequences are amplified in the first step, followed by a second exponential amplification of the same sequences during the second step.

The DOP-PCR reaction mix, containing 10X PCR Buffer without $MgCl_2$ (Invitrogen), 25 mM $MgCl_2$, 2.5 μM dNTPs mix (Promega) and 100μM 6MW Primer (CCGACTCGAGNNNNNNATGTGG) (Telenius et al., 1992), was aliquoted into 0.2 ml tubes; Taq Polymerase (Promega) and 1 μl of the Whole Chromosome Paint three were then added to each tube. The DOP-PCR reaction was then performed in 100 μl final volume as follows: denaturation at 94°C followed by 39 cycles with 30 seconds at 94°C, primer annealing at 56°C and elongation step at 72°C for 30 seconds; a final additional elongation step at 72°C for 5 minutes was also performed.

Samples (8μl) were then mixed together with 7 μl of 10X Loading Buffer (Promega) and run at 100 V on a 1% Agarose gel in 1X TAE Buffer for 30 minutes (Figure 17**a**).

After the amplification by DOP-PCR, a second DOP-PCR reaction was performed to label the Whole Chromosome Paint three. The DOP-PCR labelling reaction was performed in 100 μl final volume and the master mix was prepared as follows: 10X PCR Buffer without $MgCl_2$ (Invitrogen), 25 mM $MgCl_2$, 100 μM 6MW primer (CCGACTCGAGNNNNNNATGTGG), 2 mM dAGC (Promega) and 1mM dTTP (Promega). The mix was then aliquoted into 0.2 ml tubes and Biotin-labelled dUTPs, the amplified Chromosome Paint three and Taq Polymerase (Promega) were then added to the mix.

The DOP-PCR labelling program was run as follows: 3 minutes denaturation at 94°C followed by 39 cycles, which include 30 seconds at 94°C, primer annealing at 56°C and elongation at 72°C for 30 seconds; a final additional elongation step at 72°C for 5 minutes was also performed.

The sample was run at 100 V on 1% Agarose gel in 1X TAE Buffer for 30 minutes to check the reaction result (Figure 17**b**).

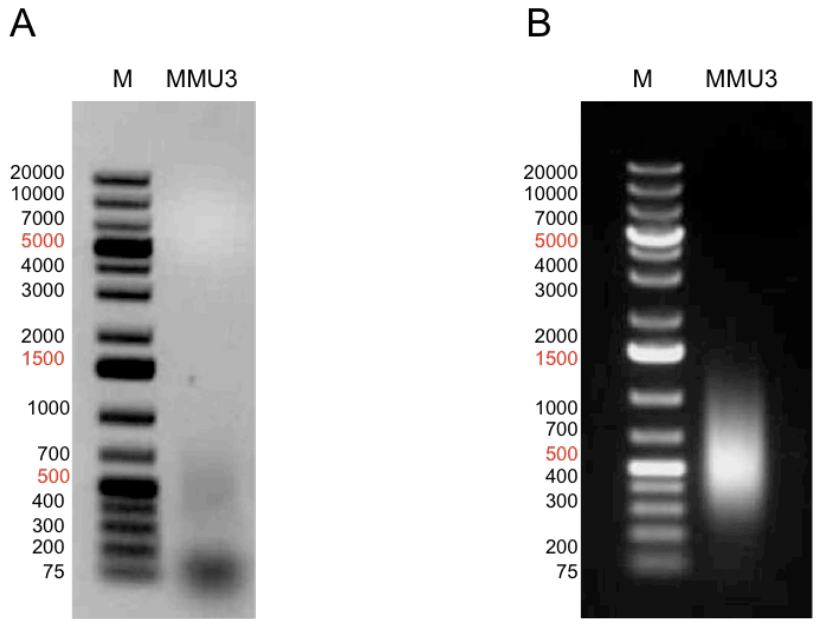

Figure 17: DOP-PCR amplification and DOP-PCR labelling of Chromosome paint 3 check, run on 1% Agarose gel in 1X TAE Buffer.

(A) DOP-PCR amplification of Whole Chromosome Paint three on 1% Agarose gel in 1X TAE Buffer. A smear between 500 bp and 75 bp was observed as a result of the random amplification using degenerated primers in the reaction, which amplified products of different size. **(B)** DOP-PCR labelling with dUTPs biotin labelled of Whole Chromosome Paint 3 on 1% Agarose gel in 1X TAE Buffer. A smear between 1000 bp and 200 bp was observed as a result of the random amplification by degenerated primers, which amplified products of different size.

1.11.3. Validation of the prepared probes using 2D FISH

1.11.3.1. Metaphase Spreads preparation

Metaphase spreads of embryonic mouse fibroblasts (MEFs) were prepared according to the recommendations of L.M Cheung et al. 1995. Previously prepared mouse embryonic fibroblasts (MEFs) by Dr Michal Gdula (University of Bradford, United Kingdom) were centrifuged at 16,000 rpm for 5 minutes. Once the supernatant was removed and the new fixative (methanol:acetic acid 3:1) was added, cells were mixed. In the meantime the water bath was set at 55°C and the water level was adjusted until the ratio between the water surface and the air volume under the waterbath cover

reached 0.23 (about 4.3 cm from the top). This step is crucial as incorrect conditions of temperature and humidity may interfere with the quality of metaphase spreads.

Next, microscope slides were placed on a trail on the water surface and two drops of MPFs per slide were added and the waterbath was covered for a couple of minutes until all the fixative was evaporated. Slides were then checked under the light microscope and if at least three metaphase spreads were observed, slides were placed in a Coplin Jar with 70% EtOH and left overnight at RT. Next day the 70% EtOH was removed and absolute Ethanol was added. Slides were left in absolute Ethanol for 10 minutes at RT and then, after the removal of Ethanol, dried for one week at RT in a closed box.

After one week incubation, slides were incubated 2 hours at 60°C and pepsin treatment was performed to remove cytoplasmatic proteins. 10% Pepsin solution was prepared and 50 μl of it were added to the pre-warmed at 37°C 0.01 M HCl solution. Slides were then incubated 10 minutes at 37°C in the 0.01 M HCl/10% pepsin solution.

After the incubation slides were washed 3X5 minutes with 1X PBS and then placed in 70% EtOH for 5 minutes at RT, additionally dehydrated by adding absolute Ethanol and left drying at RT.

1.11.3.2. 2D FISH

Reactions were prepared as follows: 1) *Loricrin*- Cy3 labelled, *Keratin 5*-Digoxigenin labelled, Chromosome Paint Three Biotin labelled and the *Mouse Hybloc Competitor DNA* (Applied Genetics Laboratories); 2) *Rps27*-Biotin labelled, *Satb1*-Digoxigenin labelled, Chromosome Paint seventeen and *Mouse Hybloc Competitor DNA* (Applied Genetics Laboratories); 3) *Eif4b*-Digoxygenin

labelled, *Acvr1b*-Biotin labelled and *Mouse Hybloc Competitor DNA*. *Mouse Hybloc Competitor DNA* is used in in situ hybridization reaction as it is enriched for DNA repetitive sequences and it is able to block non-specific hybridization in FISH assays, including repetitive sequences such as SINEs (short interspersed elements), LINEs (long interspersed elements), and sequence homology among members of the same gene family when added to the hybridization reactions, leading to cleaner and more sensitive FISH experiments.

The mixed probes were then precipitated for 1 hour at -80°C by adding three volumes of absolute Ethanol to the reaction mix. Probes were then centrifuged at 14,000 rpm for 30 minutes at 4°C. The supernatants were discarded and pellets were left drying for few minutes at RT to favour the complete evaporation of Ethanol. The hybridization mixture was then added to the pellets: firstly 2.5 μl of Formamide (Sigma-Aldrich) were added to the pellets and left dissolving for 30 minutes at 37°C, followed by the addition of 2.5 μl of Master Mix (20% Dextran Sulphate in 4X Sodium Saline Citrate Buffer).

The hybridization reaction is influenced by several factors, including melting temperature, hydrophobic interactions between opposite DNA filaments and the negative charges on the phosphate groups of the DNA. The hydrophobic interactions between the nucleotides on opposite DNA filaments are non-specific. By consequence the use of Formamide or others chemical denaturants in the Hybridization Mix plays an important role in the reduction of these non-specific interactions, increasing the specificity of the interactions between probes and their target sequences. In addition the presence of negative charges on the phosphate groups, which cause the electrostatic repulsion between the two DNA filaments, is reduced by the presence of salts,

as they are able to neutralize the negative charges. By consequence, the presence of a low concentration of salts, high temperature and the presence of formamide, increase the specificity of hybridization (high stringency conditions).

Probes were mounted on one slide with previously prepared metaphase spreads (see ***Paragraph 2.7.3.1***) and covered with 15X15 mm coverslips. The slide was sealed with rubber cement and left in a dark place at RT until the rubber cement was completely dried.

Denaturation was then performed at 75°C for 2 minutes, followed by incubation of slides in the waterbath at 37°C o.n.

The following day slides were placed in a Coplin Jar and washed 3X10 minutes with 2X SSC pH 7.0 (SSC) in the water bath at 37°C. These washings were then followed by one washing in 0.1X SSC (pH 7.0) at 60°C for 10 minutes.

To detect BACs and chromosome territory three signals, slides were incubated with mouse IgG anti-digoxigenin-Cy3 conjugated (Jackson Laboratories), Streptavidin Cy5-conjugated (Jackson Laboratories) and IgG anti-FITC-Alexa 488 conjugated (Jackson Laboratories). Both, IgG anti-digoxigenin-Cy3 and Streptavidin Cy5 conjugated were diluted 1:100, while IgG anti-FITC-Alexa 488 was diluted 1:50 in the working solution (4% BSA/0.1% Triton X-100 in 4X Saline Sodium Citrate Buffer) and incubated for 1 hour at 37°C.

After 3X5 minutes washings in 4X SSC (pH 7.0) at 37°C, 4',6-diamidino-2-phenylindole (DAPI, blue nuclear counter stain) 0.2 μg/ml was applied on the slides. After one washing in 1X PBS (pH 7.6), the VECTASHIELD Mounting Medium for fluorescence (Vector Laboratories Inc., Burlingame, CA ,USA) was

applied and slides were checked and scanned under the confocal microscope (Figure 18).

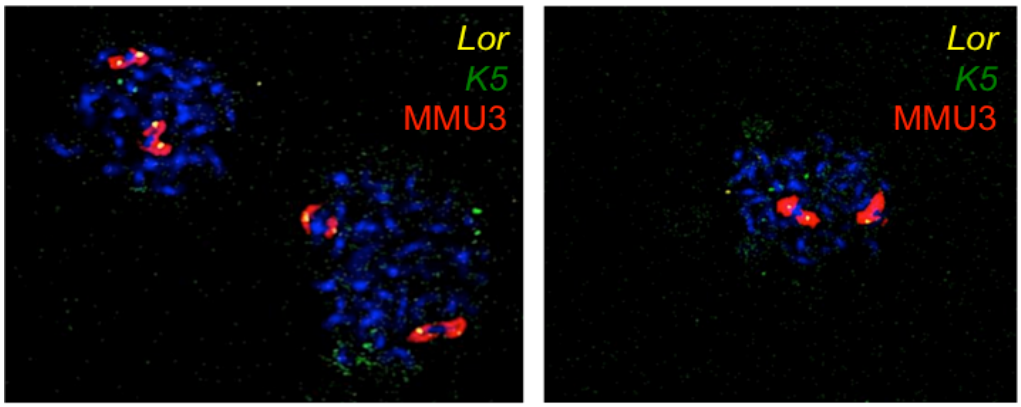

Figure 18: Example of 2D FISH on fibroblasts metaphase spreads.

Fibroblast metaphase spreads were prepared and processed for 2D FISH experiments and labelled probes for *Loricrin* (yellow), *Keratin 5* (green) and the chromosome territory 3 (MMU3) (red) were tested. Z-stacks images were acquired with the confocal laser scanning confocal microscope LSM 510 Meta (Carl Zeiss) in separate channels responding to the respective fluorophores.

1.11.4. 3D FISH on WT and keratin type II knock-out skin samples

1.11.4.1. Tissue preparation

WT and keratins type II-depleted skin samples were collected and fixed for FISH experiments at the University of Leipzig, Germany.

Cryosections (14 μm) from both WT and keratins type II-depleted skin samples were cut using a Cryostat (*Microm HM550*, Thermo Scientific) at a temperature of -22°C. Slides were incubated 30 minutes at RT. Next, slides were placed in 10 mM Sodium Citrate Buffer (pH 6.0), heated up in the microwave to partially reverse crosslink until it started boiling and cooled down for 2 minutes at RT. This step was repeated five times.

Slides were then washed once with 2X SSC (pH 7.0) for 5 minutes at 37°C and kept in 2X SSC (pH 7.0) with 50% Formamide (Sigma-Aldrich) at 4°C overnight

up to few days with the aim of reducing the hydrophobic non-specific interactions between DNA sequences, increasing, by consequence, the stringency of hybridization.

1.11.4.2. Pre-treatement of Thymocytes for 3D FISH experiments

Mice have been sacrificed and the thymus was collected.

Thymocytes have been extracted and processed for 3D FISH experiments according to Cremer M. et al. protocol (Cremer et al., 2008).

First, thymus has been placed on ice in a 6-well plate containing RPMI medium (Gibco) supplemented with 50%FBS (Gibco) and epithelial tissue has been mechanically removed from thymus. The cell lysate has been filtered through a 70 µm nylon filter (BD Bioscience) and centrifuged at 200 x g for 10 minutes at 4°C. Next, supernatant has been discarded and the cell pellet resuspended in Red Blood cells lysis Buffer (Sigma-Aldrich) and centrifuged for additional 10 minutes at 200 x g at 4°C. The supernatant containing lysed red blood cells has been discarded and the cell pellet has been resuspended in RPMI medium (Gibco) supplemented with 50% FBS (Gibco). This step is though to improve the adherence of cells to the glass surface.

Meanwhile, microscope slides have been coated with polylysine: slides were incubated in 80% ethanol for 5 minutes followed by 1 hour incubation with 150 µl of polylysine hydrobromide (1mg/mL) (Sigma-Aldrich) at RT. Next, slides were rinsed with ddH_2O, air-dried. ~1 mL of culture medium, containing from ~$1x10^5$ to $1x10^6$ cells per 20x20mm coverslips, was placed on a polylysine-coated slide. Slides were incubated at 37°C in an incubator containing 5% CO_2 for 1 hour.

After the incubation, each slide was checked under the microscope for cells attachment and the medium was briefly drained off.

Slides were then incubated in 0.3X PBS for 40 seconds. This step is crucial as it prevents the shrinkage of spherically shaped cells that are otherwise prone to collapse during the following fixation step.

Next, cells were fixed in 4% PFA/0.3X PBS for 10 minutes at RT, followed by three washings in 1X PBS. Slides were then incubated in 0.5% Triton X-100/1X PBS at RT for 20 minutes, transferred to 20% Glycerol/1X PBS and incubated at RT for 30 minutes.

Cells were frozen by dipping slides into liquid nitrogen (~30 seconds) and by thawing them on a piece of paper towel. As soon as the frozen layer disappeared, slides were put back into 20% Glycerol/1X PBS. The process has been repeated four times.

Three washings in 0.05% Triton X-100/1X PBS and a final incubation in 0.1N HCl for 5 minutes followed this step.

Slides were incubated in 2X SSC/50% Formamide from overnight up to few weeks at 4°C.

1.11.4.3. 3D FISH

Several different reactions for different 3D FISH experiments on WT and keratins type II-depleted skin samples or on freshly isolated thymocytes were prepared as follows: 1) *Loricrin*-Cy3-labelled, *Keratin 5*-Digoxigenin-labelled, Chromosome Paint 3 Biotin-labelled and mouse hybloc competitor DNA; 2) *Loricrin*-FITC labelled, *Satb1*-Digoxygenin labelled and mouse hybloc competitor DNA; 3) *Loricrin*-FITC labelled, *Acvr1b*-Biotin labelled, *Eif4b*-Digoxigenin labelled and mouse hybloc competitor DNA; 4) *Satb1*-Digoxigenin

labelled, *Acvr1b*-Biotin labelled, *Eif4b*-FITC labelled and mouse hybloc competitor DNA; 5) EDC pool-Biotin labelled, *K5*-FITC labelled, *Satb1*-Digoxygenin labelled and mouse hybloc competitor DNA; 6) *Satb1*-Digoxygenin labelled, *Keratin 5*-FITC labelled and chromosome paint 17-Biotin labelled.

Probes were then precipitated with the addition of three volumes of absolute Ethanol at -80°C for 1 hour, followed by a centrifugation at 14,000 rpm for 15 minutes at 4°C. After removal of the supernatant, probes were left drying at RT for few minutes to remove any residuals of Ethanol and pellets were then resuspended in the Hybridization Mixture (30 μl): firstly 15 μl of Deionized Formamide (Sigma-Aldrich) were added and pellets were left 30-45 minutes at 37°C to completely dissolve. Next, 15 μl of Hybridization Master Mix (20% Dextran Sulphate in 4X SSC) were added and probes were mounted on the previously prepared slides and covered with 15X15 mm coverslips; slides were sealed with rubber cement and incubated in a dark place at RT to let the rubber cement dry.

Next, slides were pre-incubated o.n. at 37°C in the water bath. This pre-incubation step allowed the completely saturation of probes with tissue.

The following day, probes were denaturated by placing slides 5 minutes in the thermo-block at 85°C. Slides were then incubated again in the water bath at 37°C and left for 48-72 additional hours. Once the incubation was finished, slides were washed and stained following the same protocol used for 2D FISH (see ***paragraph 3.3.4.2***).

Slides were checked and scanned using the confocal microscope.

1.11.5. Image processing and analysis

Microscope slides with FISH samples were scanned using confocal laser scanning microscope LSM 510 Meta (Carl Zeiss) equipped with UV laser (Enterprise, emitting light of 351nm, 364 nm wave lengths) and VIS lasers: Argon (458 nm, 477 nm, 488 nm, 514 nm), HeNe1 (543 nm) and HeNe2 (633nm). Stacks of confocal images were acquired with a 63x/1.4 plan-apochromat oil objective and a voxel size of 100nm x 100 nm x 200 nm.

Four different fluorophores with emission peaks far enough to be distinguished from each other and excited efficiently with available lasers were used for labelling: 4',6-diamidino-2-phenylindole (DAPI, blue nuclear counter stain), Fluorescein isothiocyanate (FITC, green), Indocarbocyanine (Cy3, red) and Indodicarbocyanine (Cy5, infra red). Images were recorded in separate channels responding to respective flurophores (filter settings; (Hernandez-Munoz, Taghavi et al. 2005)) (Figure 19).

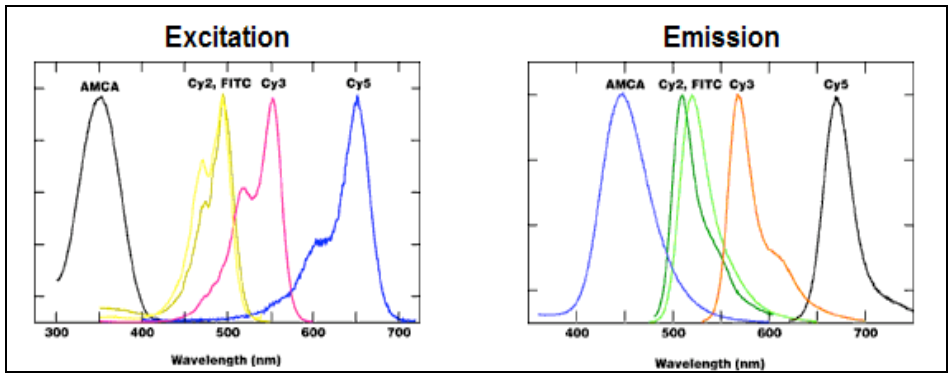

Figure 19: Representation of excitation and emission spectra of used fluorophores.

Four different fluorophores were used for labelling of DNA:DAPI (maximal absorbtion/excitation at 358 nm light wave length, maximal emission at 461 nm wave length; spectrum of DAPI is similar to AMCA), FITC (492 nm ,510 nm), Cy3 (550 nm, 570 nm) and Cy5 (650 nm, 670 nm) (Source: http://www.jacksonimmuno.com/technical/f-cy3-5.asp)

Scans of section of the whole depth of different areas of each samples were acquired and saved as three dimensional image stacks for further analysis.

1.11.5.1. Analysis of the position of Loricrin or Satb1 locus within Chromosome Territory three and seventeen respectively

Slides for the WT and keratins type II$^{-/-}$ samples were analysed for the position of *Loricrin* or *Satb1* locus within their chromosome territories. Several optical sections were analysed using *ImageJ* software and only the nuclei with detectable *Loricrin* or *Satb1* signal and no *K5* signal were considered, as these nuclei represent the effective knock-out cellular fraction. 40 nuclei (74 loci) were counted for the wild-type sample and 34 nuclei (74 loci) were counted for the knock-out sample.

Chromosome territories were divided into three parts: internal, closer to the nuclear centre, median and peripheral, closer to the nuclear border. This division was possible as the chromosome territory three as well as chromosome territory seventeen were almost in all cases close to the nuclear border.

Positional data were then exported in *Excel*, compared between the two different samples and analysed statistically.

1.11.5.2. Statistical analysis

As the aim of this part of study was not only to analyze *loricrin* or Satb1 position within its territory but also to compare these results between WT and keratins type II locus knock-out skin samples, statistical analysis using Chi-square test (X_2) of "r x k contingency tables" sets was performed.

"r x k contingency table" contains specifically ordered data where "r"stands for raw data record consisting of the distribution of one loci within its

chromosome territory in one tissue and “k” means column, represented position: peripheral, middle or internal. Null hypothesis (H0) on equality of each pair of data sets (data on particular loci in particular tissue) were tested separately assuming probability of wrongly rejection o the H0 (Type I error) below 0.05.

Finally, values of Chi-square statistic were compared with the critical values for the Chi-square test with 2 degrees of freedom (df) and the level of significance α=0.05.

$$df = (r-1)(k-1)$$

df- degrees of freedom
r - raw
k - column

1.11.5.3. Analysis of the distances between gene loci

Confocal image-stacks were processed with ImageJ and centroids of each BAC signal were found using ImageJ plugin *Centre Finder*. Coordinates of each BAC signal were corrected for chromatic aberration.

In optics, chromatic aberration is a type of distortion due to a failure of lens to focus all colours at the same convergence point and it occurs because lenses have different refractive index for different wavelengths of lights. Considering that different BACs signals, corresponding to different loci, were acquired in separate channels, it was necessary to correct coordinates for chromatic aberration.

Chromatic aberration was calculated using Tetra Speck microspheres 0.5 µm (Invitrogen T-7181). Beads were mixed, diluted 1:100 in H_2O and 50-100 µl of beads suspension was placed on a microscope slide. The suspension was spread on the microscope slide with a pipette tip as far as the surface tension permitted. Mounting medium for fluorescence (VECTASHIELD mounting medium for fluorescene, Vector Laboratories) was applied and coverslip 0.17 mm thick mounted on the microscope slide. Nail polish was used to seal the coverslip on the slide, thus preserving the fluorescence signal over time.

Slides with beads were scanned using confocal laser scanning microscope LSM 510 Meta (Carl Zeiss) equipped with UV laser (Enterprise, emitting light of 351nm, 364 nm wave lengths) and VIS lasers: Argon (458 nm, 477 nm, 488 nm, 514 nm), HeNe1 (543 nm) and HeNe2 (633nm). Stacks of confocal images were acquired with a 63x/1.4 plan-apochromat oil objective and a voxel size of 100nm x 100 nm x 200 nm. Images were recorded in separate channels responding to respective flurophores and areas with at least 20 beads were considered.

Confocal image-stacks were processed with ImageJ and each single channel was opened in separate windows. The channel opened first (DAPI) was used as reference for the other channels. The voxel sizes of the stacks was set and applied to all opened image stacks (Figure 20).

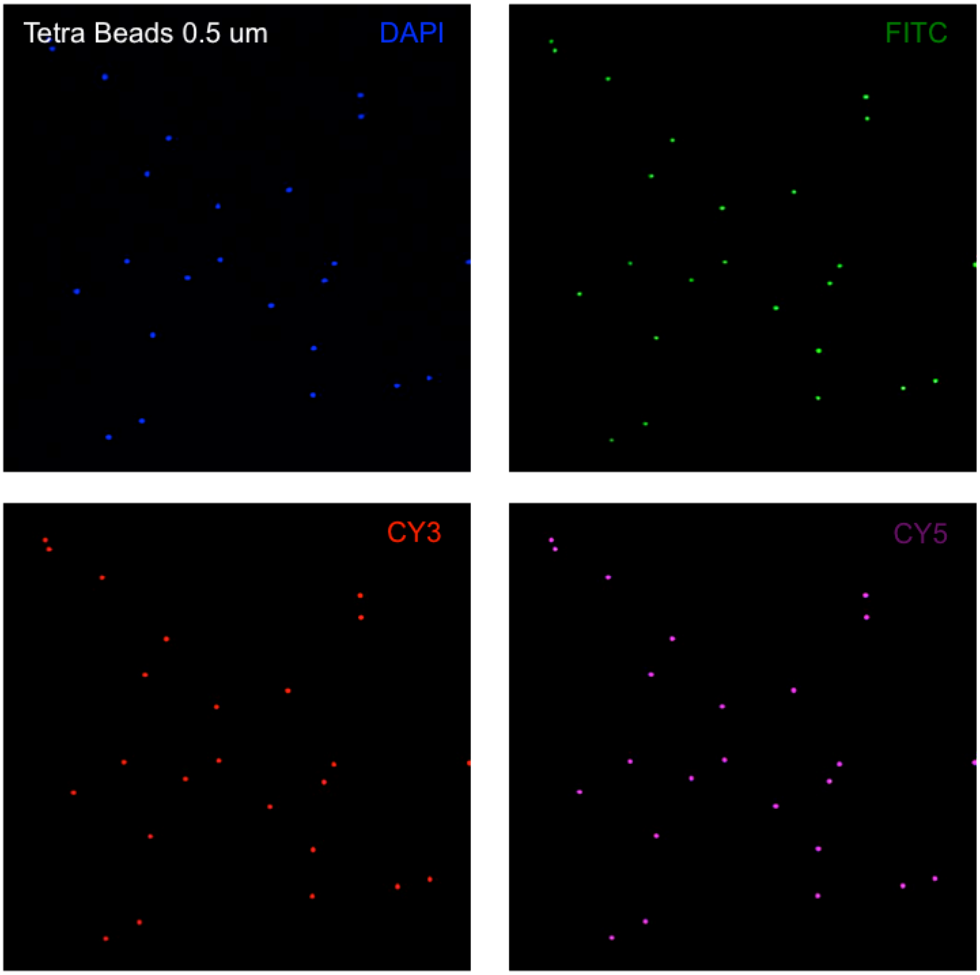

Figure 20: Confocal Z-stacks of 0.5um Tetra Beads in all four channels.

Stacks of confocal images were acquired with the laser scanning confocal microscope Zeiss Meta 510 using a 63x/1.4 plan-apochromat oil objective and a voxel size of 100nm x 100 nm x 200 nm. Images were recorded in separate channels responding to respective flurophores.

Next, ImageJ plugin *Syncronize Measure 3D* was used to synchronize all opened image stacks and a mid-section in the stacks, where the beads were approximately focused in all stacks, was chosen. The suitable threshold, that separates the bead images from the background, was then adjusted in each window.

To measure the positions of a bead image in all image stacks simultaneously, a ROI was drawn around the bead of interest and by double-clicking into the ROI,

a text window containing all the results of chromatic aberration in all three coordinates (x, y, z) and channels appeared. The process was repeated for at least 20 beads (Figure 21).

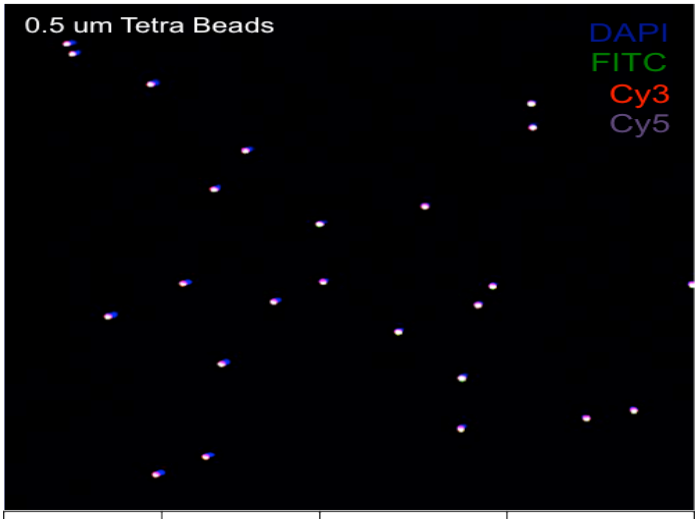

Channel	Shift x	Shift y	Shift z
Ch 1 DAPI	0,000	0,000	0,000
Ch 2 FITC	0,411	0,160	-0,362
Ch 3 Cy3	0,351	0,085	-0,246
Ch 4 Cy5	0,279	0,127	-0,300

Figure 21: Correction for chromatic aberration in all four channels.

Confocal image-stacks have been processed with ImageJ and chromatic aberration has been calculated in each separate channel using imageJ plugin *Syncronyze Measure 3D*.

Once all coordinates were corrected for chromatic aberration, the 3D Pythagoras formula was applied to calculate the distance between two or more loci within the nucleus:

$$\sqrt{(x_1-x_2)^2+(y_1-y_2)^2+(z_1-z_2)^2}$$

Distances were then normalized to the mean nucleus radius. To calculate the mean nucleus radius, few hundreds random coordinates were collected throughout the nuclear surface depicted by DAPI counterstain and the nuclear geometric centre was found by averaging all coordinates. Distances between each coordinates and the nuclear geometric centre were calculated with the 3D Pythagoras formula and results were averaged, obtaining the mean nuclear radius value.

The results obtained were compared between the two samples and analysed statistically. First, the distribution of data was checked using the Shapiro-test in "R" platform and then the appropriate statistical analysis, t-test for normal distributed data or Wilcox-test for non-normal distributed data, was applied.

1.11.6. Immuno-fluorescence experiments on WT and keratin type II knock-out mice

Cryosections of P8 WT and keratins type II-depleted skin samples were used for immuno-fluorescence analysis using Loricrin and Satb1-specific antibodies listed in Table 8 with their corresponding dilutions and secondary antibodies used. For detailed immuno-fluorescence protocol refer to ***Paragraph 2.1***.

Primary antibody	Dilution	Secondary antibody
Rabbit polyclonal Anti-Loricrin (Abcam)	1:100	Donkey anti-rabbit-Cy3 (Invitrogen)
Rabbit polyclonal Anti- Satb1 (Abcam)	1:100	Donkey anti-rabbit-Cy3 (Invitrogen)

Table 8: List of primary and secondary antibodies with their corresponding dilutions.

Chapter 3

Results

3. RESULTS

1.12. p63 deficiency leads to changes in the nuclear shape in embryonic skin epithelium and in primary mouse keratinocytes

The transcription factor p63 is the key regulator of skin development and stratification, and mice lacking the functional p63 gene are characterized by complete absence of epidermal stratification and die shortly after birth because of dehydration (Yang et al., 1999) (Mills et al., 1999).

Proper cellular and nuclear architecture are key elements for several biological mechanisms within cells, including signalling transduction, cellular migration, cell proliferation (Dechat et al., 2010; Goldman et al., 2004), gene expression regulation (Dechat et al., 2008) and mechanical stiffness (Houben et al., 2007). All these mechanisms are required for proper tissue development and differentiation and they act through proper cytoskeleton architecture as well as to a proper cross-talk between cytoskeleton and nuclear components. The defects in cell proliferation (Truong et al., 2006) and alterations in 3D nuclear organization observed in p63-null mice (Fessing et al., 2011), in addition to the fact that p63 directly regulates a subset of structural genes, including cytokeratins (Romano et al., 2009) and cell-adhesion molecules (Carroll et al., 2006), led us to further investigate whether p63 ablation could also lead to the defects in the nuclear shape of epidermal keratinocytes.

To test our hypothesis we first compared E16.5 $p63^{-/-}$ embryos with age-matched WT controls and analysed them for the presence of basal keratinocytes with misshapen nuclei. Embryonic quick frozen cryosections of both WT and p63-null embryos were stained with antibody against CD104 (also known as β_4 integrin), which binds to the cell surface of keratinocytes

attached to the basal membrane and helps to distinguish skin epithelial cells from dermal fibroblasts (Figure 22). Also, immuno-fluorescence experiments with Lamin B1-specific antibody, the major B-type lamins, was used to better discriminate between nuclei with normal and altered morphology (Figure 23**a**). DAPI was used to stain keratinocyte nuclei.

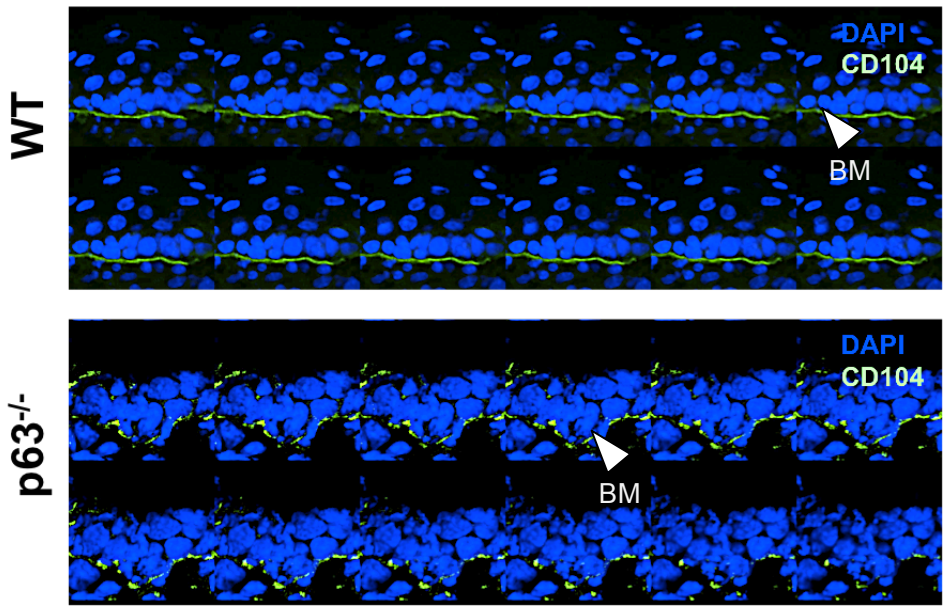

Figure 22: Z-stacks of the epidermis of WT and p63-/- embryos.

Z-stacks were acquired using the laser scanning confocal microscope LSM 510 Meta (Carl Zeiss) and 50±5 stacks/sample were acquired, using a 63x/1.4 plan-apochromat oil objective. Scans were then exported in ImageJ software and nuclei of basal epidermal cells were counted in both WT and p63-null embryonic cryosections. CD104 (β_4 integrin) (green), marker for the basement membrane was used to distinguish the epithelial cells from dermal fibroblasts and arrows indicate the basement membrane (BM). Nuclei were stained with 4',6-diamidino-2-phenylindole(DAPI, blue)

To analyse the nuclear morphology the ImageJ plugin “circularity” (*circularity = 4pi(area/perimeter^2)* has been used and 123 basal epidermal cells were counted in $p63^{-/-}$ embryos while 135 basal keratinocytes nuclei were counted in WT controls. Our analysis revealed that 32% of p63-null basal keratinocytes displayed altered nuclear morphology (mean nuclear circularity=

0.83) compared to wild-type controls (mean nuclear circularity= 0.90) (Figure 23**b**). Only nuclei with a circularity value <0.80 have been considered as abnormally shaped and used for further analyses.

To exclude the possibility that the observed defects in the nuclear shape were a consequence of apoptosis (Rao et al., 1996; Raz et al., 2006), we additionally stained embryonic skin cryosections with a caspase-3 specific antibody, an ultimate executor caspase essential for the nuclear changes associated with apoptosis (Konstantinidou et al., 2007). We found that all epidermal keratinocytes with misshapen nuclei were negative for caspase-3 (Figure 24**a**), suggesting that alterations in the nuclear shape were dependent on mechanisms other than apoptosis. As positive control for caspase-3 antibody activity, we used cryosections prepared from adult mouse skin 19 days post-depilation, because of the presence of a large number of hair follicles entering the apoptosis-driven catagen phase of hair cycle (Figure 24**a**). Furthermore, we additionally found that the majority of cells with misshapen nuclei belonged to actively proliferating cells as demonstrated by Ki67 staining (Scholzen and Gerdes, 2000) (Figure 24**b**).

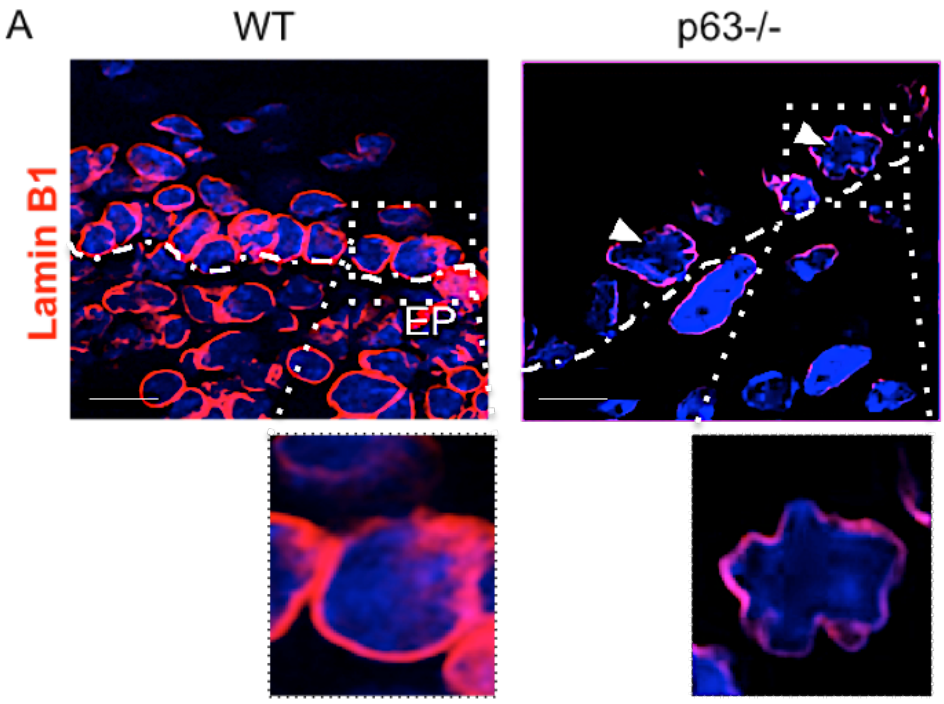

B

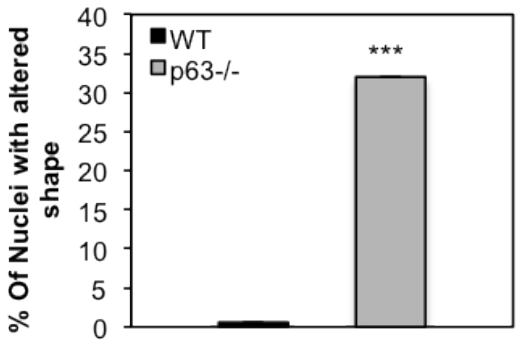

Figure 23: Nuclear shape of WT keratinocytes vs. p63-/- keratinocytes.

(A) Confocal images of basal keratinocytes nuclei of WT and p63$^{-/-}$ embryos. Nuclei were stained with 4',6-diamidino-2-phenylindole (DAPI, blue) and Lamin B1-specific antibody (red). Images were acquired with confocal microscope LSM 510 Meta (Carl Zeiss), using a 63x/1.4 plan-apochromat oil objective. p63-null keratinocytes nuclei (right) showed a lobular shape compared to controls (left). **(B) Graph with percentages of basal keratinocytes nuclei with aberrant nuclear shape in WT vs p63$^{-/-}$.** 32% of p63$^{-/-}$ basal keratinocytes displayed altered nuclear shape compared to 0.5% of WT basal keratinocytes. The statistical analysis using Peterson's Chi-square test showed a significant ($p=3x10^{-6}$) difference between the two percentages. Error bars represent SEM.

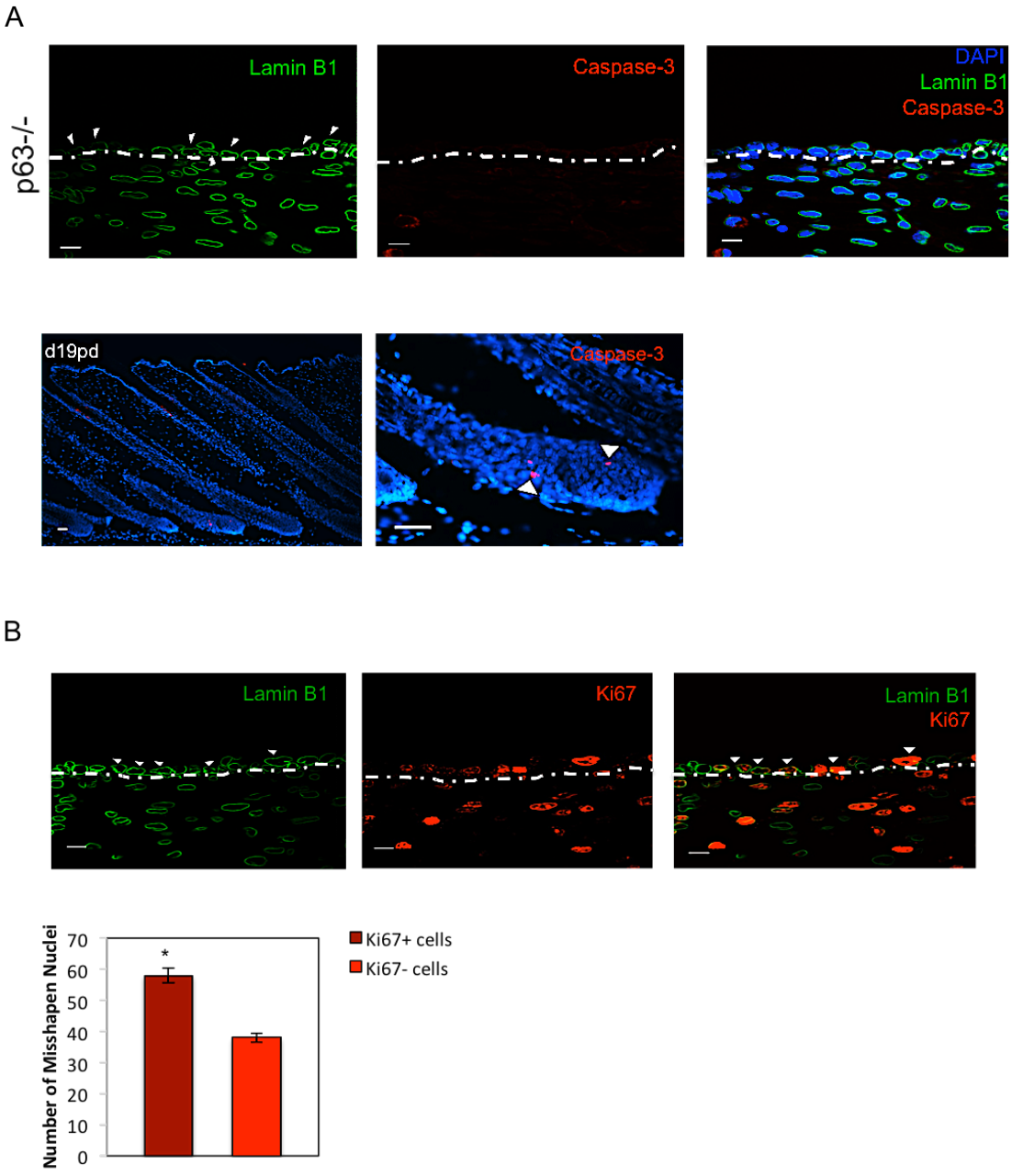

Figure 24: Analysis of apoptosis and proliferation in p63-null keratinocytes nuclei with altered shape.

Immuno-fluorescence analysis using Caspase-3 and Ki67 specific antibodies in E16.5 skin of $p63^{-/-}$ mice. **(A)** Analysis of apoptotic cells using caspase-3 specific antibody (red), showing that all keratinocytes with misshapen nuclei were negative for caspase-3. Catagen hair follicles have been used as positive control for caspase-3 antibody specificity.**(B)** Analysis of proliferation using Ki67-specific antibody (red) of keratinocytes with misshapen nuclei, showing that the majority of cells with altered nuclear morphology (n=57) were positive for this proliferation marker.

Next, we asked whether p63 knock-down using small interfering RNAs in primary keratinocytes (PMKs), isolated from wild-type mice, could also lead to defects in the nuclear shape. Cells have been transfected with p63 siRNA and control siRNA at two different concentrations, 50 nM and 100 nM, for 48 hours, fixed in 4% paraformaldehyde and stained with DAPI and Lamin B1-specific antibody (Figure 25**a**). 1395 and 1448 nuclei were counted for control siRNA and p63 siRNA treated cells respectively.

The analysis revealed that the majority of p63 siRNA-treated cells (23%) displayed nuclei with altered morphology (mean nuclear circularity= 0.85) compared to cells treated with control siRNA (3.3%) (mean nuclear circularity= 0.90) (Figure 25**b**).

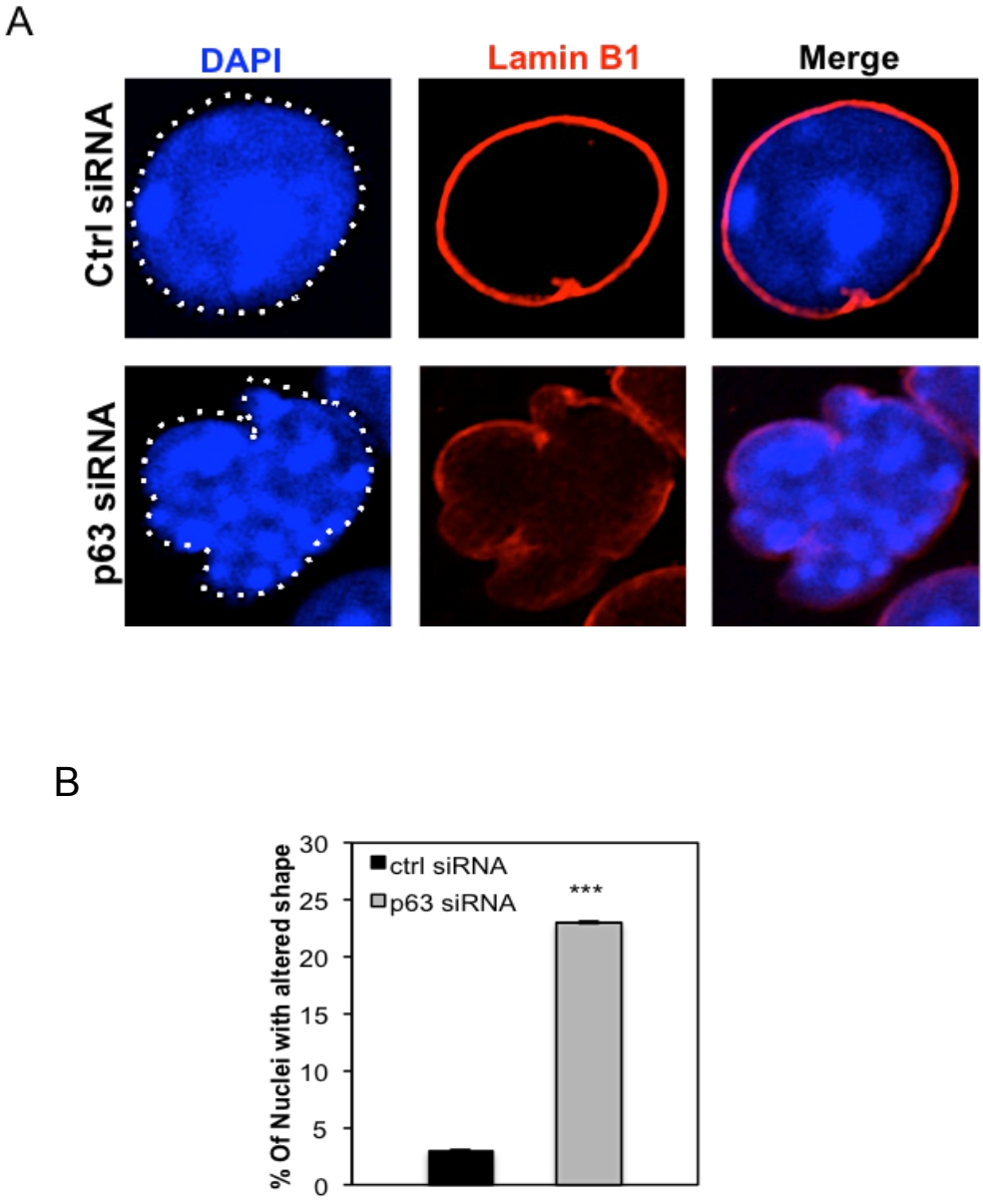

Figure 25: Analysis of the nuclear shape of ctrl siRNA treated PMKs vs. p63 siRNA treated PMKs.

(A) Confocal images of PMKs nuclei treated with ctrl siRNA and p63 siRNA. Nuclei were stained with 4',6-diamidino-2-phenylindole (DAPI, blue) and lamin B1-specific antibody (red). Images were acquired with confocal microscope LSM 510 Meta (Carl Zeiss) using a 63x/1.4 plan-apochromat oil objective. Significant high percentage of keratinocytes nuclei treated with p63 siRNA (right) showed a lobular shape compared to keratinocytes nuclei treated with ctrl siRNA (left). **B) Graph with percentages of nuclei with altered shape in ctrl siRNA treated PMKs vs. p63 siRNA treated PMKs.** 23% of p63 siRNA treated cells displayed a lobular nuclear shape compared to 3.3% of ctrl siRNA treated keratinocytes. The statistical analysis using Peterson's Chi-square test showed a significance ($p<0.0001$) difference between the two percentages. Error bars represent SEM.

1.12.1. p63 deficiency leads to decrease of the nuclear lamins expression both *in vivo* and *in vitro*

1.12.1.1. Lamin B1 and Lamin A/C expressions are reduced in p63-null epidermis

Cellular structure and nuclear architecture are integrated via links between nucleoskeleton and cytoskeleton formed via the LINC complex, able to connect nuclear lamins (Lamin A/C, Lamin B1 and Lamin B2) with cytoskeleton components (Burke and Roux, 2009; Crisp et al., 2006; Padmakumar et al., 2005; Stewart-Hutchinson et al., 2008).

Based on alterations in nuclear morphology, seen in keratinocytes from p63-deficient mice, we hypothesized that reduced expression of nuclear lamins might contribute to these changes. Indeed, previous data showed that cells lacking Lamin B1 displayed misshapen nuclei (Vergnes et al., 2004; Yang et al., 2011b) similar to those observed in p63-null keratinocytes. In addition Lamin A/C depleted murine fibroblasts also showed similar alterations in the nuclear shape (Lammerding et al., 2004).

While Lamin B1 is ubiquitously expressed during embryogenesis (Rober et al., 1989), Lamin A/C expression is developmentally regulated. However, its expression in murine epidermis starts at E15.0 (Rober et al., 1989), allowing us to perform our analyses on E16.5 $p63^{-/-}$ embryos and age-matched WT controls.

Our qRT-PCR analysis using RNA, isolated from embryonic laser captured micro-dissected epidermis from WT and $p63^{-/-}$ mice, showed significant reduction ($p=0.05$) of Lamin B1 transcript (Figure 26**a**) and a significant ($p=0.002$) increase of Lamin A/C transcript in $p63^{-/-}$ embryonic epidermis in comparison to WT control (Figure 26**b**).

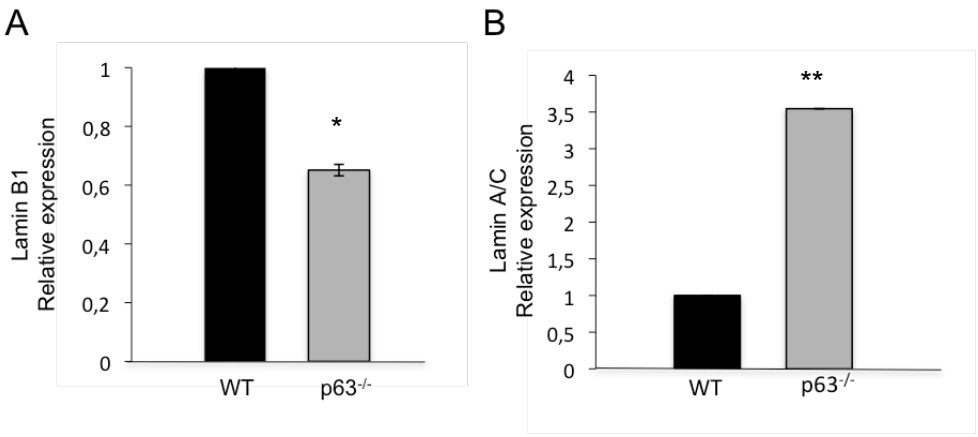

Figure 26: Relative expression of Lamin B1 and Lamin A/C in WT and p63-/- embryonic epidermis.

Primers for both Lamin B1 and Lamin A/C mRNA were designed using the Beacon Designer Software and Real-Time PCR reactions were performed. *Gapdh* gene was used as normalizer and error bars represent SEM. Four independent experiments were run in duplicate. **(A)** Significant downregulation (p=0.05) of Lamin B1 mRNA in $p63^{-/-}$ embryonic epidermis compared to WT control was observed. **(B)** Significant upregulation (p=0.002) of Lamin A/C mRNA in $p63^{-/-}$ embryonic epidermis compared to WT control was observed.

However, when the qRT-PCR analysis was performed using RNA extracted from the whole E16.5 $p63^{-/-}$ and WT embryos, no significant change in Lamin A/C expression was observed (Figure 27**a**), while Lamin B1 remained significantly reduced (p=0.006) in $p63^{-/-}$ embryos compared to WT controls (Figure 27**b**).

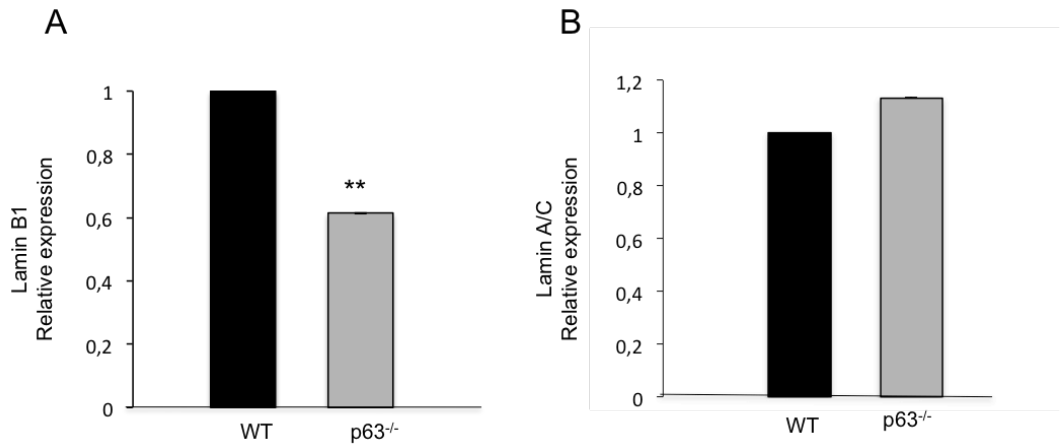

Figure 27: Relative expression of Lamin B1 and Lamin A/C in the whole p63-/- and WT embryos.

Primers for both Lamin B1 and Lamin A/C mRNA were designed using the Beacon Designer Software and Real-Time PCR reactions were performed. *Gapdh* was used as normalizer and error bars represent SEM. Four independent experiments were run in duplicate. **(A)** Relative expression of Lamin A/C mRNA with no significant change (p=0.11) between $p63^{-/-}$ and the WT control. **(B)** Relative expression of Lamin B1 mRNA in the whole $p63^{-/-}$ and WT control embryos. A significant (p=0.006) downregulation of Lamin B1 mRNA has been observed in $p63^{-/-}$ embryo compared to WT control.

To test whether the reduction of Lamin B1 mRNA led to a reduction in its protein level, we performed immuno-fluorescence analysis, using Lamin B1 specific antibody on E16.5 $p63^{-/-}$ embryonic cryosections and on age-matched WT controls. Our data showed significant reduction of Lamin B1 expression in p63-null epidermis, compared to WT controls (Figure 28**a**).

In addition our immuno-fluorescence analysis unexpectedly showed a reduction of the Lamin A/C protein in p63-null epidermis in comparison to WT controls (Figure 28**b**).

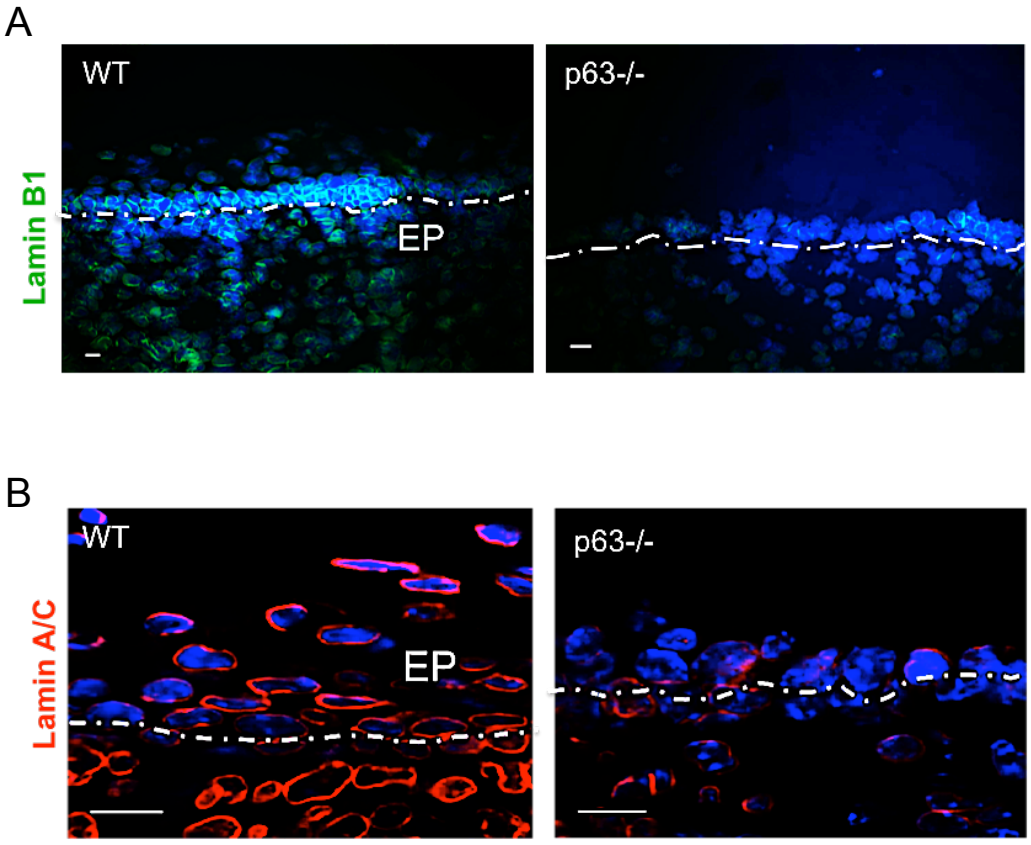

Figure 28: Fluorescence microscope images of p63-/- and WT embryonic skin after immuno-fluorescence staining using Lamin B1 and Lamin A/C-specific antibodies.

(A) Nuclei were stained with 4',6-diamidino-2-phenylindole(DAPI, blue), while Lamin B1 was stained with secondary antibody labelled with Fluorescein isothiocyanate (FITC, green). Images were acquired using the Fluorescence Microscope Eclipse 50i (Nikon), using the 40X/0.75 plan-fluor objective. **(B)** Nuclei were stained with 4',6-diamidino-2-phenylindole (DAPI, blue), while Lamin A/C was stained with secondary antibody labelled with Indocarbocyanine 3 (Cy3, red). Images were acquired with the laser scanning confocal microscope LSM 510 Meta (Carl Zeiss) using a 63x/1.4 plan-apochromat oil objective and a 2X zoom.

1.12.1.2. Lamin B1 and Lamin A/C expressions are decreased after p63 knock-down in wild-type keratinocytes

Next, we asked whether the observed defects in the nuclear morphology of primary mouse keratinocytes after p63 ablation by RNA interference experiments, were also associated with reduction of nuclear lamins expression.

To test this hypothesis we test by qRT-PCR analyses Lamin B1 and Lamin A/C expression after 48 hours of treatment with p63 siRNA at two different concentrations and compared them to cells treated with control siRNA.

The analyses showed a significant reduction of both Lamin B1 and Lamin A/C in primary mouse keratinocytes treated with p63 siRNA in comparison to keratinocytes treated with control siRNA (

Figure 29).

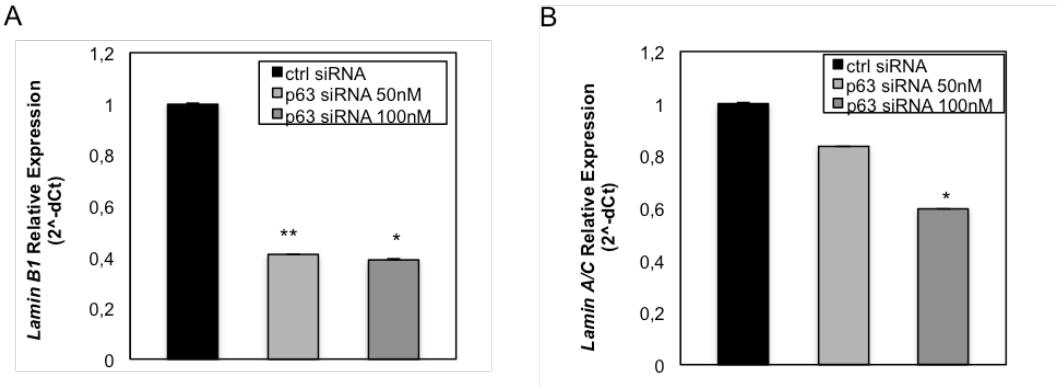

Figure 29: qRT-PCR analysis of Lamin B1 and Lamin A/C after transfection of PMKs with p63 siRNA and control siRNA.

Primary Mouse Keratinocytes have been transfected with two different contentrations of p63 siRNA (50 nM and 100 nM) and control siRNA and incubated for 48 hours. Primers specific for Lamin B1 and Lamin A/C have been used for the qRT-PCR analysis and two independent experiments have been run in duplicate. T-test results with a p-value ≤0.05 have been considered as significant. Error bars represent SEM.

1.12.2. Expressions of the components of the LINC complex are decreased in p63-null embryonic epidermis

Nuclear lamins are not the only components involved in the maintenance of nuclear integrity and nuclear positioning, so we speculated that other components of the nuclear membrane might also be affected in p63-null keratinocytes.

We asked, therefore, whether the expressions of LINC complex-associated proteins, Suns and Nesprins, are also affected in p63-null epidermis.

Sun-1 is the major protein of the LINC complex, which is important for Nesprins localization on the ONM (Padmakumar et al., 2005) and for the formation of synaptic nuclei (Lei et al., 2009). This suggests its requirement for cellular integrity maintenance during development. Based on these observations we first decided to test Sun-1 expression by qRT-PCR using p63-null embryonic epidermis and we showed a significant ($p=0.002$) reduction of Sun-1 in p63-null epidermis compared to WT control (Figure 30).

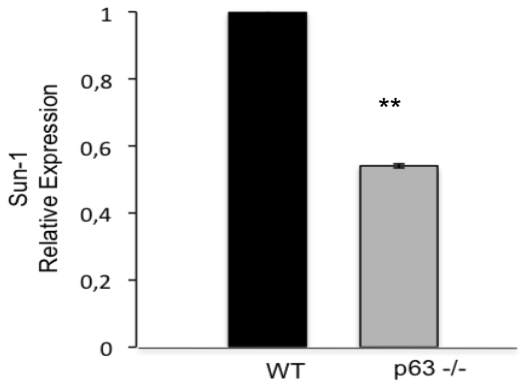

Figure 30: Relative expression of Sun-1 in the embryonic epidermis of p63-/- mice and WT controls.

(A) Primers for Sun-1 mRNA were designed using the Beacon Designer Software and a Real-Time PCR reaction was performed. *Gapdh* gene was used as normalizer and error bars represent SEM. Two independent experiments were run in duplicate. A significant (p=0.002) downregulation of Sun-1 mRNA in $p63^{-/-}$ epidermis compared to WT control has been observed.

Interestingly, immuno-fluorescence analysis on embryonic quick frozen cryosections of $p63^{-/-}$ and corresponding WT controls also showed a reduction of Sun-1 in p63-null keratinocytes (Figure 31).

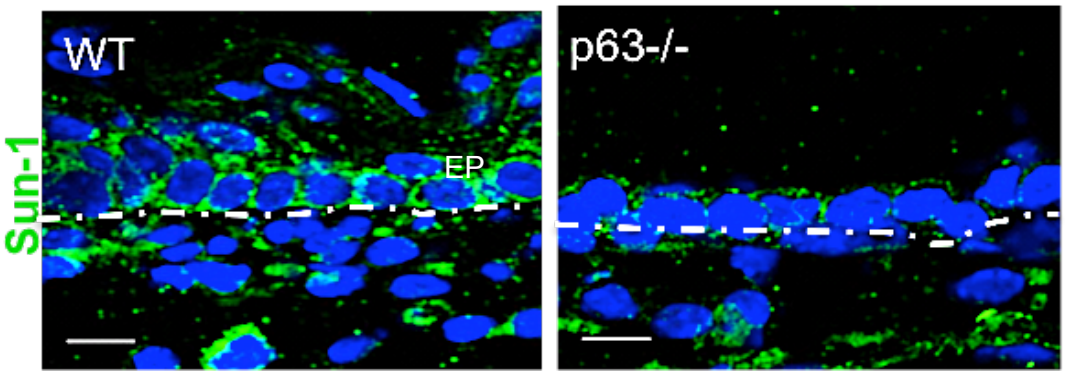

Figure 31: Immuno-fluorescence analysis using Sun-1 specific antibody in WT and p63-/- embryonic cryosections.

Nuclei were stained with 4',6-diamidino-2-phenylindole(DAPI, blue), while Sun-1 was stained with secondary antibody labelled with Fluorescein isothiocyanate (FITC, green). Images were acquired with the laser scanning confocal microscope LSM 510 Meta (Carl Zeiss), using a 63x/1.4 plan-apochromat oil objective and a 2X zoom.

Sun-1 is able to bind all three Nesprins, which have a selective binding for different cytoskeleton components: Nesprin-1 giant and Nesprin-2 giant bind to actin filaments via their actin binding domain (Padmakumar et al., 2005), while Nesprin-3 binds the versatile cytolinker Plectin via the Plectin binding domain (Wilhelmsen et al., 2005). Nesprin-3 has been shown to be essential for the maintenance of cell shape and perinuclear cytoskeleton architecture in endothelial cells (Morgan et al., 2011), as well as for keratin organization around the nucleus of Zebrafish epidermal cells (Postel et al., 2011). In addition, Lamin A/C depletion was responsible for Nesprin-3 redistribution from the nuclear envelope (NE) to the endoplasmic reticulum (ER), which resulted in disrupted attachment of the cytoskeletal components to the NE (Hale et al., 2008; Houben et al., 2009).

Taken together, these observations suggested Nesprin-3 as a good candidate for further analyses. Indeed, qRT-PCR experiments showed a significant decrease of Nesprin-3 transcript in p63-null epidermis, in comparison to WT controls (Figure 32).

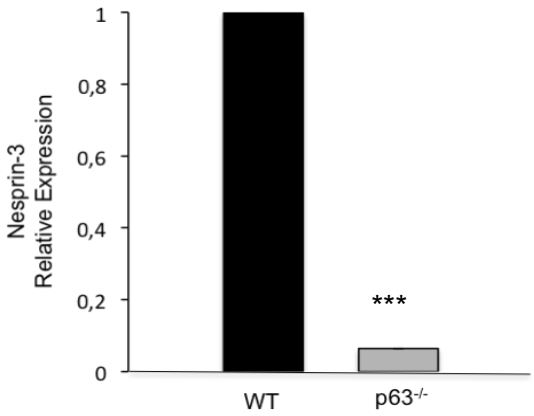

Figure 32: Relative expression of Nesprin-3 mRNA in the embryonic epidermis of p63-/- mice and WT controls.

(A) Primers for Nesprin-3 mRNA were designed using the Beacon Designer Software and a Real-Time PCR reaction was performed. *Gapdh* gene was used as normalizer and error bars represent SEM. Four independent experiments were run in duplicate. Relative expression of Nesprin-3 in embryonic epidermis of both $p63^{-/-}$ and WT control. A significant downregulation ($p=0.003$) of Nesprin-3 mRNA in $p63^{-/-}$ epidermis has been observed compared to the WT control.

Furthermore, the immuno-fluorescence experiments using Nesprin-3-specific antibody on $p63^{-/-}$ embryonic cryosections showed a significant reduction of the protein in p63-null keratinocytes compared to WT controls (Figure 33).

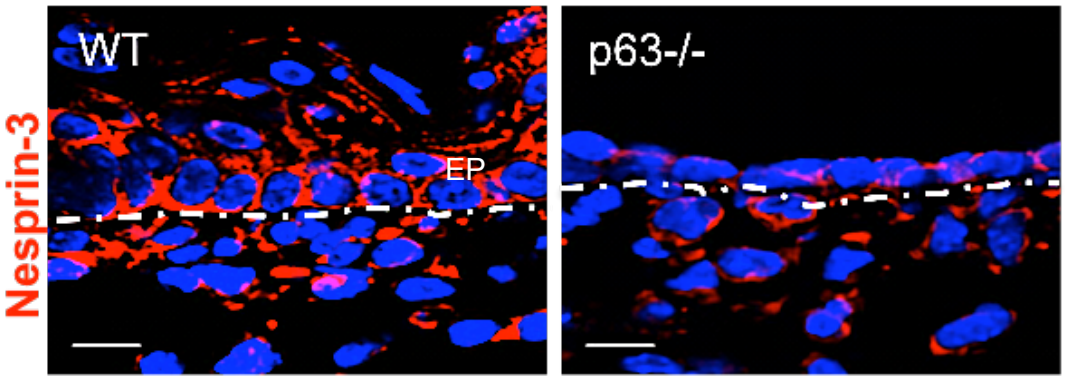

Figure 33: Immuno-fluorescence analysis using Nesprin-3-specific antibody in WT and p63-/- embryonic cryosections.

Nuclei were stained with 4',6-diamidino-2-phenylindole(DAPI, blue), while Nesprin-3 was stained with secondary antibody labelled with Indocarbocyanine 3 (Cy3, red). Images were acquired with the laser scanning confocal microscope LSM 510 Meta (Carl Zeiss), using a 63x/1.4 plan-apochromat oil objective and a 2X zoom.

1.12.2.1. Sun-1 and Nesprin-3 expressions are decreased after p63 knock-down in wild-type keratinocytes in vitro

Next, we asked whether Sun-1 and Nesprin-3 expression was also affected by p63 knock-down in primary mouse keratinocytes using RNA interference experiments. We, therefore, collected RNA from PMKs treated for 48 hours with p63 siRNA and control siRNA and analysed Sun-1 and Nesprin-3 expression by qRT-PCR.

Interestingly, p63 siRNA treated cells showed significant decreased expression of both nuclear envelope-associated components compared to cells treated with control siRNA (Figure 34).

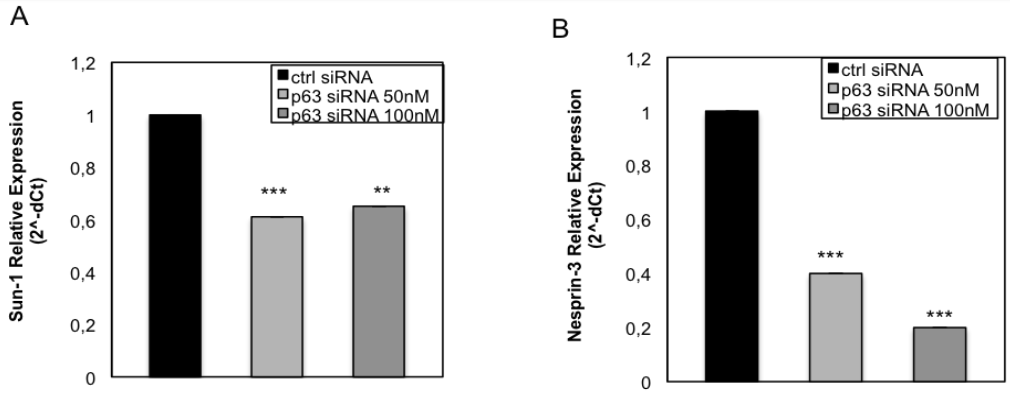

Figure 34: qRT-PCR analysis of Sun-1 and Nesprin-3 after transfection of PMKs with p63 siRNA and control siRNA.

Primary Mouse Keratinocytes have been transfected with two different contenrations of p63 siRNA (50 nM and 100 nM) and control siRNA and incubated for 48 hours. Primers specific for Sun-1 and Nesprin-3 have been used for the qRT-PCR analysis and two independent experiments have been run in duplicate. T-test results with a p-value ≤0.05 have been considered as significant. Error bars represent SEM.

1.12.3. The expression of the cytoskeleton linker Plectin is decreased in p63-null epidermis

The cytolinker Plectin is an essential protein, mediating the link between cytoskeleton components and nuclear envelope and Plectin ablation in both human and mouse has been linked to several skin defects, included the appearence of epidermal fragility and severe skin lesions (Ackerl et al., 2007). Furthermore, Plectin has been found to be associated with hemidesmosomal integrin subunit β4 and cytokeratin intermediate filaments in basal epidermal keratinocytes (Nievers et al., 2000; Rezniczek et al., 1998), which are reduced upon p63 ablation (Carroll et al., 2006; Romano et al., 2009), thus suggesting Plectin as another good candidate for further analysis.

First, we decided to analyze Plectin expression by qRT-PCR, using primers, detecting all Plectin isoforms in p63-null mice versus WT controls. When RNA extracted from total embryos was used, no significant change ($p=0.60$) in its expression between $p63^{-/-}$ and WT embryos was shown (Figure 35**a**). However, when laser captured micro-dissected epidermis has been used, a significant reduction of Plectin expression ($p=0.05$) has been shown in p63-null epidermis compared to WT controls (Figure 35**b**).

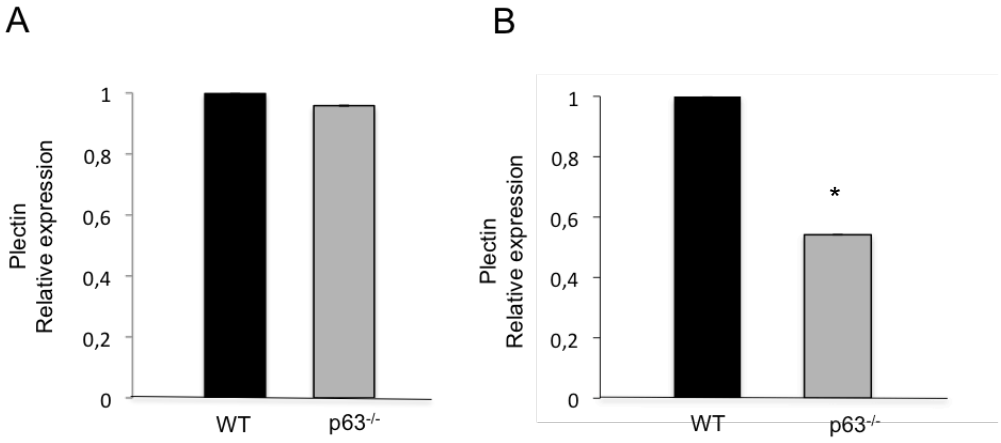

Figure 35: Relative expression of Plectin in the whole embryos and in the embryonic epidermis of both p63-/- and WT controls.

Primers for all Plectin isoforms mRNAs were designed using the Beacon Designer Software and a Real-Time PCR reaction was performed. GAPDH gene was used as normalizer and error bars represent SEM. Four independent experiments were run in duplicate**.(A)** Relative expression of Plectin mRNA in the whole embryo of both $p63^{-/-}$ and WT control with no significant change (p=0.60) in its expression. **(B)** Relative expression of Plectin mRNA in the embryonic epidermis of both $p63^{-/-}$ and WT control. A significant downregulation (p=0.05) of Plectin mRNA in $p63^{-/-}$ embryonic epidermis has been observed compared to WT control.

Additionally, our immuno-fluorescence analysis on $p63^{-/-}$ and WT embryonic cryosections showed a significant reduction of Plectin in the epidermis of p63-null embryos compared to WT controls (Figure 36).

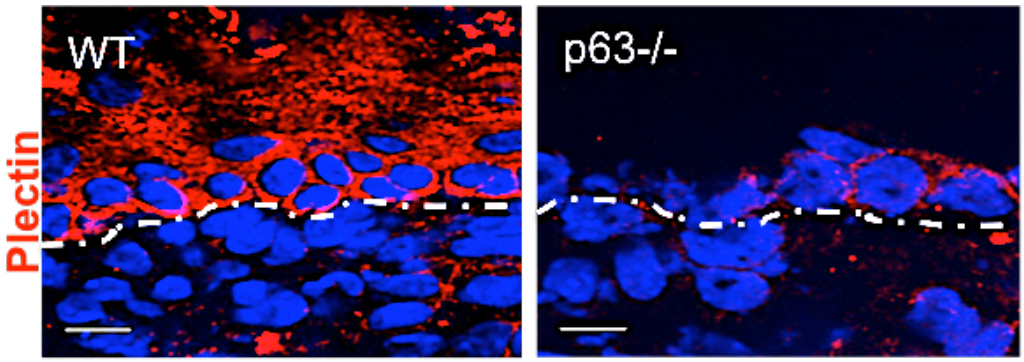

Figure 36: Immuno-fluorescence analysis using Plectin specific antibody in WT and p63-/- embryonic cryosections.

Nuclei were stained with 4',6-diamidino-2-phenylindole(DAPI, blue), while Plectin was stained with secondary antibody labelled with Indocarbocyanine 3 (Cy3, red). Images were acquired with the laser scanning confocal microscope LSM 510 Meta (Carl Zeiss), using a 63x/1.4 plan-apochromat oil objective and a 2X zoom.

1.12.4. p63 transcription factor is enriched on *Plectin 1c*, *Sun-1* and *Nesprin-3* gene promoter regions

Because Sun-1, Nesprin-3 and Plectin mRNA levels were lower in p63-null epidermis compared to the corresponding WT controls (Figure 37), we speculated that their reduction might contribute to the epidermal defects associated with p63-null phenotype. We therefore decided to test by ChIP-qPCR assay *Sun-1*, *Nesprin-3* and *Plectin* promoter regions for p63 binding, followed by qPCR analysis, using primers for different regions on the promoters of *Plectin, Sun-1* and *Nesprin-3* at distinct distances from their respective transcription start sites.

Because of the presence of 15 different *Plectin* isoforms, each regulated by a different promoter (Fuchs et al., 1999), we decided to select *Plectin 1c* isoform for our analysis, the most abundant isoform expressed in murine keratinocytes (Andra et al., 2003).

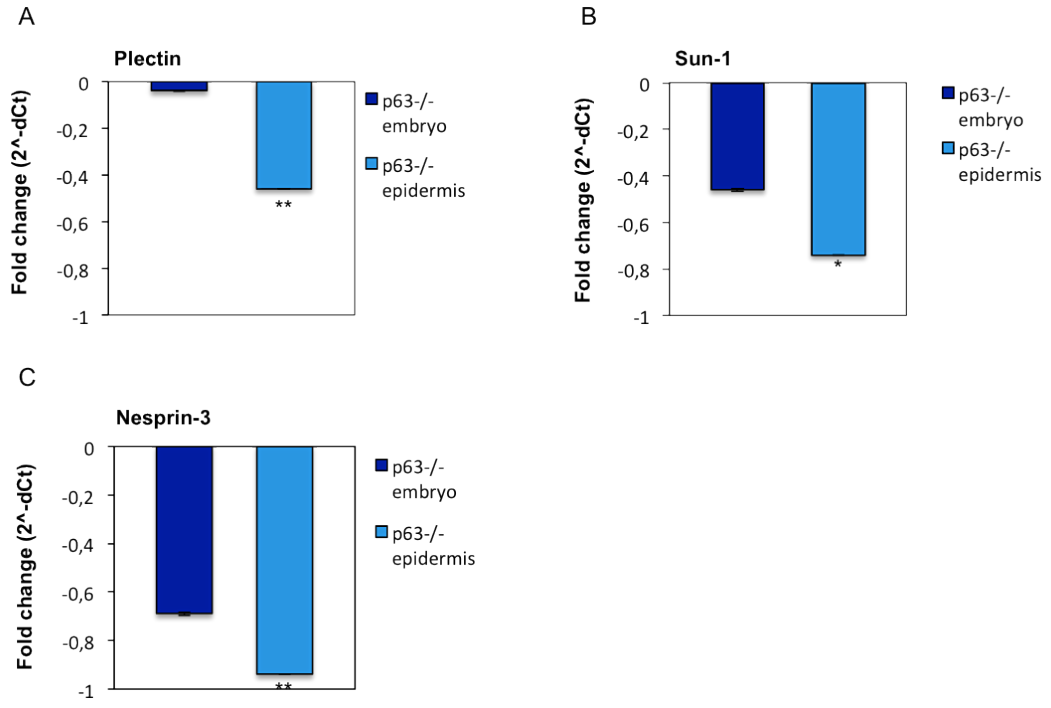

Figure 37: Nuclear envelope-associated genes and the cytolinker Plectin are specifically reduced in p63-null embryonic epidermis when compared to the corresponding p63-/- embryos.

Real-Time PCR analysis for Plectin **(A)**, Sun-1 **(B)** and Nesprin-3 **(C)** in E16.5 $p63^{-/-}$ embryos compared to age-matched p63-null epidermis, normalized to the corresponding levels in age-matched WT mice and epidermis respectively. GAPDH was used as normalizer and error bars represent SEM.

Interestingly, a significant (p=0.003) enrichment of p63 binding to DNA-containing p63 consensus sequences was observed in the upstream region at -4000 bp (p=0.05) from the *Plectin 1c* transcription start site. Significant p63 enrichment was also observed for *Nesprin-3* and *Sun-1* consensus sequences in the upstream regions at 900 bp (p=0.05) and 4000 bp (p=0.05) respectively, suggesting them as p63 transcriptional direct targets. *Claudin-1*, an established p63 direct target (Lopardo et al., 2008), has been used as positive control, while intergenic regions on chromosome 8 served as negative control for this assay (Figure 38).

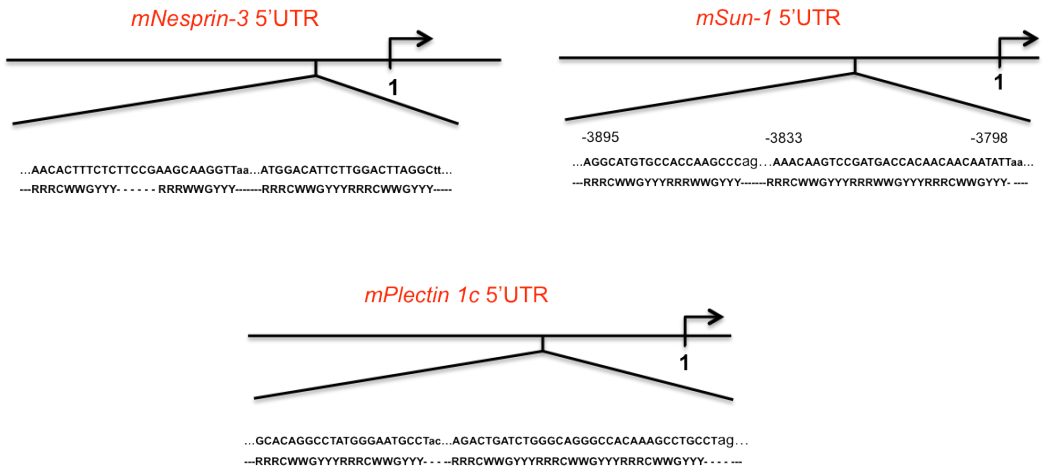

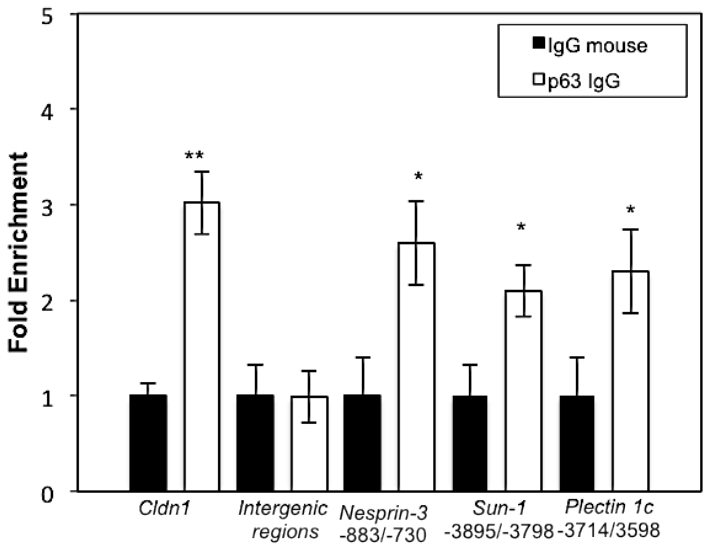

Figure 38: ChiP-quantitative PCR analysis of different promoter regions of *Nesprin-3*, *Sun-1* and *Plectin 1c* isoform.

Adult keratinocytes isolated from adult mice and fixed in 4% Formaldehyde were processed for ChIP assay with an antibody against p63 protein or purified mouse IgG. The uppercase letters of the sequence show the p63 putative binding sites in the promoter region of *Nesprin-3, Sun-1* and *Plectin 1c* genes chosen for the quantitative PCR analysis after ChIP. The promoter region of *Cldn 1* was used as positive control, while the Intergenic regions on the chromosome 8 served as negative control for this assay. The input levels of unprecipitated chromatin DNA were used as loading controls. Error bars represent SEM, and five independent experiments were run in triplicate.

1.12.5. Alterations in nuclear morphology are linked to the changes in gene expression in p63-null keratinocytes

1.12.5.1. Alterations in the distribution patterns of repressive histone modifications H3K27me3 and H3K9me3 in p63-null epidermal keratinocytes

Since several decades it has been shown that proper connections between nucleoskeleton and cytoskeleton play an essential role in driving forces for chromatin movements inside the nucleus (Dechat et al., 2010). In this context nuclear lamins have been shown to be essential for chromatin organization and gene expression regulation (Dechat et al., 2008). In *LMNA-/-* mice, loss of chromatin integrity associated with nuclear deformations was shown (Sullivan et al., 1999). In addition, Lamin B1 down-regulation resulted in the formation of microdomains characterized by the absence of heterochromatin (Shimi et al., 2008).

Therefore, reduction of both Lamin B1 and Lamin A/C expressions in p63-null keratinocytes led us to further investigate whether heterochromatin distribution was also affected in these cells.

$p63^{-/-}$ and WT embryonic cryosections were stained with anti-H3K27me3 and H3K9me3 specific antibodies and basal epidermal keratinocytes in both samples were analysed for the distribution of these repressive histone modifications. Previous data showed that absence of Lamin A/C in dermal fibroblasts was accompanied by altered distribution of H3K27me3 and H3K9me3 in these cells (Shumaker et al., 2006).

Analysis of the fluorescence distribution of H3K27me3 throughout the entire nuclear surface, performed using ImageJ plugin “plot profile”, revealed a global decrease of this repressive histone modification and loss of its

peripheral localization in p63-null keratinocytes nuclei compared to controls (Figure 39).

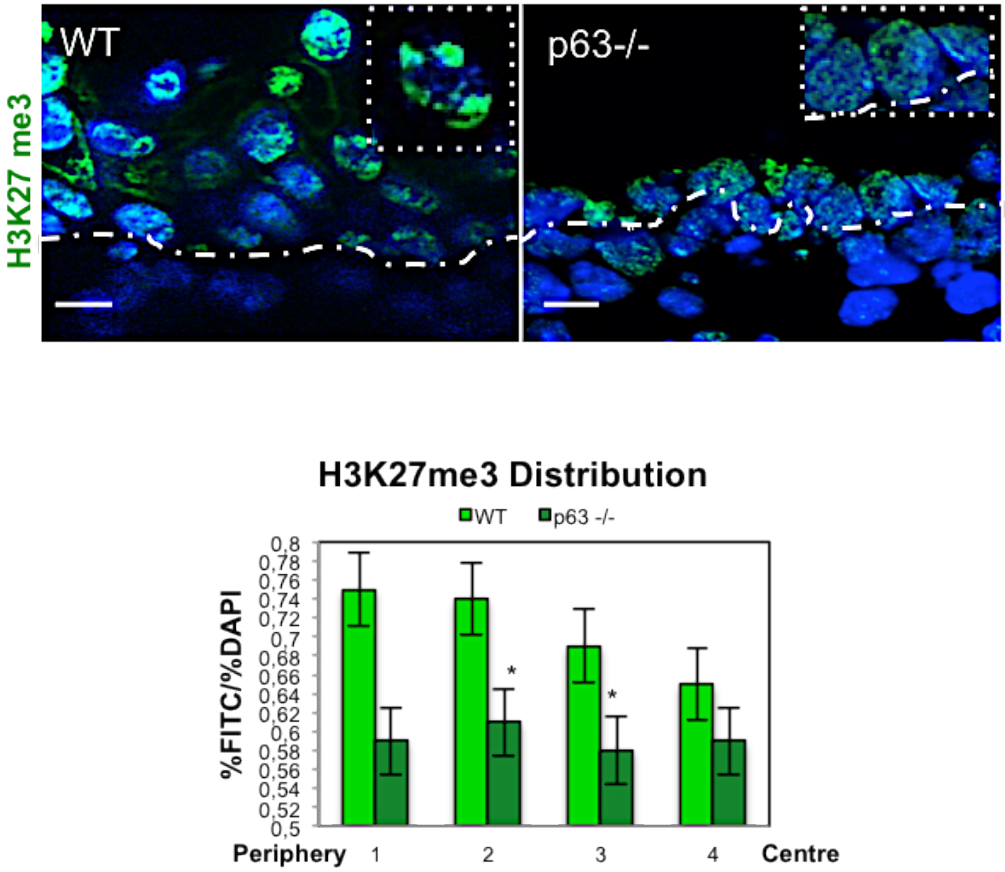

Figure 39: Immuno-fluorescence analysis using H3K27me3-specific antibody in WT and p63-/- embryonic cryosections.

Nuclei were stained with 4',6-diamidino-2-phenylindole(DAPI, blue), while H3K27me3 was stained with secondary antibody labelled with Fluorescein Isothiocyanate (FITC, green). Images were acquired with the laser scanning confocal microscope LSM 510 Meta (Carl Zeiss), using a 63x/1.4 plan-apochromat oil objective and a 2X zoom. The analysis of the distribution of fluorescence has been performed using ImageJ plugin “plot profile”. Marked decrease of the repressive histone modification H3K27me3 and a significant (p-value=0.006) loss of its peripheral distribution was observed in p63-null keratinocytes.

Analysis of the H3K9me3 histone modification associated with pericentromeric heterochromatin (Peters et al., 2003) showed alterations in its

distribution patterns and significant increase of H3K9me3 foci at the nuclear interior of p63-null keratinocytes compared to controls (Figure 40).

More detailed analysis of H3K9me3 foci revealed that they were more numerous (average foci/nucleus=12) and smaller in size in p63-null nuclei compared to controls (average foci/nucleus=8) (Figure 40).

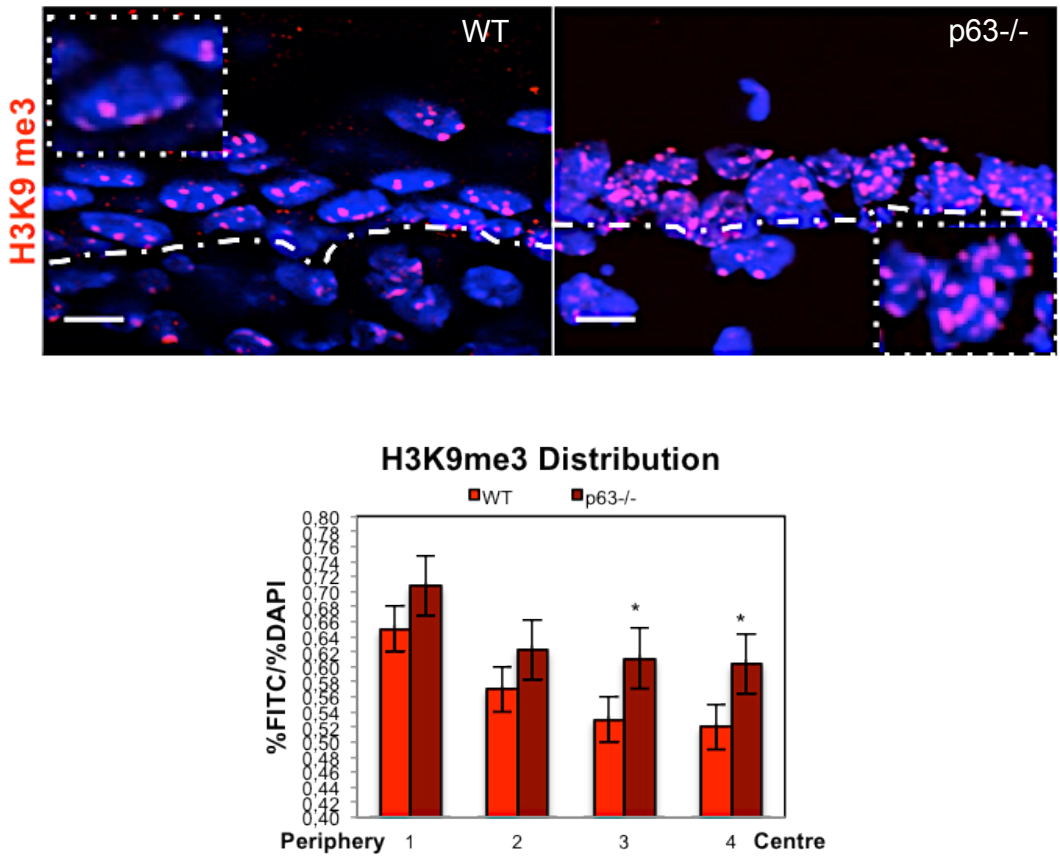

Figure 40: Immuno-fluorescence analysis using H3K9me3-specific antibody in WT and p63-/- embryonic cryosections.

Nuclei were stained with 4',6-diamidino-2-phenylindole(DAPI, blue), while H3K9me3 was stained with secondary antibody labelled with Indocarbocyanine 3 (Cy3, red). Images were acquired with the laser scanning confocal microscope LSM 510 Meta (Carl Zeiss), using a 63x/1.4 plan-apochromat oil objective and a 2X zoom. The analysis of the fluorescence distribution has been performed using ImageJ plugin “plot profile”. Altered distribution pattern of H3K9me3 with significant increase of its internal distribution (p-value=0.03) was observed in p63-null keratinocytes.

In line with these observations we also found reduced expression of heterochromatin 1α (HP1α), an established interacting partner of H3K9me3, responsible for pericentromeric heterochromatin organization and clustering (Jones et al., 2000), in p63-null keratinocytes compared to WT controls (Figure 41).

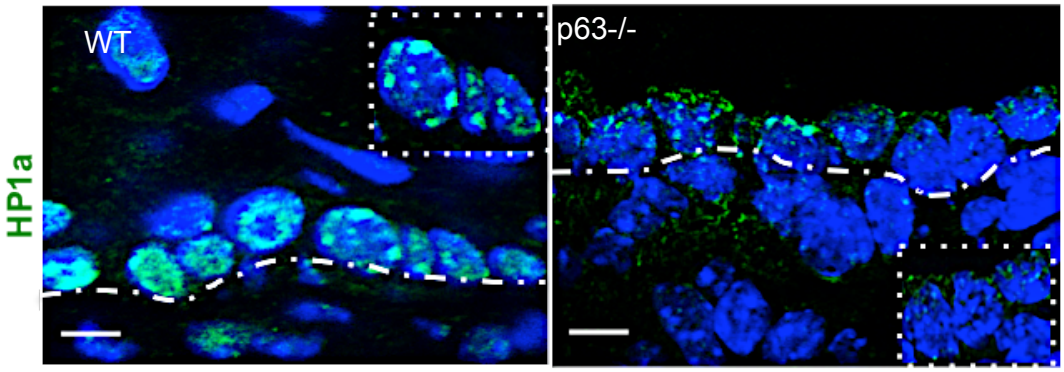

Figure 41: Immuno-fluorescence analysis using HP1α -specific antibody in WT and p63-/- embryonic cryosections.

Nuclei were stained with 4',6-diamidino-2-phenylindole (DAPI, blue), while HP1α was stained with secondary antibody labelled with Fluorescein Isothiocyanate (FITC, green). Images were acquired with the laser scanning confocal microscope LSM 510 Meta (Carl Zeiss), using a 63x/1.4 plan-apochromat oil objective and a 2X zoom. A marked decrease of HP1α has been observed in p63-null keratinocytes compared to WT controls.

Interestingly, when p63-null keratinocytes nuclei with altered shape were compared to p63-null keratinocyte nuclei with normal shape, a redistribution of H3K27me3 from the nuclear periphery to the centre was observed in misshapen nuclei (Figure 42**a**) with significant decrease of this repressive histone modification at the nuclear periphery.

With respect to H3K9me3 distribution, a global reduction of the immunostaining throughout the nucleus has been observed in p63-null keratinocytes with misshapen nuclei in comparison to normally shaped p63-null nuclei (Figure 42**b**).

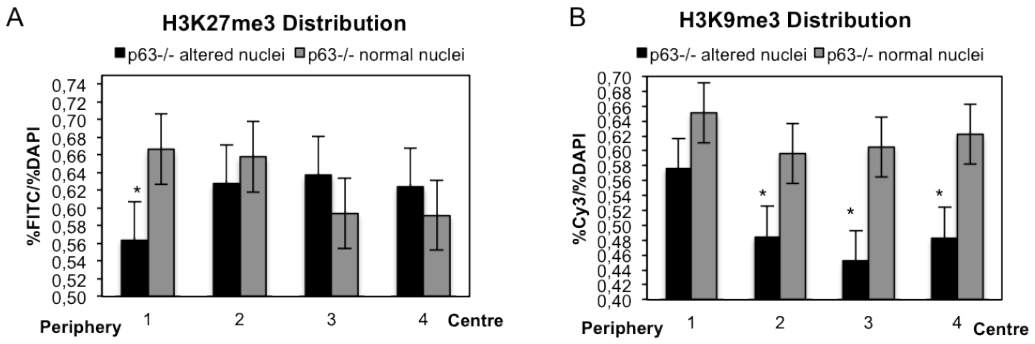

Figure 42: Alterations in the distribution patterns of repressive histone marks, H3K27me3 and H3K9me3 specifically in p63-null keratinocytes nuclei with altered shape.

(A) Analysis of the distribution of repressive histone modifications H3K27me3 and H3K9me3 in p63-null keratinocytes nuclei with normal and altered shape, showing significant (p-value=0.05) decrease of H3K27me3 at the periphery of p63-null keratinocytes nuclei with altered shape in comparison to p63-null normally shaped nuclei. **(B)** With respect to H3K9me3, a global significant reduction (p-value=0.05) in p63-null nuclei with altered shape in comparison to p63-null normally shaped keratinocytes nuclei was shown.

1.12.5.2. Ezh2 expression is decreased in p63-null mice compared to WT controls

Polycomb proteins were first identified in *Drosophila Melanogster Melanogaster* as repressors of *Hox genes*, thereby preserving body pattern along the anterior-posterior axis. In mammals they also regulate cell-cycle and they are involved in cancer development (Sparmann and van Lohuizen, 2006)

PcG proteins are classified into two groups on the basis of their association with different classes of multimeric complexes termed Polycomb Repressive Complexes (PRCs), PRC2 and PRC1. The first one is responsible for the deposition of the repressive histone modification H3K27me3 on histone tails; the second one is responsible for the recognition of H3K27me3 and chromatin silencing through different mechanisms (Sparmann and van Lohuizen, 2006)

Since the expression of H3K27me3 and nuclear lamins were decreased in p63-null epidermis, we have investigated whether Ezh2, catalytical

component of PRC2 responsible for the deposition of H3K27me3, was reduced in p63-null epidermis. Recent studies showed the reduced expression of Ezh2 in Lamin A/C depleted cells (Shumaker et al., 2006), suggesting that alterations in nuclear lamina structure might be linked with Ezh2 expression.

Indeed, qRT-PCR experiments showed a significant (p=0.006) reduction of Ezh2 in $p63^{-/-}$ embryonic epidermis compared to WT control (Figure 43).

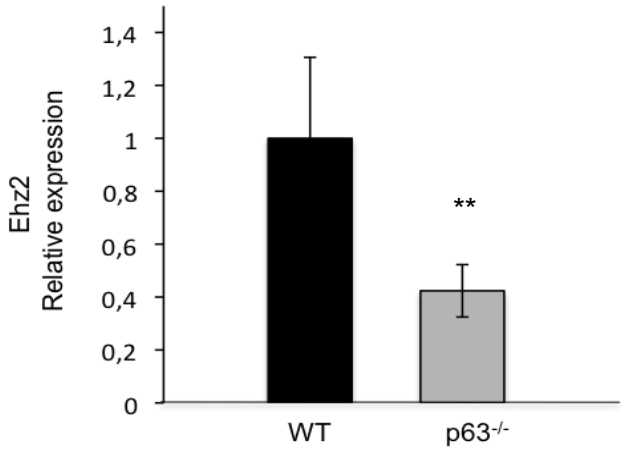

Figure 43: Relative expression of Ezh2 mRNA in the embryonic epidermis of the p63-/- mice and the WT controls.

(A) Primers for Ezh2 cDNA were designed using the Beacon Designer Software and a Real-Time PCR reaction was performed. *Gapdh* gene was used as normalizer and error bars represent SEM. Four independent experiments were run in duplicate. A significant downregulation (p=0.006) of Ezh2 mRNA in $p63^{-/-}$ epidermis has been observed compared to WT control.

To investigate whether the reduced Ezh2 mRNA level in p63-null epidermis is accompanied by the decrease of Ezh2 protein level, we additionally performed immuno-fluorescence experiments on $p63^{-/-}$ and WT skin cryosections, which showed a reduction of Ezh2 in p63-null keratinocytes compared to WT controls (Figure 44).

These data suggest that Ezh2 might contribute to the changes in heterochromatin distribution in the nuclei with abnormal shape in the epidermis of p63 knock-out mice.

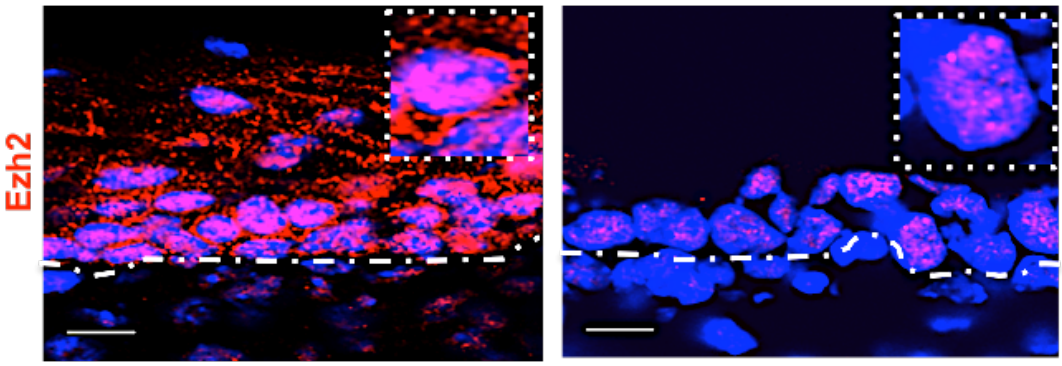

Figure 44: Confocal microscope images of immuno-fluorescence experiments on p63-/- and WT embryonic cryosections with Ezh2-specific antibody.

Nuclei were stained with 4',6-diamidino-2-phenylindole(DAPI), while Ezh2 was stained with secondary antibody labelled with Indocarbocyanine (Cy3, red). Images were acquired with the laser scanning confocal microscope LSM 510 Meta (Carl Zeiss), using a 63x/1.4 plan-apochromat oil objective and a 2X. A downregulation of Ezh2 was observed in $p63^{-/-}$ embryo compared to WT control.

1.12.6. Decreased expression of PRC1 components in p63-null epidermis

1.12.6.1. Cbx4, Cbx6 and Cbx8 but not Cbx7 are reduced in p63-null epidermis

The repressive histone modification H3K27me3 is important, although not essential, for the recruitment of PRC1, which is able to recognize H3K27me3 histone modification via the chromodomain of the mammalian Cbx proteins and to repress transcription through several possible mechanisms (Sparmann and van Lohuizen, 2006).

Preliminary data obtained in our lab by using ChIP-qPCR assay and luciferase reporter assay, showed that p63 is able to directly regulate Cbx4 transcription (data not shown). Consistently with these data, qRT-PCR analysis on p63-null epidermis and corresponding WT controls together with immuno-fluorescence experiments, showed a significant reduction of Cbx4 transcripts and protein expression in p63-null epidermis in comparison to WT control (Figure 45).

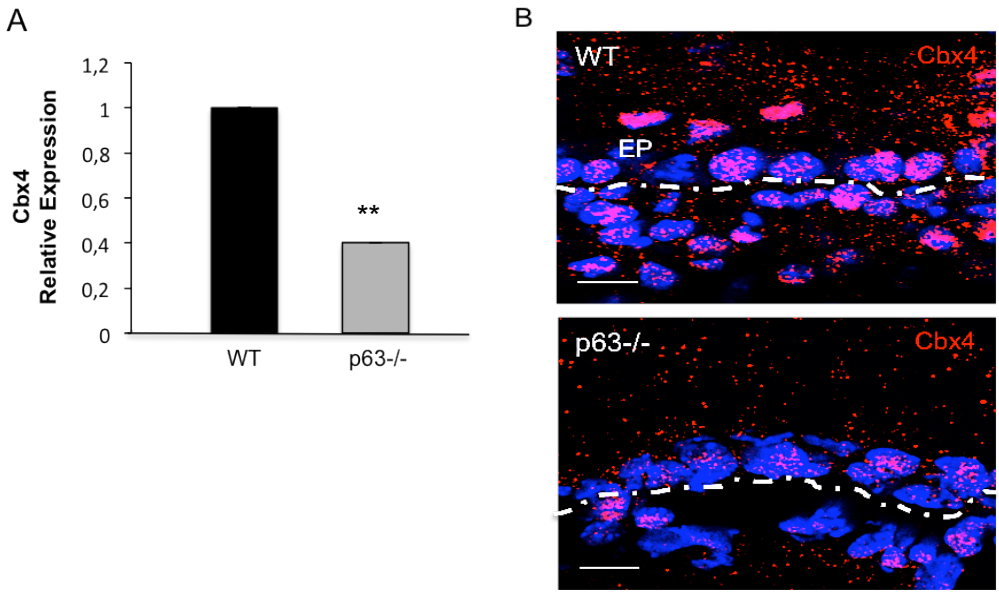

Figure 45: qRT-PCR and immuno-fluorescence analyses of Cbx4 in WT and p63-null embryonic epidermis.

(A) Primers for Cbx4 cDNA were designed using the Beacon Designer Software and a Real-Time PCR reaction was performed. *Gapdh* gene was used as normalizer and error bars represent SEM. Four independent experiments were run in duplicate. A significant reduction ($p=0.004$) of Cbx4 mRNA in $p63^{-/-}$ epidermis has been observed compared to WT controls. **(B)** Nuclei were stained with 4',6-diamidino-2-phenylindole(DAPI), while Cbx4 was stained with secondary antibody labelled with Indocarbocyanine (Cy3, red). Images were acquired with the laser scanning confocal microscope LSM 510 Meta (Carl Zeiss), using a 63x/1.4 plan-apochromat oil objective and a 2X zoom. A reduction of Cbx4 was observed in $p63^{-/-}$ embryonic epidermis compared to WT control.

Recent studies showed the existence of different functional PRC1 variants with the incorporation of different Cbx proteins (Morey et al., 2012). Based on these data, we decided to test whether other Cbx proteins were affected in p63-null mice. Interestingly, we found by qRT-PCR analyses the reduced expression of Cbx6 and Cbx8 but not of Cbx7 in p63-null epidermis compared to WT controls (Figure 46).

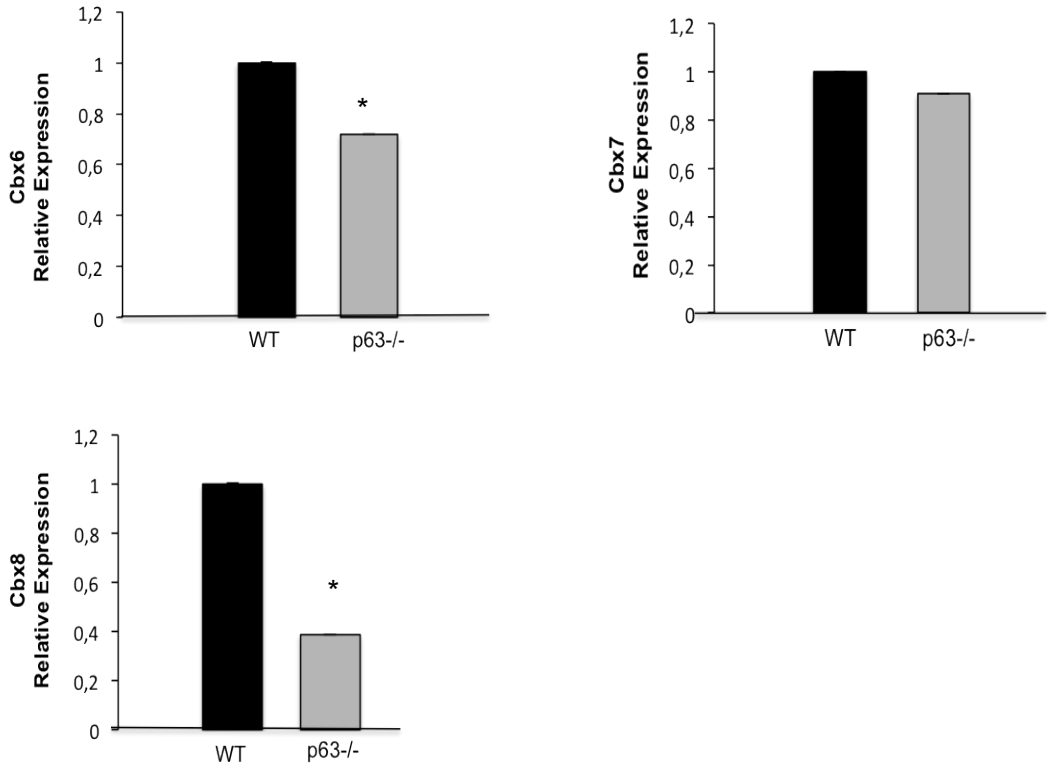

Figure 46: Relative expression of Cbx8, Cbx6, Cbx7 mRNAs in the embryonic epidermis of p63-/- mice and WT controls.

Primers for Cbx8, Cbx6 and Cbx7 cDNA were designed using the Beacon Designer Software and a Real-Time PCR reaction was performed. *Gapdh* gene was used as normalizer and error bars represent SEM. Sixteen independent experiments were run in duplicate. Significant reduction of Cbx8 (p-value=0.05) and of Cbx6 (p-value=0.04) was observed in p63-null epidermis. By contrast, Cbx7 did not show significant reduction in p63-null embryonic epidermis in comparison to WT control.

1.12.6.2. Ring 1B expression is decreased in p63-null epidermis

Gene silencing mediated by PRC1 occurs, at least in part, via the ubiquitynilation of lysine 119 on histone H2A (H2AK119ub). Ring 1B contributes to this process (Buchwald et al., 2006; Wang et al., 2004) via its RING finger motif, which has been demonstrated to contain the ubiquitin ligase activity (Wang et al., 2004). Consistent with these observations, we decided to investigate Ring 1B expression by qRT-PCR and immuno-fluorescence

analyses. We found a significant reduction of Ring 1B in p63-null epidermis compared to control (Figure 47).

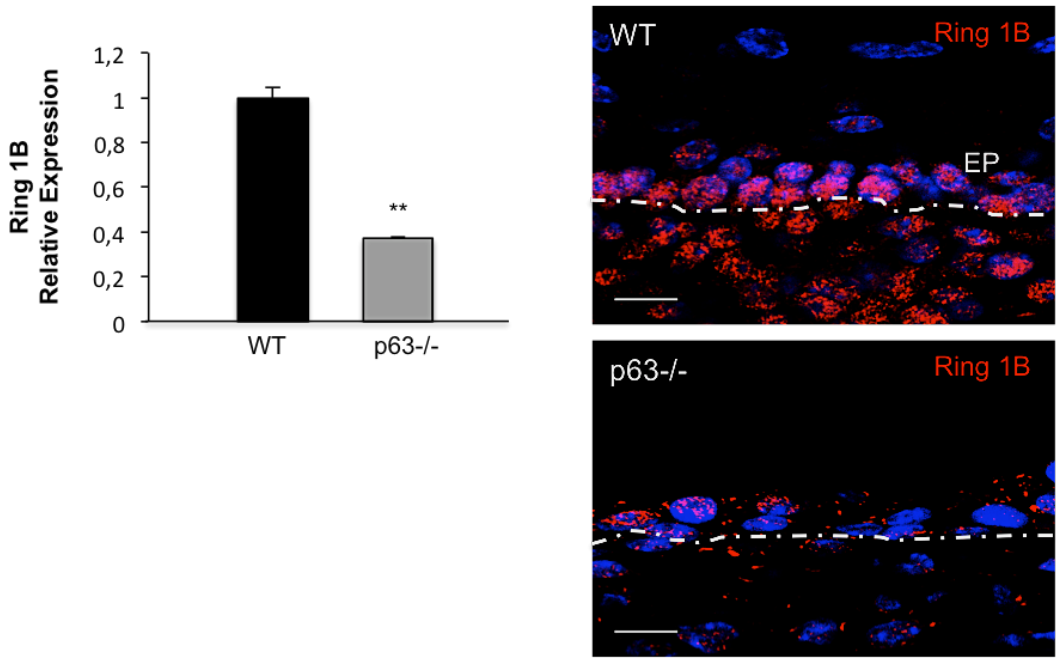

Figure 47: qRT-PCR and immuno-fluorescence analyses of Ring 1B in WT and p63-null embryonic epidermis.

(A) Primers for Ring 1B mRNA were designed using the Beacon Designer Software and a Real-Time PCR reaction was performed. *Gapdh* gene was used as normalizer and error bars represent SEM. Four independent experiments were run in duplicate. A significant reduction ($p=0.001$) of Ring 1B mRNA in $p63^{-/-}$ epidermis has been observed compared to WT controls. **(B)** Nuclei were stained with 4',6-diamidino-2-phenylindole(DAPI), while Ring 1B was stained with secondary antibody labelled with Indocarbocyanine (Cy3, red). Images were acquired with the laser scanning confocal microscope LSM 510 Meta (Carl Zeiss), using a 63x/1.4 plan-apochromat oil objective and a 2X zoom. A reduction of Ring 1B was observed in $p63^{-/-}$ epidermis compared to WT control.

Based on Ring 1B reduction of its expression, we next decided to analyse by immuno-fluorescence H2AK119ub level in $p63^{-/-}$ and WT embryonic cryosections and we found a significant reduction of this repressive histone modification in p63-null keratinocytes compared to controls (Figure 48).

These data suggest that PRC1 components Ring 1B and Cbx4 might contribute to the redistribution of heterochromatin and gene silencing in the epidermis of p63-null mice.

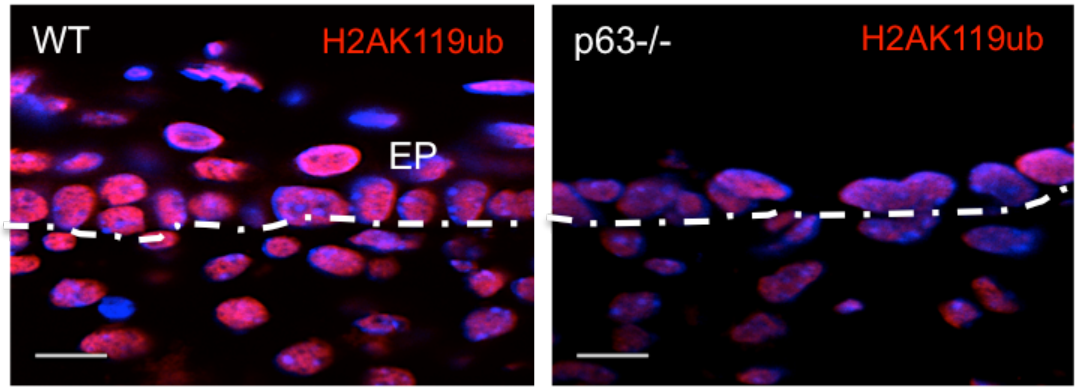

Figure 48: Confocal microscope images of immuno-fluorescence experiments on p63-/- and WT embryonic cryosections using H2AK119ub-specific antibody.

Nuclei were stained with 4',6-diamidino-2-phenylindole(DAPI), while H2AK119ub was stained with secondary antibody labelled with Indocarbocyanine (Cy3, red). Images were acquired with the laser scanning confocal microscope LSM 510 Meta (Carl Zeiss), using a 63x/1.4 plan-apochromat oil objective and a 2X zoom. Reduced H2AK119ub level was observed in $p63^{-/-}$ epidermis compared to WT control.

1.13. Cbx4$^{-/-}$ mice display an epidermal phenotype which partially resembles the phenotype of p63$^{-/-}$ mice

1.13.1. Cbx4$^{-/-}$ mice show decreased epidermal thickness and keratinocyte proliferation

Consistent with the reduced expression of several PRC1 and PRC2 components in p63$^{-/-}$ mice and with the fact that p63 directly regulates Cbx4, we hypothesized that p63-regulated gene expression program in epidermal keratinocytes might, at least in part, be mediated by PRC1 polycomb repressive complexe. This hypothesis was also consistent with recent microarray data, showing high Cbx4 and Ezh2 expressions at E16.5, thus suggesting their potential role in the control of epidermal development and stratification. We therefore decided to investigate whether Cbx4 ablation in mice could lead to epidermal defects similar to those observed in p63$^{-/-}$ mice (Figure 49).

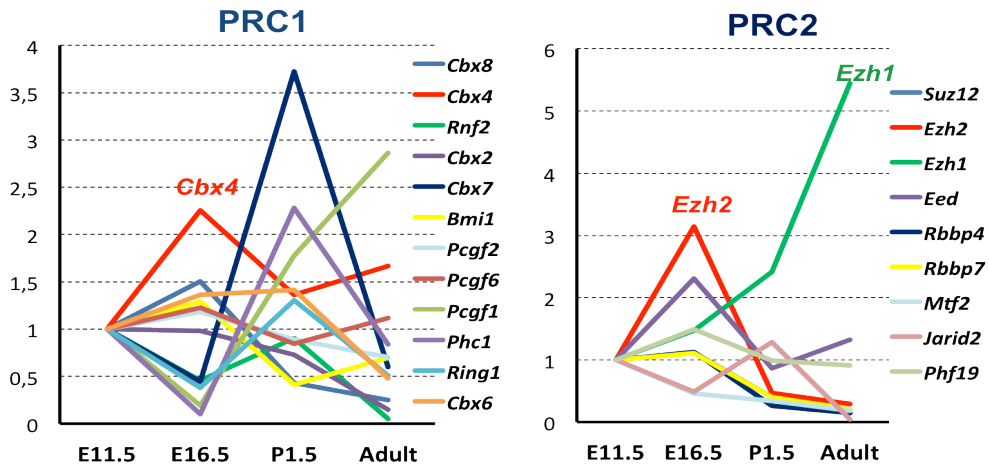

Figure 49: Microarray analysis showing the transcripts level of PRC1 and PRC2 components in the epidermis at different stages of epidermal development.

First, we performed alkaline phosphatase staining and analysed skin cryosections of Cbx4$^{-/-}$ and WT embryos from different embryonic stages (E14.5, E16.5 and E18.5).

Interestingly, morphological analysis of the epidermis in these mice showed that 11% of E14.5 Cbx4$^{-/-}$ embryos displayed a single layered epidermis (Figure 50**a**) similar to that observed in p63$^{-/-}$ mice with significant reduction in epidermal thickness (mean epidermal thickness=10µm) in comparison to controls (mean epidermal thickness=31µm). Signnificant difference in epidermal thickness was also observed in E17.5 Cbx4$^{-/-}$ embryos in comparison to WT controls (Figure 50**b**).

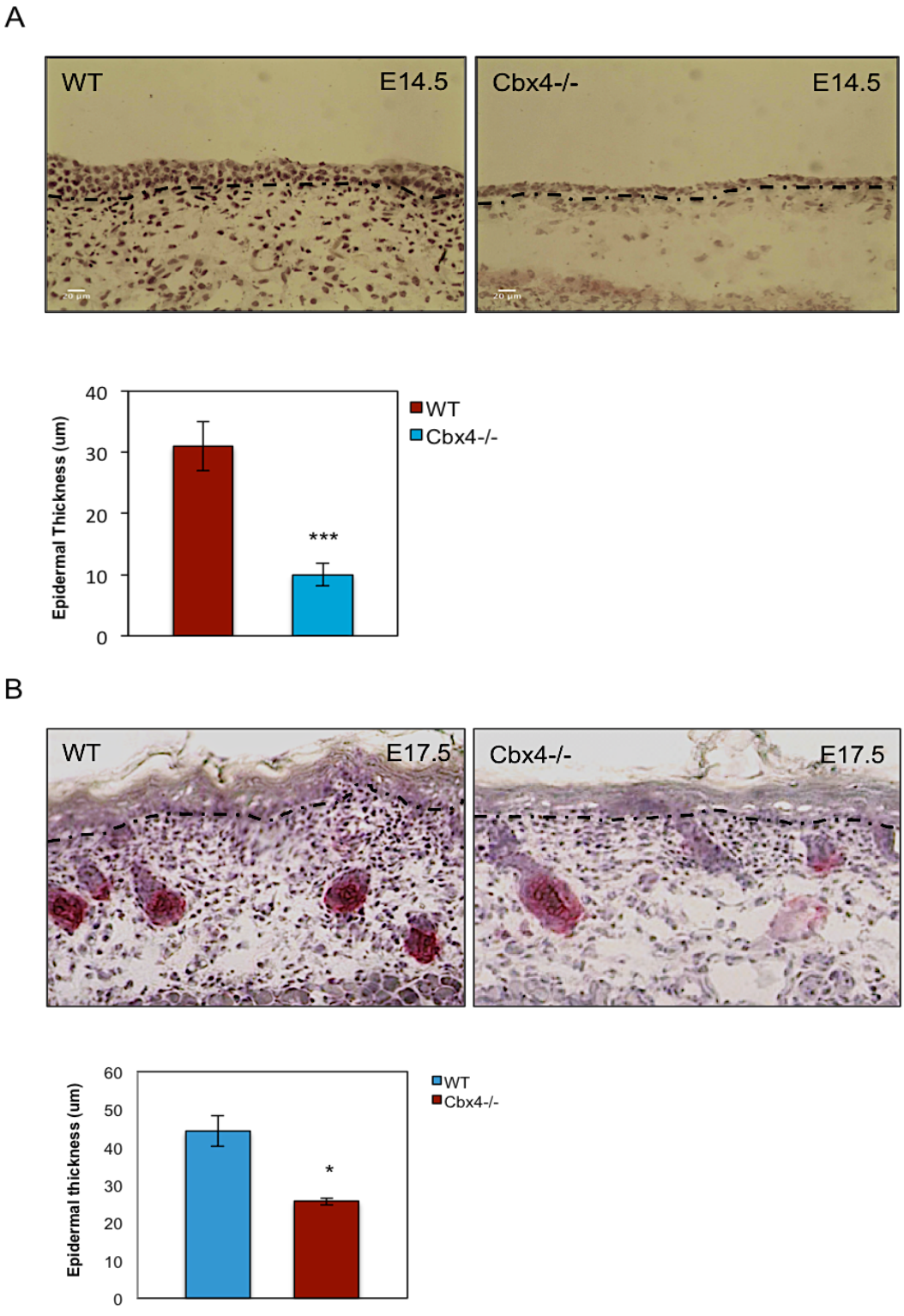

Figure 50: Alkaline phosphatase staining of Cbx4-/- and WT mice at different stages of embryonic development and analysis of epidermal thickness.

(A) Alkaline phosphatase staining of E14.5 Cbx4$^{-/-}$ and WT embryos and analysis of epidermal thickness showing a significant (p-value<0.0001) reduction in the epidermal thickness in 11% of Cbx4$^{-/-}$ embryos. **(B)** Alkaline Phosphatase staining of E17.5 Cbx4$^{-/-}$ and WT embryos showing significant difference in epidermal thickness.

The reduced epidermal thickness in E14.5 Cbx4$^{-/-}$ embryos suggested that keratinocytes proliferation rate might be decreased in these mice. We therefore stained E14.5 Cbx4$^{-/-}$ and WT skin cryosections with Ki67-specific antibody and calculated the percentage of Ki67 positive cells. We found significantly reduced proliferation rate in Cbx4-null embryos (46%) compared to WT controls (68%) (Figure 51).

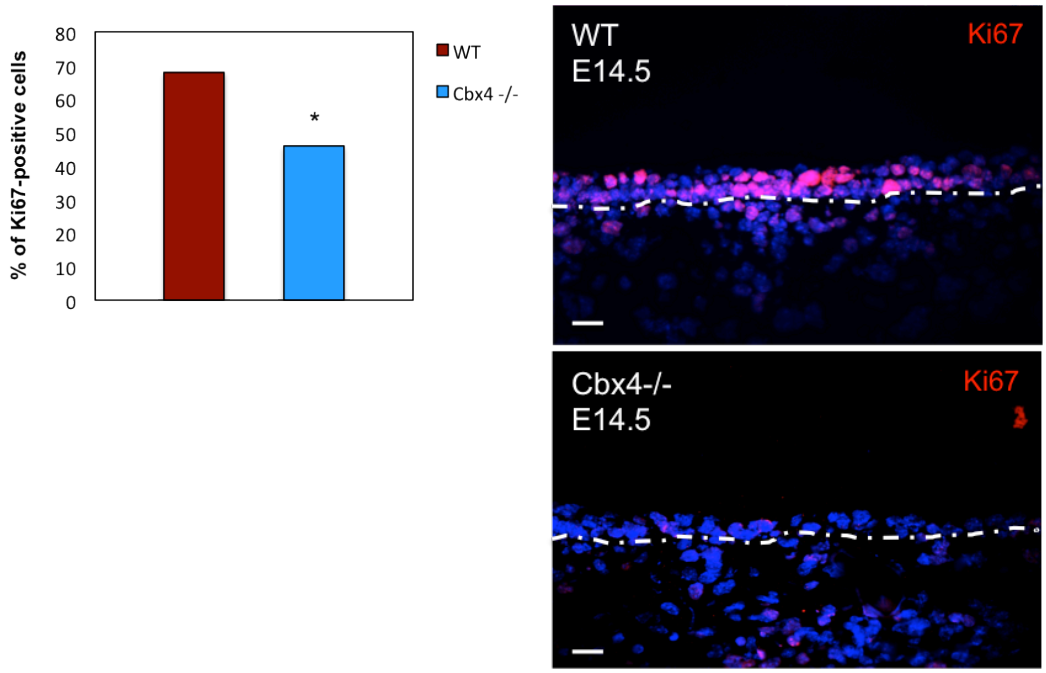

Figure 51: Analysis of proliferation using Ki67-specific antibody in E14.5 Cbx4-/- and WT embryonic cryosections.

E14.5 Cbx4$^{-/-}$ and WT embryos have been stained with Ki67-specific antibody (red) and the percentage of Ki67-positive cells has been calculated in both samples and statistically analysed using the Peterson's Chi-Square test. A significant (p-value=0.05) reduction of proliferative cells has been observed in Cbx4$^{-/-}$ embryonic epidermis in comparison to WT control.

1.13.2. Cbx4$^{-/-}$ mice show early onset of Loricrin expression in the epidermis

The epidermal stratification program starts in mice at about embryonic day E14.5. The spinous and the granular layers appear at about E16.5,

followed by the formation of a functional epidermal barrier at E18.5. Each epidermal layer is characterized by the expression of specific epidermal differentiation markers, including keratin proteins, loricrin, filaggrin and involucrin (Blanpain and Fuchs, 2009).

$p63^{-/-}$ mice lack epidermal stratification and all epidermal differentiation markers (Mills et al., 1999). We therefore asked whether $Cbx4^{-/-}$ mice also showed a similar phenotype.

E17.5 $Cbx4^{-/-}$ and WT embryonic cryosections have been analysed for K14 and loricrin expressions by immuno-fluorescence experiments. Interestingly, $Cbx4^{-/-}$ embryos showed a premature expression of loricrin in the spinous layer compared to WT controls (Figure 52), while no visible difference was observed for K14 between $Cbx4^{-/-}$ and WT controls.

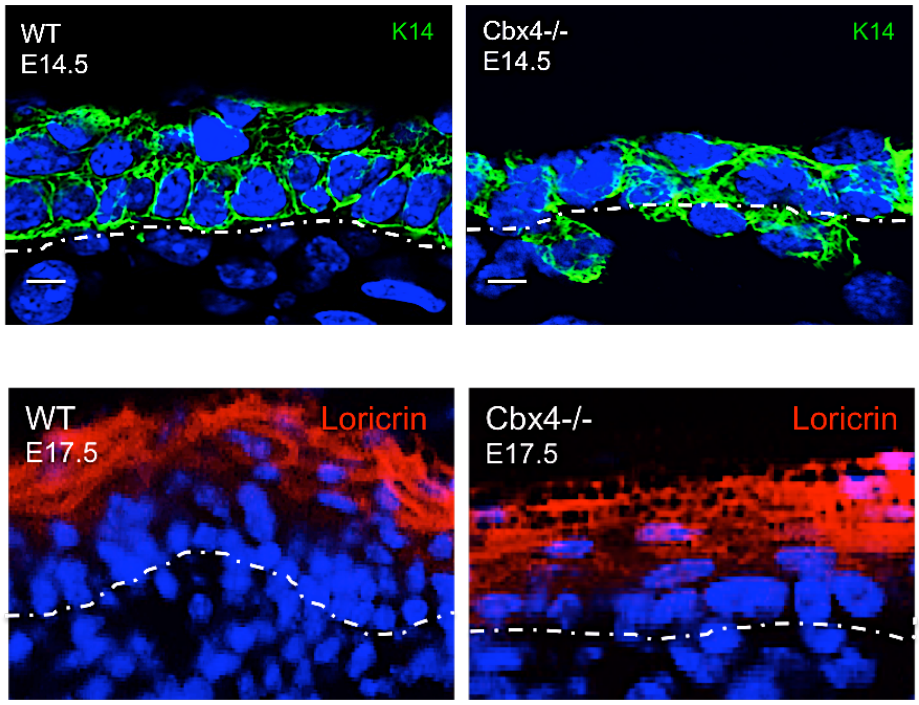

Figure 52: Immuno-fluorescence analysis of markers of early and late epidermal differentiation in WT and Cbx4-/- embryonic cryosections.

(A) E14.5 WT and Cbx4$^{-/-}$ embryos were stained with K14-specific antibody, recognized by a secondary antibody Fluoresceine Isothiocyanate labelled (Green), showing no difference in the expression of this epidermal basal layer marker. **(B)** E17.5 WT and Cbx4$^{-/-}$ embryos were stained with loricrin specific antibody (red). A premature expression of loricrin was observed in the spinous layer compared to WT controls.
Images were acquired with laser scanning microscope LSM 510 Meta (Carl Zeiss) **(A)** or with fluorescence microcope *Eclipse 50i* (Nikon) **(B)**.

1.13.3. Cbx4 ablation does not result in alterations in the expression of PRC1 components in the embryonic epidermis

Microarray data showed differential expression of PRC1 components during different stages of epidermal development (Figure 49), suggesting their requirement for epidermal development and stratification.

To test whether the epidermal defects observed in Cbx4-null mice were associated with Cbx4 ablation and not with the altered expression of other PRC1 components, we decided to analyse the expressions of the most relevant PRC1 components for epidermal development and stratification

(Figure 49), such as Cbx7, Cbx8, Phc1 and Pcgf1 in Cbx4-null epidermis from early (E14.5) and late (E18.5) embryonic stages in comparison to the corresponding WT samples.

qRT-PCR analyses showed no significant difference in the expression of these PRC1 components in E14.5 Cbx4-null laser captured microdissected epidermis as well as in E18.5 Cbx4-null epidermis in comparison to the corresponding WT controls (Figure 53).

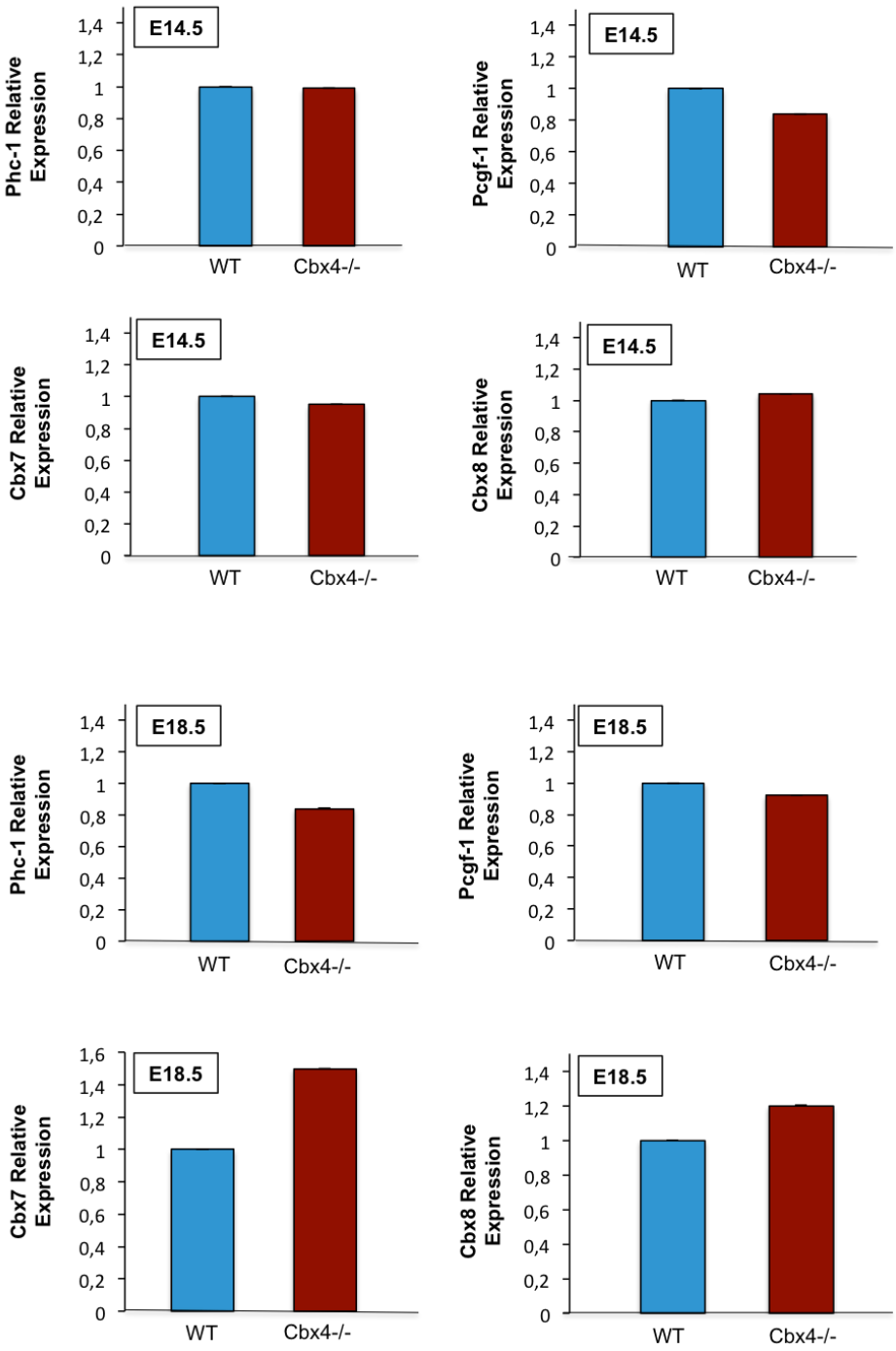

Figure 53: qRT-PCR analysis of the relative expression of several PRC1 components in E14.5 and E18.5 Cbx4-null embryonic epidermis and WT control.

Primers for Phc-1, Pcgf-1, Cbx7 and Cbx8 mRNAs were designed using the Beacon Designer Software and a Real-Time PCR reaction was performed. *Gapdh* gene was used as normalizer and error bars represent SEM. Four independent experiments were run in duplicate. No significant changes in their expression between E14.5 and E18.5 Cbx4-null epidermis and WT control shave been observed.

These data suggest that other PRC1 components are not responsible for the epidermal defects observed in Cbx4-null mice.

1.13.4. Cbx4-null epidermis and p63-null epidermis show increased expression of neural genes

Normal epidermal morphology at later stages of embryonic development (E18.5) in Cbx4-null mice (data not shown) strongly suggested that Cbx4 might play a role in epidermal commitment at earlier embryonic stages rather than in epidermal stratification process, which might be, therefore, regulated by other PRC1 components. In line with these observations, microarray data showed increased expression of Cbx4 in the epidermis at early embryonic stages (E14.5-E16.5) and its decrease at later embryonic stages (Figure 49). Conversely, the expression of other PRC1 components was lower at early embryonic stages with an increase at later embryonic stages (Figure 49).

Ectodermal commitment to an epidermal fate is dependent on the differential regulation of several pathways and on the differential expression of regulatory proteins, including transcription factors and chromatin remodelling enzymes. We therefore hypothesized that Cbx4 might be involved in this process by inhibiting the expression of neural genes and we decided to test the expression of some neural genes, which, according to microarray data, were increased in Cbx4-null epidermis, including neurofilament-1 (Nefl-1), Sodium Channel 3b (Scn3b) and Neuritin (Nrn).

Interestingly, our qRT-PCR analyses showed increased expression of Neurofilament-1, Neuritin and Sodium Channel 3b in Cbx4-null epidermis in comparison to WT control (Figure 54**a**).

Next, we asked whether the reduced expression of Cbx4 in p63-null mice could also lead to an increase in the expression of these neural genes in the epidermis (Figure 54**b**). Interestingly, qRT-PCR experiments showed increased expression of all these neural genes in p63-null epidermis in comparison to WT control. These results were also consistent with microarray data on p63-null epidermis and corresponding WT control, showing significant increase of the expression of these neural genes in p63-null epidermis (Fessing et al., 2011).

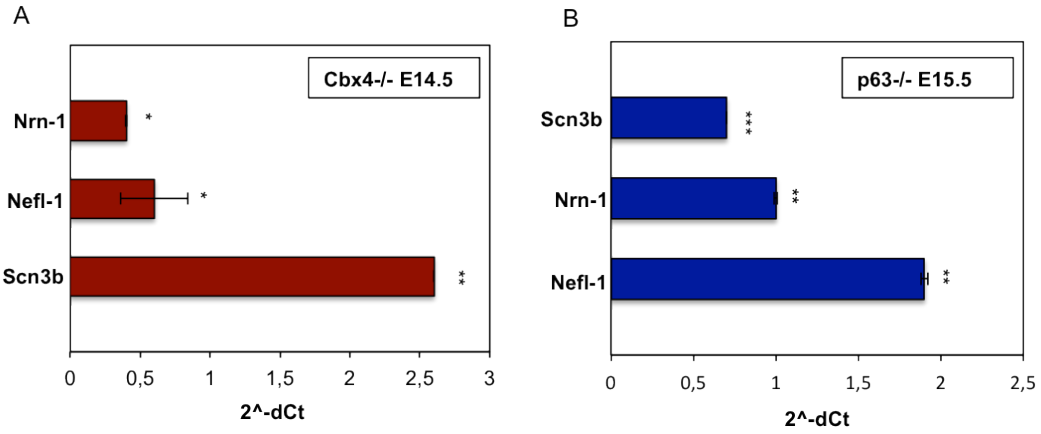

Figure 54: qRT-PCR analysis of the expression of some neural-associated genes in Cbx4-null embryonic epidermis and p63-null embryonic epidermis in comparison to their corresponding WT controls.

(A) Primers for Nrn-1, Nefl-1 and Scn3b mRNAs were designed using the Beacon Designer Software and a Real-Time PCR reaction was performed on Cbx4-null epidermis and WT control. The expression level was normalized to the corresponding levels in WT control and GAPDH gene was used as normalizer. Error bars represent SEM. Four independent experiments were run in duplicate. Significant increase of Nrn-1 (p-value=0.05), Nefl-1 (p-value=0.05) and Scn3b (p-value= 0.001) was observed in Cbx4-null epidermis in comparison to WT. **(B)** Real-Time PCR reaction was performed for Nefl-1, Nrn-1 and Scn3b genes in p63-null epidermis and WT control. Their expression level was normalized to the corresponding levels in WT control. GAPDH gene was used as normalizer and error bars represent SEM. Four independent experiments were run in duplicate. Significant increase of Nrn-1 (p-value=0.001), Nefl-1 (p-value=0.001) and Scn3b (p-value<0.0001) was observed in p63-null epidermis in comparison to WT.

Furthermore, immuno-fluorescence analysis using neurofilament-1-specific antibody on embryonic cryosections of E16.5 p63-null mice and E14.5 Cbx4-null mice together with their corresponding WT controls, showed an increase of this protein in these mice in comparison to corresponding WT controls (Figure 55).

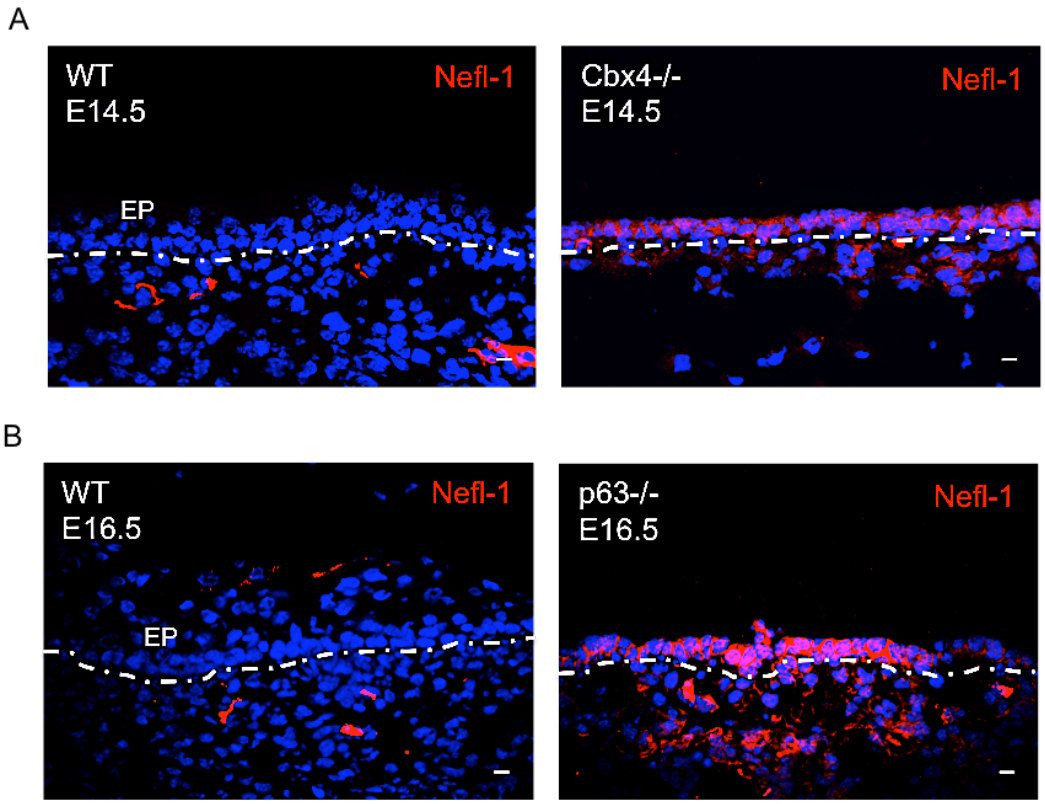

Figure 55: Immuno-fluorescence analysis of the expression of Neurofilament-1 in embryonic cryosections of Cbx4-/- and p63-/- vs corresponding WT controls.

(A) Neurofilament-1-specific antibody has been used for immuno-fluorescence analysis in E14.5 Cbx4$^{-/-}$ embryonic epidermis and corresponding WT control, showing significant increase of Nefl-1 in Cbx4-null epidermis. **(B)** Neurofilament-1-specific antibody has been used for the immuno-fluorescence analysis of its expression in E16.5 p63$^{-/-}$ embryonic epidermis and corresponding WT control, showing significant increase of Nefl-1 in p63-null epidermis.

Thus, these data suggest that p63-mediated program of epidermal differentiation is mediated, at least in part, by the PRC1 component Cbx4,

which is involved in the repression of non-epidermal (neural) genes in keratinocytes.

1.14. Deletion of keratin type II gene locus causes changes in gene expression in epidermal keratinocytes

1.14.1. Loricrin gene mainly occupies a peripheral position within chromosome territory three

Mammalian genomes encode genetic information in their linear sequence, but appropriate expression of their genes requires chromosomes to fold into complex three-dimensional structures (Gibcus and Dekker, 2013). Transcriptional control involves the formation of physical interactions between DNA sequences on the same chromosome (*in cis*) or on different chromosomes (*in trans*), leading to the formation of a complex hierarchy of structures, from chromatin loops that connect genes and enhancers to larger chromosomal domains and nuclear compartments (Gibcus and Dekker, 2013).

Keratins are essential components of the epidermis and all related epidermal appendages. Keratins play an important role in epidermal stratification as they are differentially expressed within the different epidermal layers, generating different type of connections, which are dependent on the epidermal layer (Blumenberg, 1993).

In $p63^{-/-}$ mice several keratins-encoding genes are reduced (Fessing et al., 2011), thus suggesting that keratin type I and keratin type II loci might play an important role in gene expression regulation during epidermal differentiation and epidermal barrier formation beside their structural role.

Therefore, we decided to start investigating higher order chromatin organization and the contribution of keratins in gene expression regulation in epidermal keratinocytes by using a mouse model, where keratin type II gene locus was deleted.

The conditional knock-out mice with ablation of keratin type II locus were generated at the University of Leipzig (Germany) in the lab of Prof. Thomas Magin, using a construct where Cre recombinase was expressed under the control of K14 promoter, directing its expression specifically in the basal layer of epidermis (Huelsken et al., 2001). Mice harbouring the floxed keratin type II locus were bred to K14-Cre mice. However, because of the large distance between the LoxP sites in the type II locus, only 10-15% of cells carried the deletion, resulting in patches of normal and keratins-deficient epidermal areas (Figure 56).

These mice were born alive without visible alterations in their phenotype. However, starting from post-natal day 5, they started developing hyperkeratotic, scaly, unelastic skin associated with skin fragility and lesions mainly restricted to areas frequently exposed to mechanical strain, such as limb and neck folds. This skin phenotype was accompanied by weight loss and death at 8-12 days old.

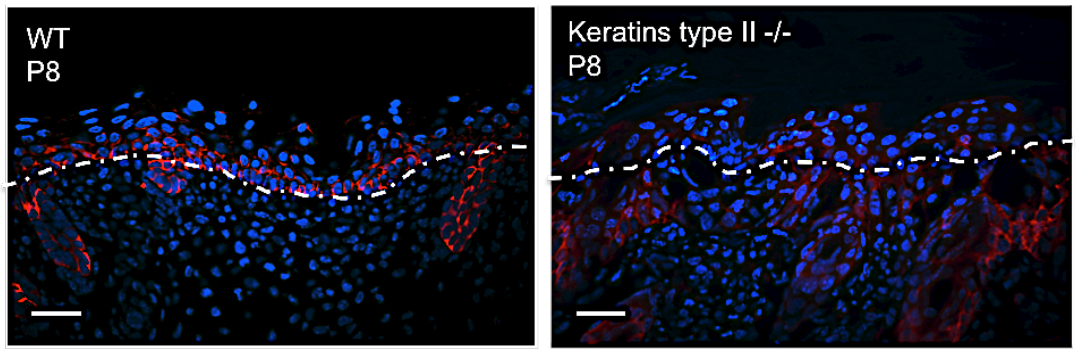

Figure 56: Immuno-fluorescence analysis of Keratin 5 expression in WT and keratin type II locus-deficient skin.

WT and keratin type II locus-deficient skin samples (P8) were stained with keratin 5-specific antibody, conjugated with a secondary antibody Indocarbocyanine 3 (Cy3) labelled (red). Keratins type II knock-out mice still retain a mosaic phenotype, resulting in patches of normal and keratins-deficient epidermis. In addition keratins type II-deficient mice display an hyperthickened disorganized epidermis in comparison to WT controls.
Images were acquired with the fluorescence microscope *Eclipse 50i* (Nikon) using a 40X objective lens.

First, we decided to analyse whether ablation of keratin II locus might influence gene expression within the EDC locus. We performed 3D fluorescence in situ hybridization (FISH) experiments, using probes directed against *Loricrin*, a gene localized within the EDC and an important marker of terminally differentiated epidermis. In parallel we used the whole Chromosome 3 paint to visualize the positioning of chromosome territory 3 (CT3).

To better discriminate between the nuclei retaining the keratin type II locus and nuclei depleted of it, we decided to additionally use a probe directed against *keratin 5* to analyse only nuclei carrying the deletion of Krt II locus (Figure 57).

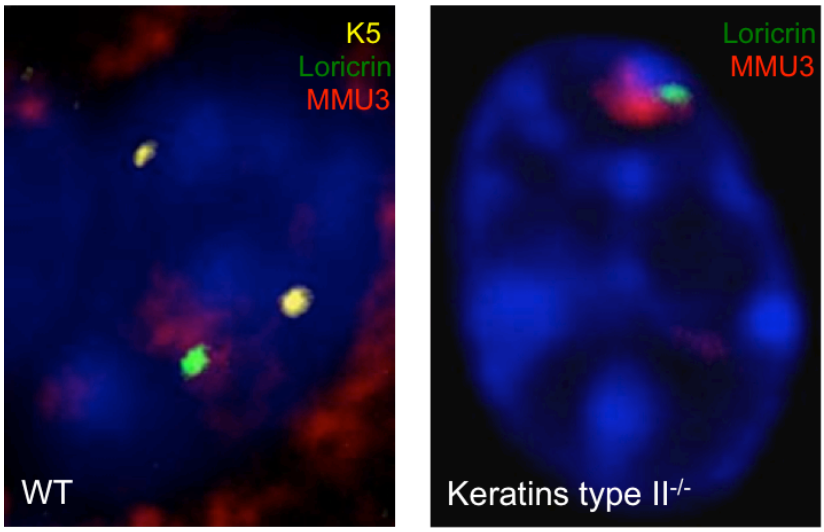

Figure 57: Confocal images of the fluorescence in situ hybridization (FISH), performed on keratins type II-/- epidermal keratinocytes and corresponding WT controls.

FISH was performed using probes against *loricrin* and *keratin 5* genes. The whole chromosome paint three (MMU3) was also used to stain the chromosome territory three and to analyze *loricrin* position within its territory. *Loricrin* probe was labelled with Indocarbocyanine 3 (Cy3, red), *K5* probe with Fluorescein isothiocyanate (FITC, green) and MMU3 with Indocarbocyanine 5 (Cy5).
Images were acquired with the laser scanning confocal microscope LSM 510 Meta (Carl Zeiss) using a 63x/1.4 plan-apochromat oil objective.

Samples were analysed for the positioning of *Loricrin* locus within the chromosome 3 territory. Z-stacks of both samples were acquired using the laser scanning confocal microscope LSM 510 Meta (Carl Zeiss) and optical sections were exported in ImageJ software and analysed, according to recommendation published previously (Fessing et al., 2011). 40 nuclei (80 loci) were analyzed for the WT sample and 34 nuclei (78 loci) were assessed in Krt II locus knock-out mice.

In our analysis, the chromosome 3 territory was divided into three parts: internal, which is closer to the nuclear centre, median and peripheral, which is closer to the nuclear border. This approach was used previously by Gdula et al. (Gdula et al., 2013) and it was based on the nuclear positioning of CT3.

Data were exported in Excel, compared between the two different samples and analysed statistically using Peterson's Chi-square test. Our results showed that *Loricrin* locus occupied significantly more peripheral position in basal epidermal cells of keratin type II gene locus knock-out cells compared to WT controls ($p=0.0169$) (Figure 58).

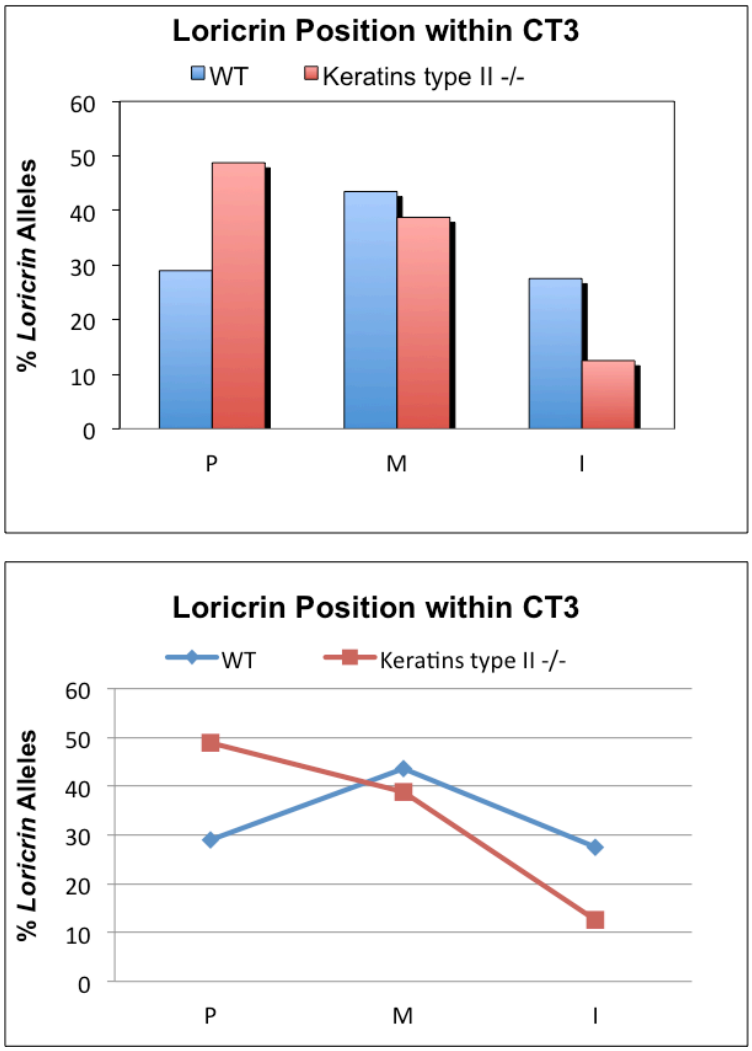

Figure 58: Analysis of *Loricrin* position within chromosome 3 territory in keratins type II-/- epidermal keratinocytes and WT controls.

40 keratinocytes nuclei (80 loci) were counted for the WT sample and 34 keratinocytes nuclei (78 loci) were counted for the knock-out sample. The chromosome territory three was divided into three parts: internal (I), median (M) and peripheral (P). *Loricrin* occupied much more peripheral position (p-value=0.0169) in the keratins type $II^{-/-}$ keratinocytes in comparison to the WT ones.

1.14.2. Loricrin expression is decreased in keratins type II locus-deficient mice

Peripheral position of the *Loricrin* gene within chromosome 3 territory, observed in Krt II locus KO mice, was similar to that of skin in E11.5 epidermis of WT mice, when Loricrin gene expression was relatively low versus E16.5 epidermis. Therefore we decided to further investigate the level of loricrin protein in the epidermis of keratin type II locus-deficient mice, consistent with the idea that peripheral genes localization has been usually associated with transcriptional repression.

We stained cryosections of P8 WT and keratins type II deficient-skin with loricrin-specific antibody and we found reduced expression of loricrin only in keratins type II-deficient epidermal areas, consistent with the mosaic pattern observed in these mice (Figure 59).

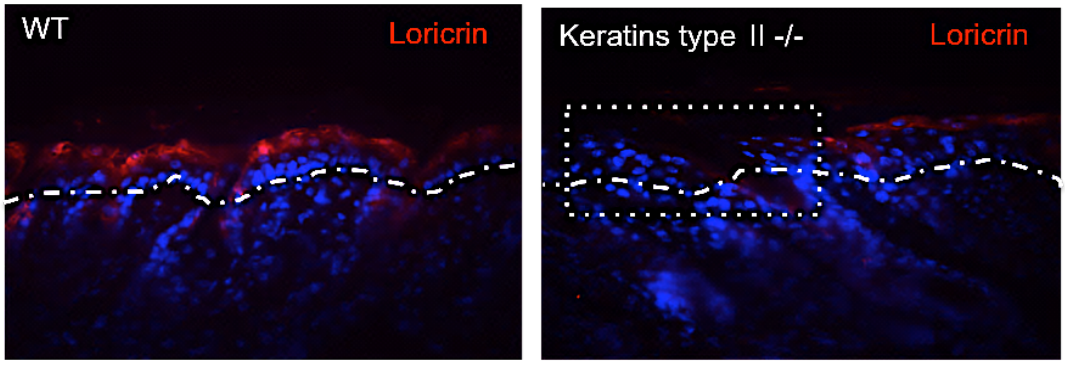

Figure 59: Immuno-fluorescence analysis of Loricrin expression in WT and keratins type II-deficient epidermis.

WT and keratins type II-deficient skin samples (P8) were stained with loricrin-specific antibody, conjugated with a secondary antibody Indocarbocyanine 3 (Cy3) labelled (red). Keratins type II-depleted skin showed significant reduced expression of loricrin in comparison to WT.
Images were acquired with the fluorescence microscope *Eclipse 50i* (Nikon) using a 40X objective lens.

These data suggest that ablation of Krt II locus results in relocation of *Loricrin* gene towards the nuclear periphery, which is associated with decrease of its expression.

1.14.3. Deletion of keratin type II locus leads to an increase in the intergenic distance between *Loricrin* and *Satb1*

The chromatin remodeller Satb1 has been shown to play a crucial role in chromatin organization within the EDC locus in epidermal keratinocytes, thus regulating the expression of epidermal-specific genes (Fessing et al., 2011). Circularized chromosome conformation capture (4C) experiments in our lab, using *Loricrin* and *Keratin 5* as baits, also showed that *Satb1* gene on chromosome 17 was part of *Loricrin* and *Keratin 5* interactomes in epidermal keratinocytes (data not shown). Furthermore, 3D FISH experiments on P0.5 WT skin using *Loricrin* and *Satb1* labelled probes, showed shorter distances between *Loricrin* and *Satb1* in epidermal keratinocytes compared to dermal fibroblasts (Figure 60). All together these findings suggest that *Loricrin*, *Satb1* and *Keratin 5* genes might be part of the same gene interactome in epidermal keratinocytes.

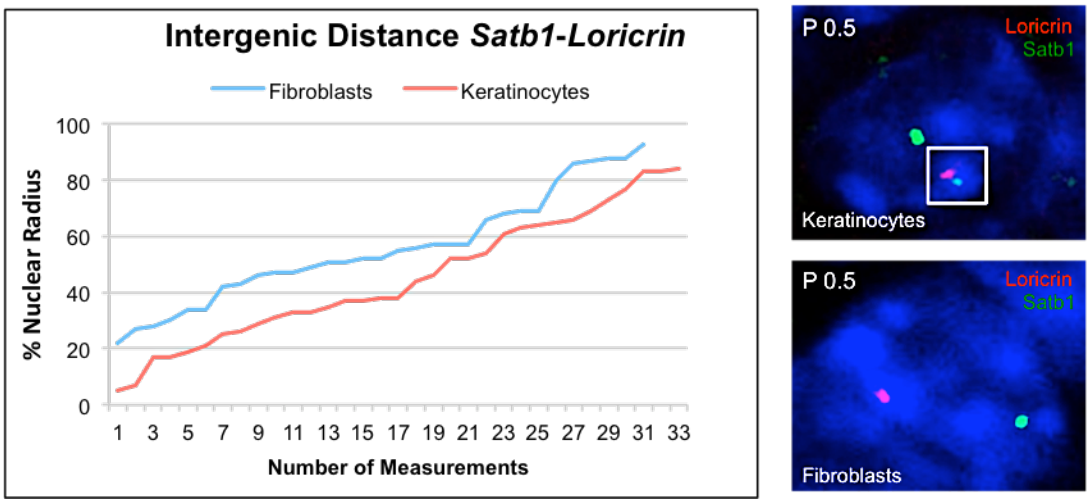

Figure 60: 3D Fluorescence in situ hybridization experiments on P0.5 samples using *Loricrin* and *Satb1* labelled probes.

P 0.5 WT mice have been processed for 3D FISH experiments using *Loricrin*-Indocarbocynine 3 (Cy3) labelled and *Satb1*-Fluoresceine Isothiocyanate (FITC) labelled and intergenic distance between them has been calculated in epidermal keratinocytes nuclei and dermal fibroblasts nuclei, used as control for the cell-specificity. The distances have been subsequently normalized for the mean nucleus radius.
The results showed significant (p-value= 0.02) shorter distance between *Loricrin* and *Satb1* in epidermal keratinocytes in comparison to dermal fibroblasts.

We, therefore, decided to test whether deletion of keratin type II locus might disrupt this interactome and alter the nuclear positioning of the *Satb1* gene versus the *Loricrin* gene or Krt II locus flanking regions.

First, we performed 3D FISH experiments using labelled probes for *loricrin* and *Satb1* on both P8 WT and keratin type II locus-depleted skin samples. 30 nuclei have been analysed in both samples and four distances between *Loricrin* alleles and *Satb1* alleles have been calculated and normalized to the average nuclear radius.

Our 3D FISH data showed increased distances between *Loricrin* and *Satb1* in the absence of keratin type II locus compared to WT controls (Figure 61).

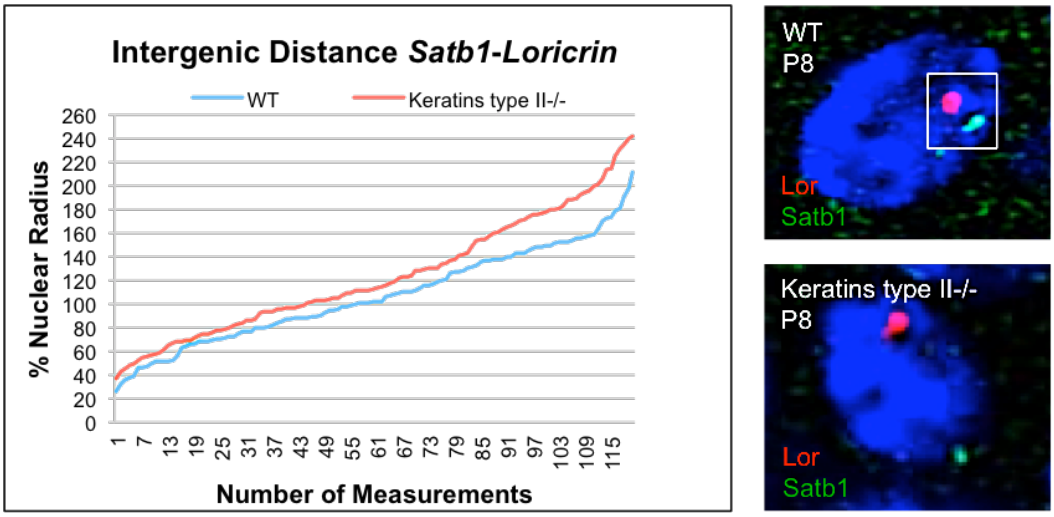

Figure 61: 3D Fluorescence in situ hybridization experiments on P8 WT and keratins type II-deficient skin samples using *Loricrin* and *Satb1* labelled probes.

P8 WT and keratins type II-depleted skin samples have been processed for 3D FISH experiments using probes for *Loricrin*-Fluorescein Isothiocyanate (FITC) labelled and *Satb1*-Indocarbocyanine 3 (Cy3) labelled and distances between them have been calculated in basal keratinocytes nuclei and normalized to the mean nucleus radius. A significant increase in the distance between *Loricrin* and *Satb1* was shown in keratins type II-deficient keratinocytes in comparison to WT controls.

1.14.4. Deletion of keratin type II locus leads to increased distance between *Loricrin* and *Satb1* gene and keratin type II locus flanking regions specifically in epidermal keratinocytes

Next, we performed additional 3D FISH experiments using labelled probes for *Satb1*, *Loricrin* and for the 5' (*Acvr1b*, activin A receptor, type 1B) and 3' flanking regions (*Eif4b* eukaryotic translation initiation factor 4B) of keratin type II locus, allowing us to analyse the intergenic distances between *Loricrin, Satb1* and keratin type II locus flanking regions in keratins type II-deficient skin samples.

Interestingly, our data showed a significant increase in the distances between *loricrin* (Figure 62) and *Satb1* (Figure 63) and keratin type II locus flanking regions in keratins type II-depleted skin in comparison to WT controls.

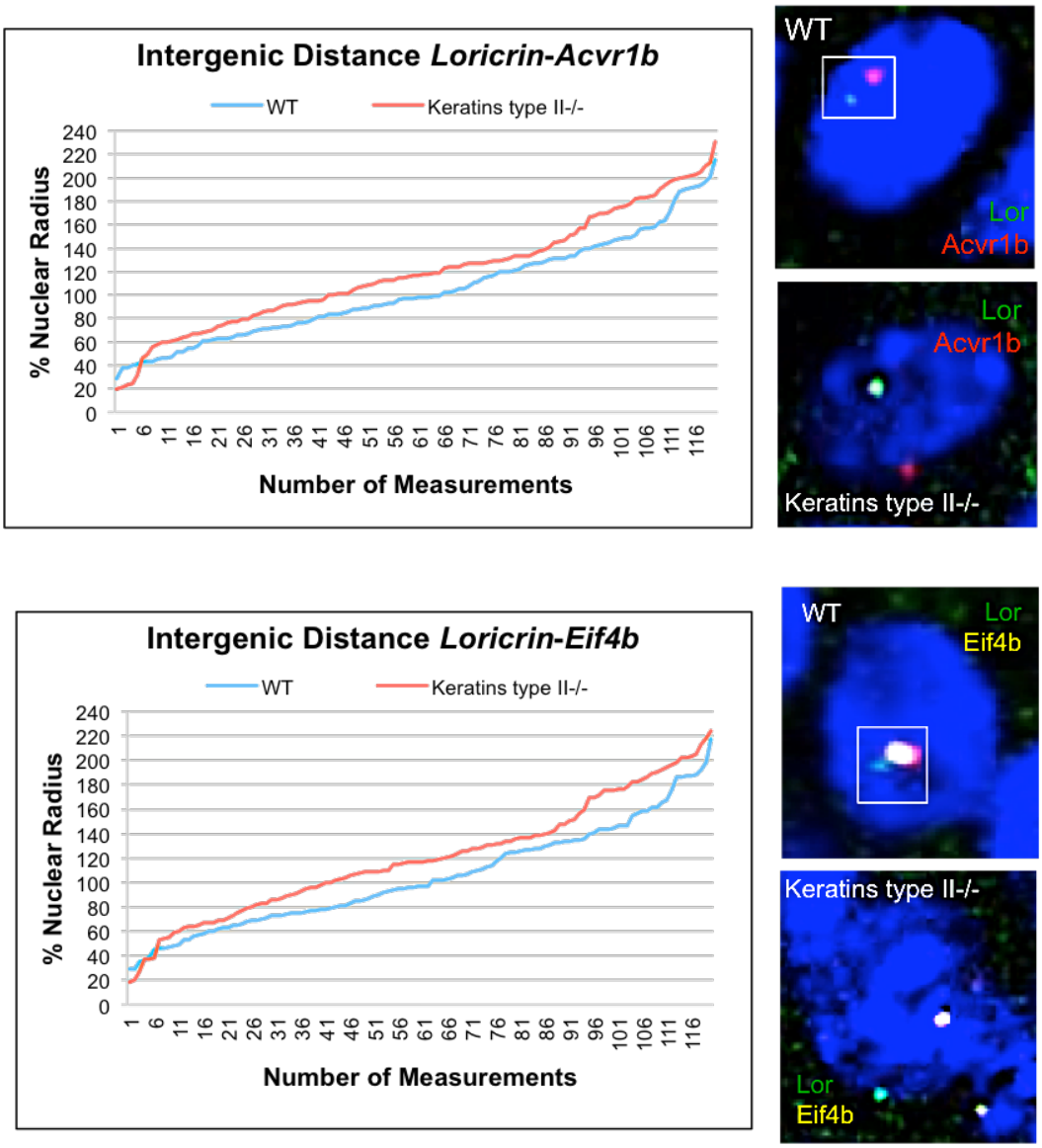

Figure 62: 3D Fluorescence in situ hybridization analysis of the intergenic distance between *Loricrin* and 5' flanking region (*Acvr1b*) and 3' flanking region (*Eif4b*) of keratins type II locus in WT and keratins type II-deficient epidermis.

Loricrin Fluorescein Isothiocyanate (FITC)-labelled, *Acvr1b*-Digoxygenin labelled and *Eif4b*-Biotin labelled have been used of 3D FISH experiments and intergenic distances between them have been calculated in both WT and keratins type II-deficient basal keratinocytes and normalized to the mean nuclear radius.
Significant increase in the intergenic distances between *Loricrin* and *Acvr1b* (p-value=0.01) as well as between *Loricrin* and *Eif4b* (p-value=0.007) in keratins type II-deficient keratinocytes have been shown.

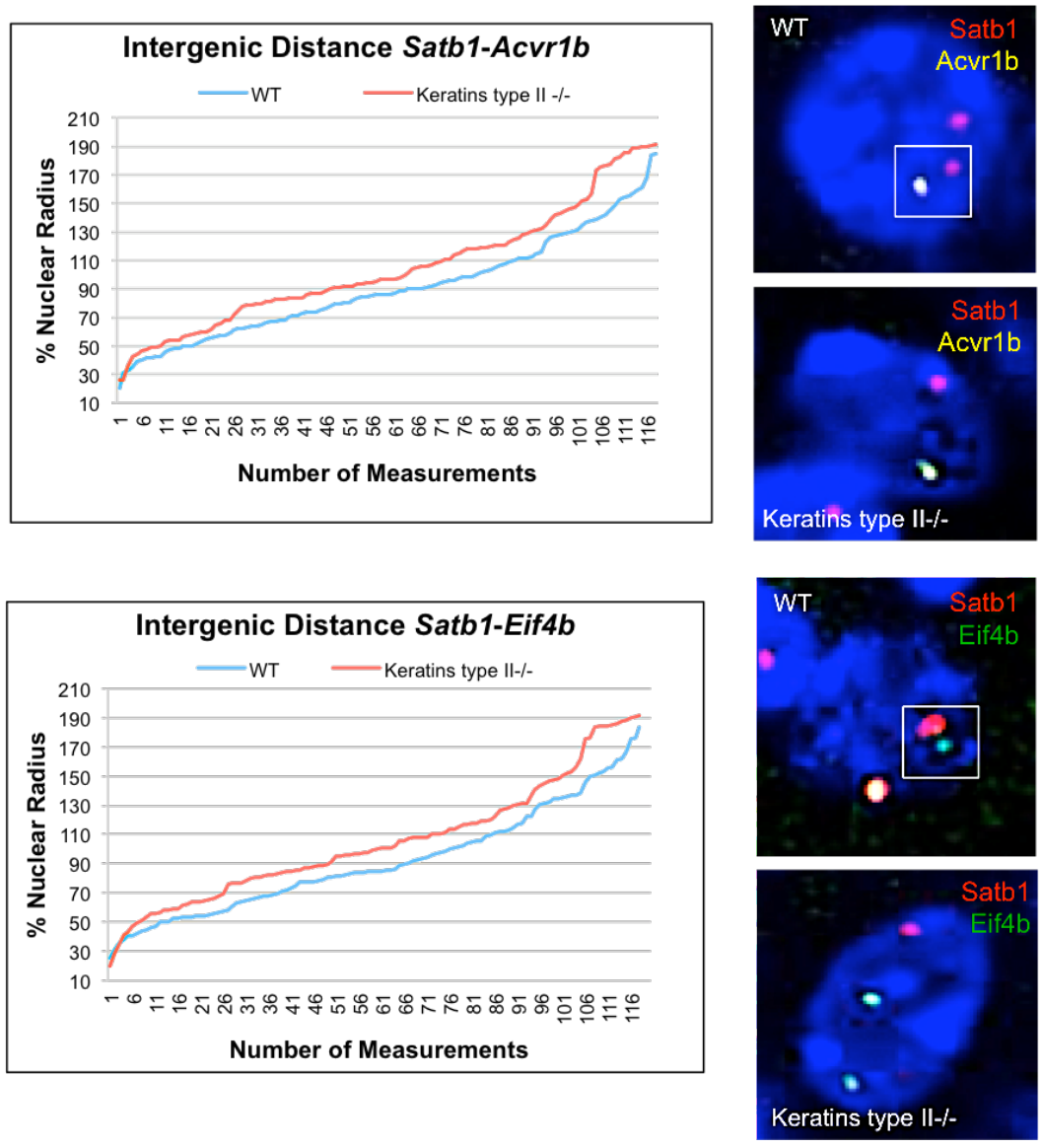

Figure 63: 3D Fluorescence in sity hybridization analysis of the intergenic distance between *Satb1* and 5' flanking region (*Acvr1b*) and 3' flanking regions (*Eif4b*) of keratins type II locus in WT and keratins type II-deficient epidermis.

Satb1 Indocarbocyanine 3-labelled (Cy3), *Acvr1b*-Biotin labelled and *Eif4b*-FITC labelled have been used of 3D FISH experiments and intergenic distances have been calculated in both WT and keratins type II-deficient basal keratinocytes and normalized to the mean nuclear radius. Significant increase in the intergenic distances between *Satb1* and *Acvr1b* (p-value=0.01) as well as between *Satb1* and *Eif4b* (p-value=0.01) in keratins type II-deficient keratinocytes have been shown.

To test whether our results were specific for epidermal keratinocytes, we decided to perform additional 3D FISH experiments on freshly isolated thymocytes using labelled probes for *Keratin 5*, *Satb1* and the EDC locus. 30 nuclei have been analysed for the intergenic distances between these loci and distances have been subsequently normalized to the average nuclear radius. Interestingly, our data showed significantly larger distances between the EDC and *keratin 5* in thymocytes in comparison to epidermal keratinocytes (Figure 64). However, no differences in the distances between *Satb1* and *keratin 5* were observed in thymocytes in comparison to keratinocytes (Figure 65).

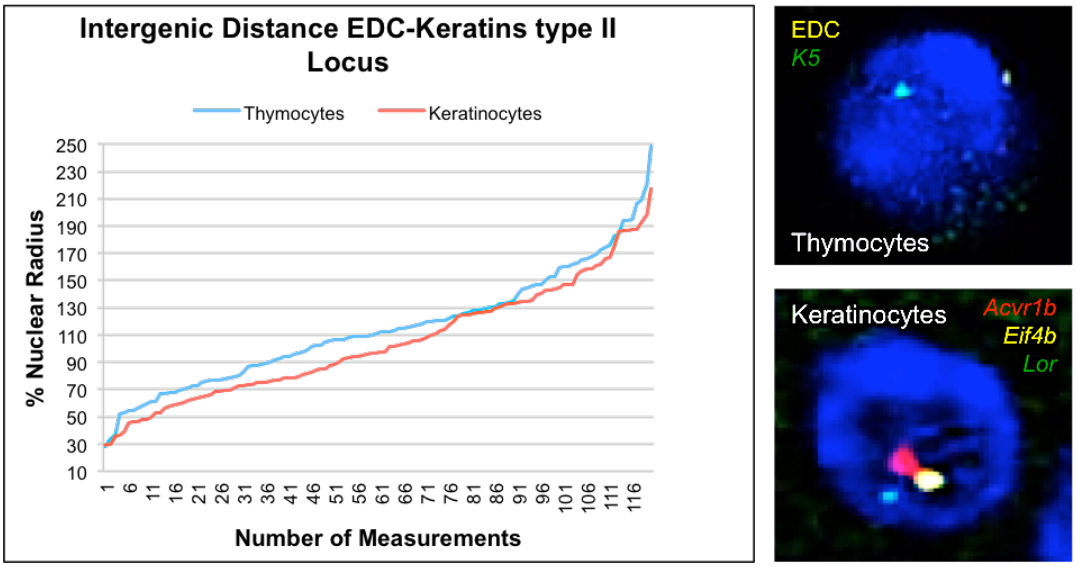

Figure 64: 3D Fluorescence in situ hybridization analysis of the intergenic distance between EDC locus and keratins type II locus in thymocytes vs epidermal keratinocytes.

EDC-Biotin labelled and *Keratin 5*-FITC labelled have been used of 3D FISH experiments on freshly isolated thymocytes and intergenic distances between them have been calculated; probes for *Acvr1b*-Digoxygenin labelled, *Eif4b*-Biotin labelled and *Loricrin*-FITC labelled have been used in epidermal keratinocytes and intergenic distances between *Loricrin* and keratins type II flanking regions have been calculated.
Significant (p-value=0.05) increase in the distance between EDC/*Loricrin* and *K5*/Keratins type II locus flanking regions was observed in thymocytes in comparison to epidermal keratinocytes.

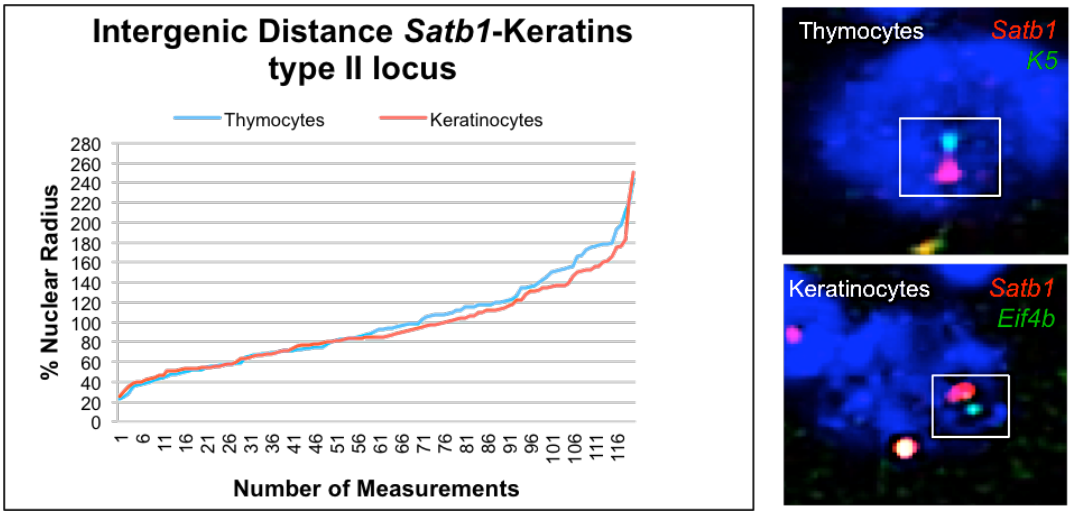

Figure 65: 3D Fluorescence in situ hybridization analysis of the intergenic distance between *Satb1* and keratins type II locus in thymocytes vs epidermal keratinocytes.

Satb1-Indocarbocyanine 3 (Cy3) labelled and *Keratin 5*-FITC labelled have been used of 3D FISH experiments on freshly isolated thymocytes and intergenic distances between them have been calculated; probes for *Eif4b*-FITC labelled and *Satb1*-Cy3 labelled have been used in epidermal keratinocytes and intergenic distances between them have been calculated.
No significant difference in the distance between *Satb1* and keratins type II locus has been shown between thymocytes and keratinocytes.

These data suggest that intranuclear positioning of the Krt II locus, Loricrin and Satb1 genes is cell type specific and spatial relationships between these genes might play a role in the control of epidermal differentiation program.

1.14.5. *Satb1* is located at the periphery of chromosome 17 territory and its expression is decreased in keratin type II-deficient mice

Ablation of keratin type II locus led to increased distances between *Loricrin* and keratin type II locus and to a relocation of Loricrin to a more peripheral position within the chromosome 3 territory, which was associated with its reduced expression in the epidermis of Krt II locus knock-out mice.

Based on these observations, we also decided to test whether changes in *Satb1* position within its chromosome 17 territory and/or changes in its expression were observed in keratin type II locus deficient-mice.

First, we performed 3D FISH experiments using *Satb1* labelled probe and the whole chromosome paint 17 and we analysed *Satb1* position within its chromosome territory.

As in the case of chromosome 3 territory (Fessing et al., 2011), chromosome territory 17 has been divided into three parts: internal, median and peripheral. This division was possible as in the majority of nuclei chromosome 17 was located at the nuclear border.

30 nuclei have been analysed in both WT and keratin type II locus-deficient mice and percentages of *Satb1* alleles occupying a peripheral, median or internal position within chromosome territory 17 have been calculated.

Our results showed that *Satb1* locus mainly occupied a peripheral position within its chromosome territory (Figure 66).

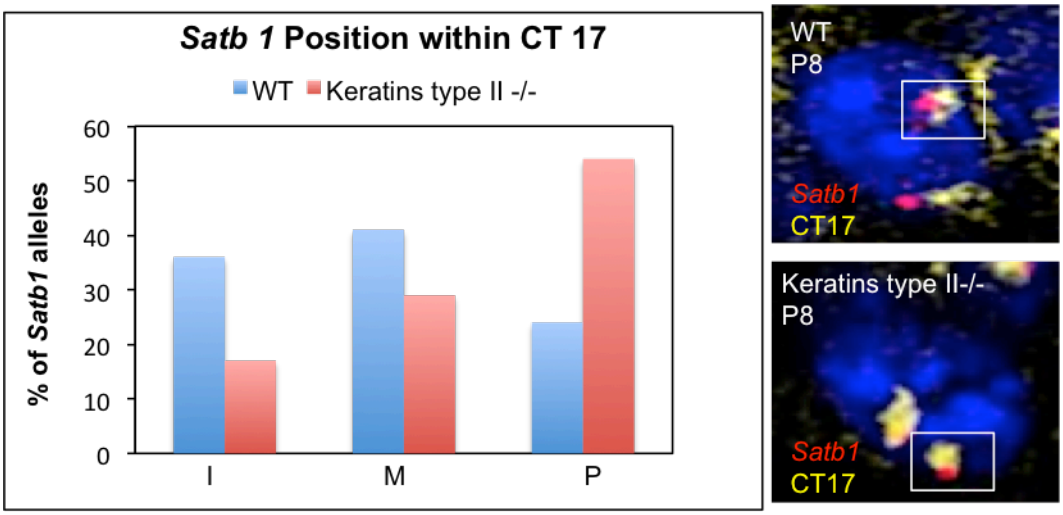

Figure 66: 3D Fluorescence in situ hybridization analysis of *Satb1* position within chromosome 17 territory in WT and keratins type II-deficient keratinocytes.

30 keratinocytes nuclei (60 loci) were counted in both WT and keratins type II–deficient skin samples. The chromosome territory seventeen was divided into three parts: internal (I), median (M) and peripheral (P). *Satb1* occupied much more peripheral position (p-value=0.007) in keratins type II-deficient keratinocytes in comparison to WT controls.

Next, we decided to test whether Satb1 protein level was also reduced in keratin type II locus-deficient mice.

Our immuno-fluorescence analysis of cryosections of P8 keratins type $II^{-/-}$ mice and corresponding WT controls using Satb1-specific antibody, showed a marked decrease of the protein in the epidermis of keratin type II locus-deficient mice in comparison to WT controls (Figure 67).

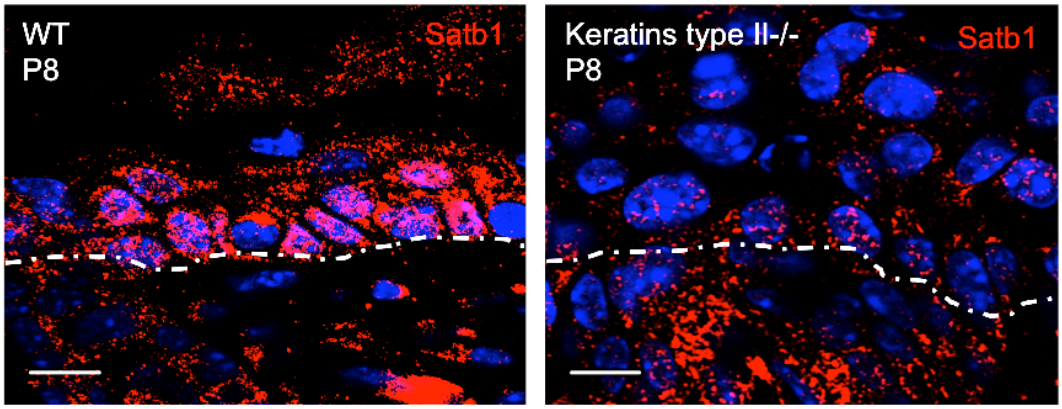

Figure 67: Immuno-fluorescence analysis of Satb1 expression in P8 WT and keratins type II-deficient epidermis.

P8 WT and keratins type II-deficient skin samples were stained with Satb1-specific antibody, conjugated with a secondary antibody Indocarbocyanine 3 (Cy3) labelled (red). Keratins type II-deficient keratinocytes showed significant reduced expression of Satb1 in comparison to WT.
Images were acquired with the laser scanning confocal microscope *LSM Meta 510* (Carl Zeiss) using a 63x/1.4 plan-apochromat oil objective.

These data suggest that similarly to *Loricrin* gene, relocation of *Satb1* gene away from the keratin type II locus resulted in marked decrease of its expression.

Taken together, these data, confirm the role of higher-order chromatin remodelling and spatial organization of the genes in the nucleus in the control of their expression during execution of lineage-specific differentiation programs.

Chapter 4

Discussion

4. DISCUSSION

1.15. p63 transcription factor controls the establishment of nuclear architecture in epidermal keratinocytes

The epidermis is the outermost component of the skin with the role of primary barrier, which protects the body from dehydration, mechanical trauma and microbial insults. Together with the dermis, it represents the main component of the skin and they function cooperatively and together during development of epidermal appendages, including hair follicles and mammary glands (Chuong et al., 1998) cit. in (Koster and Roop, 2007).

Four different layers characterize the epidermis: basal, spinous, granular layers and the cornified envelope. In mice, the epidermal stratification program occurs in a period of approximately 10 days, between E8.5 and E18.5 and starts when cells of the surface ectoderm commit to the epidermal fate.

One of the key factors in epidermal differentiation process is the transcription factor p63 as mice null for the expression of this gene, are characterised by an early block in epidermal stratification as well as truncated limbs, craniofacial malformations, abnormalities in epidermal appendages and absence of normal stratified epithelia (Mills et al., 1999; Yang et al., 1999).

p63 also plays a potentially important role in epigenetic regulation of gene expression during skin development and differentiation by controlling expression of multiple genes involved in chromatin organization and remodelling, including the genome organizer Satb1 and the ATP-dependent chromatin remodeler Brg1, both involved in higher-order chromatin folding and gene regulation within the EDC locus (Fessing et al., 2011)(Mardaryev et al., 2013).

Our data also demonstrated that p63 is important in establishing epidermal keratinocytes nuclear architecture. p63 deficiency, in fact, led to significant changes in the nuclear shape of p63-null basal keratinocytes compared to WT controls as well as of primary mouse keratinocytes after p63 knock-down by RNA interference experiments.

Alterations in the nuclear shape were accompanied both *in vivo* and *in vitro* by significant reduction of Lamin B1, the major B-type lamins, consistent with previous data showing that cells lacking Lamin B1 displayed misshapen nuclei (Vergnes et al., 2004; Yang et al., 2011b) similar to those observed in p63-null keratinocytes. Together with B-type lamins, also A-type lamins play an essential role in the maintenance of nuclear shape and stability, as demonstrated by alterations in the nuclear shape of murine fibroblasts after Lamin A/C depletion (Lammerding et al., 2004). In line with these observations, our data also showed both *in vivo* and *in vitro* a marked decrease of Lamin A/C in p63-null keratinocytes in comparison to controls.

However, while Lamin B1 transcript was reduced in p63-null laser captured micro-dissected epidermis, Lamin A/C transcript level was increased in p63-null epidermis in comparison to WT control, thus suggesting a potential negative feedback mechanism, by which the observed reduction of Lamin A protein level, possibly as a consequence of defects in its maturation process, might lead to an increase in *Lamin A* gene transcription.

Maturation of nuclear lamins is a process characterized by biochemical conversion of pre-lamins into mature lamins. Differently from B-type lamins, which remain permanently farnesylated and carboxymethylated, A-type lamins require an additional step in their transition from pre-lamin A to mature lamin A,

consisting in the removal of 15 additional amino acids from the carboxyl terminus of farnesylated/carboxymethylated pre-lamin A by Zmpste24/FACE1 (Dechat et al., 2010). Several studies showed that alterations in pre-lamin A maturation pathway were responsible for pre-lamin A accumulation, leading to premature aging Hutchinson-Gilford Progeria syndrome (HGPS) and restrictive dermopathy (Rusinol and Sinensky, 2006). Therefore, additional studies will be required to analyse the process of farnesilation of the mature Lamin A protein in p63-null keratinocytes. In addition, detailed analysis of the role of Zmpste24 enzyme in keratinocytes, whose mutations have been shown to be responsible for the reduced nuclear lamins expression and nuclear lamins mislocalization in mouse embryonic fibroblasts (Maske et al., 2003).

Besides nuclear lamins, other cellular components play an important role in the maintenance of nuclear integrity and nuclear positioning, including proteins of the LINC complex, essential in mediating the link between nuclear and cytoskeleton components (Crisp et al., 2006). One major protein of the LINC complex is Sun-1, as it has been demonstrated to be important for Nesprins localization on the ONM (Padmakumar et al., 2005) and for the formation of synaptic nuclei (Lei et al., 2009), suggesting its requirement for the maintenance of cellular integrity during development. Here, we showed a significant decrease of Sun-1 in p63-null epidermis together with the reduction of one of its interactor, Nesprin-3, another component of the LINC complex, important for the maintenance of nuclear shape and perinuclear cytoskeleton architecture in endothelial cells (Morgan et al., 2011).

Interestingly, previous studies also showed an important involvement of Sun-1 in pre-lamin A maturation process (Haque et al., 2006), thus suggesting that its

reduced expression might be, at least in part, responsible for alterations in Lamin A maturation pathway, leading to the observed lamin A reduction in these mice.

While Suns are able to bind all three Nesprins (Nesprin-1, Nesprin-2 and Nesprin-3), they, in turn, have a selective binding for different cytoskeletal components: Nesprin-1 giant and Nesprin-2 giant bind to actin filaments via their actin binding domain (Padmakumar et al., 2005), while Nesprin-3 binds the versatile cytolinker Plectin (Wilhelmsen et al., 2005). Furthermore, previous studies showed that Lamin B1 but not Lamin A/C interacts with Plectin (Foisner et al., 1991). Here, we demonstrated that Plectin level is also reduced in p63-null epidermis, strongly suggesting that nuclear lamina–cytoskeletal interactions might be affected by p63 deficiency in epidermal keratinocytes.

In contrast to Lamin B1, whose expression is reduced in both $p63^{-/-}$ whole embryo and in $p63^{-/-}$ embryonic epidermis, our data showed a reduction of Plectin, Sun-1 and Nesprin-3 expression specifically in p63-null embryonic epidermis compared to WT control, suggesting that their reduction might contribute to the epidermal defects associated with p63-null phenotype. To test this hypothesis, we performed a ChIP-qPCR assay using adult epidermal keratinoctyes and tested *Plectin*, *Sun-1* and *Nesprin-3* promoter regions for p63 binding.

Plectin gene encodes several isoforms resulted from usage of several different promoters, driving transcription of mRNAs with different 5'-parts (Fuchs et al., 1999). We decided to start our analysis with the promoter region controlling the expression of *Plectin 1c* isoform, which is the most abundant isoform expressed in murine keratinocytes (Andra et al., 2003). The analysis of different regions

within *Plectin 1c* promoter at different distances from the gene transcription start site, revealed binding of p63 to its consensus binding sites 3.8 kb upstream from the transcription start site. With respect to *Sun-1* and *Nesprin-3*, we found significant p63 enrichment to its consensus binding sequences 4.0 kb and 0.9 kb respectively from their transcription start sites, thus suggesting an important role of p63 in controlling nuclear structure in epidermal keratinocytes by directly regulating the transcription of nuclear envelope-associated genes. However, further experiments, including transient co-transfection experiments with the reporter gene driven by *Plectin 1c, Sun-1* and *Nesprin-3* promoters, will be necessary to verify the functional significance of the observed p63 binding.

Reduced expression of all these components in p63-null keratinocytes also has an important influence on epidermal development. Plectin, in fact, in addition to its structural role in connecting IFs, including keratins, to MTs, the actin cytoskeleton (Goldman et al., 1986) cit. in (Svitkina et al., 1996) and membrane adhesion sites (Bershadsky et al., 1987), including hemidesmosomes, plays an essential role in epidermal differentiation. Plectin and integrin $\alpha_6\beta_4$ expressions are decreased during keratinocyte differentiation, leading to disappearance of $\alpha_6\beta_4$ integrin-containing hemidesmosomes and Plectin in the suprabasal layer of the epidermis. This reduction is required for proper detachment of basal keratinocytes from the basal membrane prior to epidermal stratification (Kostan et al., 2009). Interestingly, β_4 integrin expression is reduced upon p63 ablation in basal epidermal keratinocytes (Carroll et al., 2006). In this context Nesprin-3 also plays an important role in organizing keratins network around the nucleus (Postel et al., 2011) as well as in linking

nuclear envelope with $\alpha_6\beta_4$ integrin-containing hemidesmosomes (Wilhelmsen et al., 2005).

Therefore, Plectin, Nesprin-3 and β_4 integrin reduction in p63-null keratinocytes might lead to alterations in the attachment of basal keratinocytes to the underlying basal membrane, essential for the maintenance of epidermal stem cell population and stem cells properties (Tani et al., 2000). These observations are consistent with the model proposed by Yang et al. in 1999, suggesting that the lack of epidermal stratification in p63-null mice was the result of the incapacity of epidermal stem cells to renew themselves (Yang et al., 1999).

By contrast, the role of nuclear lamins in epidermal development remains still controversial, as demonstrated by normal epidermal development and normal keratinocytes proliferation after Lamin B1 depletion (Yang et al., 2011a), as well as by the fact that Lamin A/C expression is detected in murine epidermis only at E15.0 after the ectoderm has committed to an epidermal fate and after the onset of epidermal stratification has begun (Blanpain and Fuchs, 2009). This suggests that nuclear lamins are not key factors in epidermal development and that they might only contribute to the observed defects in the nuclear shape of p63-null keratinocytes.

In summary, our data uncovered a novel role of p63 in the maintenance of nuclear structure in epidermal keratinocytes via direct regulation of some nuclear envelope-associated genes and cytoskeleton components. Their reduction is responsible for marked alterations in the nuclear shape of p63-null epidermal keratinocytes and for the altered epidermal development, possibly by affecting stem cell population maintenance as well as keratinocytes migration and proliferation in these mice.

1.16. Altered nuclear architecture affects heterochromatin organization in p63-null mice

Since several decades it has been shown that the proper connections between nucleoskeleton and cytoskeleton play an essential role in driving forces for chromatin movements inside the nucleus. In this context nuclear lamins have been shown to be essential for chromatin organization and gene expression regulation (Dechat et al., 2008). Indeed, in *LMNA-/-* mice, the loss of chromatin integrity is associated with nuclear deformations (Sullivan et al., 1999). In addition, Lamin B1 down-regulation results in the formation of microdomains characterized by the absence of heterochromatin (Shimi et al., 2011a).

The development of new technologies including DamID technique together with chromatin conformation capture (3C, 4C, 5C, Hi-C) (van Steensel and Dekker, 2010), helped analysing chromatin structure and chromatin organization inside the nucleus. Lamina Associated Domains (LADs), which directly interact with the nuclear lamina (Wilson and Berk, 2010), are mainly characterized by repressive histone modifications and inactive genes and gene loci are often tethered to the nuclear membrane via LADs. (Takizawa et al., 2008). LADs interactions with nuclear lamins is mediated by several lamina-associated proteins, including lamin B receptor and they have been shown to be dynamic and dependent on the differentiation process (Peric-Hupkes et al., 2010; Zullo et al., 2012).

Recent data also showed that Ezh2, important component of PRC2, responsible for gene silencing through the tri-methylation of lysine 27 on histone H3 (H3K27me3) (Sparmann and van Lohuizen, 2006), has also been found to be associated with lamin A/C. Mutations in *Lamin A* gene cause a decrease in

Ezh2 level as well as alterations in the distribution of the repressive histone modification H3K27me3 (Shumaker et al., 2006). These findings are consistent with our data, showing a significant reduction of Ezh2 in p63-null embryonic keratinocytes compared to WT controls, possibly as a consequence of the reduced Lamin A/C expression. Interestingly, in WT cells Ezh2 positive foci were mainly located at the nuclear periphery, thus confirming its already mentioned association with the nuclear lamina (Shumaker et al., 2006).

Together with Ezh2 reduction in p63-null keratinocytes, we additionally found reduced level of the repressive histone modification H3K27me3 expression. Furthermore, a more detailed analysis of H3K27me3 distribution in epidermal keratinocytes, revealed a loss of its peripheral distribution in p63-null keratinocytes in comparison to controls.

To test whether alterations in the nuclear shape were directly responsible for the altered H3K27me3 distribution patterns, we analysed only misshapen nuclei and compared them to normally shaped nuclei in p63-null mice. Interestingly, we showed a significant peripheral reduction of H3K27me3 expression in misshapen nuclei in comparison to normally shaped nuclei, strongly suggesting that reduced expression of nuclear lamins and nuclear envelope-associated components are likely to be responsible for the alterations in facultative heterochromatin distribution in p63-null keratinocytes. Our findings are also consistent with recent studies, showing movement of heterochromatin from the nuclear periphery towards the nuclear interior after depletion of Lamin A/C and/or of some of nuclear envelope-associated proteins, including Lamin B receptor (LBR), in epidermal keratinocytes (Solovei et al., 2013). However, no significant alterations in epidermal morphology and/or epidermal development

were shown (Solovei et al., 2013), raising the question regarding the involvement of the nuclear lamins in the controls of epidermal differentiation process.

Our data also showed alterations in the distribution pattern of H3K9me3, histone modification associated with pericentromeric heterochromatin (Peters et al., 2003) and significant increase of H3K9me3 foci at the nuclear interior of p63-null keratinocytes compared to controls. Detailed analysis of H3K9me3 foci revealed that they were more numerous and smaller in size in p63-null nuclei compared to controls, suggesting that heterochromatin clustering and organization might be affected in these cells. In line with these observations we also found reduced expression of HP1α, an interacting partner of H3K9me3 and responsible for pericentromeric heterochromatin organization and clustering (Jones et al., 2000), in p63-null keratinocytes compared to WT controls. However, when only misshapen nuclei have been considered for the analysis, no peripheral loss of this repressive histone modification was shown. By contrast, we found a global reduction of H3K9me3 in misshapen nuclei compared to normally shaped p63-null nuclei as well as a tendency increased number of H3K9me3 foci in misshapen nuclei, suggesting that decrease of HP1α expression rather than alterations in the nuclear shape, is likely to be responsible for the altered organization and clustering of constitutive heterochromatin in p63-null keratinocytes.

Polycomb repressive complexes (PRC1 and PRC2) act cooperatively to repress their target genes by depositing repressive histone modifications, leading to gene repression through several possible mechanisms (Sparmann and van Lohuizen, 2006). In this context, a key role is played by PRC1

catalytical component Ring1B, responsible for H2AK119 ubiquitination after recognition of histone modification H3K27me3 by Cbx proteins (Cbx4, Cbx6, Cbx7 and Cbx8). Interestingly, in p63-null epidermis we found a reduced expression of Ring1B and of the associated H2AK119ub histone modification as well as of Cbx4, Cbx6 and Cbx8, thus suggesting that alterations in the silencing mechanisms mediated by polycomb proteins might contribute to the alterations of gene expression, seen in p63-null mice. Consistent with these results, recent microarray data showed high expression of Ezh2 as well of Cbx4 in mouse epidermis at E16.5, thus suggesting an important role of polycomb repressive complexes in epidermal development and stratification. Interestingly, additional data in our lab also showed a direct transcriptional regulation of the polycomb protein Cbx4 by p63. Consistent with these findings, we found that 11% of E14.5 and E17.5 Cbx4$^{-/-}$ embryos showed epidermal defects similar to those observed in p63-null mice, including reduced epidermal thickness and reduced keratinocytes proliferation in comparison to WT controls, suggesting Cbx4 requirement for epidermal commitment. Interestingly, Cbx4 ablation did not alter the expression of other PRC1 components, essential for epidermal development (Cbx7, Cbx8, Pcgf1 and Phc1), which might therefore be able to restore epidermal stratification at later embryonic stages (E18.5) (data not shown).

By contrast, Cbx4 might play a role in ectodermal commitment to an epidermal fate by inhibiting the transcription of non-epidermal lineage specific genes. Consistent with these observations we found increased expression of several neural genes in E14.5 Cbx4-null epidermis as well as in E16.5 p63-null epidermis, strongly suggesting that Cbx4 plays a crucial role in p63-regulated

gene expression program in epidermal keratinocytes, which acts not only through the establishment and the maintenance of the expression of epidermal-specific genes but also through the repression of non-epidermal-specific genes, including neural genes, already shown to be important target genes of polycomb proteins in the nervous system, where they control neural stem cells maintenance by inhibiting genes related to differentiation into neurons and/or astrocytes (Qi et al., 2013).

In summary, all these data together suggest that the altered gene expression regulation observed in p63-null mouse epidermis, might be the result of the cooperation of several different factors, including altered nuclear structure, changes in the nuclear distribution of heterochromatin and the expression level of genes involved in chromatin organization, including polycomb proteins and chromatin remodelling factors, including Satb1 and Brg1 (Fessing et al., 2011).

Significant reduction of nuclear lamins and nuclear envelope-associated genes and the consequent changes in the peripheral organization of heterochromatin together with several polycomb components reduction, might be responsible for the aberrant silencing of chromatin regions containing epidermal-specific genes, while activating other non tissue-specific genes.

Further studies will be necessary to investigate whether changes in the interactions between nuclear lamins and chromatin occur in p63-null mouse keratinocytes. For this purpose, DamID analysis of lamina associated domains in p63-null keratinocytes and WT controls will be performed to analyse more in depth which chromatin regions lose their interaction with the nuclear lamina in p63-null keratinocytes as a consequence of nuclear lamins reduction.

Furthermore, an analysis of additional genes expression data will be useful to investigate the aberrant expression of other non-epidermal lineage specific genes in p63-null mouse keratinocytes.

1.17. $p63^{-/-}$ skin epithelium as a potential model of skin ageing?

Nuclear lamins also play an important role in ageing process (Dechat et al., 2008) and several studies have shown the existence of similarities between p63-null phenotype and senescence. One example is the premature ageing disease Hutchinson-Gilford Progeria Syndrome (HGPS), caused by mutation in *Lamin A* gene with consequent reduction in the level of the polycomb protein Ezh2 and of the repressive histone modification H3K27me3 (Shumaker et al., 2006), together with alterations in the nuclear shape (Lans and Hoeijmakers, 2006).

In addition to these findings, different studies also showed that reduced Lamin B1 expression was responsible for alterations in chromatin organization, in particular loss of H3K27me3 was observed with up-regulation of key senescence-associated genes (Shah et al., 2013), showing profound chromatin reorganization during senescence and suggesting that Lamin B1 down-regulation in senescence is a key trigger of global and local chromatin changes that impact gene expression and ageing process.

Besides alterations in chromatin organization, Lamin B1 silencing in senescent cells was also responsible for reduced cell proliferation (Shimi et al., 2011a), possibly through a mechanism involving up-regulation of p53 pathway with consequent up-regulation of p53 target genes, including the cell cycle inhibitor p21 (Shimi et al., 2011a). Interestingly, the proliferation defects, observed in

p63-null mice, strictly require p53 with up-regulation of p21 in these mice (Truong et al., 2006).

The observed reduction of some polycomb proteins in p63-null epidermis, might also be linked to the senescence process. In fact, several studies showed that reduction of Bmi-1, component of PRC1 and interacting partner of Ring1B, in primary mouse embryonic fibroblasts, led to the up-regulation of p16 gene (Jacobs et al., 1999a), codified by the *Ink4a* locus and essential in blocking the cell cycle progression via inhibition of Cdk4/6 (Agarwal et al., 2013) with consequent premature senescence in these cells (Jacobs et al., 1999a). By contrast, Bmi-1 up-regulation inhibited p16 expression allowing fibroblasts immortalization and neoplastic transformation (Jacobs et al., 1999a).

Besides Bmi-1, Cbx8 has also been shown to play a role in cell proliferation regulation and senescence process by directly regulating the Ink4a/ARF locus, inhibiting p16 expression thus preventing senescence (Dietrich et al., 2007). Interestingly, we showed thar Cbx8 is significantly reduced in p63-null skin epithelium.

Although several common features between cell senescence and p63-null phenotype are present, further experiments will be necessary to investigate whether p63-null mouse skin epithelium might be considered a model of skin ageing. Among these, analyses of the expression of the most relevant senescence-associated markers in p63-null epidermis will be performed. Furthermore, a detailed analysis of the expression of nuclear lamins and senescence-associated markers will be performed on p63 mutated human skin and compared to the corresponding normal skin samples with the main purpose to analyse whether p63 might also contribute to skin ageing in humans.

1.18. Keratin type II locus is required for the proper expression of epidermal-specific genes in keratinocytes

Other key elements in the maintenance of the proper cellular and nuclear architecture are intermediate filaments, including keratins. Keratins play an important role in epidermal stratification as they are differentially expressed within the different epidermal layers, generating different type of connections, which are dependent on the epidermal layer.

In $p63^{-/-}$ mice the expressions of several keratins-encoding genes are reduced (Fessing et al., 2011), thus suggesting that keratin type I and keratin type II loci might play an important role in gene expression regulation during epidermal differentiation and epidermal barrier formation in addition to their structural role. Consistent with this hypothesis, recent circularized chromosome conformation capture (4C) data obtained in our lab showed that *loricrin* was part of *keratin 5* interactome (unpublished observations). Consistenly with these findings we showed by 3D FISH that, in post-natal day 8 (P8) mice depleted of keratin type II locus in basal keratinocytes, *loricrin* gene occupied a more peripheral position within chromosome territory 3. Furthermore, 3D FISH analyses of the distances between *loricrin* and keratin type II locus flanking regions showed an increased distances specifically in keratins type II-depleted keratinocytes in comparison to WT controls, while no difference in the distances between *loricrin* and keratin type II locus has been shown when the same experiments were performed on freshly isolated thymocytes.

Taken together these findings suggest that keratin type II locus might contain some regulatory elements, required for proper expression of the genes within the EDC, whose coordinated expressions are important for proper epidermal development and stratification.

According to 4C data, together with l*oricrin*, *Satb1* gene was also found as part of *loricrin* and *keratin 5* interactomes (unpublished observations) and these results are also consistent with 3D FISH analyses, showing shorter distances between *loricrin* and *Satb1* in epidermal keratinocytes in comparison to dermal fibroblasts.

We further investigated *Satb1* position within chromosome territory 17 and the distances between *Satb1* and keratin type II locus flanking regions in keratins type II-depleted skin (P8) and corresponding WT control. Interestingly, *Satb1* was mainly localized at the periphery of its chromosome territory, which was accompanied by its reduced expression in keratin type II-depleted keratinocytes in comparison to controls. Additionally, distances between *Satb1* and keratin type II locus were increased in keratin type II-depleted keratinocytes compared to WT controls.

In summary, all these data strongly suggest that *loricrin*, *keratin 5* and *Satb1* might share the same interactome in the nucleus of epidermal keratinocytes, which is essential for the proper expression of these genes as well as for proper epidermal development and stratification. Ablation of keratin type II locus might lead to the disruption of this interactome with molecular and phenotypic consequences, observed in these mice at about P8-P10 of age. Because 3D FISH analyses performed on embryonic skin did not show any significant differences in the distances between *loricrin*, *Satb1* and keratin type II locus (data not shown), this suggests that alterations in gene loci interactions associated with reduced expression of these genes in epidermal keratinocytes are likely to be responsible for the defects in epidermal barrier formation observed in these mice at post-natal day 8 (P8).

Further studies will be necessary to better understand which regions of *loricrin* and *Satb1* genes are responsible for the interactions with *keratin 5* as well as which are the regulatory elements within keratin type II locus, responsible for *Satb1* and *loricrin* gene expression regulation in epidermal keratinocytes.

Taken together these data, confirm the role of higher-order chromatin remodelling and spatial organization of the genes in the nucleus of keratinocytes as essential mechanisms, required for the control of the expression of epidermal-specific genes during the execution of the epidermal stratification program.

Chapter 5

Conclusions and future directions

5. CONCLUSIONS AND FUTURE DIRECTIONS

1.19. Conclusions

Our analysis of gene expression regulation and higher-order chromatin remodelling in the nucleus of epidermal keratinocytes, led us to draw the following conclusions:

1) Our data reveal a novel role of the transcription factor p63 in the maintenance of nuclear architecture in epidermal keratinocytes via direct regulation of nuclear envelope-associated genes and cytoskeleton components, including *Plectin 1c*, *Sun-1* and *Nesprin-3*. We demonstrated that decrease of their expression is responsible, at least in part for marked alterations in the nuclear shape of p63-null epidermal keratinocytes.

Alterations in the nuclear shape in p63-deficient keratinocytes were accompanied by altered heterochromatin distribution which is evident from the global reduction of H3K27me3 and loss of its peripheral distribution, as well as from alterations in H3K9me3 distribution and clustering.

2) Altered heterochromatin organization in p63-deficient keratinocytes together with the reduced expression of several polycomb proteins (Ezh2, Cbx4, Cbx6 and Cbx8) and chromatin remodeling factors (Satb1 and Brg1), might contribute to alterations in gene expression resulting in decreased expression of epidermis-specific genes and increased expression of non-epidermal genes, including neural genes.

3) Lack of the polycomb protein Cbx4, a direct p63 transcriptional target, resulted in development of an epidermal phenotype similar to the one observed in p63-null mice with reduced epidermal thickness and keratinocyte proliferation.

Defects in epidermal morphology and keratinocytes proliferation together with an increase in the expression of neural genes in Cbx4-null epidermis, uncovered a novel role of Cbx4 in epidermal commitment as an essential part of p63-regulated gene expression program. Cbx4 operated as an important regulator that mediates p63-dependent repression of non-epidermal-specific genes.

4) Higher-order chromatin organization and spatial arrengements of lineage-specific genes in keratinocytes play important role in the control of gene expression during epidermal differentiation. In mice with genetic ablation of keratin type II locus, positioning of *Loricrin* and *Satb1* genes are shifted to the peripheral parts of chromosome 3 and 17, respectively, compared to WT controls.

Decreased expressions of Loricrin and Satb1 might be responsible for the altered gene expression within the EDC locus, leading to epidermal barrier defects observed in keratin type II locus knock-out mice.

Moreover, the increased intergenic distance between *Loricrin* and *Satb1* and keratin type II locus flanking regions in keratin type II-deficient keratinocytes compared to WT controls, suggests that these two genes together with keratin type II locus might be part of the same interactome

in the nucleus of epidermal keratinocytes, which is required for the proper expression of these genes. Indeed, keratin type II locus might contain some important regulatory elements, including enhancer and/or promoters, regulating the transcription of *Loricrin* and/or *Satb1*.

1.20. Future directions

Based on the above conclusions, we propose the following directions in the future research in this area:

1) Further studies will be necessary to investigate whether changes in the interactions between nuclear lamins and chromatin occur in p63-null mouse keratinocytes in comparison to WT controls and which chromatin regions are affected. For this purpose, DamID analysis of lamina associated domains in p63-null keratinocytes and WT controls will be helpful to analyse more in depth which chromatin regions lose their interactions with the nuclear lamina in p63-null keratinocytes, as a consequence of the reduction of the expression of nuclear lamins and nuclear envelope-associated components.

2) Further studies will be useful to better understand the molecular mechanisms underlying the role of Cbx4 in mediating gene silencing as part of p63-dependent gene expression program in epidermal keratinocytes. Therefore, p63 knock-down by RNA interference experiments in primary mouse keratinocytes, followed by infection with lentiviral vector containing Cbx4 gene sequence will be helpful to check

whether the addition of Cbx4 can rescue, at least in part, the epidermal defects associated with p63-null phenotype.

3) Additional studies will be necessary to better understand which regions of *Loricrin* and *Satb1* genes are responsible for the interactions with *keratin 5* as well as which are the regulatory elements within keratin type II locus, responsible for *Satb1* and *loricrin* gene expression regulation in epidermal keratinocytes.

4) Deeper analyses of the epigenetics regulatory mechanisms in skin pathological conditions, which affect keratinocytes differentiation, and/or in skin ageing, will be interesting to perform. These analyses will provide an important background for the development of small molecules, targeting distinct epigenetics modulators, as potential therapeutical components for the treatment of skin and/or age-associated disorders.

Chapter 6

References

6. References

Ackerl, R., Walko, G., Fuchs, P., Fischer, I., Schmuth, M., and Wiche, G. (2007). Conditional targeting of plectin in prenatal and adult mouse stratified epithelia causes keratinocyte fragility and lesional epidermal barrier defects. Journal of cell science *120*, 2435-2443.

Agarwal, P., Sandey, M., DeInnocentes, P., and Bird, R.C. (2013). Tumor suppressor gene p16/INK4A/CDKN2A-dependent regulation into and out of the cell cycle in a spontaneous canine model of breast cancer. Journal of cellular biochemistry *114*, 1355-1363.

Ahmad, K., and Henikoff, S. (2002). Histone H3 variants specify modes of chromatin assembly. Proc Natl Acad Sci U S A *99 Suppl 4*, 16477-16484.

Albiez, H., Cremer, M., Tiberi, C., Vecchio, L., Schermelleh, L., Dittrich, S., Kupper, K., Joffe, B., Thormeyer, T., von Hase, J.*, et al.* (2006). Chromatin domains and the interchromatin compartment form structurally defined and functionally interacting nuclear networks. Chromosome Res *14*, 707-733.

Alonso, L., and Fuchs, E. (2003). Stem cells of the skin epithelium. Proc Natl Acad Sci U S A *100 Suppl 1*, 11830-11835.

Andra, K., Kornacker, I., Jorgl, A., Zorer, M., Spazierer, D., Fuchs, P., Fischer, I., and Wiche, G. (2003). Plectin-isoform-specific rescue of hemidesmosomal defects in plectin (-/-) keratinocytes. J Invest Dermatol *120*, 189-197.

Bannister, A.J., and Kouzarides, T. (2011). Regulation of chromatin by histone modifications. Cell research *21*, 381-395.

Barden, H., and Levine, S. (1983). Histochemical observations on rodent brain melanin. Brain research bulletin *10*, 847-851.

Berger, S.L. (2002). Histone modifications in transcriptional regulation. Curr Opin Genet Dev *12*, 142-148.

Bernstein, B.E., Liu, C.L., Humphrey, E.L., Perlstein, E.O., and Schreiber, S.L. (2004). Global nucleosome occupancy in yeast. Genome Biol *5*, R62.

Bershadsky, A.D., Tint, I.S., and Svitkina, T.M. (1987). Association of intermediate filaments with vinculin-containing adhesion plaques of fibroblasts. Cell Motil Cytoskeleton *8*, 274-283.

Blanpain, C. (2010). Stem cells: Skin regeneration and repair. Nature *464*, 686-687.

Blanpain, C., and Fuchs, E. (2006). Epidermal stem cells of the skin. Annu Rev Cell Dev Biol *22*, 339-373.

Blanpain, C., and Fuchs, E. (2009). Epidermal homeostasis: a balancing act of stem cells in the skin. Nat Rev Mol Cell Biol *10*, 207-217.

Blanpain, C., Lowry, W.E., Pasolli, H.A., and Fuchs, E. (2006). Canonical notch signaling functions as a commitment switch in the epidermal lineage. Genes Dev *20*, 3022-3035.

Blumenberg, M. (1993). Molecular biology of human keratin genes. Academic Press, New York *Molecular Biology of the Skin: The Keratinocyte*, 1-24.

Botchkarev, V.A., Gdula, M.R., Mardaryev, A.N., Sharov, A.A., and Fessing, M.Y. (2012). Epigenetic regulation of gene expression in keratinocytes. J Invest Dermatol *132*, 2505-2521.

Boyer, L.A., Plath, K., Zeitlinger, J., Brambrink, T., Medeiros, L.A., Lee, T.I., Levine, S.S., Wernig, M., Tajonar, A., Ray, M.K.*, et al.* (2006). Polycomb complexes repress developmental regulators in murine embryonic stem cells. Nature *441*, 349-353.

Boyle, S., Gilchrist, S., Bridger, J.M., Mahy, N.L., Ellis, J.A., and Bickmore, W.A. (2001). The spatial organization of human chromosomes within the nuclei of normal and emerin-mutant cells. Hum Mol Genet *10*, 211-219.

Bracken, A.P., Dietrich, N., Pasini, D., Hansen, K.H., and Helin, K. (2006). Genome-wide mapping of Polycomb target genes unravels their roles in cell fate transitions. Genes Dev *20*, 1123-1136.

Branco, M.R., and Pombo, A. (2006). Intermingling of chromosome territories in interphase suggests role in translocations and transcription-dependent associations. PLoS Biol *4*, e138.

Brickner, D.G., Cajigas, I., Fondufe-Mittendorf, Y., Ahmed, S., Lee, P.C., Widom, J., and Brickner, J.H. (2007). H2A.Z-mediated localization of genes at the nuclear periphery confers epigenetic memory of previous transcriptional state. PLoS Biol *5*, e81.

Broers, J.L., Machiels, B.M., van Eys, G.J., Kuijpers, H.J., Manders, E.M., van Driel, R., and Ramaekers, F.C. (1999). Dynamics of the nuclear lamina as monitored by GFP-tagged A-type lamins. J Cell Sci *112 (Pt 20)*, 3463-3475.

Broers, J.L., Ramaekers, F.C., Bonne, G., Yaou, R.B., and Hutchison, C.J. (2006). Nuclear lamins: laminopathies and their role in premature ageing. Physiol Rev *86*, 967-1008.

Buchwald, G., van der Stoop, P., Weichenrieder, O., Perrakis, A., van Lohuizen, M., and Sixma, T.K. (2006). Structure and E3-ligase activity of the Ring-Ring complex of polycomb proteins Bmi1 and Ring1b. EMBO J *25*, 2465-2474.

Burke, B., and Roux, K.J. (2009). Nuclei take a position: managing nuclear location. Dev Cell *17*, 587-597.

Candi, E., Schmidt, R., and Melino, G. (2005). The cornified envelope: a model of cell death in the skin. Nat Rev Mol Cell Biol *6*, 328-340.

Caretti, G., Di Padova, M., Micales, B., Lyons, G.E., and Sartorelli, V. (2004). The Polycomb Ezh2 methyltransferase regulates muscle gene expression and skeletal muscle differentiation. Genes Dev *18*, 2627-2638.

Carroll, D.K., Carroll, J.S., Leong, C.O., Cheng, F., Brown, M., Mills, A.A., Brugge, J.S., and Ellisen, L.W. (2006). p63 regulates an adhesion programme and cell survival in epithelial cells. Nat Cell Biol *8*, 551-561.

Chepelev, I., Wei, G., Wangsa, D., Tang, Q., and Zhao, K. (2012). Characterization of genome-wide enhancer-promoter interactions reveals co-expression of interacting genes and modes of higher order chromatin organization. Cell research *22*, 490-503.

Chomiczewska, D., Trznadel-Budzko, E., Kaczorowska, A., and Rotsztejn, H. (2009). [The role of Langerhans cells in the skin immune system]. Polski merkuriusz lekarski : organ Polskiego Towarzystwa Lekarskiego *26*, 173-177.

Chopra, V.S., Hendrix, D.A., Core, L.J., Tsui, C., Lis, J.T., and Levine, M. (2011). The polycomb group mutant esc leads to augmented levels of paused Pol II in the Drosophila embryo. Mol Cell *42*, 837-844.

Chuong, C.M., Jung, H.S., Noden, D., and Widelitz, R.B. (1998). Lineage and pluripotentiality of epithelial precursor cells in developing chicken skin. Biochem Cell Biol *76*, 1069-1077.

Clapier, C.R., and Cairns, B.R. (2009). The biology of chromatin remodeling complexes. Annu Rev Biochem *78*, 273-304.

Constantinescu, D., Gray, H.L., Sammak, P.J., Schatten, G.P., and Csoka, A.B. (2006). Lamin A/C expression is a marker of mouse and human embryonic stem cell differentiation. Stem Cells *24*, 177-185.

Cotsarelis, G. (2006). Epithelial stem cells: a folliculocentric view. J Invest Dermatol *126*, 1459-1468.

Cotsarelis, G., Sun, T.T., and Lavker, R.M. (1990). Label-retaining cells reside in the bulge area of pilosebaceous unit: implications for follicular stem cells, hair cycle, and skin carcinogenesis. Cell *61*, 1329-1337.

Cremer, C., Cremer, T., and Gray, J.W. (1982). Induction of chromosome damage by ultraviolet light and caffeine: correlation of cytogenetic evaluation and flow karyotype. Cytometry *2*, 287-290.

Cremer, M., Grasser, F., Lanctot, C., Muller, S., Neusser, M., Zinner, R., Solovei, I., and Cremer, T. (2008). Multicolor 3D fluorescence in situ hybridization for imaging interphase chromosomes. Methods Mol Biol *463*, 205-239.

Cremer, T., and Cremer, M. (2010). Chromosome territories. Cold Spring Harb Perspect Biol *2*, a003889.

Crisp, M., Liu, Q., Roux, K., Rattner, J.B., Shanahan, C., Burke, B., Stahl, P.D., and Hodzic, D. (2006). Coupling of the nucleus and cytoplasm: role of the LINC complex. J Cell Biol *172*, 41-53.

Dai, Z., and Dai, X. (2011). Nuclear colocalization of transcription factor target genes strengthens coregulation in yeast. Nucleic Acids Res.

Daujat, S., Zeissler, U., Waldmann, T., Happel, N., and Schneider, R. (2005). HP1 binds specifically to Lys26-methylated histone H1.4, whereas simultaneous Ser27 phosphorylation blocks HP1 binding. J Biol Chem *280*, 38090-38095.

de Guzman Strong, C., Conlan, S., Deming, C.B., Cheng, J., Sears, K.E., and Segre, J.A. (2010). A milieu of regulatory elements in the epidermal differentiation complex syntenic block: implications for atopic dermatitis and psoriasis. Hum Mol Genet *19*, 1453-1460.

Dechat, T., Adam, S.A., Taimen, P., Shimi, T., and Goldman, R.D. (2010). Nuclear lamins. Cold Spring Harb Perspect Biol *2*, a000547.

Dechat, T., Pfleghaar, K., Sengupta, K., Shimi, T., Shumaker, D.K., Solimando, L., and Goldman, R.D. (2008). Nuclear lamins: major factors in the structural organization and function of the nucleus and chromatin. Genes Dev *22*, 832-853.

Dellino, G.I., Schwartz, Y.B., Farkas, G., McCabe, D., Elgin, S.C., and Pirrotta, V. (2004). Polycomb silencing blocks transcription initiation. Mol Cell *13*, 887-893.

Dhillon, N., and Kamakaka, R.T. (2000). A histone variant, Htz1p, and a Sir1p-like protein, Esc2p, mediate silencing at HMR. Mol Cell *6*, 769-780.

Dietrich, N., Bracken, A.P., Trinh, E., Schjerling, C.K., Koseki, H., Rappsilber, J., Helin, K., and Hansen, K.H. (2007). Bypass of senescence by the polycomb group protein CBX8 through direct binding to the INK4A-ARF locus. EMBO J *26*, 1637-1648.

Dion, M.F., Altschuler, S.J., Wu, L.F., and Rando, O.J. (2005). Genomic characterization reveals a simple histone H4 acetylation code. Proc Natl Acad Sci U S A *102*, 5501-5506.

DiSepio, D., Jones, A., Longley, M.A., Bundman, D., Rothnagel, J.A., and Roop, D.R. (1995). The proximal promoter of the mouse loricrin gene contains a functional AP-1 element and directs keratinocyte-specific but not differentiation-specific expression. J Biol Chem *270*, 10792-10799.

Eberharter, A., Langst, G., and Becker, P.B. (2004). A nucleosome sliding assay for chromatin remodeling factors. Methods in enzymology *377*, 344-353.

Elder, J.T., and Zhao, X. (2002). Evidence for local control of gene expression in the epidermal differentiation complex. Exp Dermatol *11*, 406-412.

Elefanty, A.G., Antoniou, M., Custodio, N., Carmo-Fonseca, M., and Grosveld, F.G. (1996). GATA transcription factors associate with a novel class of nuclear bodies in erythroblasts and megakaryocytes. EMBO J *15*, 319-333.

Eskeland, R., Leeb, M., Grimes, G.R., Kress, C., Boyle, S., Sproul, D., Gilbert, N., Fan, Y., Skoultchi, A.I., Wutz, A.*, et al.* (2010). Ring1B compacts chromatin structure and represses gene expression independent of histone ubiquitination. Mol Cell *38*, 452-464.

Ezhkova, E., Lien, W.H., Stokes, N., Pasolli, H.A., Silva, J.M., and Fuchs, E. (2011). EZH1 and EZH2 cogovern histone H3K27 trimethylation and are essential for hair follicle homeostasis and wound repair. Genes Dev *25*, 485-498.

Ezhkova, E., Pasolli, H.A., Parker, J.S., Stokes, N., Su, I.H., Hannon, G., Tarakhovsky, A., and Fuchs, E. (2009). Ezh2 orchestrates gene expression for the stepwise differentiation of tissue-specific stem cells. Cell *136*, 1122-1135.

Fan, J.Y., Gordon, F., Luger, K., Hansen, J.C., and Tremethick, D.J. (2002). The essential histone variant H2A.Z regulates the equilibrium between different chromatin conformational states. Nat Struct Biol *9*, 172-176.

Felsenfeld, G., and Groudine, M. (2003). Controlling the double helix. Nature *421*, 448-453.

Feng, S., Jacobsen, S.E., and Reik, W. (2010). Epigenetic reprogramming in plant and animal development. Science *330*, 622-627.

Fessing, M.Y., Mardaryev, A.N., Gdula, M.R., Sharov, A.A., Sharova, T.Y., Rapisarda, V., Gordon, K.B., Smorodchenko, A.D., Poterlowicz, K., Ferone, G.*, et al.* (2011). p63 regulates Satb1 to control tissue-specific chromatin remodeling during development of the epidermis. J Cell Biol *194*, 825-839.

Fields, A.P., and Thompson, L.J. (1995). The regulation of mitotic nuclear envelope breakdown: a role for multiple lamin kinases. Prog Cell Cycle Res *1*, 271-286.

Fischle, W., Wang, Y., and Allis, C.D. (2003). Histone and chromatin cross-talk. Curr Opin Cell Biol *15*, 172-183.

Foisner, R., Traub, P., and Wiche, G. (1991). Protein kinase A- and protein kinase C-regulated interaction of plectin with lamin B and vimentin. Proc Natl Acad Sci U S A *88*, 3812-3816.

Francis, N.J., Kingston, R.E., and Woodcock, C.L. (2004). Chromatin compaction by a polycomb group protein complex. Science *306*, 1574-1577.

Fuchs, E. (1995). Keratins and the skin. Annu Rev Cell Dev Biol *11*, 123-153.

Fuchs, E. (2007). Scratching the surface of skin development. Nature *445*, 834-842.

Fuchs, E., and Raghavan, S. (2002). Getting under the skin of epidermal morphogenesis. Nat Rev Genet *3*, 199-209.

Fuchs, P., Zorer, M., Rezniczek, G.A., Spazierer, D., Oehler, S., Castanon, M.J., Hauptmann, R., and Wiche, G. (1999). Unusual 5' transcript complexity of plectin isoforms: novel tissue-specific exons modulate actin binding activity. Hum Mol Genet *8*, 2461-2472.

Gdula, M.R., Poterlowicz, K., Mardaryev, A.N., Sharov, A.A., Peng, Y., Fessing, M.Y., and Botchkarev, V.A. (2013). Remodeling of three-dimensional organization of the nucleus during terminal keratinocyte differentiation in the epidermis. J Invest Dermatol *133*, 2191-2201.

Geyer, P.K., Vitalini, M.W., and Wallrath, L.L. (2011). Nuclear organization: taking a position on gene expression. Curr Opin Cell Biol *23*, 354-359.

Ghioni, P., Bolognese, F., Duijf, P.H., Van Bokhoven, H., Mantovani, R., and Guerrini, L. (2002). Complex transcriptional effects of p63 isoforms: identification of novel activation and repression domains. Mol Cell Biol *22*, 8659-8668.

Gibcus, J.H., and Dekker, J. (2013). The hierarchy of the 3D genome. Mol Cell *49*, 773-782.

Goldman, A.E., Maul, G., Steinert, P.M., Yang, H.Y., and Goldman, R.D. (1986). Keratin-like proteins that coisolate with intermediate filaments of BHK-21 cells are nuclear lamins. Proc Natl Acad Sci U S A *83*, 3839-3843.

Goldman, R.D., Shumaker, D.K., Erdos, M.R., Eriksson, M., Goldman, A.E., Gordon, L.B., Gruenbaum, Y., Khuon, S., Mendez, M., Varga, R.*, et al.* (2004). Accumulation of mutant lamin A causes progressive changes in nuclear architecture in Hutchinson-Gilford progeria syndrome. Proc Natl Acad Sci U S A *101*, 8963-8968.

Gonczy, P. (2008). Mechanisms of asymmetric cell division: flies and worms pave the way. Nat Rev Mol Cell Biol *9*, 355-366.

Gong, F., Sun, L., Wang, Z., Shi, J., Li, W., Wang, S., Han, X., and Sun, Y. (2011). The BCL2 gene is regulated by a special AT-rich sequence binding protein 1-mediated long range chromosomal interaction between the promoter and the distal element located within the 3'-UTR. Nucleic Acids Res *39*, 4640-4652.

Grande, M.A., van der Kraan, I., de Jong, L., and van Driel, R. (1997). Nuclear distribution of transcription factors in relation to sites of transcription and RNA polymerase II. J Cell Sci *110 (Pt 15)*, 1781-1791.

Gros-Louis, F., Dupre, N., Dion, P., Fox, M.A., Laurent, S., Verreault, S., Sanes, J.R., Bouchard, J.P., and Rouleau, G.A. (2007). Mutations in SYNE1 lead to a newly discovered form of autosomal recessive cerebellar ataxia. Nature genetics *39*, 80-85.

Guo, C., Gerasimova, T., Hao, H., Ivanova, I., Chakraborty, T., Selimyan, R., Oltz, E.M., and Sen, R. (2011). Two forms of loops generate the chromatin conformation of the immunoglobulin heavy-chain gene locus. Cell *147*, 332-343.

Halata, Z., Grim, M., and Baumann, K.I. (2003). [The Merkel cell: morphology, developmental origin, function]. Casopis lekaru ceskych *142*, 4-9.

Hale, C.M., Shrestha, A.L., Khatau, S.B., Stewart-Hutchinson, P.J., Hernandez, L., Stewart, C.L., Hodzic, D., and Wirtz, D. (2008). Dysfunctional connections between the nucleus and the actin and microtubule networks in laminopathic models. Biophysical journal *95*, 5462-5475.

Haque, F., Lloyd, D.J., Smallwood, D.T., Dent, C.L., Shanahan, C.M., Fry, A.M., Trembath, R.C., and Shackleton, S. (2006). SUN1 interacts with nuclear lamin A and cytoplasmic nesprins to provide a physical connection between the nuclear lamina and the cytoskeleton. Mol Cell Biol *26*, 3738-3751.

Hernandez-Munoz, I., Taghavi, P., Kuijl, C., Neefjes, J., and van Lohuizen, M. (2005). Association of BMI1 with polycomb bodies is dynamic and requires PRC2/EZH2 and the maintenance DNA methyltransferase DNMT1. Mol Cell Biol *25*, 11047-11058.

Herrmann, H., Hesse, M., Reichenzeller, M., Aebi, U., and Magin, T.M. (2003). Functional complexity of intermediate filament cytoskeletons: from structure to assembly to gene ablation. International review of cytology *223*, 83-175.

Hodawadekar, S.C., and Marmorstein, R. (2007). Chemistry of acetyl transfer by histone modifying enzymes: structure, mechanism and implications for effector design. Oncogene *26*, 5528-5540.

Horn, P.J., and Peterson, C.L. (2002). Molecular biology. Chromatin higher order folding--wrapping up transcription. Science *297*, 1824-1827.

Houben, F., Ramaekers, F.C., Snoeckx, L.H., and Broers, J.L. (2007). Role of nuclear lamina-cytoskeleton interactions in the maintenance of cellular strength. Biochim Biophys Acta *1773*, 675-686.

Houben, F., Willems, C.H., Declercq, I.L., Hochstenbach, K., Kamps, M.A., Snoeckx, L.H., Ramaekers, F.C., and Broers, J.L. (2009). Disturbed nuclear orientation and cellular migration in A-type lamin deficient cells. Biochim Biophys Acta *1793*, 312-324.

Huelsken, J., Vogel, R., Erdmann, B., Cotsarelis, G., and Birchmeier, W. (2001). beta-Catenin controls hair follicle morphogenesis and stem cell differentiation in the skin. Cell *105*, 533-545.

Hunkapiller, J., Shen, Y., Diaz, A., Cagney, G., McCleary, D., Ramalho-Santos, M., Krogan, N., Ren, B., Song, J.S., and Reiter, J.F. (2012). Polycomb-like 3 promotes polycomb repressive complex 2 binding to CpG islands and embryonic stem cell self-renewal. PLoS genetics *8*, e1002576.

Indra, A.K., Dupe, V., Bornert, J.M., Messaddeq, N., Yaniv, M., Mark, M., Chambon, P., and Metzger, D. (2005). Temporally controlled targeted somatic mutagenesis in embryonic surface ectoderm and fetal epidermal keratinocytes unveils two distinct developmental functions of BRG1 in limb morphogenesis and skin barrier formation. Development *132*, 4533-4544.

Iozzo, R.V. (2005). Basement membrane proteoglycans: from cellar to ceiling. Nat Rev Mol Cell Biol *6*, 646-656.

Ishii, K., Arib, G., Lin, C., Van Houwe, G., and Laemmli, U.K. (2002). Chromatin boundaries in budding yeast: the nuclear pore connection. Cell *109*, 551-562.

Jacobs, J.J., Kieboom, K., Marino, S., DePinho, R.A., and van Lohuizen, M. (1999a). The oncogene and Polycomb-group gene bmi-1 regulates cell proliferation and senescence through the ink4a locus. Nature *397*, 164-168.

Jacobs, J.J., Scheijen, B., Voncken, J.W., Kieboom, K., Berns, A., and van Lohuizen, M. (1999b). Bmi-1 collaborates with c-Myc in tumorigenesis by inhibiting c-Myc-induced apoptosis via INK4a/ARF. Genes Dev *13*, 2678-2690.

Jenuwein, T., and Allis, C.D. (2001). Translating the histone code. Science *293*, 1074-1080.

Jones, D.O., Cowell, I.G., and Singh, P.B. (2000). Mammalian chromodomain proteins: their role in genome organisation and expression. Bioessays *22*, 124-137.

Kamminga, L.M., Bystrykh, L.V., de Boer, A., Houwer, S., Douma, J., Weersing, E., Dontje, B., and de Haan, G. (2006). The Polycomb group gene Ezh2 prevents hematopoietic stem cell exhaustion. Blood *107*, 2170-2179.

Kashiwagi, M., Morgan, B.A., and Georgopoulos, K. (2007). The chromatin remodeler Mi-2beta is required for establishment of the basal epidermis and normal differentiation of its progeny. Development *134*, 1571-1582.

Kelly, P., Katema, M., Amadi, B., Zimba, L., Aparicio, S., Mudenda, V., Baboo, K.S., and Zulu, I. (2008). Gastrointestinal pathology in the University Teaching Hospital, Lusaka, Zambia: review of endoscopic and pathology records. Trans R Soc Trop Med Hyg *102*, 194-199.

Ketema, M., and Sonnenberg, A. (2011). Nesprin-3: a versatile connector between the nucleus and the cytoskeleton. Biochem Soc Trans *39*, 1719-1724.

Kharchenko, P.V., Alekseyenko, A.A., Schwartz, Y.B., Minoda, A., Riddle, N.C., Ernst, J., Sabo, P.J., Larschan, E., Gorchakov, A.A., Gu, T.*, et al.* (2011). Comprehensive analysis of the chromatin landscape in Drosophila melanogaster. Nature *471*, 480-485.

Kim, C.A., and Bowie, J.U. (2003). SAM domains: uniform structure, diversity of function. Trends Biochem Sci *28*, 625-628.

Kim, S.I., Bultman, S.J., Kiefer, C.M., Dean, A., and Bresnick, E.H. (2009). BRG1 requirement for long-range interaction of a locus control region with a downstream promoter. Proc Natl Acad Sci U S A *106*, 2259-2264.

Kim, Y.J., Cecchini, K.R., and Kim, T.H. (2011). Conserved, developmentally regulated mechanism couples chromosomal looping and heterochromatin barrier activity at the homeobox gene A locus. Proc Natl Acad Sci U S A *108*, 7391-7396.

Kirmizis, A., Bartley, S.M., and Farnham, P.J. (2003). Identification of the polycomb group protein SU(Z)12 as a potential molecular target for human cancer therapy. Molecular cancer therapeutics *2*, 113-121.

Klymenko, T., Papp, B., Fischle, W., Kocher, T., Schelder, M., Fritsch, C., Wild, B., Wilm, M., and Muller, J. (2006). A Polycomb group protein complex with sequence-specific DNA-binding and selective methyl-lysine-binding activities. Genes Dev *20*, 1110-1122.

Knoblich, J.A. (2008). Mechanisms of asymmetric stem cell division. Cell *132*, 583-597.

Konstantinidou, A.E., Givalos, N., Gakiopoulou, H., Korkolopoulou, P., Kotsiakis, X., Boviatsis, E., Agrogiannis, G., Mahera, H., and Patsouris, E. (2007). Caspase-3 immunohistochemical expression is a marker of apoptosis, increased grade and early recurrence in intracranial meningiomas. Apoptosis : an international journal on programmed cell death *12*, 695-705.

Kornberg, R.D. (1974). Chromatin structure: a repeating unit of histones and DNA. Science *184*, 868-871.

Kosak, S.T., and Groudine, M. (2004). Gene order and dynamic domains. Science *306*, 644-647.

Kostan, J., Gregor, M., Walko, G., and Wiche, G. (2009). Plectin isoform-dependent regulation of keratin-integrin alpha6beta4 anchorage via Ca2+/calmodulin. J Biol Chem *284*, 18525-18536.

Koster, M.I., Dai, D., Marinari, B., Sano, Y., Costanzo, A., Karin, M., and Roop, D.R. (2007). p63 induces key target genes required for epidermal morphogenesis. Proc Natl Acad Sci U S A *104*, 3255-3260.

Koster, M.I., Kim, S., Mills, A.A., DeMayo, F.J., and Roop, D.R. (2004). p63 is the molecular switch for initiation of an epithelial stratification program. Genes Dev *18*, 126-131.

Koster, M.I., and Roop, D.R. (2007). Mechanisms regulating epithelial stratification. Annu Rev Cell Dev Biol *23*, 93-113.

Krivega, I., and Dean, A. (2012). Enhancer and promoter interactions-long distance calls. Curr Opin Genet Dev *22*, 79-85.

Ku, M., Koche, R.P., Rheinbay, E., Mendenhall, E.M., Endoh, M., Mikkelsen, T.S., Presser, A., Nusbaum, C., Xie, X., Chi, A.S.*, et al.* (2008). Genomewide analysis of PRC1 and PRC2 occupancy identifies two classes of bivalent domains. PLoS genetics *4*, e1000242.

Kurdistani, S.K., Tavazoie, S., and Grunstein, M. (2004). Mapping global histone acetylation patterns to gene expression. Cell *117*, 721-733.

Kurokawa, I., Takahashi, K., Moll, I., and Moll, R. (2011). Expression of keratins in cutaneous epithelial tumors and related disorders--distribution and clinical significance. Exp Dermatol *20*, 217-228.

Lagarou, A., Mohd-Sarip, A., Moshkin, Y.M., Chalkley, G.E., Bezstarosti, K., Demmers, J.A., and Verrijzer, C.P. (2008). dKDM2 couples histone H2A ubiquitylation to histone H3 demethylation during Polycomb group silencing. Genes Dev *22*, 2799-2810.

Lammerding, J., Schulze, P.C., Takahashi, T., Kozlov, S., Sullivan, T., Kamm, R.D., Stewart, C.L., and Lee, R.T. (2004). Lamin A/C deficiency causes defective nuclear mechanics and mechanotransduction. The Journal of clinical investigation *113*, 370-378.

Lans, H., and Hoeijmakers, J.H. (2006). Cell biology: ageing nucleus gets out of shape. Nature *440*, 32-34.

LeBoeuf, M., Terrell, A., Trivedi, S., Sinha, S., Epstein, J.A., Olson, E.N., Morrisey, E.E., and Millar, S.E. (2010). Hdac1 and Hdac2 act redundantly to control p63 and p53 functions in epidermal progenitor cells. Dev Cell *19*, 807-818.

Lee, H., and Kimelman, D. (2002). A dominant-negative form of p63 is required for epidermal proliferation in zebrafish. Dev Cell *2*, 607-616.

Lee, J.S., Shukla, A., Schneider, J., Swanson, S.K., Washburn, M.P., Florens, L., Bhaumik, S.R., and Shilatifard, A. (2007). Histone crosstalk between H2B monoubiquitination and H3 methylation mediated by COMPASS. Cell *131*, 1084-1096.

Lee, T.I., Jenner, R.G., Boyer, L.A., Guenther, M.G., Levine, S.S., Kumar, R.M., Chevalier, B., Johnstone, S.E., Cole, M.F., Isono, K.*, et al.* (2006). Control of developmental regulators by Polycomb in human embryonic stem cells. Cell *125*, 301-313.

Lei, K., Zhang, X., Ding, X., Guo, X., Chen, M., Zhu, B., Xu, T., Zhuang, Y., Xu, R., and Han, M. (2009). SUN1 and SUN2 play critical but partially redundant roles in anchoring nuclei in skeletal muscle cells in mice. Proc Natl Acad Sci U S A *106*, 10207-10212.

Leung, C., Lingbeek, M., Shakhova, O., Liu, J., Tanger, E., Saremaslani, P., Van Lohuizen, M., and Marino, S. (2004). Bmi1 is essential for cerebellar development and is overexpressed in human medulloblastomas. Nature *428*, 337-341.

Li, B., Carey, M., and Workman, J.L. (2007). The role of chromatin during transcription. Cell *128*, 707-719.

Li, B., Pattenden, S.G., Lee, D., Gutierrez, J., Chen, J., Seidel, C., Gerton, J., and Workman, J.L. (2005). Preferential occupancy of histone variant H2AZ at inactive promoters influences local histone modifications and chromatin remodeling. Proc Natl Acad Sci U S A *102*, 18385-18390.

Light, W.H., Brickner, D.G., Brand, V.R., and Brickner, J.H. (2010). Interaction of a DNA zip code with the nuclear pore complex promotes H2A.Z incorporation and INO1 transcriptional memory. Mol Cell *40*, 112-125.

Lin, F., and Worman, H.J. (1993). Structural organization of the human gene encoding nuclear lamin A and nuclear lamin C. J Biol Chem *268*, 16321-16326.

Loebel, D.A., Watson, C.M., De Young, R.A., and Tam, P.P. (2003). Lineage choice and differentiation in mouse embryos and embryonic stem cells. Dev Biol *264*, 1-14.

Loewinger, L., and McKeon, F. (1988). Mutations in the nuclear lamin proteins resulting in their aberrant assembly in the cytoplasm. EMBO J *7*, 2301-2309.

Lopardo, T., Lo Iacono, N., Marinari, B., Giustizieri, M.L., Cyr, D.G., Merlo, G., Crosti, F., Costanzo, A., and Guerrini, L. (2008). Claudin-1 is a p63 target gene with a crucial role in epithelial development. PloS one *3*, e2715.

Luger, K. (2003). Structure and dynamic behavior of nucleosomes. Curr Opin Genet Dev *13*, 127-135.

Luger, K., Mader, A.W., Richmond, R.K., Sargent, D.F., and Richmond, T.J. (1997). Crystal structure of the nucleosome core particle at 2.8 A resolution. Nature *389*, 251-260.

Luis, N.M., Morey, L., Mejetta, S., Pascual, G., Janich, P., Kuebler, B., Cozutto, L., Roma, G., Nascimento, E., Frye, M.*, et al.* (2011). Regulation of human epidermal stem cell proliferation and senescence requires polycomb- dependent and -independent functions of Cbx4. Cell stem cell *9*, 233-246.

MacPherson, M.J., Beatty, L.G., Zhou, W., Du, M., and Sadowski, P.D. (2009). The CTCF insulator protein is posttranslationally modified by SUMO. Mol Cell Biol *29*, 714-725.

Marella, N.V., Seifert, B., Nagarajan, P., Sinha, S., and Berezney, R. (2009). Chromosomal rearrangements during human epidermal keratinocyte differentiation. J Cell Physiol *221*, 139-146.

Margueron, R., Trojer, P., and Reinberg, D. (2005). The key to development: interpreting the histone code? Curr Opin Genet Dev *15*, 163-176.

Marsman, J., and Horsfield, J.A. (2012). Long distance relationships: enhancer-promoter communication and dynamic gene transcription. Biochim Biophys Acta *1819*, 1217-1227.

Maske, C.P., Hollinshead, M.S., Higbee, N.C., Bergo, M.O., Young, S.G., and Vaux, D.J. (2003). A carboxyl-terminal interaction of lamin B1 is dependent on the CAAX endoprotease Rce1 and carboxymethylation. J Cell Biol *162*, 1223-1232.

Matharu, N.K., Hussain, T., Sankaranarayanan, R., and Mishra, R.K. (2010). Vertebrate homologue of Drosophila GAGA factor. J Mol Biol *400*, 434-447.

McDade, S.S., and McCance, D.J. (2010). The role of p63 in epidermal morphogenesis and neoplasia. Biochem Soc Trans *38*, 223-228.

Mendenhall, E.M., Koche, R.P., Truong, T., Zhou, V.W., Issac, B., Chi, A.S., Ku, M., and Bernstein, B.E. (2010). GC-rich sequence elements recruit PRC2 in mammalian ES cells. PLoS genetics *6*, e1001244.

Meneghini, M.D., Wu, M., and Madhani, H.D. (2003). Conserved histone variant H2A.Z protects euchromatin from the ectopic spread of silent heterochromatin. Cell *112*, 725-736.

Menon, G.K., Grayson, S., and Elias, P.M. (1985). Ionic calcium reservoirs in mammalian epidermis: ultrastructural localization by ion-capture cytochemistry. J Invest Dermatol *84*, 508-512.

Meshorer, E., and Misteli, T. (2006). Chromatin in pluripotent embryonic stem cells and differentiation. Nat Rev Mol Cell Biol *7*, 540-546.

Mikkola, M.L. (2007). p63 in skin appendage development. Cell cycle *6*, 285-290.

Mills, A.A., Zheng, B., Wang, X.J., Vogel, H., Roop, D.R., and Bradley, A. (1999). p63 is a p53 homologue required for limb and epidermal morphogenesis. Nature *398*, 708-713.

Min, I.M., Waterfall, J.J., Core, L.J., Munroe, R.J., Schimenti, J., and Lis, J.T. (2011). Regulating RNA polymerase pausing and transcription elongation in embryonic stem cells. Genes Dev *25*, 742-754.

Mohd-Sarip, A., van der Knaap, J.A., Wyman, C., Kanaar, R., Schedl, P., and Verrijzer, C.P. (2006). Architecture of a polycomb nucleoprotein complex. Mol Cell *24*, 91-100.

Moir, R.D., Spann, T.P., Lopez-Soler, R.I., Yoon, M., Goldman, A.E., Khuon, S., and Goldman, R.D. (2000). Review: the dynamics of the nuclear lamins during the cell cycle-- relationship between structure and function. J Struct Biol *129*, 324-334.

Molofsky, A.V., Pardal, R., Iwashita, T., Park, I.K., Clarke, M.F., and Morrison, S.J. (2003). Bmi-1 dependence distinguishes neural stem cell self-renewal from progenitor proliferation. Nature *425*, 962-967.

Morey, L., Pascual, G., Cozzuto, L., Roma, G., Wutz, A., Benitah, S.A., and Di Croce, L. (2012). Nonoverlapping functions of the Polycomb group Cbx family of proteins in embryonic stem cells. Cell stem cell *10*, 47-62.

Morgan, J.T., Pfeiffer, E.R., Thirkill, T.L., Kumar, P., Peng, G., Fridolfsson, H.N., Douglas, G.C., Starr, D.A., and Barakat, A.I. (2011). Nesprin-3 regulates endothelial cell morphology, perinuclear cytoskeletal architecture, and flow-induced polarization. Molecular biology of the cell *22*, 4324-4334.

Moriyama, M., Durham, A.D., Moriyama, H., Hasegawa, K., Nishikawa, S., Radtke, F., and Osawa, M. (2008). Multiple roles of Notch signaling in the regulation of epidermal development. Dev Cell *14*, 594-604.

Morrison, K.M., Miesegaes, G.R., Lumpkin, E.A., and Maricich, S.M. (2009). Mammalian Merkel cells are descended from the epidermal lineage. Dev Biol *336*, 76-83.

Morrison, S.J., and Kimble, J. (2006). Asymmetric and symmetric stem-cell divisions in development and cancer. Nature *441*, 1068-1074.

Muller, J., and Kassis, J.A. (2006). Polycomb response elements and targeting of Polycomb group proteins in Drosophila. Curr Opin Genet Dev *16*, 476-484.

Muller, J., and Verrijzer, P. (2009). Biochemical mechanisms of gene regulation by polycomb group protein complexes. Curr Opin Genet Dev *19*, 150-158.

Muller, M., Hagstrom, K., Gyurkovics, H., Pirrotta, V., and Schedl, P. (1999). The mcp element from the Drosophila melanogaster bithorax complex mediates long-distance regulatory interactions. Genetics *153*, 1333-1356.

Murray-Zmijewski, F., Lane, D.P., and Bourdon, J.C. (2006). p53/p63/p73 isoforms: an orchestra of isoforms to harmonise cell differentiation and response to stress. Cell Death Differ *13*, 962-972.

Nechaev, S., and Adelman, K. (2011). Pol II waiting in the starting gates: Regulating the transition from transcription initiation into productive elongation. Biochim Biophys Acta *1809*, 34-45.

Nekrasov, M., Klymenko, T., Fraterman, S., Papp, B., Oktaba, K., Kocher, T., Cohen, A., Stunnenberg, H.G., Wilm, M., and Muller, J. (2007). Pcl-PRC2 is needed to generate high levels of H3-K27 trimethylation at Polycomb target genes. EMBO J *26*, 4078-4088.

Newport, J.W., Wilson, K.L., and Dunphy, W.G. (1990). A lamin-independent pathway for nuclear envelope assembly. J Cell Biol *111*, 2247-2259.

Nguyen, B.C., Lefort, K., Mandinova, A., Antonini, D., Devgan, V., Della Gatta, G., Koster, M.I., Zhang, Z., Wang, J., Tommasi di Vignano, A.*, et al.* (2006). Cross-regulation between Notch and p63 in keratinocyte commitment to differentiation. Genes Dev *20*, 1028-1042.

Nichols, J., Zevnik, B., Anastassiadis, K., Niwa, H., Klewe-Nebenius, D., Chambers, I., Scholer, H., and Smith, A. (1998). Formation of pluripotent stem cells in the mammalian embryo depends on the POU transcription factor Oct4. Cell *95*, 379-391.

Nievers, M.G., Kuikman, I., Geerts, D., Leigh, I.M., and Sonnenberg, A. (2000). Formation of hemidesmosome-like structures in the absence of ligand binding by the (alpha)6(beta)4 integrin requires binding of HD1/plectin to the cytoplasmic domain of the (beta)4 integrin subunit. J Cell Sci *113 (Pt 6)*, 963-973.

O'Carroll, D., Erhardt, S., Pagani, M., Barton, S.C., Surani, M.A., and Jenuwein, T. (2001). The polycomb-group gene Ezh2 is required for early mouse development. Mol Cell Biol *21*, 4330-4336.

O'Connell, S., Wang, L., Robert, S., Jones, C.A., Saint, R., and Jones, R.S. (2001). Polycomblike PHD fingers mediate conserved interaction with enhancer of zeste protein. J Biol Chem *276*, 43065-43073.

Ohno, K., McCabe, D., Czermin, B., Imhof, A., and Pirrotta, V. (2008). ESC, ESCL and their roles in Polycomb Group mechanisms. Mechanisms of development *125*, 527-541.

Onodera, C.S., Underwood, J.G., Katzman, S., Jacobs, F., Greenberg, D., Salama, S.R., and Haussler, D. (2012). Gene isoform specificity through enhancer-associated antisense transcription. PloS one *7*, e43511.

Osborne, C.S., Chakalova, L., Brown, K.E., Carter, D., Horton, A., Debrand, E., Goyenechea, B., Mitchell, J.A., Lopes, S., Reik, W.*, et al.* (2004). Active genes dynamically colocalize to shared sites of ongoing transcription. Nature genetics *36*, 1065-1071.

Ostlund, C., Folker, E.S., Choi, J.C., Gomes, E.R., Gundersen, G.G., and Worman, H.J. (2009). Dynamics and molecular interactions of linker of nucleoskeleton and cytoskeleton (LINC) complex proteins. J Cell Sci *122*, 4099-4108.

Padmakumar, V.C., Libotte, T., Lu, W., Zaim, H., Abraham, S., Noegel, A.A., Gotzmann, J., Foisner, R., and Karakesisoglou, I. (2005). The inner nuclear membrane protein Sun1 mediates the anchorage of Nesprin-2 to the nuclear envelope. Journal of cell science *118*, 3419-3430.

Pardal, R., Clarke, M.F., and Morrison, S.J. (2003). Applying the principles of stem-cell biology to cancer. Nat Rev Cancer *3*, 895-902.

Park, I.K., Qian, D., Kiel, M., Becker, M.W., Pihalja, M., Weissman, I.L., Morrison, S.J., and Clarke, M.F. (2003). Bmi-1 is required for maintenance of adult self-renewing haematopoietic stem cells. Nature *423*, 302-305.

Parry, D.A., Conway, J.F., and Steinert, P.M. (1986). Structural studies on lamin. Similarities and differences between lamin and intermediate-filament proteins. Biochem J *238*, 305-308.

Parthun, M.R. (2007). Hat1: the emerging cellular roles of a type B histone acetyltransferase. Oncogene *26*, 5319-5328.

Perez, C.A., Ott, J., Mays, D.J., and Pietenpol, J.A. (2007). p63 consensus DNA-binding site: identification, analysis and application into a p63MH algorithm. Oncogene *26*, 7363-7370.

Perez-Moreno, M., Jamora, C., and Fuchs, E. (2003). Sticky business: orchestrating cellular signals at adherens junctions. Cell *112*, 535-548.

Peric-Hupkes, D., Meuleman, W., Pagie, L., Bruggeman, S.W., Solovei, I., Brugman, W., Graf, S., Flicek, P., Kerkhoven, R.M., van Lohuizen, M.*, et al.* (2010). Molecular

maps of the reorganization of genome-nuclear lamina interactions during differentiation. Mol Cell *38*, 603-613.

Peter, M., Kitten, G.T., Lehner, C.F., Vorburger, K., Bailer, S.M., Maridor, G., and Nigg, E.A. (1989). Cloning and sequencing of cDNA clones encoding chicken lamins A and B1 and comparison of the primary structures of vertebrate A- and B-type lamins. J Mol Biol *208*, 393-404.

Peterlin, B.M., and Price, D.H. (2006). Controlling the elongation phase of transcription with P-TEFb. Mol Cell *23*, 297-305.

Peters, A.H., Kubicek, S., Mechtler, K., O'Sullivan, R.J., Derijck, A.A., Perez-Burgos, L., Kohlmaier, A., Opravil, S., Tachibana, M., Shinkai, Y.*, et al.* (2003). Partitioning and plasticity of repressive histone methylation states in mammalian chromatin. Mol Cell *12*, 1577-1589.

Phatnani, H.P., and Greenleaf, A.L. (2006). Phosphorylation and functions of the RNA polymerase II CTD. Genes Dev *20*, 2922-2936.

Pirrotta, V., and Li, H.B. (2012). A view of nuclear Polycomb bodies. Curr Opin Genet Dev *22*, 101-109.

Postel, R., Ketema, M., Kuikman, I., de Pereda, J.M., and Sonnenberg, A. (2011). Nesprin-3 augments peripheral nuclear localization of intermediate filaments in zebrafish. J Cell Sci *124*, 755-764.

Qi, L., Cao, J.L., Hu, Y., Yang, J.G., Ji, Y., Huang, J., Zhang, Y., Sun, D.G., Xia, H.F., and Ma, X. (2013). The dynamics of polycomb group proteins in early embryonic nervous system in mouse and human. International journal of developmental neuroscience : the official journal of the International Society for Developmental Neuroscience *31*, 487-495.

Rao, L., Perez, D., and White, E. (1996). Lamin proteolysis facilitates nuclear events during apoptosis. J Cell Biol *135*, 1441-1455.

Raz, V., Carlotti, F., Vermolen, B.J., van der Poel, E., Sloos, W.C., Knaan-Shanzer, S., de Vries, A.A., Hoeben, R.C., Young, I.T., Tanke, H.J.*, et al.* (2006). Changes in lamina

structure are followed by spatial reorganization of heterochromatic regions in caspase-8-activated human mesenchymal stem cells. J Cell Sci *119*, 4247-4256.

Redon, C., Pilch, D., Rogakou, E., Sedelnikova, O., Newrock, K., and Bonner, W. (2002). Histone H2A variants H2AX and H2AZ. Curr Opin Genet Dev *12*, 162-169.

Reik, W. (2007). Stability and flexibility of epigenetic gene regulation in mammalian development. Nature *447*, 425-432.

Ren, X., Vincenz, C., and Kerppola, T.K. (2008). Changes in the distributions and dynamics of polycomb repressive complexes during embryonic stem cell differentiation. Mol Cell Biol *28*, 2884-2895.

Rezniczek, G.A., de Pereda, J.M., Reipert, S., and Wiche, G. (1998). Linking integrin alpha6beta4-based cell adhesion to the intermediate filament cytoskeleton: direct interaction between the beta4 subunit and plectin at multiple molecular sites. J Cell Biol *141*, 209-225.

Rishi, V., Bhattacharya, P., Chatterjee, R., Rozenberg, J., Zhao, J., Glass, K., Fitzgerald, P., and Vinson, C. (2010). CpG methylation of half-CRE sequences creates C/EBPalpha binding sites that activate some tissue-specific genes. Proc Natl Acad Sci U S A *107*, 20311-20316.

Rober, R.A., Weber, K., and Osborn, M. (1989). Differential timing of nuclear lamin A/C expression in the various organs of the mouse embryo and the young animal: a developmental study. Development *105*, 365-378.

Romano, R.A., Ortt, K., Birkaya, B., Smalley, K., and Sinha, S. (2009). An active role of the DeltaN isoform of p63 in regulating basal keratin genes K5 and K14 and directing epidermal cell fate. PloS one *4*, e5623.

Roth, S.Y., Denu, J.M., and Allis, C.D. (2001). Histone acetyltransferases. Annu Rev Biochem *70*, 81-120.

Roth, W., Kumar, V., Beer, H.D., Richter, M., Wohlenberg, C., Reuter, U., Thiering, S., Staratschek-Jox, A., Hofmann, A., Kreusch, F.*, et al.* (2012). Keratin 1 maintains skin

integrity and participates in an inflammatory network in skin through interleukin-18. J Cell Sci *125*, 5269-5279.

Rusinol, A.E., and Sinensky, M.S. (2006). Farnesylated lamins, progeroid syndromes and farnesyl transferase inhibitors. J Cell Sci *119*, 3265-3272.

Sasaki, M., Abe, R., Fujita, Y., Ando, S., Inokuma, D., and Shimizu, H. (2008). Mesenchymal stem cells are recruited into wounded skin and contribute to wound repair by transdifferentiation into multiple skin cell type. Journal of immunology *180*, 2581-2587.

Sato, H., Koide, T., Sagai, T., Ishiguro, S.I., Tamai, M., Saitou, N., and Shiroishi, T. (1999). The genomic organization of type I keratin genes in mice. Genomics *56*, 303-309.

Saurin, A.J., Shiels, C., Williamson, J., Satijn, D.P., Otte, A.P., Sheer, D., and Freemont, P.S. (1998). The human polycomb group complex associates with pericentromeric heterochromatin to form a novel nuclear domain. J Cell Biol *142*, 887-898.

Schirmer, E.C. (2008). The epigenetics of nuclear envelope organization and disease. Mutat Res *647*, 112-121.

Scholzen, T., and Gerdes, J. (2000). The Ki-67 protein: from the known and the unknown. Journal of cellular physiology *182*, 311-322.

Sen, G.L., Webster, D.E., Barragan, D.I., Chang, H.Y., and Khavari, P.A. (2008). Control of differentiation in a self-renewing mammalian tissue by the histone demethylase JMJD3. Genes Dev *22*, 1865-1870.

Shah, P.P., Donahue, G., Otte, G.L., Capell, B.C., Nelson, D.M., Cao, K., Aggarwala, V., Cruickshanks, H.A., Rai, T.S., McBryan, T.*, et al.* (2013). Lamin B1 depletion in senescent cells triggers large-scale changes in gene expression and the chromatin landscape. Genes Dev *27*, 1787-1799.

Shao, Z., Raible, F., Mollaaghababa, R., Guyon, J.R., Wu, C.T., Bender, W., and Kingston, R.E. (1999). Stabilization of chromatin structure by PRC1, a Polycomb complex. Cell *98*, 37-46.

Shi, Y., Lan, F., Matson, C., Mulligan, P., Whetstine, J.R., Cole, P.A., Casero, R.A., and Shi, Y. (2004). Histone demethylation mediated by the nuclear amine oxidase homolog LSD1. Cell *119*, 941-953.

Shiio, Y., and Eisenman, R.N. (2003). Histone sumoylation is associated with transcriptional repression. Proc Natl Acad Sci U S A *100*, 13225-13230.

Shimi, T., Butin-Israeli, V., Adam, S.A., Hamanaka, R.B., Goldman, A.E., Lucas, C.A., Shumaker, D.K., Kosak, S.T., Chandel, N.S., and Goldman, R.D. (2011a). The role of nuclear lamin B1 in cell proliferation and senescence. Genes Dev *25*, 2579-2593.

Shimi, T., Butin-Israeli, V., and Goldman, R.D. (2011b). The roles of the nuclear envelope in mediating the molecular crosstalk between the nucleus and the cytoplasm. Curr Opin Cell Biol.

Shimi, T., Pfleghaar, K., Kojima, S., Pack, C.G., Solovei, I., Goldman, A.E., Adam, S.A., Shumaker, D.K., Kinjo, M., Cremer, T.*, et al.* (2008). The A- and B-type nuclear lamin networks: microdomains involved in chromatin organization and transcription. Genes Dev *22*, 3409-3421.

Shumaker, D.K., Dechat, T., Kohlmaier, A., Adam, S.A., Bozovsky, M.R., Erdos, M.R., Eriksson, M., Goldman, A.E., Khuon, S., Collins, F.S.*, et al.* (2006). Mutant nuclear lamin A leads to progressive alterations of epigenetic control in premature aging. Proc Natl Acad Sci U S A *103*, 8703-8708.

Simon, J.A., and Kingston, R.E. (2009). Mechanisms of polycomb gene silencing: knowns and unknowns. Nat Rev Mol Cell Biol *10*, 697-708.

Simon, J.A., and Kingston, R.E. (2013). Occupying chromatin: Polycomb mechanisms for getting to genomic targets, stopping transcriptional traffic, and staying put. Mol Cell *49*, 808-824.

Sing, A., Pannell, D., Karaiskakis, A., Sturgeon, K., Djabali, M., Ellis, J., Lipshitz, H.D., and Cordes, S.P. (2009). A vertebrate Polycomb response element governs segmentation of the posterior hindbrain. Cell *138*, 885-897.

Solovei, I., Wang, A.S., Thanisch, K., Schmidt, C.S., Krebs, S., Zwerger, M., Cohen, T.V., Devys, D., Foisner, R., Peichl, L.*, et al.* (2013). LBR and lamin A/C sequentially tether peripheral heterochromatin and inversely regulate differentiation. Cell *152*, 584-598.

Sparmann, A., and van Lohuizen, M. (2006). Polycomb silencers control cell fate, development and cancer. Nat Rev Cancer *6*, 846-856.

Squazzo, S.L., O'Geen, H., Komashko, V.M., Krig, S.R., Jin, V.X., Jang, S.W., Margueron, R., Reinberg, D., Green, R., and Farnham, P.J. (2006). Suz12 binds to silenced regions of the genome in a cell-type-specific manner. Genome research *16*, 890-900.

Stadhouders, R., Thongjuea, S., Andrieu-Soler, C., Palstra, R.J., Bryne, J.C., van den Heuvel, A., Stevens, M., de Boer, E., Kockx, C., van der Sloot, A.*, et al.* (2012). Dynamic long-range chromatin interactions control Myb proto-oncogene transcription during erythroid development. EMBO J *31*, 986-999.

Starr, D.A., and Fischer, J.A. (2005). KASH 'n Karry: the KASH domain family of cargo-specific cytoskeletal adaptor proteins. Bioessays *27*, 1136-1146.

Steinmetz, E.J., Warren, C.L., Kuehner, J.N., Panbehi, B., Ansari, A.Z., and Brow, D.A. (2006). Genome-wide distribution of yeast RNA polymerase II and its control by Sen1 helicase. Mol Cell *24*, 735-746.

Stern, C.D. (2005). Neural induction: old problem, new findings, yet more questions. Development *132*, 2007-2021.

Stewart-Hutchinson, P.J., Hale, C.M., Wirtz, D., and Hodzic, D. (2008). Structural requirements for the assembly of LINC complexes and their function in cellular mechanical stiffness. Experimental cell research *314*, 1892-1905.

Strahl, B.D., and Allis, C.D. (2000). The language of covalent histone modifications. Nature *403*, 41-45.

Su, I.H., Dobenecker, M.W., Dickinson, E., Oser, M., Basavaraj, A., Marqueron, R., Viale, A., Reinberg, D., Wulfing, C., and Tarakhovsky, A. (2005). Polycomb group protein ezh2 controls actin polymerization and cell signaling. Cell *121*, 425-436.

Sullivan, T., Escalante-Alcalde, D., Bhatt, H., Anver, M., Bhat, N., Nagashima, K., Stewart, C.L., and Burke, B. (1999). Loss of A-type lamin expression compromises nuclear envelope integrity leading to muscular dystrophy. J Cell Biol *147*, 913-920.

Sutherland, H., and Bickmore, W.A. (2009). Transcription factories: gene expression in unions? Nat Rev Genet *10*, 457-466.

Svitkina, T.M., Verkhovsky, A.B., and Borisy, G.G. (1996). Plectin sidearms mediate interaction of intermediate filaments with microtubules and other components of the cytoskeleton. J Cell Biol *135*, 991-1007.

Swaminathan, J., Baxter, E.M., and Corces, V.G. (2005). The role of histone H2Av variant replacement and histone H4 acetylation in the establishment of Drosophila heterochromatin. Genes Dev *19*, 65-76.

Taddei, A., Van Houwe, G., Hediger, F., Kalck, V., Cubizolles, F., Schober, H., and Gasser, S.M. (2006). Nuclear pore association confers optimal expression levels for an inducible yeast gene. Nature *441*, 774-778.

Tahiliani, M., Koh, K.P., Shen, Y., Pastor, W.A., Bandukwala, H., Brudno, Y., Agarwal, S., Iyer, L.M., Liu, D.R., Aravind, L.*, et al.* (2009). Conversion of 5-methylcytosine to 5-hydroxymethylcytosine in mammalian DNA by MLL partner TET1. Science *324*, 930-935.

Takizawa, T., Gudla, P.R., Guo, L., Lockett, S., and Misteli, T. (2008). Allele-specific nuclear positioning of the monoallelically expressed astrocyte marker GFAP. Genes Dev *22*, 489-498.

Tani, H., Morris, R.J., and Kaur, P. (2000). Enrichment for murine keratinocyte stem cells based on cell surface phenotype. Proc Natl Acad Sci U S A *97*, 10960-10965.

Telenius, H., Carter, N.P., Bebb, C.E., Nordenskjold, M., Ponder, B.A., and Tunnacliffe, A. (1992). Degenerate oligonucleotide-primed PCR: general amplification of target DNA by a single degenerate primer. Genomics *13*, 718-725.

Tjeertes, J.V., Miller, K.M., and Jackson, S.P. (2009). Screen for DNA-damage-responsive histone modifications identifies H3K9Ac and H3K56Ac in human cells. EMBO J *28*, 1878-1889.

Tolhuis, B., Blom, M., Kerkhoven, R.M., Pagie, L., Teunissen, H., Nieuwland, M., Simonis, M., de Laat, W., van Lohuizen, M., and van Steensel, B. (2011). Interactions among Polycomb domains are guided by chromosome architecture. PLoS genetics *7*, e1001343.

Tolhuis, B., Palstra, R.J., Splinter, E., Grosveld, F., and de Laat, W. (2002). Looping and interaction between hypersensitive sites in the active beta-globin locus. Mol Cell *10*, 1453-1465.

Trempus, C.S., Morris, R.J., Bortner, C.D., Cotsarelis, G., Faircloth, R.S., Reece, J.M., and Tennant, R.W. (2003). Enrichment for living murine keratinocytes from the hair follicle bulge with the cell surface marker CD34. J Invest Dermatol *120*, 501-511.

Truong, A.B., Kretz, M., Ridky, T.W., Kimmel, R., and Khavari, P.A. (2006). p63 regulates proliferation and differentiation of developmentally mature keratinocytes. Genes Dev *20*, 3185-3197.

Tsukada, Y., Fang, J., Erdjument-Bromage, H., Warren, M.E., Borchers, C.H., Tempst, P., and Zhang, Y. (2006). Histone demethylation by a family of JmjC domain-containing proteins. Nature *439*, 811-816.

Tumbar, T., Guasch, G., Greco, V., Blanpain, C., Lowry, W.E., Rendl, M., and Fuchs, E. (2004). Defining the epithelial stem cell niche in skin. Science *303*, 359-363.

Tzur, Y.B., Wilson, K.L., and Gruenbaum, Y. (2006). SUN-domain proteins: 'Velcro' that links the nucleoskeleton to the cytoskeleton. Nat Rev Mol Cell Biol *7*, 782-788.

Valk-Lingbeek, M.E., Bruggeman, S.W., and van Lohuizen, M. (2004). Stem cells and cancer; the polycomb connection. Cell *118*, 409-418.

van der Lugt, N.M., Domen, J., Linders, K., van Roon, M., Robanus-Maandag, E., te Riele, H., van der Valk, M., Deschamps, J., Sofroniew, M., van Lohuizen, M.*, et al.* (1994). Posterior transformation, neurological abnormalities, and severe hematopoietic defects in mice with a targeted deletion of the bmi-1 proto-oncogene. Genes Dev *8*, 757-769.

van Steensel, B., and Dekker, J. (2010). Genomics tools for unraveling chromosome architecture. Nature biotechnology *28*, 1089-1095.

Vanbokhoven, H., Melino, G., Candi, E., and Declercq, W. (2011). p63, a story of mice and men. J Invest Dermatol *131*, 1196-1207.

Vaquerizas, J.M., Kummerfeld, S.K., Teichmann, S.A., and Luscombe, N.M. (2009). A census of human transcription factors: function, expression and evolution. Nat Rev Genet *10*, 252-263.

Varambally, S., Dhanasekaran, S.M., Zhou, M., Barrette, T.R., Kumar-Sinha, C., Sanda, M.G., Ghosh, D., Pienta, K.J., Sewalt, R.G., Otte, A.P.*, et al.* (2002). The polycomb group protein EZH2 is involved in progression of prostate cancer. Nature *419*, 624-629.

Vergnes, L., Peterfy, M., Bergo, M.O., Young, S.G., and Reue, K. (2004). Lamin B1 is required for mouse development and nuclear integrity. Proc Natl Acad Sci U S A *101*, 10428-10433.

Vire, E., Brenner, C., Deplus, R., Blanchon, L., Fraga, M., Didelot, C., Morey, L., Van Eynde, A., Bernard, D., Vanderwinden, J.M.*, et al.* (2006). The Polycomb group protein EZH2 directly controls DNA methylation. Nature *439*, 871-874.

Volz, A., Korge, B.P., Compton, J.G., Ziegler, A., Steinert, P.M., and Mischke, D. (1993). Physical mapping of a functional cluster of epidermal differentiation genes on chromosome 1q21. Genomics *18*, 92-99.

Voncken, J.W., Roelen, B.A., Roefs, M., de Vries, S., Verhoeven, E., Marino, S., Deschamps, J., and van Lohuizen, M. (2003). Rnf2 (Ring1b) deficiency causes gastrulation arrest and cell cycle inhibition. Proc Natl Acad Sci U S A *100*, 2468-2473.

Wang, H., Wang, L., Erdjument-Bromage, H., Vidal, M., Tempst, P., Jones, R.S., and Zhang, Y. (2004). Role of histone H2A ubiquitination in Polycomb silencing. Nature *431*, 873-878.

Wang, Q., Du, X., Cai, Z., and Greene, M.I. (2006). Characterization of the structures involved in localization of the SUN proteins to the nuclear envelope and the centrosome. DNA and cell biology *25*, 554-562.

Wang, X., Pasolli, H.A., Williams, T., and Fuchs, E. (2008). AP-2 factors act in concert with Notch to orchestrate terminal differentiation in skin epidermis. J Cell Biol *183*, 37-48.

Wang, Y., and Sassoon, D. (1995). Ectoderm-mesenchyme and mesenchyme-mesenchyme interactions regulate Msx-1 expression and cellular differentiation in the murine limb bud. Dev Biol *168*, 374-382.

Watt, F.M. (1998). Epidermal stem cells: markers, patterning and the control of stem cell fate. Philos Trans R Soc Lond B Biol Sci *353*, 831-837.

Watt, F.M., Estrach, S., and Ambler, C.A. (2008). Epidermal Notch signalling: differentiation, cancer and adhesion. Curr Opin Cell Biol *20*, 171-179.

Whetstine, J.R., Nottke, A., Lan, F., Huarte, M., Smolikov, S., Chen, Z., Spooner, E., Li, E., Zhang, G., Colaiacovo, M.*, et al.* (2006). Reversal of histone lysine trimethylation by the JMJD2 family of histone demethylases. Cell *125*, 467-481.

Wiche, G., and Winter, L. (2011). Plectin isoforms as organizers of intermediate filament cytoarchitecture. Bioarchitecture *1*, 14-20.

Wilhelmsen, K., Litjens, S.H., Kuikman, I., Tshimbalanga, N., Janssen, H., van den Bout, I., Raymond, K., and Sonnenberg, A. (2005). Nesprin-3, a novel outer nuclear membrane protein, associates with the cytoskeletal linker protein plectin. J Cell Biol *171*, 799-810.

Wilson, K.L., and Berk, J.M. (2010). The nuclear envelope at a glance. J Cell Sci *123*, 1973-1978.

Winter-Vann, A.M., and Casey, P.J. (2005). Post-prenylation-processing enzymes as new targets in oncogenesis. Nat Rev Cancer *5*, 405-412.

Woo, C.J., Kharchenko, P.V., Daheron, L., Park, P.J., and Kingston, R.E. (2010). A region of the human HOXD cluster that confers polycomb-group responsiveness. Cell *140*, 99-110.

Wu, H., D'Alessio, A.C., Ito, S., Xia, K., Wang, Z., Cui, K., Zhao, K., Sun, Y.E., and Zhang, Y. (2011). Dual functions of Tet1 in transcriptional regulation in mouse embryonic stem cells. Nature *473*, 389-393.

Xu, M., and Cook, P.R. (2008). Similar active genes cluster in specialized transcription factories. J Cell Biol *181*, 615-623.

Yang, A., Schweitzer, R., Sun, D., Kaghad, M., Walker, N., Bronson, R.T., Tabin, C., Sharpe, A., Caput, D., Crum, C*., et al.* (1999). p63 is essential for regenerative proliferation in limb, craniofacial and epithelial development. Nature *398*, 714-718.

Yang, S.H., Chang, S.Y., Yin, L., Tu, Y., Hu, Y., Yoshinaga, Y., de Jong, P.J., Fong, L.G., and Young, S.G. (2011a). An absence of both lamin B1 and lamin B2 in keratinocytes has no effect on cell proliferation or the development of skin and hair. Hum Mol Genet *20*, 3537-3544.

Yang, S.H., Jung, H.J., Coffinier, C., Fong, L.G., and Young, S.G. (2011b). Are B-type lamins essential in all mammalian cells? Nucleus *2*, 562-569.

Yang, X.J. (2004). The diverse superfamily of lysine acetyltransferases and their roles in leukemia and other diseases. Nucleic Acids Res *32*, 959-976.

Yang, X.J., and Seto, E. (2007). HATs and HDACs: from structure, function and regulation to novel strategies for therapy and prevention. Oncogene *26*, 5310-5318.

Yao, J., Ardehali, M.B., Fecko, C.J., Webb, W.W., and Lis, J.T. (2007). Intranuclear distribution and local dynamics of RNA polymerase II during transcription activation. Mol Cell *28*, 978-990.

Yasui, D., Miyano, M., Cai, S., Varga-Weisz, P., and Kohwi-Shigematsu, T. (2002). SATB1 targets chromatin remodelling to regulate genes over long distances. Nature *419*, 641-645.

Yi, R., Poy, M.N., Stoffel, M., and Fuchs, E. (2008). A skin microRNA promotes differentiation by repressing 'stemness'. Nature *452*, 225-229.

Yu, M., Mazor, T., Huang, H., Huang, H.T., Kathrein, K.L., Woo, A.J., Chouinard, C.R., Labadorf, A., Akie, T.E., Moran, T.B.*, et al.* (2012). Direct recruitment of polycomb repressive complex 1 to chromatin by core binding transcription factors. Mol Cell *45*, 330-343.

Zhang, Q., Bethmann, C., Worth, N.F., Davies, J.D., Wasner, C., Feuer, A., Ragnauth, C.D., Yi, Q., Mellad, J.A., Warren, D.T.*, et al.* (2007). Nesprin-1 and -2 are involved in the pathogenesis of Emery Dreifuss muscular dystrophy and are critical for nuclear envelope integrity. Hum Mol Genet *16*, 2816-2833.

Zhao, J., Sun, B.K., Erwin, J.A., Song, J.J., and Lee, J.T. (2008). Polycomb proteins targeted by a short repeat RNA to the mouse X chromosome. Science *322*, 750-756.

Zhou, P., Byrne, C., Jacobs, J., and Fuchs, E. (1995). Lymphoid enhancer factor 1 directs hair follicle patterning and epithelial cell fate. Genes Dev *9*, 700-713.

Zullo, J.M., Demarco, I.A., Pique-Regi, R., Gaffney, D.J., Epstein, C.B., Spooner, C.J., Luperchio, T.R., Bernstein, B.E., Pritchard, J.K., Reddy, K.L.*, et al.* (2012). DNA sequence-dependent compartmentalization and silencing of chromatin at the nuclear lamina. Cell *149*, 1474-1487.

Published September 19, 2011

p63 regulates *Satb1* to control tissue-specific chromatin remodeling during development of the epidermis

Michael Y. Fessing,[1] Andrei N. Mardaryev,[1] Michal R. Gdula,[1] Andrey A. Sharov,[2] Tatyana Y. Sharova,[2] Valentina Rapisarda,[1] Konstantin B. Gordon,[1] Anna D. Smorodchenko,[2] Krzysztof Poterlowicz,[1] Giustina Ferone,[5] Yoshinori Kohwi,[3] Caterina Missero,[4,5] Terumi Kohwi-Shigematsu,[3] and Vladimir A. Botchkarev[1,2]

[1]Centre for Skin Sciences, University of Bradford, Bradford BD7 1DP, England, UK
[2]Department of Dermatology, Boston University School of Medicine, Boston, MA 02118
[3]Life Sciences Division, Lawrence Berkeley National Laboratory, University of California, Berkeley, Berkeley, CA 94720
[4]CEINGE Biotechnologie Avanzate, 80145 Naples, Italy
[5]Fondazione SDN Istituto di Ricovero e Cura a Carattere Scientifico, 80143 Napoli, Italy

During development, multipotent progenitor cells establish tissue-specific programs of gene expression. In this paper, we show that p63 transcription factor, a master regulator of epidermal morphogenesis, executes its function in part by directly regulating expression of the genome organizer Satb1 in progenitor cells. p63 binds to a proximal regulatory region of the *Satb1* gene, and p63 ablation results in marked reduction in the Satb1 expression levels in the epidermis. Satb1$^{-/-}$ mice show impaired epidermal morphology. In Satb1-null epidermis, chromatin architecture of the epidermal differentiation complex locus containing genes associated with epidermal differentiation is altered primarily at its central domain, where Satb1 binding was confirmed by chromatin immunoprecipitation–on-chip analysis. Furthermore, genes within this domain fail to be properly activated upon terminal differentiation. Satb1 expression in p63$^{+/-}$ skin explants treated with p63 small interfering ribonucleic acid partially restored the epidermal phenotype of p63-deficient mice. These data provide a novel mechanism by which Satb1, a direct downstream target of p63, contributes in epidermal morphogenesis via establishing tissue-specific chromatin organization and gene expression in epidermal progenitor cells.

Introduction

During the execution of developmental programs, the components of the chromatin-remodeling and transcription machinery are expressed in a highly organized manner, resulting in the establishment of tissue-specific patterns of gene activation and silencing (Hemberger et al., 2009). However, the mechanisms underlying these series of events to achieve terminal differentiation of specific cell types are still unclear.

The program of epidermal differentiation and barrier formation in mice begins at about embryonic day 14.5 (E14.5) followed by the appearance of the spinous and granular layers at E16.5 and establishment of a functional epidermal barrier at E18.5 (Fuchs, 2007; Koster and Roop, 2007; Blanpain and Fuchs, 2009). This program is tightly controlled by several transcription regulators, including the p63 transcription factor (Koster and Roop, 2007; Truong and Khavari, 2007; Crum and McKeon, 2010), as well as by the DNA- and chromatin-remodeling factors (DNA methyltransferase DNMT1, histone demethylase JMJD3, histone deacetylases 1/2, ATP-dependent chromatin-modifying enzymes Brg1 and Mi-2β, and the polycomb group protein Ezh2; Indra et al., 2005; Kashiwagi et al., 2007; Sen et al., 2008, 2010; Ezhkova et al., 2009; LeBoeuf et al., 2010). It remains to be explored how transcription factors and chromatin-remodeling enzymes are coordinately regulated to establish tissue-specific gene expression programs during terminal differentiation of epidermal progenitor cells.

M.Y. Fessing and A.N. Mardaryev contributed equally to this paper.

Correspondence to Vladimir A. Botchkarev: v.a.botchkarev@bradford.ac.uk; or Terumi Kohwi-Shigematsu: TKohwi-Shigematsu@lbl.gov

Abbreviations used in this paper: BAC, bacterial artificial chromosome; ChIP, chromatin immunoprecipitation; EDC, epidermal differentiation complex; LCM, laser capture microdissection; WT, wild type.

Supplemental Material can be found at:
http://jcb.rupress.org/content/suppl/2011/09/15/jcb.201101148.DC1.html

The Rockefeller University Press $30.00
J. Cell Biol. Vol. 194 No. 6 825–839
www.jcb.org/cgi/doi/10.1083/jcb.201101148

Published September 19, 2011

The p63 transcription factor serves as a master regulator of epidermal development, and p63 knockout (−/−) mice fail to form stratified epithelium and to express several epidermis-specific genes (Mills et al., 1999; Yang et al., 1999). In keratinocytes, p63 regulates a large number of genes that encode distinct adhesion/signaling molecules, transcription factors, and cell cycle–associated proteins as well as tissue-specific proteins, such as keratins, involucrin, and loricrin (Viganò and Mantovani, 2007).

Eukaryotic genomes appear to be organized for gene regulation with a tendency of linear clustering of coexpressed genes, often related in function (Kosak and Groudine, 2004). In the mammalian epidermis, differentiation of the multipotent progenitor cells in the basal epidermal layer into keratinocytes of the suprabasal layer is accompanied by coordinated activation of the specific sets of genes; e.g., a cluster of such genes is found in the epidermal differentiation complex (EDC) located in the gene-rich region of mouse chromosome 3 (Fig. S1). Genes in the EDC encode the components of the cornified cell envelope (involucrin, loricrin, filaggrin, small proline-rich and late-cornified envelope proteins, etc.) essential for epidermal barrier function (Marshall et al., 2001; Martin et al., 2004; Bazzi et al., 2007; Brown et al., 2007).

It is well accepted now that higher-order chromatin organization and spatial arrangement of genes within the nuclear space, as well as nuclear compartmentalization of chromatin-remodeling complexes and transcription machinery, all play an important role in controlling gene expression (Fraser and Bickmore, 2007; Lanctôt et al., 2007; Takizawa et al., 2008; Rando and Chang, 2009; Zhao et al., 2009; Joffe et al., 2010; Naumova and Dekker, 2010; Schoenfelder et al., 2010). It has been previously shown that the differentiation process in cultured epidermal keratinocytes is also associated with changes in intranuclear positioning of the EDC and distinct chromosomes (Elder and Zhao, 2002; Marella et al., 2009). siRNA knockdown of p63 in keratinocytes results in marked alterations of gene expression in the EDC (Truong et al., 2006). However, it remains to be determined whether the p63 protein itself directly regulates some of these events during epidermal differentiation or whether the proteins encoded by p63 downstream target genes play a role in some of these processes.

In several other tissue-specific gene loci (e.g., T_H2 cytokine locus and β-globin locus), higher-order chromatin remodeling for establishing specific 3D conformations is regulated by the specialized adenine and thymine–rich binding protein Satb1, which functions as the genome organizer (Dickinson et al., 1992; Alvarez et al., 2000; Cai et al., 2003, 2006; Kumar et al., 2007; Han et al., 2008; Wang et al., 2009). Satb1 targets chromatin-remodeling enzymes and transcription factors to specific genomic regions, establishes region-specific epigenomic modification status, and plays a fundamental role in the execution of tissue-specific gene expression programs (Yasui et al., 2002; Cai et al., 2006; Pavan Kumar et al., 2006). However, the upstream mechanisms controlling Satb1 expression in distinct cell types are unknown.

Here, we show that during epidermal morphogenesis, p63 transcription factor directly regulates expression of the genome organizer Satb1. Satb1 remodels chromatin architecture at the tissue-specific EDC gene locus, as indicated by compression of the central domain of this locus where terminal differentiation–associated genes are clustered. Upon *Satb1* ablation, these genes cannot be properly activated, and the epidermal morphology becomes impaired, thus demonstrating an essential role for Satb1 as a part of the p63-dependent developmental program, through higher-order chromatin remodeling and gene regulation in epidermal progenitor cells.

Results

Expression of genes encoding chromatin-remodeling factors is markedly altered in the p63-null epidermis

Because p63 transcription factor is a master regulator for epidermal development, we hypothesized that it may regulate expression of a multitude of genes encoding chromatin-remodeling factors to establish specific chromatin architecture in epidermal progenitor cells. Global gene expression profiles were compared between the epidermis isolated by laser capture microdissection (LCM) from E16.5 $p63^{-/-}$ and wild-type (WT) mice, as previously described (Fig. 1 A; Mammucari et al., 2005; Sharov et al., 2006). This approach allowed us to compare gene expression profiles between the epidermal cells of $p63^{-/-}$ and WT mice in situ and to exclude alterations in gene expression induced by the proteolysis-associated cell separation procedures (Zhou et al., 2006). Global microarray analysis showed ≥1.8-fold changes in expression of 2,522 up-regulated and 998 down-regulated genes between the epidermis of $p63^{-/-}$ and WT mice (Fig. 1 B and Tables S1 and S2).

Among the distinct groups of genes, the expression of which was either down- or up-regulated in $p63^{-/-}$ mice versus WT mice, gene ontology analysis revealed a significant enrichment of the genes ($P < 0.05$) involved in the control of nuclear and chromatin assembly and remodeling (Fig. 1 B). These genes constituted ∼11 and 5% of the total number of down-regulated or up-regulated genes, respectively. Interestingly, in the epidermis of $p63^{-/-}$ mice versus WT controls, the expression of the genes encoding several key regulators of the higher-order chromatin structure and ATP-dependent chromatin remodeling (Satb1, Mi-2α, and Mi-2β) was down-regulated, whereas the expression of some other ATP-dependent chromatin-remodeling factors (Chd1 and Brm) was up-regulated. The top list of most affected genes is shown in Fig. 1 B (see the entire list in Tables S1 and S2). The relative expression levels of some of the most down-regulated genes between the WT and $p63^{-/-}$ mice were further validated by RT-PCR (Fig. 1 C). These data suggest that the genes encoding chromatin-remodeling factors represent a novel class of the p63 targets, raising a possibility that some of these factors may be in charge of the remodeling of the higher-order and/or local chromatin structures and tissue-specific gene expression during differentiation of the epidermal progenitor cells.

p63 controls the expression of Satb1 in epidermal progenitor cells

We studied whether p63 controls tissue-specific chromatin organization and gene expression during development of the epidermis

Published September 19, 2011

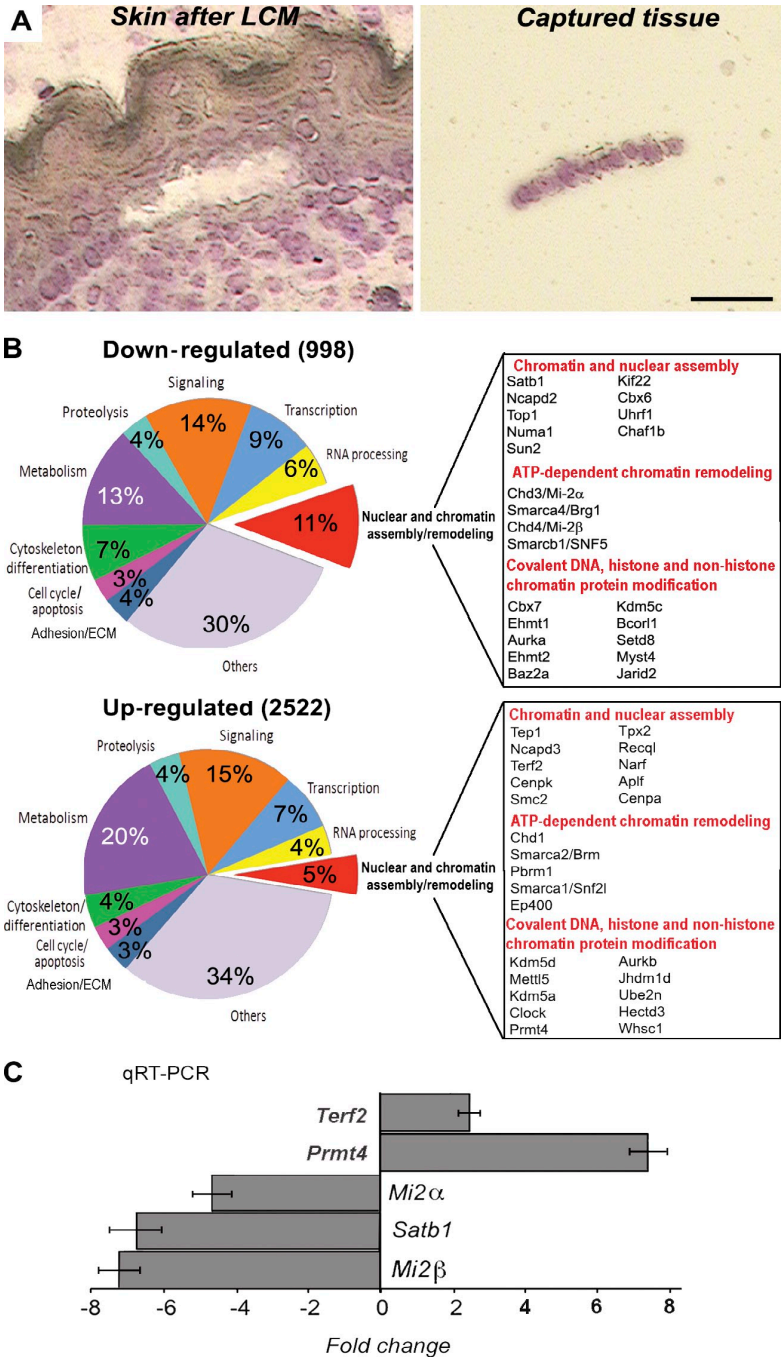

Figure 1. **Changes in global transcription profile and expression of the genes encoding chromatin-remodeling factors in the epidermis of p63$^{-/-}$ mice.** The skin of E16.5 p63$^{-/-}$ and WT mice was processed for LCM to isolate fragments of the epidermis. RNA was isolated from captured tissue, amplified, and processed for microarray and RT-PCR analyses. (A) Cryosection of the skin after LCM including a fragment of the captured epidermis. Bar, 25 µm. (B) Agilent microarray analysis of the laser-captured epidermis of p63$^{-/-}$ and WT mice. Diagrams showing the ontology of the down- and up-regulated genes in p63-null versus WT epidermis. Selected genes involved in the control of nuclear structure and chromatin remodeling, the expression of which was changed in the epidermis of p63$^{-/-}$ versus WT mice, are listed (a full list of the genes is shown in Tables S1 and S2). (C) Real-time PCR for *Satb1*, *Mi-2α*, *Mi-2β*, *Terf2*, and *Prmt4* in the E16.5 epidermis of p63$^{-/-}$ mice normalized to the corresponding levels in age-matched WT mice. Error bars represent SEM.

through regulation of some of the chromatin-remodeling factors. For this purpose, we focused on the genome organizer Satb1 as a potential p63 target because of its known function in regulating large-scale chromatin remodeling in several cell type–specific gene loci (e.g., T_H2 cytokine locus and β-globin locus; Cai et al., 2003; Wang et al., 2009) as well as cancer-related gene loci in aggressive breast cancer (Han et al., 2008). We found that Satb1 was coexpressed with p63 in basal cells of the epidermis of embryonic (E16.5) and postnatal skin (Fig. 2 A and not depicted). Skin epithelium of p63$^{-/-}$ mice expressing Keratin 18 as a marker of undifferentiated epithelial cells showed strongly reduced Satb1 protein levels (Fig. 2, B and C), which was consistent with greatly reduced *Satb1* transcript expression in the epidermis of p63$^{-/-}$ mice versus WT controls (Fig. 1 C).

In addition, the expression of the Satb1 protein was strongly reduced in the E13.5 skin explants of heterozygous p63 knockout (+/−) mice treated with p63 siRNA when compared with age-matched skin samples treated by the control siRNA (Figs. 2 D and S2 [A and B]). The expression of Loricrin, a marker of differentiated keratinocytes, was also decreased in

Published September 19, 2011

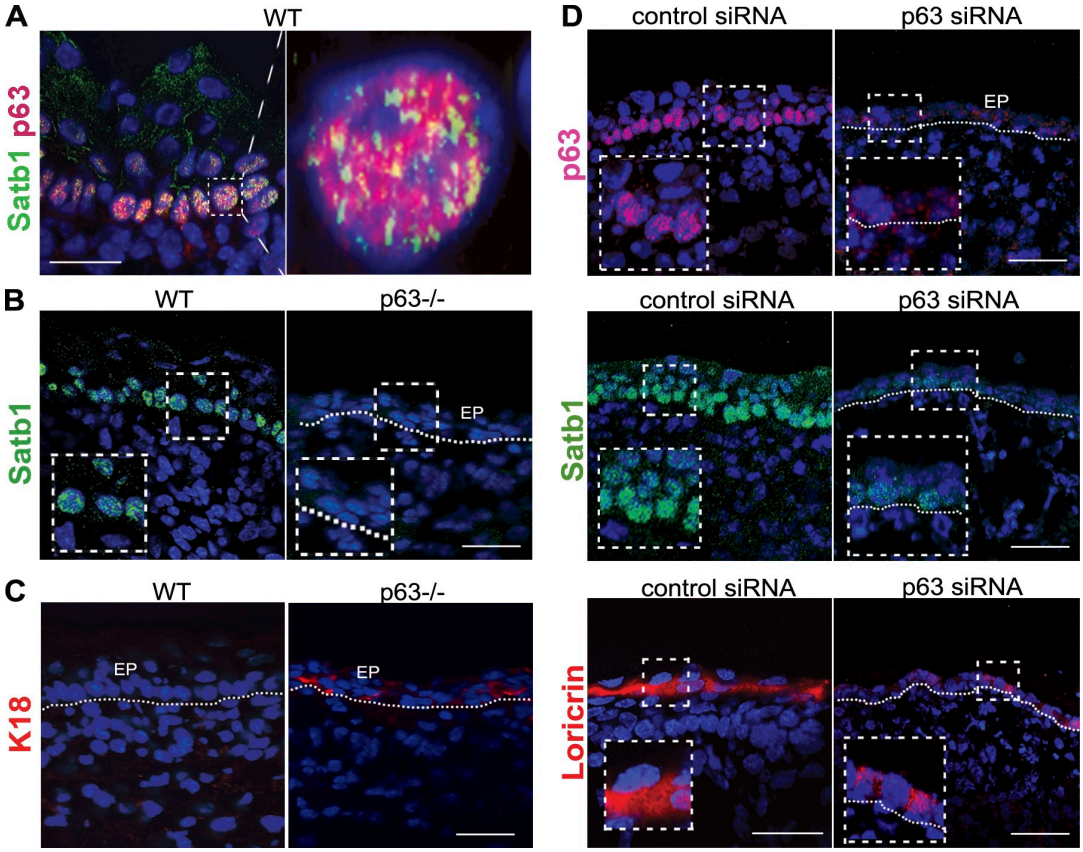

Figure 2. **p63 controls the expression of Satb1 in epidermal progenitor cells.** The skin of p63-deficient and WT embryos was processed for immunofluorescent analyses as well as for modulation of gene expression in organ culture experiments with p63 siRNA. (A) Double immunofluorescence showing coexpression of p63 and Satb1 in the nuclei of basal epidermal cells in E16.5 WT mice. (B and C) Immunostaining for Satb1 (B) and K18 (C) in the E16.5 skin of WT and $p63^{-/-}$ mice. Marked decrease of Satb1 expression in the epidermis (EP) of $p63^{-/-}$ mice is magnified in the dashed boxes. (D) Immunostaining for p63, Satb1, and Loricrin in the E13.5 skin samples of heterozygous p63 knockout (+/−) mice cultured in the presence of p63 siRNA or control siRNA for 48 h. In epidermis, the expression of p63, Satb1, and Loricrin proteins in the p63 siRNA–treated samples was decreased compared with the controls. (B and D) The epidermal–dermal junction is shown by dotted lines. Bars, 25 µm.

the epidermis of embryonic skin explants after treatment with p63 siRNA compared with controls (Fig. 2 D).

Furthermore, chromatin immunoprecipitation (ChIP) assays using primary epidermal keratinocytes isolated from E16.5 embryos or newborn mice revealed binding of the p63 to the consensus sequence identified in the upstream region at −1662 to −1738 bp from the *Satb1* transcription start site (Fig. 3, A and B). p63 binding was also seen at the consensus sequence in the *Cldn1* promoter region, an established p63 target gene (Fig. 3 B; Lopardo et al., 2008). However, no binding was seen at the predicted p63 site located in the first intron of the *Satb1* gene, serving as a negative control for this assay (Fig. 3 B).

To assess whether p63 controls the activity of the *Satb1* promoter, HaCaT keratinocytes were cotransfected with a luciferase reporter plasmid containing a mouse *Satb1* promoter (pSatb1luc; unpublished data) and either the ΔNp63 expression vector (pΔNp63) or a control vector (pcDNA3). Transfection of cells with pΔNp63, but not with pcDNA3, resulted in an increase of the Satb1 promoter–driven luciferase activity by threefold compared with control (Fig. 3 C). These data strongly suggest that *Satb1* is indeed a direct target gene of p63 in keratinocytes.

p63 or *Satb1* ablation results in altered conformation of the chromatin domain containing the EDC locus

We further investigated whether there is any evidence for changes as a result of either *p63* or *Satb1* ablation in the higher-order chromatin organization in epidermal progenitor cells during development. Using 3D FISH, we analyzed the conformation of the 5 Mbp chromatin domain of mouse chromosome 3 that contains the tissue-specific EDC gene locus in the epidermis of E16.5 $p63^{-/-}$, $Satb1^{-/-}$, and corresponding WT embryos. The EDC occupies ∼3.1 Mbp in this domain located in the gene-rich region of mouse chromosome 3 and is flanked by several genes that are expressed in the epidermis, including *Rps27* and *Gabpb2*, encoding ribosomal protein S27 and guanine and adenine–binding protein subunit 2, respectively (Fig. 4 A).

Despite the fact that the mean radius of the nuclei of basal epidermal cells was quite similar in $p63^{-/-}$, $Satb1^{-/-}$, and corresponding WT embryos, the distances between the *Rps27* and *Lor* genes in the E16.5 epidermis of both $p63^{-/-}$ and $Satb1^{-/-}$ mice (without or after normalization to the corresponding nuclear radius) were significantly increased ($P < 0.05$) versus the

Published September 19, 2011

corresponding controls, whereas distances between the *Lor* and *Gabpb2* genes remained unchanged (Figs. 4 [B–D] and S2 C). Distribution of the distances between the *Rps27* and *Lor* in individual nuclei showed a lack of peaks in the corresponding histograms, thus suggesting similarities in the positioning of both alleles of each gene relative to other genes in the keratinocyte nuclei (Fig. S2 D). However, there was no significant difference observed in the distances between any of those genes in dermal cells of the p63$^{-/-}$ or Satb1$^{-/-}$ mice and WT controls, indicating that the effects of p63 and Satb1 on 3D chromatin structure in keratinocytes are tissue specific (Fig. 4 D).

Next, we examined whether there is any correlation of the changes in chromatin organization and gene expression at the EDC locus for E16.5 epidermis of p63$^{-/-}$ and Satb1$^{-/-}$ embryos. The EDC contains several genes, including those activated during terminal keratinocyte differentiation (Fig. 4 A). Using quantitative RT-PCR, we observed that genes within the EDC and its flanking regions (*Rps27* and *Gabpb2*) showed quite similar changes in expression in the epidermis of E16.5 p63$^{-/-}$ and Satb1$^{-/-}$ embryos versus the WT controls (Fig. 4 E).

In both p63$^{-/-}$ and Satb1$^{-/-}$ mice, the expression of the genes located in the central EDC domain and involved in the epidermal barrier formation, such as *Lor*, *Inv*, *Lce1b*, and *Lce3c*, was decreased, whereas the expression of the *S100a9* located at the EDC 5′ end increased versus the corresponding WT controls (Fig. 4 E). In Satb1$^{-/-}$ mice, similar changes in gene expression in the EDC were observed in both dorsal skin and foot pads (Figs. 4 E and S2 E). The higher levels of reduction in expression for some of the genes tested in the epidermis of p63$^{-/-}$ mice compared with those of the Satb1$^{-/-}$ mice at E16.5 suggest the requirement of additional factors downstream of p63 for regulation of their expression. Expression of *Fil*, located at the EDC 3′ end, is solely dependent on p63 and not on Satb1, indicating that Satb1 is insufficient to replace global gene regulation by p63 (Fig. 4 E). Nevertheless, a similarity in altered expression patterns of the EDC genes seen in the p63$^{-/-}$ and Satb1$^{-/-}$ mice, paralleled by similar changes in the conformation of the 5 Mbp chromatin domain containing EDC, suggests a role for Satb1 in mediating, at least in part, the p63 functions in the developing epidermis.

Satb1$^{-/-}$ mice have impaired epidermal morphology and altered gene expression in keratinocyte-specific genomic loci

If *Satb1* is a critical downstream target gene of p63 in epidermal progenitor cells, it is expected that the skin of Satb1$^{-/-}$ mice will exhibit altered epidermal morphogenesis. In fact, Satb1$^{-/-}$ mice at postnatal day 0.5 (P0.5) show a significant decrease ($P < 0.01$) of the epidermal thickness, as well as a thinning of the granular epidermal layer compared with WT mice, more pronounced in the foot pads versus dorsal skin (Fig. 5, A and B). In addition, Satb1$^{-/-}$ mice showed significantly ($P < 0.05$) decreased epidermal proliferation compared with WT controls (Fig. 5 C).

To gain mechanistic insight into the role of Satb1 in the regulation of the keratinocyte terminal differentiation, samples of total RNA isolated from the skin of newborn Satb1$^{-/-}$ and

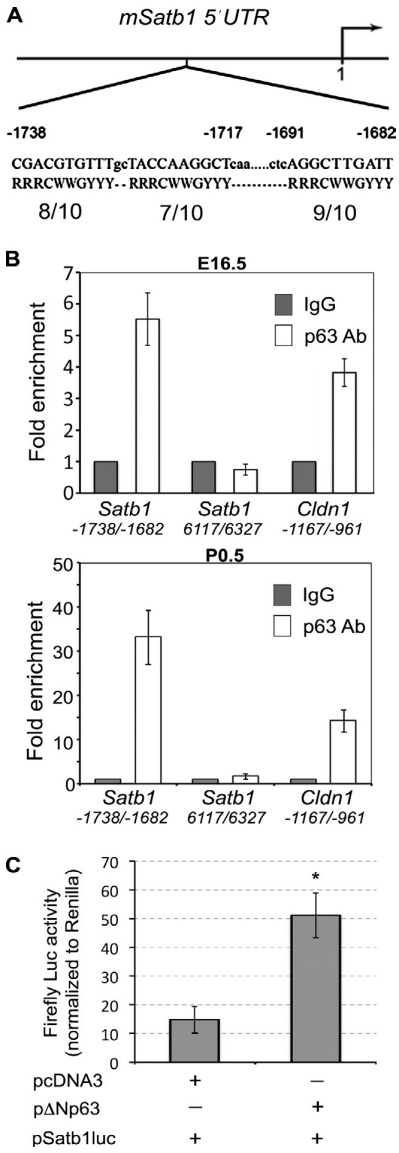

Figure 3. **Satb1 is a direct target of p63 in keratinocytes.** Primary keratinocytes isolated from E16.5 embryos or newborn mice were processed for ChIP analysis with an antibody against the p63 protein or purified rabbit IgGs. HaCaT cells were used in cotransfection experiments with Satb1 promoter–driven reporter construct. (A and B) Quantitative RT-PCR analysis of two distinct regions of the *Satb1* (a predicted high-affinity p63-binding site and a negative control site) showing a specific high-affinity p63-binding site at the *Satb1* promoter. In A, the position 1 refers to 5′ of Satb1 transcript (AK037740). The uppercase letters of the sequence show the p63 putative binding sites in the promoter region of the Satb1 gene chosen for the quantitative PCR analysis after ChIP. The promoter region of the *Cldn1* was used as a positive control. The input levels of unprecipitated chromatin DNA were used as loading controls. Error bars represent SEM, and three independent experiments were run in triplicate. (C) HaCaT keratinocytes were cotransfected with the luciferase reporter plasmid containing a mouse Satb1 promoter fragment and pΔNp63 expression plasmid or control pcDNA3 plasmid. The increase in the pSatb1-luc activities by cotransfection with pΔNp63 compared with the control pcDNA3 was ~3.3 fold (mean ± SEM, $n = 3$; *, $P < 0.05$, Student's *t* test).

Published September 19, 2011

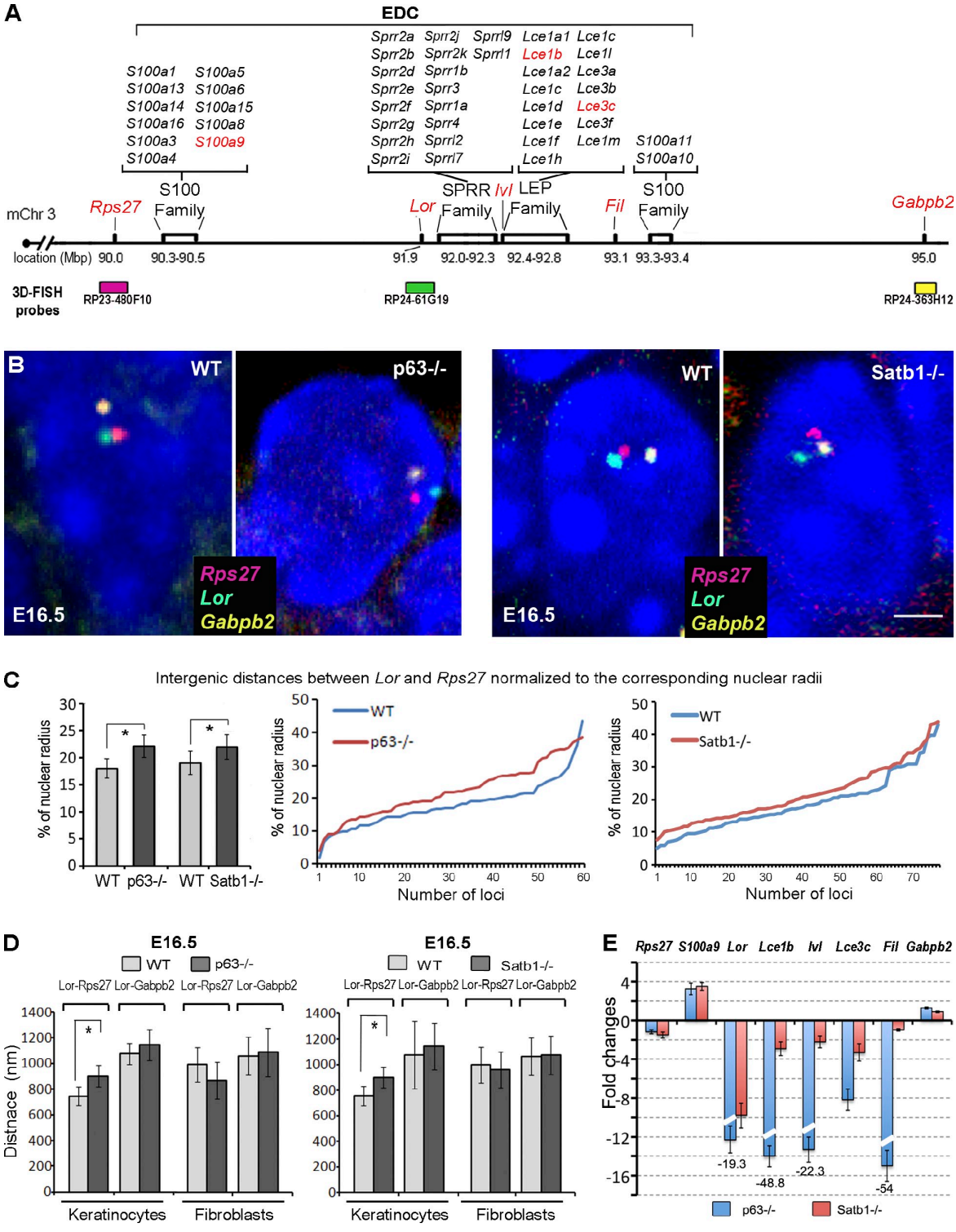

Figure 4. **Alterations in the conformation of the 5 Mb chromatin domain containing EDC in the epidermis of p63$^{-/-}$ and Satb1$^{-/-}$ mice.** The skin of E16.5 p63$^{-/-}$, Satb1$^{-/-}$, and corresponding WT mice was processed for 3D FISH analyses, which were correlated with changes in gene expression determined by quantitative RT-PCR. (A) A schematic structure of the 5 Mb domain on mouse chromosome 3 (mChr3) containing the EDC locus, *Rps27*, and *Gabpb2* genes. 3D FISH DNA probes detecting the corresponding domains are shown in green (*Loricrin*), pink (*Rps27*), and yellow (*Gabpb2*). Genes selected for quantitative RT-PCR analysis (shown in E) are shown in red. LEP, late-cornified envelope protein. (B) Multicolor 3D FISH with BACs covering the *Rps27*, *Lor*, and *Gabpb2* in the epidermal cells of p63$^{-/-}$, Satb1$^{-/-}$, and corresponding WT mice at E16.5 (representative single Z sections). Bar, 2 µm. (C) 3D FISH distances between the *Rps27*and *Lor* normalized to the radius of each nuclei in basal epidermal cells of p63$^{-/-}$, Satb1$^{-/-}$, and corresponding WT mice.

Published September 19, 2011

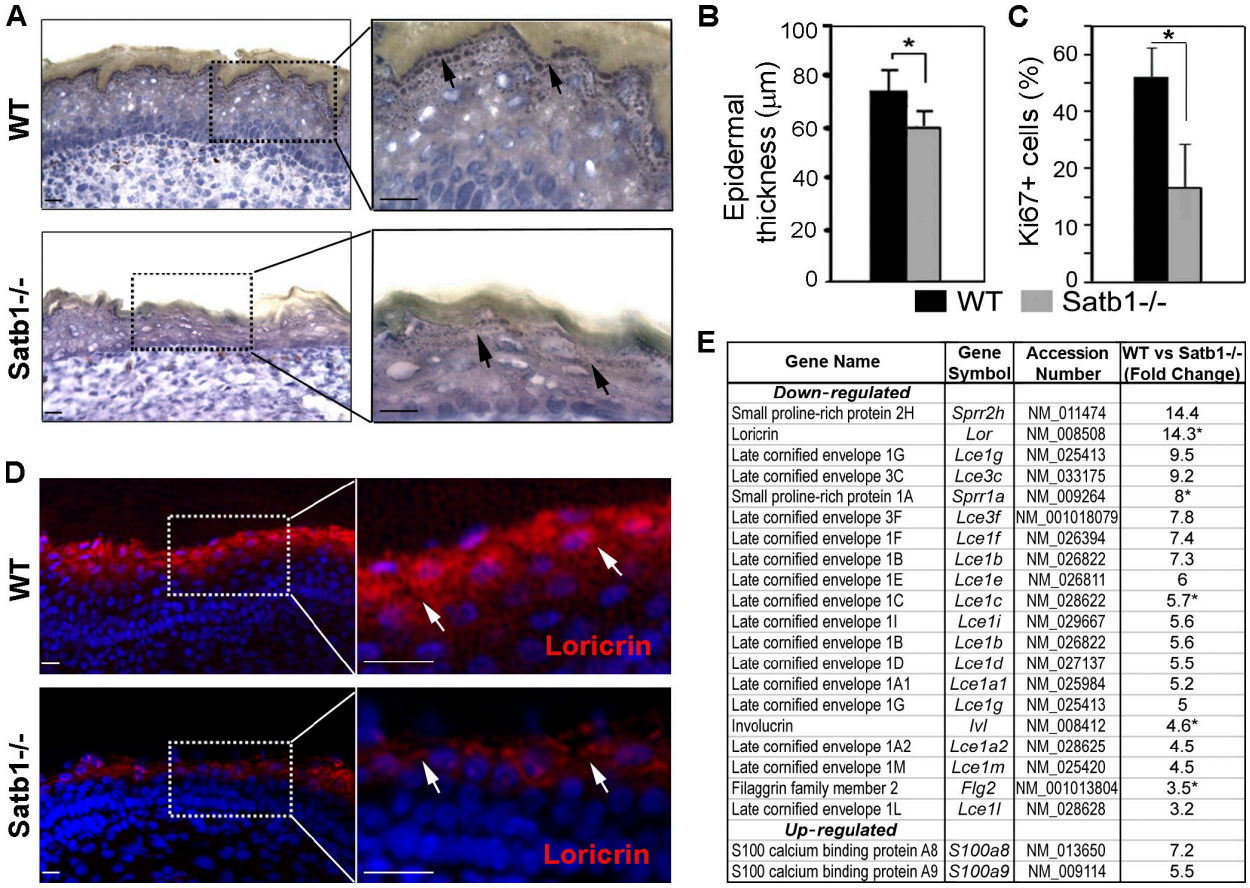

E

Gene Name	Gene Symbol	Accession Number	WT vs Satb1-/- (Fold Change)
Down-regulated			
Small proline-rich protein 2H	*Sprr2h*	NM_011474	14.4
Loricrin	*Lor*	NM_008508	14.3*
Late cornified envelope 1G	*Lce1g*	NM_025413	9.5
Late cornified envelope 3C	*Lce3c*	NM_033175	9.2
Small proline-rich protein 1A	*Sprr1a*	NM_009264	8*
Late cornified envelope 3F	*Lce3f*	NM_001018079	7.8
Late cornified envelope 1F	*Lce1f*	NM_026394	7.4
Late cornified envelope 1B	*Lce1b*	NM_026822	7.3
Late cornified envelope 1E	*Lce1e*	NM_026811	6
Late cornified envelope 1C	*Lce1c*	NM_028622	5.7*
Late cornified envelope 1I	*Lce1i*	NM_029667	5.6
Late cornified envelope 1B	*Lce1b*	NM_026822	5.6
Late cornified envelope 1D	*Lce1d*	NM_027137	5.5
Late cornified envelope 1A1	*Lce1a1*	NM_025984	5.2
Late cornified envelope 1G	*Lce1g*	NM_025413	5
Involucrin	*Ivl*	NM_008412	4.6*
Late cornified envelope 1A2	*Lce1a2*	NM_028625	4.5
Late cornified envelope 1M	*Lce1m*	NM_025420	4.5
Filaggrin family member 2	*Flg2*	NM_001013804	3.5*
Late cornified envelope 1L	*Lce1l*	NM_028628	3.2
Up-regulated			
S100 calcium binding protein A8	*S100a8*	NM_013650	7.2
S100 calcium binding protein A9	*S100a9*	NM_009114	5.5

Figure 5. **Satb1 knockout mice show alterations in the epidermal structure and Loricrin expression.** Cryosections of the footpad skin of newborn Satb1$^{-/-}$ and WT mice were processed for morphometric and immunofluorescent analyses. (A) Alterations in the structure and thinning of granular layer (arrows) in the epidermis of Satb1$^{-/-}$ mice compared with WT mice. Bars, 25 µm. (B) Significant (*, P < 0.05) decrease of the epidermal thickness in the epidermis of Satb1$^{-/-}$ mice compared with WT mice. Measurements of the epidermal thickness were performed in three Satb1$^{-/-}$ and three WT mice. 20 measurements were performed in each mouse. (C) Significant (*, P < 0.05) decrease of cell proliferation in the epidermis of Satb1$^{-/-}$ mice versus WT controls. The percentages of the Ki-67+ nuclei were determined in the epidermis of two Satb1$^{-/-}$ and two WT mice; 40–50 nuclei were analyzed in each animal. (B and C) Error bars represent SEM. (D) Decrease of Loricrin expression in the epidermis of Satb1$^{-/-}$ versus WT mice. Bars, 25 µm. (E) Agilent microarray data demonstrating changes in gene expression in the EDC between P0.5 Satb1$^{-/-}$ and WT mice. Asterisks indicate the fold changes in gene expression levels validated by quantitative RT-PCR.

WT mice were processed for microarray analysis (Sharov et al., 2006). In addition, the formaldehyde–cross-linked chromatin fragments from primary epidermal keratinocytes were immunoprecipitated with anti-Satb1 antibody, and a NimbleGen MM8 Deluxe Promoter HX1 array analysis was performed. ChIP-on-chip analysis showed that Satb1 does not always bind in the vicinity of the transcription start sites of the genes. In some cases, it binds sites remote from the gene proximal regulatory regions (Tables S4–S6), which is consistent with its role as a genome organizer important for the proper higher-order chromatin folding previously shown (Cai et al., 2003, 2006; Wang et al., 2009). Microarray and ChIP-on-chip data were merged, and 2,503 genes whose expression was significantly changed in *Satb1*$^{-/-}$ mice (≥1.8-fold) and showed Satb1 binding within 200 kb from the corresponding transcription start sites were selected as targets for Satb1 in keratinocytes (Fig. S3 A and Tables S4 and S5).

Interestingly, bioinformatic analyses on the Satb1 target genes involved in many biological processes (viz., regulation in cell adhesion/ECM remodeling, metabolism, cytoskeleton,

Pairwise comparisons represent a significant increase in the *Lor-Rps27* distances between the E16.5 WT versus p63$^{-/-}$ or Satb1$^{-/-}$ mice (mean ± SEM, *n* = 60; *, P < 0.01, Newman–Keuls test after a one-way ANOVA test). (D) 3D FISH distances between the *Rps27*and *Lor* and the *Lor* and *Gabpb2* in basal epidermal cells and dermal cells of p63$^{-/-}$, Satb1$^{-/-}$, and corresponding WT mice. Pairwise comparisons represent a significant increase in the *Lor-Rps27* distances between the E16.5 WT versus p63$^{-/-}$ or Satb1$^{-/-}$ mice (mean ± SEM, *n* = 60; P < 0.01, Newman–Keuls test after a one-way ANOVA test). (E) Quantitative RT-PCR analyses of gene expression in the 5 Mb domain containing EDC in the epidermis of E16.5 p63$^{-/-}$ and Satb1$^{-/-}$ mice normalized to the expression levels in the corresponding WT mice. White slashes represent the interruption of these bars to indicate that they show the fold changes in gene expression levels higher than the maximum value in the y axis. The exact fold changes are indicated under each bar. SEM is shown in the appropriate scale (relative to the y axis). Three independent experiments were run in triplicate.

Published September 19, 2011

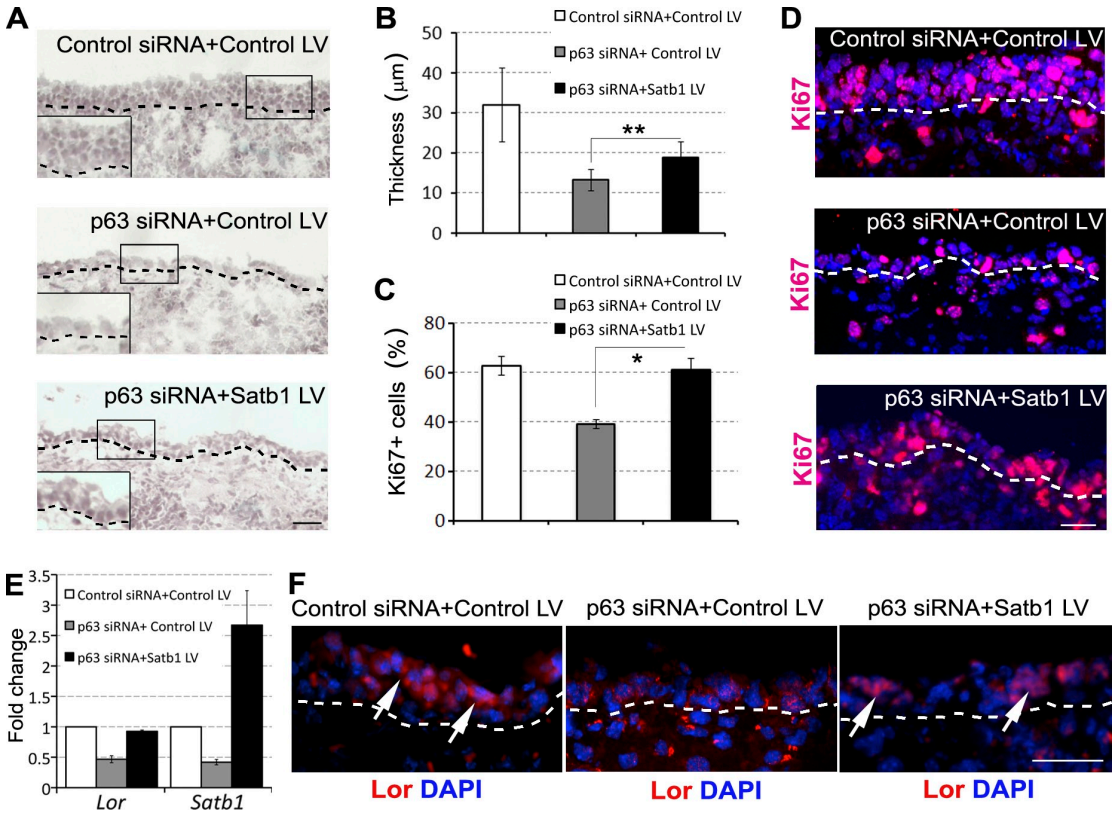

Figure 6. **Treatment with Satb1-expressing lentivirus partially rescues alterations of epidermal phenotype in skin explants caused by p63 deficiency.** The skin of $p63^{+/-}$ and WT E13.5 embryos was processed for modulation of gene expression in organ culture with p63 siRNA and Satb1-expressing lentivirus. (A and B) Morphology of E13.5 skin explants of $p63^{+/-}$ mice treated with combinations of p63 or control siRNAs and Satb1-expressing or control lentiviruses (LV) for 48 h. The decrease of the epidermal thickness induced by p63 siRNA is significantly (**, $P < 0.01$) rescued by the cotreatment with Satb1-expressing lentivirus compared with corresponding controls. Epidermal thickness was measured in three samples for each experimental group; 60 measurements were conducted in each sample. (C and D) Cotreatment with Satb1-expressing lentivirus prevents the decrease of cell proliferation in the epidermis of skin explants induced by p63 siRNA compared with controls (*, $P < 0.05$). The percentages of Ki-67+ cells were analyzed in three samples for each experimental group; 30 cells were analyzed in each sample. (A and D) The dotted lines show the position of the basement membrane separating the epidermis and dermis. (E and F) Quantitative RT-PCR for Loricrin and Satb1 (E) and immunostaining for Loricrin (F). Levels of Loricrin transcripts and the expression of protein decreased after p63 siRNA treatment restored in the epidermis after cotreatment with Satb1-expressing lentivirus compared with the controls (F, arrows). Treatment with Satb1-expressing lentivirus resulted in a marked increase of Satb1 transcript levels in the epidermis after decrease induced by p63 siRNA (E). (A, D, and F) The epidermal–dermal junction is shown by dotted lines. (B, C, and E) Error bars represent SEM. Bars: (A and F) 50 μm; (D) 25 μm.

signaling, and transcription) revealed that a large number of those genes are grouped into large genomic loci (>0.5 Mbp each) of gene clusters, containing >20 functionally relevant genes per locus, and that such genomic loci include epidermis-specific loci (Fig. S3 B and Tables S4 and S5). In fact, analyses of 33 such loci that are distributed genome wide showed significant preferential binding ($P < 0.05$) of Satb1 and Satb1-dependent changes in gene expression in the keratinocyte-specific loci (EDC, keratin type I/II loci, and keratin-associated protein locus) located on mouse chromosomes 3, 11, 15, and 16 (Fig. S3 B). Many of those genes found in the keratinocyte-specific loci were altered in expression upon p63 ablation (Fig. 5 E and Tables S1 and S2).

Microarray analysis revealed a profound decrease in gene expression in all keratinocyte-specific loci in $Satb1^{-/-}$ mice compared with WT controls (Fig. 3 B and Tables S4 and S5). Similarly to $p63^{-/-}$ mice, the expression of Krt10, Krt23, and Krt78 decreased in $Satb1^{-/-}$ mice compared with WT controls (Tables S1 and S4). In the EDC locus, Satb1 ablation resulted in decreased expression of a large number of genes that belong to the small proline-rich and late-cornified envelope families involved in the control of terminal keratinocyte differentiation, whereas an increase in expression was detected for selected members of the S100 family (Fig. 5 E). Consistent with microarray and quantitative RT-PCR data (Fig. 4 E), immunohistochemical analysis revealed markedly reduced expression of the Loricrin in Satb1-null epidermis versus the controls (Fig. 5 D). Thus, alterations of epidermal morphology in $Satb1^{-/-}$ mice and marked similarity in the Satb1- and p63-dependent changes in gene expression in four major keratinocyte-specific loci suggest that Satb1 is indeed a significant component of p63-regulated molecular network in the epidermis.

Gain of Satb1 expression partially rescues the epidermal phenotype in embryonic skin explants of p63-deficient mice

To assess whether the restoration of Satb1 expression is capable of partially rescuing the skin phenotype of $p63^{-/-}$ mice, E13.5 skin explants isolated from heterozygous (+/−) p63 knockout

Published September 19, 2011

mice were cultured ex vivo and treated with p63 siRNA in combination with either Satb1-expressing or control lentiviruses (Fig. 6). Treatment of $p63^{+/-}$ skin explants with p63 siRNA resulted in an ∼80–90% decrease of the p63 mRNA levels compared with WT skin (Fig. S2 A). p63 siRNA treatment also caused marked decrease of the Satb1 mRNA levels, which, however, were restored by cotreatment with Satb1-expressing but not the control lentiviruses (Fig. 6 E).

In contrast to the $p63^{+/-}$ skin explants treated by control siRNA, treatment with p63 siRNA alone or in combination with control lentivirus caused a marked decrease of the epidermal thickness, cell proliferation, and Loricrin expression, thus reproducing in part the skin phenotype of $p63^{-/-}$ mice (Fig. 6, A–F). However, cotreatment of $p63^{+/-}$ skin samples with p63 siRNA and Satb1-expressing lentivirus resulted in a significant increase in epidermal thickness, cell proliferation, and Loricrin expression compared with the samples treated with p63 siRNA and control lentivirus (Fig. 6 A–F). Restoration of epidermal proliferation after treatment with Satb1-expressing lentivirus was consistent with data showing the reduced cell proliferation in the epidermis of $Satb1^{-/-}$ mice compared with WT controls (Fig. 5 C). Therefore, it is likely that Satb1 plays a role in regulating both keratinocyte proliferation and differentiation and is capable of partially restoring the epidermal phenotype of p63-deficient mice.

Satb1 binds to the distinct genomic regions within the EDC locus in keratinocytes

Because the distance between the *Lor* and *Rps27* in the 5 Mbp chromatin domain is increased in $Satb1^{-/-}$ epidermis in comparison with WT mice (Fig. 4, B–D), we hypothesized that Satb1 may bind to specific sites in the EDC locus to regulate the EDC chromatin conformation. To determine whether any regions within the EDC locus are direct binding targets of Satb1, the formaldehyde–cross-linked chromatin fragments from keratinocytes isolated from E16.5 embryos or newborn skin were immunoprecipitated with anti-Satb1 antibody, and ChIP-on-chip analysis was performed (Fig. 7 A).

Analyses of the ChIP-on-chip data revealed Satb1 binding to many genomic sites, and these sites are found enriched in three distinct regions within the EDC locus (at the 5′ end domain adjacent to the gene desert region, the central domain, and the 3′ end domain). Importantly, Satb1-binding sites in the central domain correspond to the small proline-rich protein (Sprr) and late-cornified envelope (Lce) gene families (Fig. 7 A and Table S6), which are activated during terminal keratinocyte differentiation (Marshall et al., 2001; Martin et al., 2004; Bazzi et al., 2007; Brown et al., 2007). ChIP-on-chip data were further validated by ChIP–quantitative PCR, and the results confirmed that, in both E16.5 and newborn mice, Satb1 binds to the proximal regulatory regions of the *Sprr1b* and *Lce3b* genes located at the central EDC domain (Fig. S4).

Satb1 compresses chromatin conformation of the EDC locus and its central domain

To further examine the potential roles of Satb1 in chromatin remodeling and the execution of gene expression programs in epidermal progenitor cells, 3D FISH analysis of the chromatin conformation was performed in the epidermis of E16.5 and P0.5 $Satb1^{-/-}$ and age-matched WT mice, focusing on total EDC and its central domain containing a large number of the keratinocyte-specific genes (such as genes belonging to the Sprr and Lce families as well as *Lor* and *Inv*). Using DNA probes corresponding to *S100a6* (5′ end), *Lor-Lce3c* (the central domain), and *S100a10* (3′ end), we analyzed the 3D structure of the EDC locus by measuring the volume of its central domain as well as distances between its 5′ end, central domain, and 3′ end. We found that in E16.5 or P0.5 $Satb1^{-/-}$ and WT mice, the EDC locus was localized in the nuclear interior of epidermal progenitor cells, and *Satb1* ablation did not significantly alter its radial positions compared with WT mice (Fig. S5, A and B).

However, the most striking feature of the EDC conformation in the E16.5 and P0.5 $Satb1^{-/-}$ epidermis, in comparison with age-matched WT mice, was the significantly ($P < 0.001$) expanded central domain, determined as the volume of the *Lor-Lce3c* signal (representative Z optical sections of the corresponding DNA FISH images are shown in Fig. 7 B, and continuous Z section images are shown in Fig. S5 E). As evident from the distribution of the data, we consistently observed the increased volume of the central domain in each individual nuclei of epidermal cells in P0.5 $Satb1^{-/-}$ mice compared with aged-matched WT mice (Fig. 7 C). In contrast to the epidermal cells, a lack of changes in the volume of the central EDC domain was seen between dermal cells of $Satb1^{-/-}$ and WT mice (Fig. S5 D), thus suggesting that the effects of the Satb1 ablation on its conformation are indeed keratinocyte specific.

In addition, we found an overall expansion in the length of the whole EDC in P0.5 $Satb1^{-/-}$ epidermis ($P < 0.01$) compared with age-matched WT mice (Figs. 7 [C and D] and S5 C), which is likely a result of elongation of its 5′ domain, determined as a distance between the *S100a6* and the center of the *Lor-Lce3c* signal (Table S7). These results are consistent with data demonstrating the significant elongation of the distance between *Lor* and *Rps27* genes in $Satb1^{-/-}$ embryos versus WT mice (Fig. 4, B–D) and suggest that *Satb1* ablation leads to significant decompression of the locus.

Interestingly, Satb1 binding at specific sites within the EDC locus was not always detected at the proximal promoter regions of the genes whose expression was markedly altered in the $Satb^{-/-}$ epidermis (e.g., *Lor*; Fig. 7 A and Table S6). Our 3D FISH data indicate that Satb1 compresses the chromatin conformation at the EDC locus, including the regions enriched in genes activated during terminal keratinocyte differentiation (Fig. 7, B–D). We observed marked differences in the expression of the genes located in the EDC central domain upon either *Satb1* or *p63* ablation (Figs. 4 E and 5 E). Therefore, it is likely that Satb1 regulates gene expression in the EDC locus in epidermal progenitor cells by establishing its tissue-specific chromatin conformations and potentially by forming a densely looped chromatin structure, rather than by directly targeting proximal cis-regulatory elements of individual genes.

Published September 19, 2011

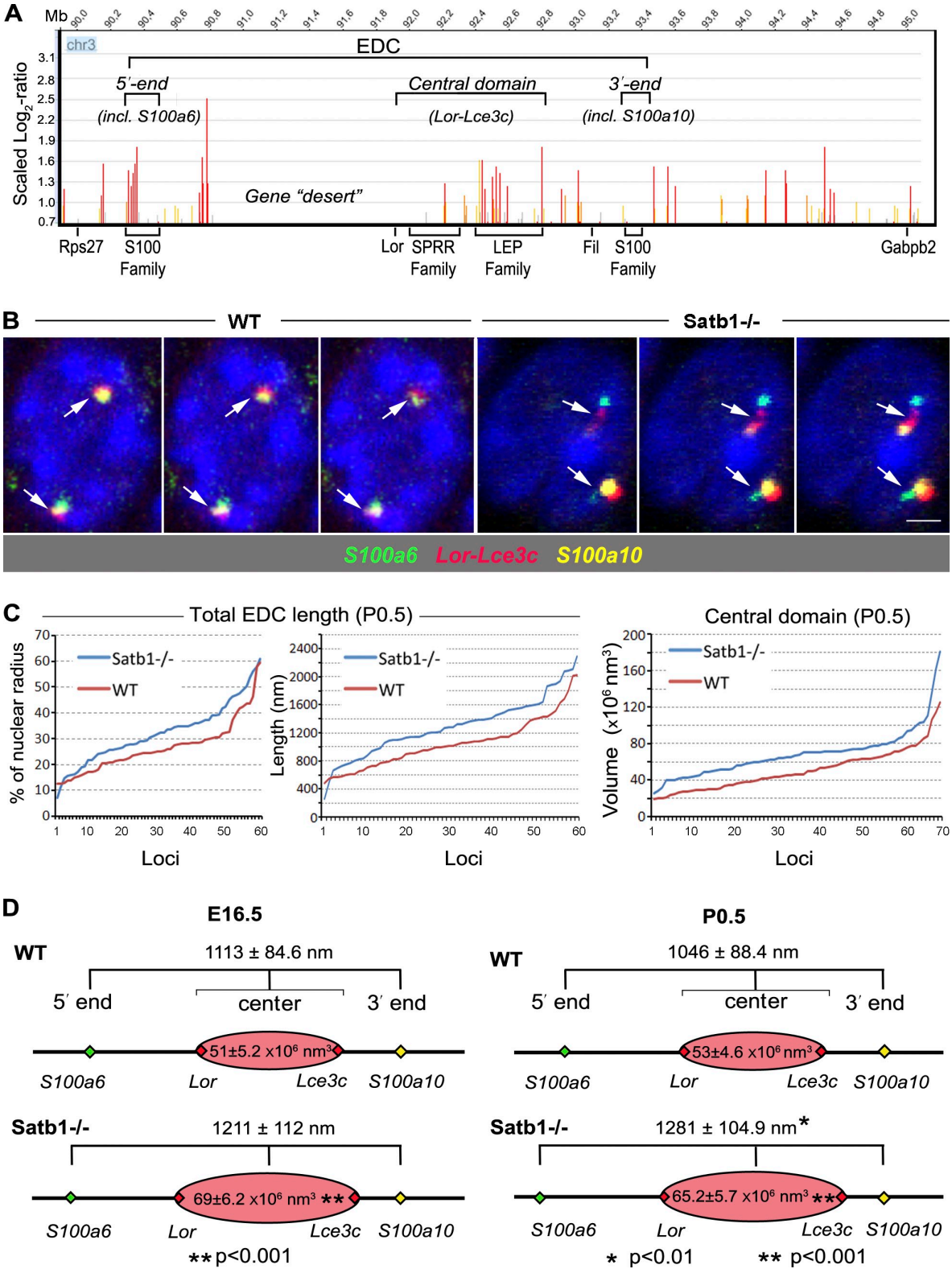

Figure 7. **Satb1 binds the central EDC domain and regulates its conformation in epidermal cells.** Primary mouse keratinocytes were processed for ChIP-on-chip analyses with Satb1 antibody, and skin cryosections of E16.5 and P0.5 Satb1$^{-/-}$ and WT mice were processed for 3D FISH analyses of the EDC chromatin structure. (A) ChIP-on-chip analysis of the Satb1 binding to the distinct genomic regions of the 5 Mb chromatin domain on mouse chromosome 3 (chr3) containing EDC in primary keratinocytes. Enrichment of the Satb1-binding sites at the distinct EDC regions including the central domain. Lack of

Published September 19, 2011

Discussion

Here, we show that p63 transcription factor governs a program of the development of stratified epithelia (Koster and Roop, 2007; Truong and Khavari, 2007; Crum and McKeon, 2010) via regulating expression of the genes that control higher-order chromatin remodeling, covalent histone modifications, and nuclear assembly. Among the genes that regulate chromatin structure and gene expression, we focused on Satb1, which is known to regulate large-scale chromatin remodeling in selected cell types and progenitor cells (Cai et al., 2003, 2006; Kumar et al., 2007; Han et al., 2008; Agrelo et al., 2009). Satb1 was identified among the genes involved in chromatin remodeling that were down-regulated in $p63^{-/-}$ epidermis, consistent with data previously reported using cultured epithelial cells (Carroll et al., 2006; Truong et al., 2006; Pozzi et al., 2009). Our data unveil a novel mechanism by which p63 functions in epidermal development, at least in part, via direct regulation of *Satb1*.

We demonstrate that in keratinocytes, Satb1 shows preferential binding to four major tissue-specific gene loci (EDC, keratin type I/II loci, and keratin-associated protein locus). Satb1 ablation, in striking similarity to p63 deficiency, results in profound alterations of expression of a large number of epidermis-specific genes. Furthermore, we show that the restoration of Satb1 levels partially rescues the epidermal phenotype of embryonic skin explants from p63-deficient mice, further suggesting Satb1 as an important part of the p63-regulated network in the skin.

Among many chromatin-remodeling factors (such as Smarca4/Brg1, Mi-2α, Mi-2β, etc.) that are altered in $p63^{-/-}$ mice and other p63 targets previously identified (Koster and Roop, 2007; Viganò and Mantovani, 2007), Satb1 represents an important functional component of the p63-regulated genetic network because of its ability to reorganize chromatin structure and regulate higher-order chromatin remodeling in epidermal progenitor cells. In fact, our expression data together with ChIP-on-chip data for Satb1-binding sites indicate that once Satb1 is induced by p63, it establishes its own regulatory network, binding to the target gene loci and controlling the expression of ∼2,500 genes, including those not associated with the epidermis-specific gene loci. Among these genes, cell cycle–associated genes are of interest because we found that Satb1 has an effect in promoting cell proliferation in the developing epidermis, which is consistent with data obtained from the studies on aggressive breast cancer cells (Han et al., 2008). The mechanisms underlying Satb1-induced cell proliferation need to be studied in the future.

Differences in gene expression profiles in keratinocytes observed after either *p63* or *Satb1* ablation in many gene groups may suggest that the roles of p63 and Satb1 in the control of expression of the genes located outside of the epidermis-specific loci are quite distinct. However, we must be aware that p63 ablation, which deregulates many key transcriptional repressors/activators and chromatin-remodeling factors, in addition to Satb1, could alter expression of many Satb1 target genes beyond the effect of Satb1 ablation alone. This could explain, at least for some gene groups, why their expression profiles are quite distinct between $p63^{-/-}$ and $Satb1^{-/-}$ mice. Nevertheless, we provide compelling evidence that within a spiderweb of a gene regulatory network governed by p63, Satb1, as its direct downstream target gene, constitutes an important component driving epidermal development via regulating the epidermis-specific gene loci. It still remains to be investigated whether Satb1 acts together with p63 or whether it acts independently from p63 in controlling the establishment of specific conformation of the EDC and other genomic loci in keratinocytes.

We show here that Satb1 binds to distinct genomic regions including the central domain of the EDC locus, which consists of a large number of genes activated during terminal keratinocyte differentiation (Martin et al., 2004; Brown et al., 2007) and which regulates the establishment of its specific conformations in keratinocytes. It has been previously shown that intranuclear EDC positioning in cultured keratinocytes is cell type specific, whereas their treatment with 5-azacytidine and sodium butyrate results in an increase of gene expression within the EDC (Elder and Zhao, 2002; Williams et al., 2002). These and other studies suggest that changes in local epigenomic modification of the EDC gene locus are required for efficient expression of keratinocyte-specific genes (Frye et al., 2007; Ezhkova et al., 2009; Sen et al., 2010).

Furthermore, we demonstrate that Satb1 deficiency results in decompression of the EDC locus, specifically its central domain. These alterations are associated with a marked decrease in expression of terminal differentiation–associated genes and are accompanied by morphological changes in the epidermis (thinning of the granular layer and decrease of the epidermal thickness). Lack of similar dynamics in the nuclei of dermal cells suggests that the developmentally regulated remodeling of the higher-order chromatin structure in the EDC associated with increase of its transcription activity is indeed a tissue-specific event and that other factors may control EDC condensation in dermal cells.

During the execution of cell differentiation programs, tissue-specific genes organized into large genomic loci are expressed in a tightly coordinated manner to achieve the proper balance of the distinct proteins in differentiated cells (Kosak and Groudine, 2004). Increased evidence of data suggests that for such coordinated regulation, distinct spatial organization of tissue-specific

Satb1 binding to the gene desert region between the 5′ end and the central domain of the locus. LEP, late-cornified envelope protein. (B) 3D FISH analyses of the volume of central EDC domain as well as the EDC length with probes detecting the 5′ and 3′ ends of the EDC (*S100a6* and *S100a10* genes, respectively) and the central domain (*Lor-Lce3c)* in the basal epidermal cells of $Satb1^{-/-}$ and WT mice. Representative single Z optical sections of newborn WT and Satb1 knockout keratinocyte nuclei are shown. Consecutive Z sections of the same nuclei are shown in Fig. S5 E. Arrows indicate the FISH signals. Bar, 2 µm. (C) The volume of the EDC central domain and the length of the total EDC locus were measured and compared between nuclei of basal epidermal cells of $Satb1^{-/-}$ and WT mice. The distribution of the data after measuring the total EDC length with or without normalization to the corresponding nuclear radii (left and middle, respectively) and the volume of the central domain (right) in 60–70 loci of basal epidermal cells at P0.5 $Satb1^{-/-}$ and WT mice is shown. Individual loci are shown in the x axis. (D) Statistical analysis shows a significant increase of the volume of central EDC domain in $Satb1^{-/-}$ mice compared with that of WT mice. The length of the total EDC increases in P0.5 $Satb1^{-/-}$ mice compared with WT mice.

Published September 19, 2011

gene loci is required, and Satb1 was shown to be an essential factor in controlling formation of the specific loop structures in many tissue-specific gene loci (Cai et al., 2003, 2006). It has been shown that during T_H2 lymphocyte activation, Satb1 promotes the formation of a specific 3D structure of the cytokine locus, in which chromatin is folded into numerous small loops that bring proximal and distal gene regulatory elements together to activate the gene expression (Cai et al., 2006). More recent data demonstrate that Satb1 also controls the formation of the chromatin loops in the β-globin locus (Wang et al., 2009). We hypothesize that Satb1 may form a similar chromatin structure, characterized by dense chromatin loops, in the EDC central domain and the flanking regions, which may result in reduction of the total physical volume of chromatin in these regions. Such a higher-order transcriptionally active chromatin structure may facilitate the accessibility of protein complexes to target gene loci as well as interactions between proximal and distal regulatory gene regions.

If this hypothesis is correct, in the absence of Satb1, the EDC locus cannot be properly folded, and, therefore, this region on mouse chromosome 3 will remain more decompressed (or elongated) compared with WT cells and will not be able to support efficient expression of the terminal differentiation–associated genes. To test this hypothesis, additional studies using the chromatin conformation capture techniques will be required to identify the role of Satb1 in the formation of such chromatin loop–like structures within the EDC. However, significant changes in the volume of the central EDC domain and total EDC length upon Satb1 ablation provide strong support for this hypothesis.

Importantly, these data are also consistent with previous observations that strong Satb1 binding may not be necessarily detected at the proximal promoter regions of its target genes. This is because the main binding targets of Satb1 are the specialized DNA domains called base unpairing regions (Kohwi-Shigematsu and Kohwi, 1990; Bode et al., 1992), which are enriched in the gene-rich regions throughout the genome (Cai et al., 2006). For instance, Satb1 binding was undetected at the proximal regulatory region of the *Lor* gene per se, and yet *Lor* appears to be regulated in the context of Satb1-dependent 3D chromatin folding.

The data presented in this paper link, for the first time, the functions of a master regulator of tissue development (viz., p63) with a protein that controls higher-order chromatin remodeling (viz., Satb1), and this link provides an important foundation for further studies of the role of p63 as a potential upstream regulator of Satb1 activity in other cell types. Because the Satb1-dependent step in the p63-mediated program of higher-order chromatin remodeling in the EDC locus is highly important for the proper execution of differentiation programs in epidermal progenitor cells, it remains to be determined whether similar mechanisms underlie the involvement of p63 and Satb1 during the developmentally regulated activation of gene expression in other keratinocyte-specific loci as well as during activation of the epidermis-specific gene expression programs in epithelial stem cells in adult skin (Ito et al., 2007; Watt et al., 2008; Blanpain and Fuchs, 2009). Importantly, recent data indeed revealed that Satb1 has a critical role in regulating the differentiation potential of embryonic stem cells (Savarese et al., 2009).

Collectively, our data demonstrate that Satb1 is an important hitherto unrecognized component of the global regulatory network of p63, a master regulator of epidermal morphogenesis. These data provide a novel fundamental mechanism showing how master regulators of tissue morphogenesis establish tissue- and developmental stage–specific patterns of chromatin organization and remodeling to control the fate of multipotent progenitor cells.

Materials and methods

Experimental animals and tissue collection

All animal studies were performed under protocols approved by the Boston University and University of California Berkeley Institutional Animal Care and Use Committee and the Home Office Project License. C57Bl/6 mice were purchased from Charles River. Skin samples were collected from mice at distinct days of embryonic and postnatal development (E16.5 and P0.5). $p63^{-/-}$ and $p63^{+/+}$ control embryos at E16.5 were obtained by breeding $p63^{+/-}$ animals purchased from The Jackson Laboratory. Genotyping of mice was performed using PCR, as recommended by the supplier. For each developmental stage, six to seven samples were collected. Tissue samples were frozen in liquid nitrogen and processed for immunofluorescent or microarray analyses as previously described (Sharov et al., 2003, 2005b).

In brief, for FISH and immunofluorescent analysis of 3D preserved nuclei, skin samples were processed through the fixation protocol with formaldehyde and gradual equilibration in buffered sucrose solutions according to previously published recommendations (Solovei et al., 2009). The embryos or tissues were fixed in 4% formaldehyde at 4°C overnight and incubated in 50 mM ammonium chloride solution at room temperature for 5 min followed by washes with 0.1 M phosphate buffer (pH 7.0) and by incubations in 5 and 12.5% sucrose solution in the phosphate buffer (1 h at room temperature) and in 20% sucrose solution (overnight at 4°C). Finally, the samples were frozen and embedded into optimal cutting temperature medium.

LCM, microarray, and quantitative RT-PCR analysis

LCM of whole mouse epidermis at selected stages of development was performed followed by RNA isolation, amplification, and microarray analysis as previously described (Sharov et al., 2006). In brief, 8-µm-thick frozen skin cryosections were dehydrated to preserve RNA integrity, and LCM was performed from the epidermis of WT and $p63^{-/-}$ mice at E16.5 using an LCM microscope (Life Technologies). Total RNAs were isolated using the PicoPure RNA isolation kit (Life Technolgoies) followed by two rounds of linear RNA amplification using the RiboAmp RNA amplification kit (Life Technologies). Equal amounts of RNA from each sample were labeled by Cy3 using a fluorescent labeling kit (Agilent Technologies). Quality and size distribution of targets was determined by RNA 6000 Nano Laboratory–on-chip assay (Agilent Technologies), and quantification was determined using a microscale spectrophotometer (NanoDrop). After one round of linear amplification in all analyses, Universal Mouse Reference RNA (Agilent Technologies) was used as a control. All microarray analyses were performed by MOgene, LC using the 41K Whole Mouse Genome 60-mer Oligo Microarray kit (Agilent Technologies). Real-time PCR of unamplified reference RNA and reference RNA obtained after two rounds of amplification was used for validation of possible alterations in gene expression caused by the amplification procedure. All microarray data on gene expression were normalized to the corresponding data obtained from the reference RNA. Two independent datasets were obtained from WT and transgenic mice, and p values were calculated by Feature Extraction software (version 7.5; Agilent Technologies) using distribution of the background intensity values to signal intensity and using a Student's *t* test. For quantitative RT-PCR analysis of RNA isolated and amplified after LCM, PCR primers were designed on Beacon Designer software (Table S6; PREMIER Biosoft International). Real-time PCR was performed using iQ SYBR green Supermix and the MyiQ Single-Color Real-Time PCR Detection System (Bio-Rad Laboratories). Differences between samples and controls were calculated using the Gene Expression Macro program (Bio-Rad Laboratories) based on the $\Delta\Delta C_t$ equitation method with glyceraldehyde 3-phosphate dehydrogenase and peptidylprolyl isomerase A genes as internal housekeeping controls.

3D FISH and immunofluorescent analyses

Labeled DNA probes were prepared, and 3D FISH analysis was performed on 20-µm tissue sections as previously described (Solovei et al., 2009).

Published September 19, 2011

Individual or pooled bacterial artificial chromosome (BAC) DNA for the genetic loci of interest was used for the probe synthesis (Table S3). The probes were synthesized by nick translation using Biotin-dUTP, FITC-dUTP, or Cy3-dUTP. Whole chromosome paints were labeled with Biotin-dUTP by degenerate oligonucleotide–primed PCR. The frozen sections were briefly dried, heated in 10 mM sodium citrate (pH 6.0) to partially reverse cross-linking, and equilibrated in 50% formamide/2× SSC. Labeled DNA probe mixtures were dissolved in hybridization buffer and applied on the tissue under glass chambers. Genomic and probe DNA were denatured by incubating slides at 85°C for 5 min, and hybridization was performed at 37°C for 2 d. After hybridization, slides were washed three times at 2× SSC for 10 min at 37°C followed by one wash in 0.1× SSC for 10 min at 60°C. When biotinylated probes were used, the slides were incubated with avidin–Alexa Fluor 488 (Invitrogen), streptavidin-Cy3, or streptavidin-Cy5 (Rockland Immunochemicals). DNA was stained with DAPI (Sigma-Aldrich), and slides were embedded using VectaShield medium (Vector Laboratories). Immunofluorescent analysis was performed on 10–20-µm quickly frozen or 3D preserved tissue with antibodies (Table S10) using standard protocols (Fessing et al., 2006).

Microscopy and image analyses

For analysis of epidermal morphology, images of the tissue after staining with hemotoxylin were acquired at room temperature using a microscope (Eclipse 50i; Nikon) equipped with a Plan Fluor 20×/0.50 or 40×/0.75 objective lens (Nikon), VisiCam 3.0 camera (VWR International), and VisiCam Image Analyzer software. The morphometric analysis was performed using ImageJ software (National Institutes of Health). Immunofluorescent images were acquired at room temperature using a microscope (Eclipse 50i), EXi Aqua camera (QImaging), and Image-Pro Express software (version 6.3; Media Cybernetics).

3D FISH images were collected using a laser-scanning confocal microscope (510 META; Carl Zeiss), Plan Apochromat 63×/1.4 oil differential interference contrast objective lens, and laser-scanning microscopy software (510 META). Imaging was performed at room temperature using Immersol immersion oil (Carl Zeiss). For 3D image analysis, the nuclei were scanned with a Z axial distance of 200 nm yielding separate stacks of 8-bit grayscale images for each fluorescent channel with a pixel size of 100–200 nm. For each optical section, images were collected sequentially for all fluorophores, and axial chromatic shift was corrected for each channel using 500-nm TetraSpeck beads (Invitrogen; Solovei et al., 2009). The images were processed and analyzed using ImageJ software. For the illustration purposes, 3D FISH and immunofluorescent images of the skin cryosections were adjusted using the levels and brightness/contrast tools in Photoshop (CS4; Adobe); separate adjustments were applied to every pixel in each RGB channel.

To determine radial positions of the loci, coordinates of at least 200 random points from the nuclear surface depicted by DAPI counterstain were acquired and exported to Excel (Microsoft), where the nuclear geometric center was calculated by coordinate averaging (Höfers et al., 1993). The mean nuclear radius for each nucleus was calculated as a mean of distances from the nuclear geometric center to all surface points. Distances between the centers of the nucleus and distinct loci were calculated on the basis of their spatial coordinates and were normalized to the mean nuclear radius using Excel (Ronneberger et al., 2008). Distances between individual gene loci were calculated after determination of the spatial coordinates of the corresponding centers of the signals using ImageJ software. The distances were normalized to the mean radii of the corresponding nuclei, determined as described above.

The volume of the central EDC domain was calculated using the approach previously described (Rauch et al., 2008). First, the threshold of the fluorescent signal was determined via selection of 1% of the brightest voxels from 3D intensity histograms using ImageJ software. Second, using this threshold, the number of voxels within each fluorescent signal was calculated. Next, the physical volume indicated by the fluorescent signal was determined as a sum of the volumes from all voxels after correction for optical aberrations by normalizing the data to the volume of beads of distinct size (100 nm, 500 nm, and 4 µm; TetraSpeck).

Embryonic tissue culture

Whole dorsal skin culture from E13.5 $p63^{+/-}$ embryos were prepared and maintained as previously described (Botchkarev et al., 1999). In brief, skin samples were dissected from embryos and cultured in the 6-well plates containing Williams' E culture medium for 48 h. Within 2 h after the culture preparation, tissue samples were transfected with Stealth siRNA, recognizing all isoforms of p63 (Antonini et al., 2006), or medium containing negative control Stealth siRNA (Invitrogen) at 100 nM final concentration using the RNAiMax reagent (Invitrogen). Samples were also incubated with combinations of p63 siRNA or control siRNA and Satb1-expressing lentivirus or control lentivirus (10 µg/ml) for 48 h. The tissue was frozen and embedded into optimal cutting temperature medium as described in the Experimental animals and tissue collection section for subsequent immunofluorescent analyses. The penetration of the RNAi into the tissue under the used experimental conditions was demonstrated using BLOCK-iT Fluorescent Oligo (Invitrogen) in parallel experiments.

Western blot analysis

Proteins were extracted from snap-frozen skin samples or cultured keratinocytes with lysis buffer as previously described (Antonini et al., 2006). 5 µg of protein was processed for Western blot analysis followed by incubation with primary antibodies against p63 or Erk (Table S10) overnight at 4°C. HRP-tagged IgG antibody was used as a secondary antibody (1:5,000; Thermo Fisher Scientific). Antibody binding was visualized using an ECL system (SuperSignal West Pico kit; Thermo Fisher Scientific) followed by autoradiography with x-ray film (Thermo Fisher Scientific).

ChIP and ChIP-on-chip assays

ChIP assay was performed using epidermal keratinocytes isolated from E16.5 or newborn mouse skin with anti-p63 or anti-Satb1 antibodies (Table S8) as previously described (Antonini et al., 2006; Nguyen et al., 2006). PCR analysis for enrichment in the promoter sequences of *Satb1*, *Cldn1*, *Lor*, *Sprr1b*, *Lce3b*, *or Inv* genes in precipitated DNA was performed using the PCR primers listed in Table S7. For ChIP-on-chip analysis, precipitated DNA was analyzed by quantitative PCR or after one round of amplification (WGA2; Sigma-Aldrich) and applied to a general extended NimbleGen MM8 Deluxe Promoter HX1 array (MOgene, LC).

Reporter assay

Plasmids expressing pSatb1-luc construct bearing a promoter region containing the far-upstream CpG island and the p63 consensus sequence of mouse *Satb1* were generated. For reporter assay, HaCaT cells were seeded into 96-well plates (10^4 cells per well) 1 d before transfection. Cells were cotransfected with pΔNp63 (Antonini et al., 2006) or pcDNA3 plasmids (120 ng/well; Invitrogen) along with the reporter pSatb1-Luc construct using Lipofectamine 2000 (0.5 µl/well; Invitrogen). After 48 h, reporter activity was detected using the Dual-Glo Luciferase Assay System (Promega). Two independent assays were performed in triplicate, and results were normalized to the pNull-Renilla construct activity, the data were pooled, a mean ± SEM was calculated, and statistical analysis was performed using a Student's *t* test.

Statistical analysis and gene ontology analysis

For statistical evaluation of differences in radial positions, intergene distances, and 3D FISH signal volumes, normality of data distributions was evaluated by plotting them on histograms. Equality of their variances was tested by the Levene's test. Significance of the differences for the pairwise comparisons was analyzed by a two-tailed *t* test ($\alpha = 0.05$). For more than two-sample comparisons, a one-way analysis of variance (ANOVA) followed by the Newman–Keuls test ($\alpha = 0.05$) was performed. Enrichment of the Satb1 target genes in the distinct genomic loci was assessed by using the hypergeometric or Fisher's exact tests. Functional annotation of the overrepresented and underrepresented genes was performed as previously described (Sharov et al., 2009; Fessing et al., 2010) using the National Institute on Aging Array Analysis software (National Institutes of Health) according to previously published recommendations (Sharov et al., 2005a).

Online supplemental material

Fig. S1 shows localization of the EDC in gene-dense regions of mouse chromosome 3. Fig. S2 shows validation of the effects of p63 knockdown after siRNA treatment in skin explants and keratinocytes as well as the data on the analyses of 3D FISH distances and gene expression in the epidermis of $p63^{-/-}$, $Satb1^{-/-}$, and corresponding WT mice. Fig. S3 shows the results of the microarray, ChIP-on-chip, and bioinformatic analyses of the genes whose expression was altered in the skin of $Satb1^{-/-}$ mice versus WT controls and which showed association of Satb1 with the genomic regions within 200 kb from the transcription start sites in the ChIP-on-chip assay. Fig. S4 shows the results of ChIP–quantitative PCR analyses of keratinocytes demonstrating binding of Satb1 to the promoter regions of the distinct genes within the EDC. Fig. S5 shows the results of 3D FISH analyses of radial positions of *Rps27* and *Lor* genes and differences in

Published September 19, 2011

the intergene distances in the EDC locus as well as the confocal stacks demonstrating intranuclear localization of the distinct EDC domains in the epidermis of Satb1$^{-/-}$ and WT mice. Tables S1 and S2 show the lists of the genes down- and up-regulated in the skin epithelium of the E16.5 p63$^{-/-}$ versus WT mice, respectively. Table S3 shows the list of 3D FISH BAC probes generated to the distinct regions of mouse chromosome 3. Tables S4 and S5 show the list of genes that demonstrate Satb1 binding to their regulatory regions and down- and up-regulated in the skin of the P0.5 Satb1$^{-/-}$ versus WT mice, respectively. Table S6 shows SATB1 binding sites in the EDC locus and its 5′ and 3′ flanking regions based on the ChIP-on-chip analysis. Table S7 shows the length of the distinct EDC domains in Satb1$^{-/-}$ and WT mice. Tables S8 and S9 show the list of the primers used for quantitative RT-PCR and ChIP–quantitative PCR analyses, respectively. Table S10 shows the list of primary antibodies used for immunohistochemical analyses. Online supplemental material is available at http://www.jcb.org/cgi/content/full/jcb.201101148/DC1.

The authors greatly appreciate the invaluable help and support of Prof. T. Cremer, Dr. I. Solovei, and Dr. B. Joffe (University of Munich, Munich, Germany) in establishing 3D FISH technique and analyzing the data.

This study was supported in part by the grants from the Medical Research Council (G0901666) to V.A. Botchkarev, from the National Institutes of Health (R37CA039681) to T. Kohwi-Shigematsu (under the Department of Energy Contract no. DE-AC02-05CH11231), and from the Fondazione Telethon (GGP09230) to C. Missero.

Submitted: 31 January 2011
Accepted: 22 August 2011

References

Agrelo, R., A. Souabni, M. Novatchkova, C. Haslinger, M. Leeb, V. Komnenovic, H. Kishimoto, L. Gresh, T. Kohwi-Shigematsu, L. Kenner, and A. Wutz. 2009. SATB1 defines the developmental context for gene silencing by Xist in lymphoma and embryonic cells. *Dev. Cell*. 16:507–516. http://dx.doi.org/10.1016/j.devcel.2009.03.006

Alvarez, J.D., D.H. Yasui, H. Niida, T. Joh, D.Y. Loh, and T. Kohwi-Shigematsu. 2000. The MAR-binding protein SATB1 orchestrates temporal and spatial expression of multiple genes during T-cell development. *Genes Dev.* 14:521–535.

Antonini, D., B. Rossi, R. Han, A. Minichiello, T. Di Palma, M. Corrado, S. Banfi, M. Zannini, J.L. Brissette, and C. Missero. 2006. An autoregulatory loop directs the tissue-specific expression of p63 through a long-range evolutionarily conserved enhancer. *Mol. Cell. Biol.* 26:3308–3318. http://dx.doi.org/10.1128/MCB.26.8.3308-3318.2006

Bazzi, H., K.A. Fantauzzo, G.D. Richardson, C.A. Jahoda, and A.M. Christiano. 2007. Transcriptional profiling of developing mouse epidermis reveals novel patterns of coordinated gene expression. *Dev. Dyn.* 236:961–970. http://dx.doi.org/10.1002/dvdy.21099

Blanpain, C., and E. Fuchs. 2009. Epidermal homeostasis: a balancing act of stem cells in the skin. *Nat. Rev. Mol. Cell Biol.* 10:207–217. http://dx.doi.org/10.1038/nrm2636

Bode, J., Y. Kohwi, L. Dickinson, T. Joh, D. Klehr, C. Mielke, and T. Kohwi-Shigematsu. 1992. Biological significance of unwinding capability of nuclear matrix-associating DNAs. *Science*. 255:195–197. http://dx.doi.org/10.1126/science.1553545

Botchkarev, V.A., N.V. Botchkareva, W. Roth, M. Nakamura, L.-H. Chen, W. Herzog, G. Lindner, J.A. McMahon, C. Peters, R. Lauster, et al. 1999. Noggin is a mesenchymally derived stimulator of hair-follicle induction. *Nat. Cell Biol.* 1:158–164. http://dx.doi.org/10.1038/11078

Brown, S.J., C.M. Tilli, B. Jackson, A.A. Avilion, M.C. MacLeod, L.J. Maltais, R.C. Lovering, and C. Byrne. 2007. Rodent Lce gene clusters; new nomenclature, gene organization, and divergence of human and rodent genes. *J. Invest. Dermatol.* 127:1782–1786.

Cai, S., H.J. Han, and T. Kohwi-Shigematsu. 2003. Tissue-specific nuclear architecture and gene expression regulated by SATB1. *Nat. Genet.* 34:42–51. http://dx.doi.org/10.1038/ng1146

Cai, S., C.C. Lee, and T. Kohwi-Shigematsu. 2006. SATB1 packages densely looped, transcriptionally active chromatin for coordinated expression of cytokine genes. *Nat. Genet.* 38:1278–1288. http://dx.doi.org/10.1038/ng1913

Carroll, D.K., J.S. Carroll, C.O. Leong, F. Cheng, M. Brown, A.A. Mills, J.S. Brugge, and L.W. Ellisen. 2006. p63 regulates an adhesion programme and cell survival in epithelial cells. *Nat. Cell Biol.* 8:551–561. http://dx.doi.org/10.1038/ncb1420

Crum, C.P., and F.D. McKeon. 2010. p63 in epithelial survival, germ cell surveillance, and neoplasia. *Annu. Rev. Pathol.* 5:349–371. http://dx.doi.org/10.1146/annurev-pathol-121808-102117

Dickinson, L.A., T. Joh, Y. Kohwi, and T. Kohwi-Shigematsu. 1992. A tissue-specific MAR/SAR DNA-binding protein with unusual binding site recognition. *Cell*. 70:631–645. http://dx.doi.org/10.1016/0092-8674(92)90432-C

Elder, J.T., and X. Zhao. 2002. Evidence for local control of gene expression in the epidermal differentiation complex. *Exp. Dermatol.* 11:406–412. http://dx.doi.org/10.1034/j.1600-0625.2002.110503.x

Ezhkova, E., H.A. Pasolli, J.S. Parker, N. Stokes, I.H. Su, G. Hannon, A. Tarakhovsky, and E. Fuchs. 2009. Ezh2 orchestrates gene expression for the stepwise differentiation of tissue-specific stem cells. *Cell*. 136:1122–1135. http://dx.doi.org/10.1016/j.cell.2008.12.043

Fessing, M.Y., T.Y. Sharova, A.A. Sharov, R. Atoyan, and V.A. Botchkarev. 2006. Involvement of the Edar signaling in the control of hair follicle involution (catagen). *Am. J. Pathol.* 169:2075–2084. http://dx.doi.org/10.2353/ajpath.2006.060227

Fessing, M.Y., R. Atoyan, B. Shander, A.N. Mardaryev, V.V.J. Botchkarev Jr., K. Poterlowicz, Y. Peng, T. Efimova, and V.A. Botchkarev. 2010. BMP signaling induces cell-type-specific changes in gene expression programs of human keratinocytes and fibroblasts. *J. Invest. Dermatol.* 130:398–404. http://dx.doi.org/10.1038/jid.2009.259

Fraser, P., and W. Bickmore. 2007. Nuclear organization of the genome and the potential for gene regulation. *Nature*. 447:413–417. http://dx.doi.org/10.1038/nature05916

Frye, M., A.G. Fisher, and F.M. Watt. 2007. Epidermal stem cells are defined by global histone modifications that are altered by Myc-induced differentiation. *PLoS ONE*. 2:e763. http://dx.doi.org/10.1371/journal.pone.0000763

Fuchs, E. 2007. Scratching the surface of skin development. *Nature*. 445:834–842. http://dx.doi.org/10.1038/nature05659

Han, H.J., J. Russo, Y. Kohwi, and T. Kohwi-Shigematsu. 2008. SATB1 reprogrammes gene expression to promote breast tumour growth and metastasis. *Nature*. 452:187–193. http://dx.doi.org/10.1038/nature06781

Hemberger, M., W. Dean, and W. Reik. 2009. Epigenetic dynamics of stem cells and cell lineage commitment: digging Waddington's canal. *Nat. Rev. Mol. Cell Biol.* 10:526–537. http://dx.doi.org/10.1038/nrm2727

Höfers, C., P. Baumann, G. Hummer, T.M. Jovin, and D.J. Arndt-Jovin. 1993. The localization of chromosome domains in human interphase nuclei. Three-dimensional distance determinations of fluorescence in situ hybridization signals from confocal laser scanning microscopy. *Bioimaging*. 1:96–106. http://dx.doi.org/10.1002/1361-6374(199306)1:2<96::AID-BIO4>3.3.CO;2-4

Indra, A.K., V. Dupé, J.M. Bornert, N. Messaddeq, M. Yaniv, M. Mark, P. Chambon, and D. Metzger. 2005. Temporally controlled targeted somatic mutagenesis in embryonic surface ectoderm and fetal epidermal keratinocytes unveils two distinct developmental functions of BRG1 in limb morphogenesis and skin barrier formation. *Development*. 132:4533–4544. http://dx.doi.org/10.1242/dev.02019

Ito, M., Z. Yang, T. Andl, C. Cui, N. Kim, S.E. Millar, and G. Cotsarelis. 2007. Wnt-dependent de novo hair follicle regeneration in adult mouse skin after wounding. *Nature*. 447:316–320. http://dx.doi.org/10.1038/nature05766

Joffe, B., H. Leonhardt, and I. Solovei. 2010. Differentiation and large scale spatial organization of the genome. *Curr. Opin. Genet. Dev.* 20:562–569. http://dx.doi.org/10.1016/j.gde.2010.05.009

Kashiwagi, M., B.A. Morgan, and K. Georgopoulos. 2007. The chromatin remodeler Mi-2beta is required for establishment of the basal epidermis and normal differentiation of its progeny. *Development*. 134:1571–1582. http://dx.doi.org/10.1242/dev.001750

Kohwi-Shigematsu, T., and Y. Kohwi. 1990. Torsional stress stabilizes extended base unpairing in suppressor sites flanking immunoglobulin heavy chain enhancer. *Biochemistry*. 29:9551–9560. http://dx.doi.org/10.1021/bi00493a009

Kosak, S.T., and M. Groudine. 2004. Gene order and dynamic domains. *Science*. 306:644–647. http://dx.doi.org/10.1126/science.1103864

Koster, M.I., and D.R. Roop. 2007. Mechanisms regulating epithelial stratification. *Annu. Rev. Cell Dev. Biol.* 23:93–113. http://dx.doi.org/10.1146/annurev.cellbio.23.090506.123357

Kumar, P.P., O. Bischof, P.K. Purbey, D. Notani, H. Urlaub, A. Dejean, and S. Galande. 2007. Functional interaction between PML and SATB1 regulates chromatin-loop architecture and transcription of the MHC class I locus. *Nat. Cell Biol.* 9:45–56. http://dx.doi.org/10.1038/ncb1516

Lanctôt, C., T. Cheutin, M. Cremer, G. Cavalli, and T. Cremer. 2007. Dynamic genome architecture in the nuclear space: regulation of gene expression in three dimensions. *Nat. Rev. Genet.* 8:104–115. http://dx.doi.org/10.1038/nrg2041

LeBoeuf, M., A. Terrell, S. Trivedi, S. Sinha, J.A. Epstein, E.N. Olson, E.E. Morrisey, and S.E. Millar. 2010. Hdac1 and Hdac2 act redundantly to control p63 and p53 functions in epidermal progenitor cells. *Dev. Cell*. 19:807–818. http://dx.doi.org/10.1016/j.devcel.2010.10.015

Lopardo, T., N. Lo Iacono, B. Marinari, M.L. Giustizieri, D.G. Cyr, G. Merlo, F. Crosti, A. Costanzo, and L. Guerrini. 2008. Claudin-1 is a p63 target gene with a crucial role in epithelial development. *PLoS ONE*. 3:e2715. http://dx.doi.org/10.1371/journal.pone.0002715

Mammucari, C., A. Tommasi di Vignano, A.A. Sharov, J. Neilson, M.C. Havrda, D.R. Roop, V.A. Botchkarev, G.R. Crabtree, and G.P. Dotto. 2005. Integration of Notch 1 and calcineurin/NFAT signaling pathways in keratinocyte growth and differentiation control. *Dev. Cell*. 8:665–676. http://dx.doi.org/10.1016/j.devcel.2005.02.016

Marella, N.V., B. Seifert, P. Nagarajan, S. Sinha, and R. Berezney. 2009. Chromosomal rearrangements during human epidermal keratinocyte differentiation. *J. Cell. Physiol.* 221:139–146. http://dx.doi.org/10.1002/jcp.21855

Marshall, D., M.J. Hardman, K.M. Nield, and C. Byrne. 2001. Differentially expressed late constituents of the epidermal cornified envelope. *Proc. Natl. Acad. Sci. USA*. 98:13031–13036. http://dx.doi.org/10.1073/pnas.231489198

Martin, N., S. Patel, and J.A. Segre. 2004. Long-range comparison of human and mouse Sprr loci to identify conserved noncoding sequences involved in coordinate regulation. *Genome Res.* 14:2430–2438. http://dx.doi.org/10.1101/gr.2709404

Mills, A.A., B. Zheng, X.J. Wang, H. Vogel, D.R. Roop, and A. Bradley. 1999. p63 is a p53 homologue required for limb and epidermal morphogenesis. *Nature*. 398:708–713. http://dx.doi.org/10.1038/19531

Naumova, N., and J. Dekker. 2010. Integrating one-dimensional and three-dimensional maps of genomes. *J. Cell Sci.* 123:1979–1988. http://dx.doi.org/10.1242/jcs.051631

Nguyen, B.C., K. Lefort, A. Mandinova, D. Antonini, V. Devgan, G. Della Gatta, M.I. Koster, Z. Zhang, J. Wang, A. Tommasi di Vignano, et al. 2006. Cross-regulation between Notch and p63 in keratinocyte commitment to differentiation. *Genes Dev.* 20:1028–1042. http://dx.doi.org/10.1101/gad.1406006

Pavan Kumar, P., P.K. Purbey, C.K. Sinha, D. Notani, A. Limaye, R.S. Jayani, and S. Galande. 2006. Phosphorylation of SATB1, a global gene regulator, acts as a molecular switch regulating its transcriptional activity in vivo. *Mol. Cell.* 22:231–243. http://dx.doi.org/10.1016/j.molcel.2006.03.010

Pozzi, S., F. Zambelli, D. Merico, G. Pavesi, A. Robert, P. Maltère, X. Gidrol, R. Mantovani, and M.A. Vigano. 2009. Transcriptional network of p63 in humankeratinocytes.*PLoSONE*.4:e5008.http://dx.doi.org/10.1371/journal.pone.0005008

Rando, O.J., and H.Y. Chang. 2009. Genome-wide views of chromatin structure. *Annu. Rev. Biochem.* 78:245–271. http://dx.doi.org/10.1146/annurev.biochem.78.071107.134639

Rauch, J., T.A. Knoch, I. Solovei, K. Teller, S. Stein, K. Buiting, B. Horsthemke, J. Langowski, T. Cremer, M. Hausmann, and C. Cremer. 2008. Light optical precision measurements of the active and inactive Prader-Willi syndrome imprinted regions in human cell nuclei. *Differentiation*. 76:66–82.

Ronneberger, O., D. Baddeley, F. Scheipl, P.J. Verveer, H. Burkhardt, C. Cremer, L. Fahrmeir, T. Cremer, and B. Joffe. 2008. Spatial quantitative analysis of fluorescently labeled nuclear structures: problems, methods, pitfalls. *Chromosome Res.* 16:523–562. http://dx.doi.org/10.1007/s10577-008-1236-4

Savarese, F., A. Dávila, R. Nechanitzky, I. De La Rosa-Velazquez, C.F. Pereira, R. Engelke, K. Takahashi, T. Jenuwein, T. Kohwi-Shigematsu, A.G. Fisher, and R. Grosschedl. 2009. Satb1 and Satb2 regulate embryonic stem cell differentiation and Nanog expression. *Genes Dev.* 23:2625–2638. http://dx.doi.org/10.1101/gad.1815709

Schoenfelder, S., I. Clay, and P. Fraser. 2010. The transcriptional interactome: gene expression in 3D. *Curr. Opin. Genet. Dev.* 20:127–133. http://dx.doi.org/10.1016/j.gde.2010.02.002

Sen, G.L., D.E. Webster, D.I. Barragan, H.Y. Chang, and P.A. Khavari. 2008. Control of differentiation in a self-renewing mammalian tissue by the histone demethylase JMJD3. *Genes Dev.* 22:1865–1870. http://dx.doi.org/10.1101/gad.1673508

Sen, G.L., J.A. Reuter, D.E. Webster, L. Zhu, and P.A. Khavari. 2010. DNMT1 maintains progenitor function in self-renewing somatic tissue. *Nature*. 463:563–567. http://dx.doi.org/10.1038/nature08683

Sharov, A.A., L. Weiner, T.Y. Sharova, F. Siebenhaar, R. Atoyan, A.M. Reginato, C.A. McNamara, K. Funa, B.A. Gilchrest, J.L. Brissette, and V.A. Botchkarev. 2003. Noggin overexpression inhibits eyelid opening by altering epidermal apoptosis and differentiation. *EMBO J.* 22:2992–3003. http://dx.doi.org/10.1093/emboj/cdg291

Sharov, A.A., D.B. Dudekula, and M.S. Ko. 2005a. A web-based tool for principal component and significance analysis of microarray data. *Bioinformatics*. 21:2548–2549. http://dx.doi.org/10.1093/bioinformatics/bti343

Sharov, A.A., M. Fessing, R. Atoyan, T.Y. Sharova, C. Haskell-Luevano, L. Weiner, K. Funa, J.L. Brissette, B.A. Gilchrest, and V.A. Botchkarev. 2005b. Bone morphogenetic protein (BMP) signaling controls hair pigmentation by means of cross-talk with the melanocortin receptor-1 pathway. *Proc. Natl. Acad. Sci. USA*. 102:93–98. http://dx.doi.org/10.1073/pnas.0408455102

Sharov, A.A., T.Y. Sharova, A.N. Mardaryev, A. Tommasi di Vignano, R. Atoyan, L. Weiner, S. Yang, J.L. Brissette, G.P. Dotto, and V.A. Botchkarev. 2006. Bone morphogenetic protein signaling regulates the size of hair follicles and modulates the expression of cell cycle-associated genes. *Proc. Natl. Acad. Sci. USA*. 103:18166–18171. http://dx.doi.org/10.1073/pnas.0608899103

Sharov, A.A., A.N. Mardaryev, T.Y. Sharova, M. Grachtchouk, R. Atoyan, H.R. Byers, J.T. Seykora, P. Overbeek, A. Dlugosz, and V.A. Botchkarev. 2009. Bone morphogenetic protein antagonist noggin promotes skin tumorigenesis via stimulation of the Wnt and Shh signaling pathways. *Am. J. Pathol.* 175:1303–1314. http://dx.doi.org/10.2353/ajpath.2009.090163

Solovei, I., M. Kreysing, C. Lanctôt, S. Kösem, L. Peichl, T. Cremer, J. Guck, and B. Joffe. 2009. Nuclear architecture of rod photoreceptor cells adapts to vision in mammalian evolution. *Cell*. 137:356–368. http://dx.doi.org/10.1016/j.cell.2009.01.052

Takizawa, T., K.J. Meaburn, and T. Misteli. 2008. The meaning of gene positioning. *Cell*. 135:9–13. http://dx.doi.org/10.1016/j.cell.2008.09.026

Truong, A.B., and P.A. Khavari. 2007. Control of keratinocyte proliferation and differentiation by p63. *Cell Cycle*. 6:295–299. http://dx.doi.org/10.4161/cc.6.3.3753

Truong, A.B., M. Kretz, T.W. Ridky, R. Kimmel, and P.A. Khavari. 2006. p63 regulates proliferation and differentiation of developmentally mature keratinocytes. *Genes Dev.* 20:3185–3197. http://dx.doi.org/10.1101/gad.1463206

Viganò, M.A., and R. Mantovani. 2007. Hitting the numbers: the emerging network of p63 targets. *Cell Cycle*. 6:233–239. http://dx.doi.org/10.4161/cc.6.3.3802

Wang, L., L.J. Di, X. Lv, W. Zheng, Z. Xue, Z.C. Guo, D.P. Liu, and C.C. Liang. 2009. Inter-MAR association contributes to transcriptionally active looping events in human beta-globin gene cluster. *PLoS ONE*. 4:e4629. http://dx.doi.org/10.1371/journal.pone.0004629

Watt, F.M., M. Frye, and S.A. Benitah. 2008. MYC in mammalian epidermis: how can an oncogene stimulate differentiation? *Nat. Rev. Cancer*. 8:234–242. http://dx.doi.org/10.1038/nrc2328

Williams, R.R., S. Broad, D. Sheer, and J. Ragoussis. 2002. Subchromosomal positioning of the epidermal differentiation complex (EDC) in keratinocyte and lymphoblast interphase nuclei. *Exp. Cell Res.* 272:163–175. http://dx.doi.org/10.1006/excr.2001.5400

Yang, A., R. Schweitzer, D. Sun, M. Kaghad, N. Walker, R.T. Bronson, C. Tabin, A. Sharpe, D. Caput, C. Crum, and F. McKeon. 1999. p63 is essential for regenerative proliferation in limb, craniofacial and epithelial development. *Nature*. 398:714–718. http://dx.doi.org/10.1038/19539

Yasui, D., M. Miyano, S. Cai, P. Varga-Weisz, and T. Kohwi-Shigematsu. 2002. SATB1 targets chromatin remodelling to regulate genes over long distances. *Nature*. 419:641–645. http://dx.doi.org/10.1038/nature01084

Zhao, R., M.S. Bodnar, and D.L. Spector. 2009. Nuclear neighborhoods and gene expression. *Curr. Opin. Genet. Dev.* 19:172–179. http://dx.doi.org/10.1016/j.gde.2009.02.007

Zhou, M., X.M. Li, and R.M. Lavker. 2006. Transcriptional profiling of enriched populations of stem cells versus transient amplifying cells. A comparison of limbal and corneal epithelial basal cells. *J. Biol. Chem.* 281:19600–19609. http://dx.doi.org/10.1074/jbc.M600777200

Development 138, 4843-4852 (2011) doi:10.1242/dev.070284

Lhx2 differentially regulates Sox9, Tcf4 and Lgr5 in hair follicle stem cells to promote epidermal regeneration after injury

Andrei N. Mardaryev[1], Natalia Meier[2], Krzysztof Poterlowicz[1], Andrey A. Sharov[3], Tatyana Y. Sharova[3], Mohammed I. Ahmed[1], Valentina Rapisarda[1], Christopher Lewis[1], Michael Y. Fessing[1], Thomas M. Ruenger[3], Jag Bhawan[3], Sabine Werner[4], Ralf Paus[2,5] and Vladimir A. Botchkarev[1,3,*]

SUMMARY

The Lhx2 transcription factor plays essential roles in morphogenesis and patterning of ectodermal derivatives as well as in controlling stem cell activity. Here, we show that during murine skin morphogenesis, Lhx2 is expressed in the hair follicle (HF) buds, whereas in postnatal telogen HFs Lhx2$^+$ cells reside in the stem cell-enriched epithelial compartments (bulge, secondary hair germ) and co-express selected stem cell markers (Sox9, Tcf4 and Lgr5). Remarkably, Lhx2$^+$ cells represent the vast majority of cells in the bulge and secondary hair germ that proliferate in response to skin injury. This is functionally important, as wound re-epithelization is significantly retarded in heterozygous *Lhx2* knockout (+/–) mice, whereas anagen onset in the HFs located closely to the wound is accelerated compared with wild-type mice. Cell proliferation in the bulge and the number of Sox9$^+$ and Tcf4$^+$ cells in the HFs closely adjacent to the wound in *Lhx2*$^{+/-}$ mice are decreased in comparison with wild-type controls, whereas expression of Lgr5 and cell proliferation in the secondary hair germ are increased. Furthermore, acceleration of wound-induced anagen development in *Lhx2*$^{+/-}$ mice is inhibited by administration of *Lgr5* siRNA. Finally, Chip-on-chip/ChIP-qPCR and reporter assay analyses identified *Sox9*, *Tcf4* and *Lgr5* as direct Lhx2 targets in keratinocytes. These data strongly suggest that Lhx2 positively regulates *Sox9* and *Tcf4* in the bulge cells, and promotes wound re-epithelization, whereas it simultaneously negatively regulates Lgr5 in the secondary hair germ and inhibits HF cycling. Thus, Lhx2 operates as an important regulator of epithelial stem cell activity in the skin response to injury.

KEY WORDS: Skin, Stem cells, Wound healing

INTRODUCTION

Skin development is governed by interactions between the epithelium and mesenchyme, which result in formation of the epidermis and a number of skin appendages, including hair follicles (HFs) (Driskell et al., 2011; Fuchs, 2007; Schmidt-Ullrich and Paus, 2005). During postnatal life, epidermis and HFs self-renew and regenerate with an involvement of stem cells that are capable of differentiating into distinct epithelial cell lineages (Ambler and Maatta, 2009; Blanpain and Fuchs, 2009; Cotsarelis, 2006; Watt and Jensen, 2009). Epithelial stem cells also contribute to epidermal regeneration after injury, a complex process that includes tightly regulated recruitment of undifferentiated progenitor cells to the wound epithelium (Gurtner et al., 2008; Lau et al., 2009; Schafer and Werner, 2007).

The HF is an important source of epithelial stem cells, which are capable of generating daughter cells that re-build epithelial hair bulb during the hair cycle or migrate to the wound epithelium and promote the regenerative process (Cotsarelis et al., 1990; Ghazizadeh and Taichman, 2001; Hsu et al., 2011; Ito et al., 2005; Ito et al., 2007; Kasper et al., 2011; Langton et al., 2008; Levy et al., 2005; Levy et al., 2007; Snippert et al., 2010; Taylor et al., 2000). HFs contain several populations of epithelial stem cells, each characterized by distinct, yet partially overlapping, expression patterns of surface receptors (Cd34, Cd71, Cd200, Lgr5, Lgr6, Lrig1, Sca-1), cytoskeletal proteins (keratins 15 and 19), signalling/transcriptional regulators (Lhx2, Sox9, Tcf3/4, Nfatc1, Gli-1) and epigenetic markers (Blanpain et al., 2004; Brownell et al., 2011; Frye et al., 2007; Garza et al., 2011; Horsley et al., 2008; Jaks et al., 2008; Jensen et al., 2009; Jensen et al., 2008; Morris et al., 2004; Nguyen et al., 2009; Nowak et al., 2008; Rhee et al., 2006; Snippert et al., 2010; Trempus et al., 2007; Tumbar et al., 2003).

In normal skin, distinct populations of epithelial stem cells residing in the bulge, secondary hair germ or infundibulum of the HFs differentially contribute to the renewal of the epidermis versus the regeneration of the HF during the hair cycle (Ito et al., 2005; Jaks et al., 2008; Jensen et al., 2009; Li and Clevers, 2010). However, wounding perturbs homeostasis, resulting in activation of those populations of epithelial stem cells that normally supply progenies only into the HF during hair cycling (Ito et al., 2005; Kasper et al., 2011; Levy et al., 2007). Although HFs are not absolutely required for skin regeneration after injury, re-epithelization in hair-bearing skin occurs faster and more efficiently when compared with non-hair-bearing areas (Ansell et al., 2011; Ito and Cotsarelis, 2008; Langton et al., 2008; Romagosa et al., 2008).

The Lim-homeodomain transcription factor Lhx2 is an important regulator controlling the switch between stem cell maintenance and activation in the HFs (Rhee et al., 2006; Tiede and Paus, 2006;

[1]Centre for Skin Sciences, School of Life Sciences, University of Bradford, UK. [2]Department of Dermatology, University of Lübeck, Germany. [3]Department of Dermatology, Boston University School of Medicine, Boston, MA, USA. [4]Department of Biology, Institute of Cell Biology, Swiss Federal Institute of Technology (ETH), Zürich, Switzerland. [5]School of Translational Medicine, University of Manchester, UK.

*Author for correspondence (v.a.botchkarev@bradford.ac.uk; vladbotc@bu.edu)

Accepted 12 September 2011

Tornqvist et al., 2010). Lhx2 is expressed in the bulge and hair germ of mouse telogen (resting) HFs, and *Lhx2* deficiency in mice leads to incapability in maintaining a quiescent state in the bulge stem cells (Rhee et al., 2006). In human HFs, Lhx2 shows more broad expression patterns and, in addition to the bulge cells, is seen in the isthmus, the infundibulum and the lower outer root sheath (Kloepper et al., 2008). In other organs (eye, pituitary gland, limb, brain, hematopoietic system), Lhx2 operates as a central link in the genetic networks that coordinate multiple signalling pathways controlling organ development and cell fate determination, as well as stem cell maintenance, differentiation and self-renewal (Chou et al., 2009; Dahl et al., 2008; Hirota and Mombaerts, 2004; Porter et al., 1997; Tetreault et al., 2009; Yun et al., 2009).

Despite the advantages in identification of distinct stem cell populations in the skin achieved during past few years (Blanpain and Fuchs, 2009; Watt and Jensen, 2009), regulatory mechanisms involved in controlling their activity and expression of stem cell markers (membrane receptors, cytoskeleton components, transcription factors) during their transition towards the epidermal or HF cell lineages in normal and injured skin are still unclear. In addition, the mechanisms underlying differential involvement of these stem cell populations in the control of distinct types of the regenerative processes in the epithelial tissues (epidermal regeneration after injury, physiological or wound-induced hair follicle cycling) remain to be elucidated.

Here, we show that Lhx2 plays an important role as a switchboard regulator of the activity of distinct epithelial stem cell populations in the HF during wound healing. In particular, we demonstrate that Lhx2 promotes wound re-epithelization via positive regulation of *Sox9*, and *Tcf4*, while simultaneously inhibiting HF cycling via negative regulation of *Lgr5*. Thus, Lhx2 serves as a key factor integrating signalling and transcriptional networks that modulate activity of the HF stem cells during epidermal regeneration after injury.

MATERIALS AND METHODS

Animal experiments

All animal experiments were performed under the Home Office Project License (University of Bradford, UK). *Lhx2*$^{+/-}$ mice (Porter et al., 1997) were crossbred to obtain homozygous *Lhx2*$^{-/-}$ and wild-type embryos, which were collected on embryonic day 16.5 (E16.5), as described before (Botchkarev et al., 1999a). A full-thickness 3 mm wound was introduced by punch biopsy onto back skin of 8-week-old *Lhx2*$^{+/-}$ and wild-type mice at the telogen stage of the hair cycle (8-10 female mice of each strain per time point, one wound per mouse). *Lgr5* siRNA or control siRNA (Dharmacon, Chicago, IL) were injected into the wounds of *Lhx2*$^{+/-}$ mice at a concentration of 20 μM as described previously (Mardaryev et al., 2010). siRNA treatment was performed on days 1-6 after wound infliction, and skin samples were collected on day 7 of the experiment. In each experiment, at least 4-5 mice per time point were used for analyses in both experimental and control groups. Samples of the skin closely (within 5 mm) and distantly located to the wound edge were collected at days 0, 1, 3 and 5 after wounding and were snap-frozen in liquid nitrogen.

Human skin biopsies and wound healing organ culture assay

Biopsies of human skin with chronic wounds after diagnostic skin surgery and scalp skin of patients undergoing elective cosmetic surgery were obtained after informed consent and Ethics Committee Approval according to the Helsinki Ethical Guidelines for medical research involving human subjects. For skin organ culture, 2 mm punches were cut into full-thickness skin samples from patients. Then, 4 mm punches were set in the skin surrounding each 2 mm hole to obtain 'punch within a punch' skin samples (Moll et al., 1998). Samples were frozen immediately for analysis (day 0) or transferred to six-well plates containing Williams E culture medium supplemented with insulin and hydrocortisone (Philpott et al., 1990; Lu et al., 2007). Each well contained two skin punches in 3 ml medium. After 48 hours the incubation medium was changed, and skin punches from each experimental condition were frozen at day 3. All experiments were performed in triplicates.

Microarray and qRT-PCR analyses

Total RNA was isolated from snap-frozen tissue samples using miRNeasy kit (Qiagen, Hilden, Germany). For microarray analysis, 0.5 μg of total RNA was processed for one-round amplification using RiboAmp RNA Amplification Kit (Molecular Devices, Sunnyvale, CA). mRNA microarray analysis was performed by Mogene (St Louis, MO) using 41K Whole Mouse Genome 60-mer oligo-microarray (manufactured by Agilent Technologies). For qRT-PCR, 1 μg of total RNA was converted into cDNA using Reverse Transcription System (Promega, Madison, WI). Gene expression was performed on a MyiQ single-colour real-time PCR detection system (Bio-Rad, Hercules, CA) using PerfeCta SYBR Green FastMix for iQ (Quanta BioSciences, Gaithersburg, MD), as described previously (Sharov et al., 2003). PCR primers were designed using the Beacon Designer software (Premier Biosoft International, Palo Alto, CA; supplementary material Table S2). Differences between samples were calculated using the Genex database software (Bio-Rad) based on the Ct ($^{\Delta\Delta}C_t$) equitation method and normalized to the house-keeping gene *Gapdh*. Data from triplicates were pooled, mean±s.e.m. was calculated, and statistical analysis was performed using unpaired Student's *t*-test. Microarray data have been deposited in the Gene Expression Omnibus database (Accession Numbers GSE32511 and GSE32514)

Chip-on-chip and Chip-qPCR

Mouse embryonic, neonatal and adult epidermal keratinocytes were isolated from E16.5 embryos, 2- to 3-day-old and 8-week-old FVB mice, respectively, as described previously (Sharov et al., 2006) with modifications. Single cell suspensions were prepared after overnight digestion in 0.25% trypsin (Invitrogen) and epidermal separation. Cells were dual cross-linked with 2 mM disuccinimidyl glutarate (DSG) for 45 minutes and then in 1% paraformaldehyde for 15 minutes at room temperature as described previously (Nowak et al., 2005). Fixed cells were lysed in 10 ml of Lysis Buffer 1 [50 mM HEPES (pH 7.5), 140 mM NaCl, 1 mM EDTA, 0.1% IGEPAL 630 (Sigma-Aldrich)], containing 0.05% Triton X100, 2.5 % glycerol and supplemented with 1× protease inhibitor cocktail (Roche, Rotkreuz, Switzerland) for 10 minutes on ice, followed by incubation in Buffer 2 [0.1 M Tris HCl (pH 8) and 200 mM NaCl with protease inhibitors] for 15 minutes at room temperature. Chromatin was sonicated at 30% of amplitude for 10 minutes on a Branson Sonifier 450 (Branson Ultrasonics, Danbury, CT) using a cup horn. The samples were centrifuged (2×14,000 ***g*** for 5 minutes each), and soluble chromatin was transferred to a fresh tube. Crosslinked DNA after sonication was precipitated with 5 μg of anti-Lhx2 antibody (C-20, sc-19344, Santa Cruz, Santa Cruz, CA) or non-immune goat IgG (Vector Laboratories, Burlingame, CA) overnight at 4ºC. Chromatin/antibody complex was pulled down with Dynal Protein G magnetic beads (Invitrogen, Carlsbad, CA) and washed in the low- and high-salt buffers. After de-crosslinking (65ºC for 4 hours) and Proteinase K treatment, chromatin was purified by phenol-chloroform extraction and ethanol precipitation. Precipitated DNA after one round of amplification (WGA2, Sigma) was processed with NimbleGen MM8 Deluxe Promoter HX1 array (Mogene, St Louis, MO), or was analyzed by qPCR using primers generated for predicted Lhx2 binding sites (supplementary material Table S2). ChIP-qPCR data were pooled, mean±s.e.m. was calculated, and statistical analysis was performed using Student's *t*-test.

Reporter assay

Lhx2 expressing plasmid (pLhx2) was generated by subcloning the mouse *Lhx2* cDNA from an I.M.A.G.E. clone (6413339, Gene Service Ltd, UK) into the pCMV-SPORT6 vector (Invitrogen) at *Sal*I and *Not*I sites. pSox9-luc construct (also known as pGL6.8-luc) bearing –6.8 kb promoter region of the mouse *Sox9* gene was kindly provided by Dr P. Koopman (Kanai and Koopman, 1999). To generate a Tcf4 reporter construct, the *Tcf4* promoter region (–3598/+462) was PCR amplified from mouse genomic

DNA with Advantage HD DNA polymerase (Clontech) using the following primers (*Bgl*II and *Hin*dIII restriction sites are underlined): 5′-CCCGGGCTCGAGATCTTGACCACACCCCCACCACTT-3′ (F) and 5′-CCGGAATGCCAAGCTTGCATTTTTCACCCACCAGCAGC-3′ (R). The purified fragment was then cloned into pGl3-basic vector (Promega) at *Bgl*II and *Hin*dIII sites using In-Fusion HD Cloning System (Clontech, Mountain View, CA). For reporter assay, HaCaT cells were seeded into 96-well plates (10^4 cells per well) 1 day before transfection. Cells were co-transfected with pLhx2 or pCDN3 plasmids (120 ng/well) along with one of the reporter constructs (pSox9-Luc or pTcf4-Luc; 80 ng/well) using Lipofectamine 2000 (0.5 μl/well) (Invitrogen). After 48 hours, reporter activity was detected using the Dual-Glo Luciferase Assay System (Promega) on Infinite 200 PRO microplate reader (Tecan, Männedorf, Switzerland). Two independent assays were performed in triplicates and results were normalized to the pnull-Renilla construct activity. Data were pooled, mean±s.e.m. was calculated, and statistical analysis was performed using Student's *t*-test.

Western blotting

Proteins were extracted from snap-frozen skin samples or cultured cells with lysis buffer as described previously (Sharov et al., 2005; Sharov et al., 2006). Protein (5 μg) was processed for western blot analysis as described previously, followed by incubation with primary antibodies against Lhx2 [goat, 1:100, Santa Cruz (sc19344)] or Lgr5 [rabbit, 1:100, Abcam (ab75732)] overnight at 4ºC. Horseradish peroxidase-tagged IgG antibody was used as secondary antibody (1:5000; Thermo Scientific, Rockford, IL). Antibody binding was visualized using an enhanced chemiluminescence system (SuperSignal West Pico Kit, Thermo Scientific) followed by autoradiography with X-ray film (CL-Xposure Film, Thermo Scientific). Densitometric analysis was performed using Total Lab v1.10 software (Biogenetic, USA).

Histology, histomorphometry and immunohistochemistry

For histological analyses, 8 μm sections from the central parts of the wounds were stained with Hematoxylin-Eosin and photographed using an Eclipse 50i microscope equipped with a DS-C1 digital camera and ACT-2U image analysis software (Nikon, Tokyo, Japan). The length and area of the hyperproliferative wound epithelium were determined using the ImageJ software (http://rsbweb.nih.gov/ij/) as described previously (Kumin et al., 2007). Histomorphometry of the distinct hair cycle stages was performed on skin cryosections stained by alkaline phosphatase as described previously (Botchkarev et al., 1999b; Botchkareva et al., 2000).

For immunohistochemical analyses, cryosections were incubated with primary antisera against Lhx2, Sox9, Tcf4, Lgr5, Ki-67, Lef1, Krt16, Krt17, CD4, F4/80 and Ly-6G [CD4, rat, 1:100, Dako; F4/80, rat, 1:100, Dianova (T-2006); Ki-67, rabbit, 1:100, Abcam (ab15580); Krt14, rabbit, 1:200, Sigma (c-8791); Krt16, rabbit, 1:100, Abcam (ab76416); Krt17, rabbit, 1:5000, Abcam (ab53707); Lef1, rabbit, 1:100, Cell Signaling (C12A5); Lhx2, goat, 1:100, Santa Cruz (sc-19344); Ly-6G, rat, 1:150, BD Farmingen (551459); Sox9, rabbit, 1:100, Santa Cruz (sc20095); Tcf4, rabbit, 1:100, Cell Signaling (c48H11)] overnight at 4°C, followed by application of corresponding Alexa-488 and Cy-555-coupled secondary antibodies (Invitrogen; 1:200) for 60 minutes at 37°C, as described previously (Botchkareva et al., 2000). Image acquisition was performed on a Zeiss confocal microscope or a Nikon fluorescent microscope. Statistical analysis of the histomorphometric parameters and the number of $Ki67^+$ cells was performed using an unpaired Student's *t*-test or Mann-Whitney's test after the data from triplicate experiments were pooled and mean±s.e.m. was calculated.

In vitro migration assay

Primary keratinocytes from $Lhx2^{+/-}$ and $Lhx2^{+/+}$ mice were isolated as mentioned above and plated on collagen-coated dishes. Cells were grown at 33°C with 5% CO_2 until 100% confluency. Using a P10 tip, a scratch was made in the middle of the plate. The distance between leading edges of the migrating keratinocytes was measured using the ImageJ software, as described previously (Chmielowiec et al., 2007). Data from triplicates were pooled, mean±s.d. was calculated, and statistical analysis was performed using unpaired Student's *t*-test.

RESULTS

Lhx2 ablation results in altered expression of stem cells markers in the skin

Lhx2 is one of the hair bud-specific markers, whereas in postnatal telogen HFs Lhx2 is expressed in the bulge and secondary hair germ, the compartments enriched by epithelial stem cells (Rhee et al., 2006). To gain mechanistic insight into the role of Lhx2 in the regulation of the activity of epithelial stem cells, samples of total RNA isolated from E16.5 $Lhx2^{-/-}$ and wild-type embryos were processed for microarray analysis (Sharov et al., 2006). In addition, the formaldehyde-cross-linked chromatin fragments from primary epidermal keratinocytes were immunoprecipitated with anti-Lhx2 antibody, and ChiP-on-chip analysis was performed. Microarray and ChiP-on-chip data were merged, and 621 genes, the expression of which was significantly (two-fold and higher) changed in $Lhx2^{-/-}$ mice and showed association of Lhx2 with the corresponding promoter regions, were selected as the genuine Lhx2 targets in keratinocytes (Fig. 1A).

Interestingly, among the Lhx2 targets involved in the control of cell adhesion/extracellular matrix remodelling, metabolism, cytoskeleton, signalling and transcription, several genes were implicated in the control of stem cell activity (Fig. 1B; supplementary material Table S1). These included *Sox9*, *Tcf3* and *Tcf4*, which were downregulated in the $Lhx2^{-/-}$ mice, as well as *Lgr5*, which was upregulated (Fig. 1B, supplementary material Table S1). Alterations in the expression of these genes in $Lhx2^{-/-}$ versus wild-type mice were confirmed by qRT-PCR and immunohistochemistry (Fig. 1B,C). In particular, Sox9 and Tcf4 were not seen in the HF placodes in the embryonic $Lhx2^{-/-}$ skin, thus serving as an additional control for the microarray and Chip-on-chip data (Fig. 1C). Interestingly, expression of Lef1, which is closely related to Tcf3 and Tcf4 (Nguyen et al., 2009; Nguyen et al., 2006), was not affected by the deletion of *Lhx2* (Fig. 1C). This is consistent with data demonstrating differential expression patterns and functional roles for Lef1 versus Tcf3/4 in the developing and postnatal skin (DasGupta and Fuchs, 1999; Merrill et al., 2001; Nguyen et al., 2009).

Lhx2 expression is increased in the skin during wound healing

Regeneration of skin after injury includes not only re-epithelization of the epidermis, but also growth activation in the HFs closely adjacent to the wound (Ansell et al., 2011; Ito and Cotsarelis, 2008; Langton et al., 2008; Romagosa et al., 2008). To determine a potential role of Lhx2 in wound repair, we first studied its expression in mouse skin at distinct time-points after wounding, as well as in human skin biopsies obtained from individuals with chronic wounds and in punch-wounded human skin cultured under serum-free conditions (Moll et al., 1998; Lu et al., 2007). In the skin of 8- to 9-week-old mice, levels of *Lhx2* transcripts increased on days 3 and 5 after application of full-thickness 3 mm wounds (Fig. 2A). $Lhx2^+$ cells showed a marked increase in their proliferation on days 3 and 5 after wounding (Fig. 2B,C). In both bulge and secondary hair germ of the HFs adjacent to the wound more than 80% of proliferating cells were $Lhx2^+$ (Fig. 2C). However, similar to unwounded skin (Rhee et al., 2006), $Lhx2^+$ cells were seen only in the bulge and secondary hair germ of mouse HFs adjacent to the wound, whereas lack of Lhx2 expression was seen in the infundibulum, interfollicular epidermis and wound epithelium (Fig. 2D).

In normal human skin, Lhx2 was expressed in the HF bulge and outer root sheath, whereas in the skin biopsies from chronic wounds, $Lhx2^+$ cells were seen in the wound edge epithelium and upper region of the infundibulum of the HFs located closely to the

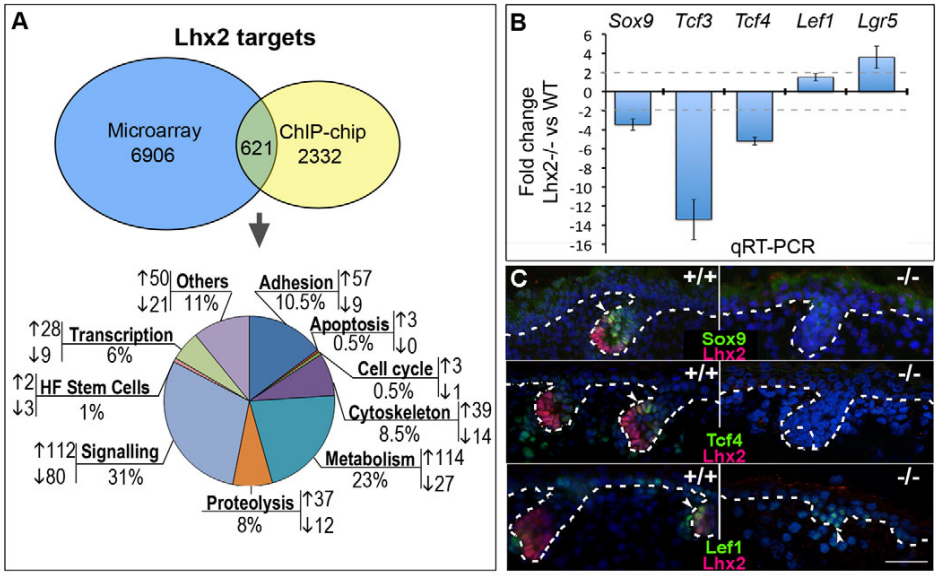

Fig. 1. Altered expression of stem cell markers in the *Lhx2*-null skin. E16.5 *Lhx2*$^{-/-}$ and wild-type embryos were processed for RNA extraction and subsequent microarray studies and qRT-PCR analyses, as well as for immunohistochemistry. Primary keratinocytes isolated from mouse back skin were processed for ChIP-on-chip analysis with an antibody against the Lhx2 or purified goat IgG. (**A**) The ontology of the genes whose expression was altered in the E16.5 *Lhx2*$^{-/-}$ mice versus wild-type controls and which showed association of Lhx2 with the corresponding promoter regions in ChIP-on-chip assay. Full list of the genes is shown in Table S1 (supplementary material). (**B**) qRT-PCR analysis of the stem cell markers and regulators of stem cell activity in the *Lhx2*$^{-/-}$ versus wild-type skin. Data are mean±s.e.m. (**C**) Hair follicle buds of *Lhx2*$^{-/-}$ mice show lack of the Sox9- and Tcf4-positive cells, and presence of Lef1, which are all visible in wild-type mice (arrowheads). Borders between the epithelial and mesenchymal skin compartments are indicated by a broken line. Scale bar: 50 μm.

wound edge (Fig. 2E,G). In organ-cultured full-thickness fragments of normal human skin, the Lhx2^{+} cells (expressing also keratin 14) were located in the bulge and outer root sheath of the HFs and their number was significantly (P<0.05) increased on day 3 after injury compared with unwounded skin (Fig. 2F,H,I).

Lhx2 deficiency results in impaired wound repair and accelerated entry of the hair follicles into anagen

To assess the role of Lhx2 in the control of wound re-epithelization after injury, *Lhx2* heterozygous knockout (+/–) mice were used as a model (Porter et al., 1997). *Lhx2* knockout (–/–) mice die between E15.5 and E16.5 from abnormalities in the development of the liver, brain and hematopoietic system (Porter et al., 1997). *Lhx2*$^{+/-}$ mice were viable, fertile and showed ~50% decrease of Lhx2 protein and mRNA levels in the skin compared with wild-type mice (Fig. 3A,B).

Histological and histomorphometric analysis of the skin sections at distinct time-points after wound infliction showed progressive alterations in the development of the hyperproliferative wound epithelium in *Lhx2*$^{+/-}$ mice compared with wild-type mice (Fig. 3C-E). Despite the fact that on day 3 after wounding the length and area of the hyperproliferative wound epithelium used as established parameters of the regenerative process (Kumin et al., 2007) were quite similar between wild-type and *Lhx2*$^{+/-}$ mice, both parameters were significantly reduced (P<0.05) in *Lhx2*$^{+/-}$ mice on day 5 after wounding compared to wild-type controls (Fig. 3C-E). Interestingly, on days 5-7 after wounding, HFs in *Lhx2*$^{+/-}$ mice located closely (within 5 mm) to the wound showed significantly more advanced anagen development compared with the HFs in wild-type mice (Fig. 3F,G; supplementary material Fig. S1A), whereas no differences in hair cycle progression between *Lhx2*$^{+/-}$ and wild-type mice were seen in the HFs distantly located to the wounds (data not shown).

Analysis of cell proliferation in the distinct epithelial skin compartments (wound epithelium, interfollicular epidermis, HF infundibulum, bulge and secondary germ) on days 1-5 after wounding revealed significant differences between *Lhx2*$^{+/-}$ and WT mice only in the bulge and secondary hair germ of the HFs (Fig. 3H,I; supplementary material Fig. S1B). Interestingly, cell proliferation in the bulge of the HFs in *Lhx2*$^{+/-}$ mice was significantly lower (P<0.05) on day 3 after wounding compared with wild-type mice, whereas the number of Ki67^{+} cells in the secondary hair germ was significantly higher (P<0.001) compared with wild-type mice at this time point (Fig. 3H,I). However, other parameters of the wound-healing process, such as expression of wound-associated keratins (Krt16, Krt17), presence of immune cells (macrophages, neutrophils, CD4^{+} T cells) in the dermis/granulation tissue, as well as keratinocyte migration (as determined by scratch assay with cultured keratinocytes) were not changed in the *Lhx2*$^{+/-}$ versus wild-type mice (supplementary material Fig. S1C-H).

Thus, the impaired re-epithelization in *Lhx2*$^{+/-}$ mice was accompanied by inverse changes in cell proliferation in the bulge versus secondary hair germ and by more rapid development of anagen in the HFs adjacent to the wound (Fig. 3C-I). These data suggest that Lhx2 differentially regulates the activity of those populations of the HF stem cells that respond to skin injury versus those that regulate HF cycling by supplying their progenies either into the wound epithelium or into the growing HF, respectively (Ito et al., 2005).

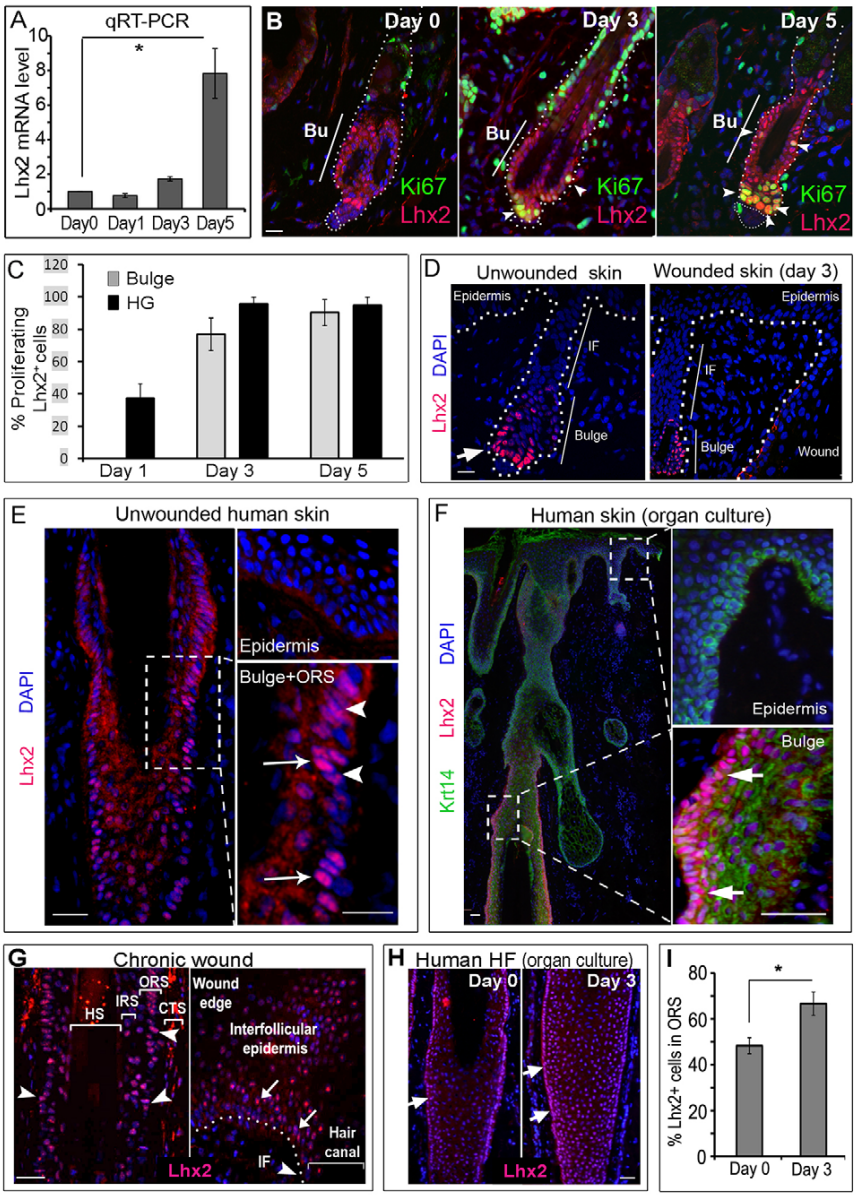

Fig. 2. Lhx2 expression increases in hair follicles during wound healing. qRT-PCR for Lhx2 was performed with RNA from mouse skin wounds at different days after wounding. Cryosections of the wounded human and mouse skin were immunolabelled with anti-Lhx2 antiserum alone or together with anti-Ki-67 or CK14 antibody. In microscopic images, borders between the epidermis or HF and dermis are depicted by the broken line. (**A**) Increase in *Lhx2* transcripts in mouse skin 5 days after wounding (mean±s.e.m.; **P*<0.05, Student's *t*-test); (**B**,**C**) Lhx2$^+$ cells proliferate in response to skin wounding in mice. Double immunodetection shows localization of the proliferating Lhx2$^+$ cells in the hair germ and bulge of HFs adjacent to the wound (B, arrowheads). The majority (>80%) of proliferating cells in the hair germ and bulge are Lhx2 positive (C). Bu, bulge. Data are mean±s.e.m. (**D**) During wound healing, Lhx2$^+$ cells are seen only in the hair follicle bulge and secondary hair germ (arrow) and are absent in the wound epithelium. (**E**) In normal unwounded human skin, Lhx2 shows nuclear (arrows) and cytoplasmic (arrowheads) expression only in the HF bulge and outer root sheath (bottom image, arrows), and is absent in the epidermis (upper image). (**F**) In organ cultures of human skin, Lhx2$^+$ cells that also expressed keratin 14 are seen in the bulge/outer root sheath (lower inset, arrows). Lack of Lhx2 is seen in the epidermis (upper inset, arrow). (**G**) In the biopsies of chronic skin wounds, Lhx2 is expressed in the wound edge epithelium and interfollicular epidermis (arrows), as well as in the follicular infundibulum (arrowheads). (**H**,**I**) Increase in the number of Lhx2$^+$ cells in the HF outer root sheath in organ cultured human skin after wounding (mean±s.e.m., **P*<0.05, Student's *t*-test). Arrows indicate Lhx2$^+$ cells in the outer root sheath. CTS, connective tissue sheath; HS, hair shaft; IF, infundibulum; IRS, inner root sheath; ORS, outer root sheath. Scale bars: 50 μm; 25 μm in insets.

Lhx2 stimulates the expression of Sox9, Tcf4 and inhibits Lgr5 expression in hair follicle stem cells during wound healing

Because, in mice, Lhx2 was expressed exclusively in the bulge and secondary hair germ and was not seen in the follicular infundibulum, inter-follicular epidermis or wound epithelium (Fig. 2B,D), we hypothesized that Lhx2 contributes to wound re-epithelization rather indirectly and most likely via regulation of *Sox9* and *Tcf4* in hair follicle stem cells. Genetic ablation of *Sox9* or *Tcf3/4* resulted in marked retardation of the wound-healing process (Nguyen et al., 2009; Nowak et al., 2008). In addition, Sox9 and Tcf3 proteins are ectopically expressed in the epidermis of K14-Lhx2 transgenic mice, suggesting an involvement of Lhx2 in the control of their expression in keratinocytes (Rhee et al., 2006).

In early anagen HFs of unwounded adult mouse skin, Sox9$^+$ and Tcf4$^+$ cells were only seen in the bulge, but were absent in the follicular infundibulum (supplementary material Fig. S2A). In wounded skin, double immunolabelling of Lhx2 with Sox9 or Tcf4 revealed their colocalization within the bulge area (Fig. 4A). However, in wounded skin Sox9$^+$ and Tcf4$^+$ cells were also seen in the follicular infundibulum (Fig. 4B), and these cells did not express Lhx2 (data not shown). To assess whether *Lhx2* deficiency may affect the expression of Sox9 and Tcf4, the number Sox9$^+$ and Tcf4$^+$ cells was compared in the HFs closely adjacent to the wounds between the *Lhx2*$^{+/-}$ and wild-type mice. The percentage of Sox9$^+$ and Tcf4$^+$ cells was markedly decreased in the infundibulum but not in the bulge of the HFs adjacent to the wound in *Lhx2*$^{+/-}$ mice versus wild-type controls (Fig. 4B,C; supplementary material Fig. S2B). Furthermore, qRT-PCR data showed significant decrease of the *Sox9*

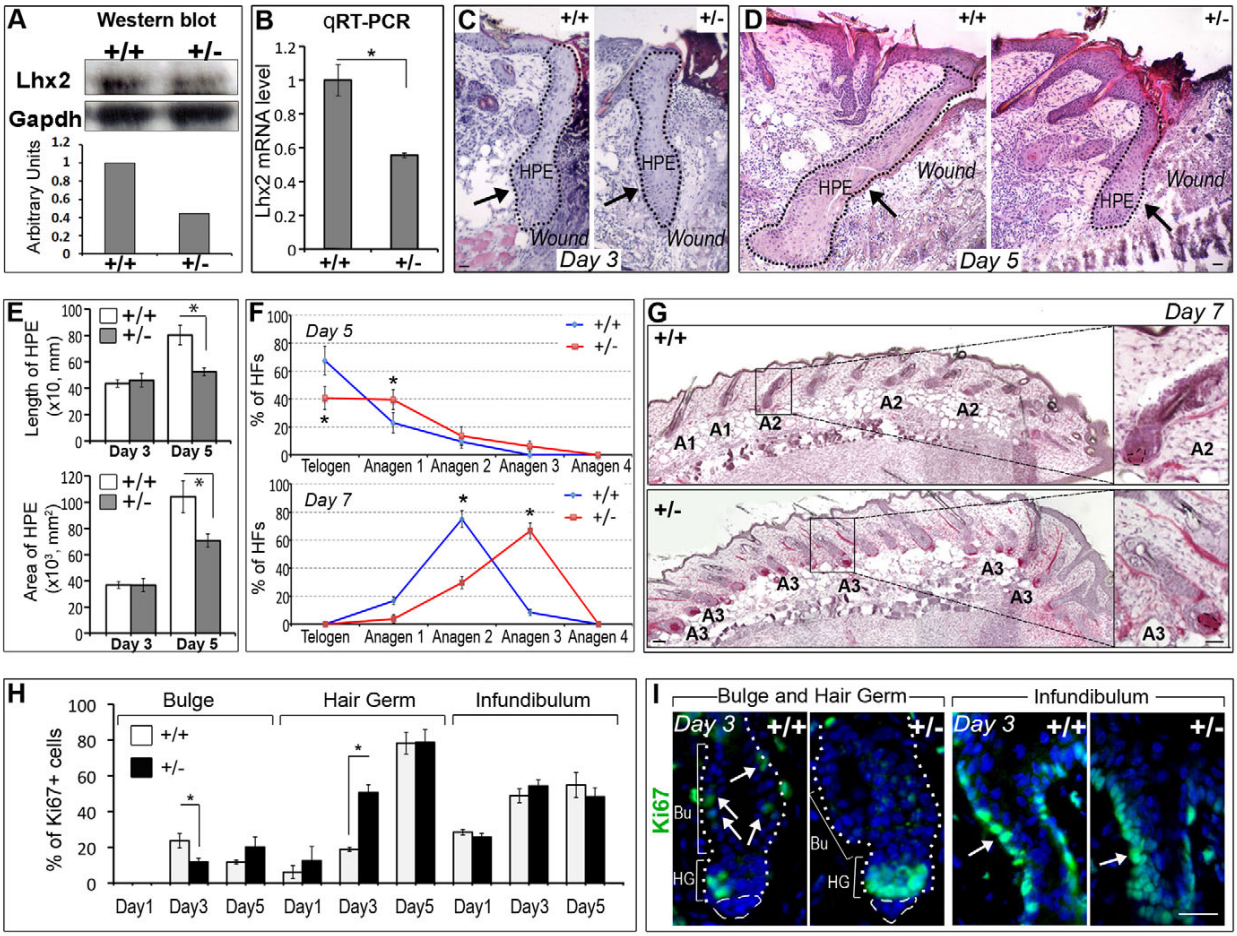

Fig. 3. *Lhx2*$^{+/-}$ mice show impaired wound re-epithelization and accelerated anagen development associated with alterations of cell proliferation in the hair follicles. Full-thickness wounds were introduced to back skin of 8-week-old wild-type (+/+) or Lhx2 heterozygous (+/–) mice, and skin was collected at days 1-7 after wounding. Skin samples (n=8-10 from each strain) from the central part of the wounds were processed for Hematoxylin and Eosin, alkaline phosphatase or Ki67 staining, and morphometric analyses. (**A**,**B**) Decrease in levels of Lhx2 protein (A) and transcripts (B) in the skin of 8-week-old Lhx2$^{+/-}$ mice versus age-matched wild-type controls, as determined by western blot analysis (A) or qRT-PCR (B). Data are mean±s.e.m. (**C**,**D**) Impaired development of the wound epithelium in *Lhx2*$^{+/-}$ skin on day 5 post wounding (D) compared with day 3 (C) and with corresponding wild-type controls. Broken line and arrows show the areas of hyper-proliferative epithelium (HPE). (**E**) Significantly reduced area and length of the hyper-proliferative epithelium (HPE) in the *Lhx2*$^{+/-}$ skin at day 5 after wounding versus the controls (mean±s.e.m., *P<0.05). (**F**,**G**) Acceleration of anagen development in the HFs located closely to the wounds in *Lhx2*$^{+/-}$ mice versus wild-type controls on days 5 and 7 after wound infliction (mean±s.e.m., *P<0.05). HFs at distinct stages of the hair cycle on day 7 of experiment are shown [G; T, telogen or resting stage; A1, anagen 1, a stage characterized by onset of keratinocyte proliferation resulted in the enlargement of secondary hair germ; A2, anagen 2, a stage characterized by partial incorporation of the dermal papilla into enlarged secondary hair germ; A3, a stage characterized by full incorporation of the dermal papilla into the forming hair bulb (see Muller-Rover et al., 2001)]. Images of the skin on day 5 of the experiment are shown in Fig. S1A (supplementary material). (**H**,**I**) Analysis of cell proliferation in distinct HF compartments (days 1-5 after wounding) shows inverse changes in the number of Ki67^{+} cells in the bulge versus secondary hair germ of the HFs in *Lhx2*$^{+/-}$ mice compared with wild-type controls on day 3 after wound infliction (mean±s.e.m., *P<0.05, Student's t-test). Number of Ki67^{+} cells in the infundibulum (I, arrows) does not change between the *Lhx2*$^{+/-}$ mice and wild-type controls. Data on cell proliferation in the interfollicular epidermis and wound epithelium in *Lhx2*$^{+/-}$ and wild-type mice at distinct time-points after wounding are shown in Fig. S1B (supplementary material). Bu, bulge; HG, secondary hair germ. Scale bars: 50 μm; 100 μm in G (insets).

and *Tcf4* transcript levels in wounded skin of *Lhx2*$^{+/-}$ mice compared with wild-type controls, whereas no such changes were seen in unwounded skin (supplementary material Fig. S2C). These data suggest that Lhx2 is indeed involved in regulating the expression of *Sox9* and *Tcf4* in the bulge progenitor cells during wound healing.

Lgr5 also showed colocalization with Lhx2 in the secondary hair germ (Fig. 4A). Furthermore, expression of Lgr5 in the secondary hair germ, as well as Lgr5 mRNA and protein levels were increased in total skin of *Lhx2*$^{+/-}$ mice on day 5 after wounding compared with wild-type controls, but not in the unwounded skin (Fig. 4D-F; supplementary material Fig. S2C). Importantly, acceleration of anagen development in *Lhx2*$^{+/-}$ mice versus wild-type mice on day 7 after wounding was significantly (P<0.05) inhibited by intracutaneous administration of *Lgr5* siRNA (Fig. 4G,H). *Lgr5* siRNA treatment also inhibited wound-associated anagen development in wild-type mice (data not shown). The efficient *Lgr5*

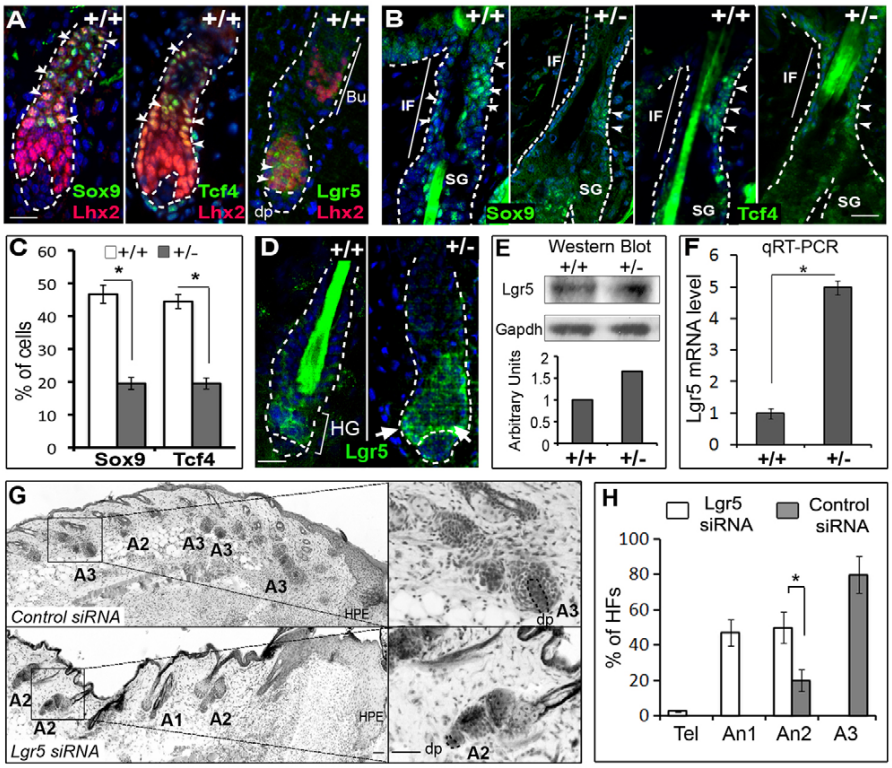

Fig. 4. Interrelations between Lhx2 and Sox9, Tcf4 and Lgr5 in hair follicle progenitor cells during wound healing. Skin of *Lhx2*$^{+/-}$ and wild-type mice at days 5-7 after wounding was processed for immunohistochemical detection of Lhx2 and/or Sox9, Tcf4, Lgr5 (A-D), as well as processed for detection of the Lgr5 proteins and transcripts by western blot and qRT-PCR (E,F). *Lhx2*$^{+/-}$ mice were treated with Lgr5 or control siRNA on days 1-6 after wound infliction, and skin was processed for histoenzymatic detection of alkaline phosphatase and histomorphometry of hair cycle stages (G,H). (**A**) Co-expression of Lhx2 and/or Sox9, Tcf4 and Lgr5 in HFs of wild-type mice (arrowheads). Borders between the epidermis or HF and dermis are depicted by the broken line. (**B**,**C**) Immunodetection of the Sox9$^+$ and Tcf4$^+$ cells in the HFs of wild-type and *Lhx2*$^{+/-}$ mice 5 days after wounding. The percentage of Sox9$^+$ and Tcf4$^+$ cells (B, arrowheads) is reduced in the infundibulum of Lhx2$^{+/-}$ mice versus wild-type controls (C, mean±s.e.m., *P<0.05, Student's t-test). (**D**) Expression of Lgr5 increased in the secondary hair germ of the HFs in *Lhx2*$^{+/-}$ mice (arrows) compared with wild-type controls on day 5 after wounding. (**E**,**F**) Increase in expression of Lgr5 protein (E) and transcripts (F) in the skin of *Lhx2*$^{+/-}$ mice versus age-matched wild-type controls on day 5 after wounding, as determined by western blot analysis (E) or qRT-PCR (F) (mean±s.e.m., *P<0.05). (**G**,**H**) Inhibition of wound-induced anagen development and significant increase in the number of anagen 2 HFs and decrease of anagen 3 HFs on day 7 of experiment in *Lhx2*$^{+/-}$ mice after treatment with *Lgr5* siRNA compared with control siRNA (mean±s.e.m., *P<0.05, Student's t-test). High magnifications of the HFs at distinct stages of the hair cycle are shown in the insets (G; T, telogen; A1-A3, anagen 1-3; dermal papilla of the HFs is depicted by a broken line). Data on the validations of the *Lgr5* siRNA activity are shown in Fig. S2 (supplementary material). Bu, bulge; DP, dermal papilla; HF, secondary hair germ; IF, infundibulum; SG, sebaceous gland. Scale bars: 50 μm; 100 μm in G (insets).

knockdown was verified by the detection of significantly reduced levels of *Lgr5* transcripts in the skin, as well as of the levels of Lgr5 protein and mRNA in primary keratinocytes after *Lgr5* siRNA treatment (supplementary material Fig. S3A,B). These data suggest that Lhx2 inhibits wound-induced anagen development, at least in part, via negative regulation of Lgr5 expression in the HF progenitor cells residing in the secondary hair germ.

Sox9, Tcf4 and Lgr5 are direct Lhx2 targets in keratinocytes

To further validate whether *Sox9, Tcf4 and Lgr5* are indeed direct targets of Lhx2, MatInspector analysis (Cartharius et al., 2005) for putative Lhx2-binding sites was performed and revealed several AT-rich Lim-homeodomain DNA-binding sites within the promoter regions of the *Sox9*, *Tcf4* and *Lgr5* genes. To confirm the ChIP-on-chip data, we carried out ChIP-qPCR on chromatin samples isolated from keratinocytes of E16.5 embryos, newborn or adult mice (Fig. 5A,B; supplementary material Fig. S4). ChIP-qPCR analyses of newborn or adult keratinocytes showed Lhx2 association with chromatin at distinct sites in the genomic regions of the *Sox9, Tcf4* and *Lgr5* promoters. In all three promoters tested, several sites among the predicted binding regions showed distinct (from twofold to fourfold) degrees of enrichment of binding to anti-Lhx2 antibody versus controls (Fig. 5A,B). Lhx2 binding to the *Sox9* and *Tcf4* promoters was also seen in keratinocytes isolated from E16.5 embryos (supplementary material Fig. S4). However, in contrast to keratinocytes from newborn or adult mice, lack of Lhx2 binding to the *Lgr5* promoter was seen in E16.5 keratinocytes (supplementary material Fig. S4). This is consistent with low Lgr5 expression levels in embryonic skin (Jaks et al., 2008) and suggests that Lhx2 controls expression of *Lgr5* only in postnatal skin. However, there was no difference in precipitation with the anti-Lhx2 antibody of the control sites on each promoter compared with control IgG, thus serving as internal negative control for this assay (Fig. 5B).

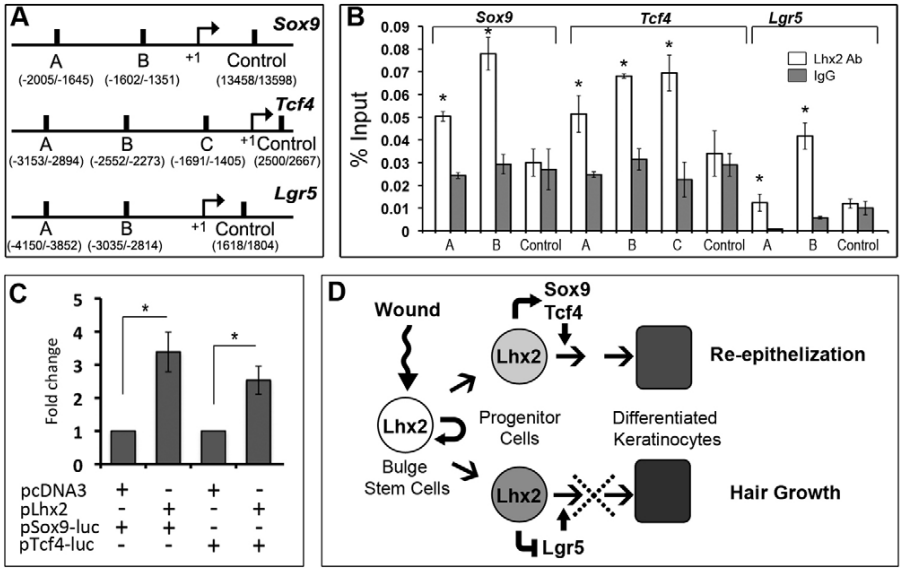

Fig. 5. Lhx2 binds to the promoter regions of the *Sox9*, *Tcf4* and *Lgr5* genes in keratinocytes. Mouse keratinocytes isolated from adult telogen skin were processed for ChIP-qPCR analysis with an antibody against Lhx2 or purified goat IgG. HaCaT keratinocytes were processed for detection of the *Sox9* and *Tcf4* promoter activities. (**A**) *Sox9*, *Tcf4* and *Lgr5* promoter regions with putative Lim-homeodomain DNA-binding sites or control sites predicted by bioinformatic analysis. (**B**) ChIP-qPCR analysis of the distinct regions in the *Sox9, Tcf4* and *Lgr5* promoters, showing enrichment with Lhx2 antibody compared with IgG controls (mean±s.e.m., n=3; *P<0.05, Student's t-test). (**C**) HaCaT keratinocytes were transfected with the reporter plasmids containing mouse *Sox9* or *Tcf4* promoter fragments, as well as with Lhx2-containing vector or with pCDN3 control vector. Increase in the pSox9-Luc or pTcf4-Luc activities versus controls (mean±s.e.m., n=3; *P<0.05, Student's t-test). (**D**) The involvement of Lhx2 in the control of the hair follicle response to skin injury.

To assess whether Lhx2 controls the activities of the *Sox9* and *Tcf4* promoters, HaCaT keratinocytes were transfected with the corresponding reporter plasmids containing mouse *Sox9* or *Tcf4* promoters, respectively. Cells were co-transfected with an Lhx2 expressing vector, which resulted in a 2.5- to 3.5-fold increase in pSox9-Luc or pTcf4-Luc activities when compared with control (Fig. 5C). These data suggested that Lhx2 positively regulates the activity of the both promoters. They are consistent with the results of microarray, ChIP-on-chip and immunohistochemical analyses (Figs 1, 4) and demonstrate that Lhx2 indeed controls the expression of these markers in distinct populations of HF progenitor cells during epidermal regeneration after injury.

DISCUSSION

Skin repair after injury is a complex process, which involves recruitment of distinct populations of undifferentiated progenitor cells from adjacent HFs into regenerating epidermis (Blanpain and Fuchs, 2009; Cotsarelis, 2006; Gurtner et al., 2008; Lau et al., 2009). The data presented in this manuscript unravel a previously unrecognized role for Lhx2 in the promotion of epidermal regeneration after wounding and demonstrate that Lhx2 operates as one of the key regulators controlling the differential response of the distinct populations of the HF stem cells to skin injury.

We show that Lhx2$^+$ cells residing in the bulge and secondary hair germ of the HF represent the vast majority of cells that proliferate after skin injury in mice and expand in number in the HF outer root sheath in human skin (Fig. 2). This suggests a high degree of conservation of the molecular control of the wound healing response between humans and mice. Although the precise choreography of the molecular events by which Lhx2 impacts on epidermal regeneration in human skin remain to be defined, we demonstrate here that in mice Lhx2 causes opposite effects on cell proliferation in the bulge and secondary hair germ and differentially regulates the activity of the distinct populations of the progenitor cells residing in these follicular compartments.

Because, in mice, Lhx2 is not expressed in the wound epithelium or interfollicular epidermis (Fig. 2), we hypothesize that it contributes to the wound-healing process rather indirectly and, at least in part, via positive regulation of *Sox9* and *Tcf4* in the bulge stem cells. Sox9 and Tcf4 transcription factors play essential roles in the control of HF morphogenesis and in the maintenance of the HF stem cells during postnatal life (Nguyen et al., 2009; Nowak et al., 2008), and Lhx2 co-localizes with these markers in the HF bulge (Fig. 4). Furthermore, lineage tracing experiments showed that bulge-derived Sox9$^+$ and Tcf4$^+$ progenitor cells contribute to wound re-epithelization, and genetic ablation of *Sox9* or *Tcf3/4* resulted in marked retardation of the wound-healing process (Nguyen et al., 2009; Nowak et al., 2008). ChIP-on-chip/Chip-qPCR and reporter assay data presented here provide evidence that Lhx2 serves as a direct upstream regulator of *Sox9* and *Tcf4* and, most likely, promotes expansion of the Sox9$^+$ and Tcf4$^+$ progenitor cells towards the regenerating epidermis during the response of the skin to injury (Figs 4, 5).

In addition to the marked retardation of wound re-epithelization, *Lhx2*$^{+/-}$ mice show significant acceleration of anagen development in the HFs adjacent to the wounds (Fig. 3; supplementary material Fig. S1). We demonstrate here that Lhx2 negatively regulates the expression of *Lgr5* (Figs 4, 5), a marker of the cycling population of the HF stem cells predominantly residing in secondary hair germ and lower bulge, which is capable of generating all HF cell lineages during the hair cycle (Jaks et al., 2008). It has recently been shown that Lgr5-*lacZ*-expressing cells could also be seen in

the bulge and interfollicular epidermis at late stages of the healing process, suggesting their contribution to re-epithelization (Kasper et al., 2011). We show that Lhx2 and Lgr5 are co-expressed in the progenitor cells residing in secondary hair germ, that levels of Lgr5 transcripts and protein are increased in the skin of *Lhx2*$^{+/-}$ mice, and that acceleration of the wound-induced anagen development in *Lhx2*$^{+/-}$ mice is inhibited by administration of *Lgr5* siRNA (Fig. 4). Together with the ChIP-on-chip and Chip-qPCR data (Fig. 5), these data strongly suggest that, during wound healing, Lhx2 inhibits HF cycling, most likely via negative regulation of *Lgr5* in the progenitor cell population located in the secondary hair germ.

It has previously been shown that Lhx2 operates as a transcriptional activator or repressor during development depending on the site, timing and levels of expression, as well as on the availability of distinct co-factors that form the Lhx2 transcription complexes (Chou et al., 2009; Hobert and Westphal, 2000; Xu et al., 2007; Yun et al., 2009). Our data on the wound-induced acceleration of anagen development in *Lhx2*$^{+/-}$ mice are consistent with data showing accelerated entry of the HFs into anagen phase during the normal hair cycle in the *Lhx2*-null skin grafted onto nude mice (Rhee et al., 2006). However, these data are quite opposite to the results obtained with *CreER:Lhx2*$^{fl/fl}$ mice, in which the *Lhx2* gene is inactivated in adult skin after topical tamoxifen application leading to retardation of anagen development (Tornqvist et al., 2010). It remains to be determined whether timing and/or degree of *Lhx2* inactivation, as well as availability of its co-factors in the skin may contribute to the differences in hair growth phenotype between two genetic models. These data also suggest that the role of Lhx2 in the control of hair-specific genetic programs in the follicular stem cells is more complex than previously anticipated. Elucidating its precise role in different developmental processes will require further investigations using mice with tissue-specific knockout or overexpression of *Lhx2*.

Interestingly, Lhx2 protein was not seen in the isthmus and infundibulum of the HFs during wound healing, the areas containing two other stem cell populations expressing *Lgr6* and *Lrig1*, respectively (Jensen et al., 2009; Snippert et al., 2010). Thus, Lhx2 involvement in the control of Lgr6^{+} and Lrig1^{+} stem cell populations is rather unlikely, supporting a concept that several independent mechanisms control the recruitment of the distinct HF stem cell populations to the regenerating epidermis in wounded skin (Ito et al., 2005; Jaks et al., 2008; Jensen et al., 2009; Levy et al., 2005; Levy et al., 2007; Snippert et al., 2010).

Taken together, our data demonstrating that Lhx2 positively regulates *Sox9* and *Tcf4* and negatively regulates *Lgr5* in the bulge and secondary hair germ progenitor cells, suggest that Lhx2 operates as a central switchboard controlling the differential response of the distinct HF stem cell populations to wounding. Indeed, by stimulating the expression of *Sox9* and *Tcf4*, Lhx2 may promote generation of the HF-derived progenitor cells that contribute to regeneration of the epidermis after injury. Instead, by inhibiting *Lgr5* expression, Lhx2 suppresses stem cell activation for construction of new anagen HF, and thereby HF entry into anagen (Fig. 5D).

Through its dual activity, which includes stimulation of epidermal regeneration on the one hand and inhibition of hair cycling on the other hand, Lhx2 serves as one of the key regulators in the molecular network that control the response of the HFs to skin injury. Although detailed mechanisms underlying its involvement in reciprocal control of the activity of distinct HF stem cell populations remain to be further defined, these data suggest that Lhx2 may serve as a novel target for promoting the production and recruitment of the progenitor cells into regenerating epithelia in conditions associated with an impaired stem cell activity, including ageing and chronic inflammation.

Acknowledgements
We thank Dr H. Westphal and Dr P. Koopman for providing *Lhx2*$^{+/-}$ mice and Sox9-Luc plasmid, respectively.

Funding
This study was supported by the grants from the Biotechnology and Biological Sciences Research Council [BB/E023010/1 to V.A.B.] and from Deutsche Forschungsgemeinschaf [Pa 345/12-2 to R.P.].

Competing interests statement
The authors declare no competing financial interests.

Supplementary material
Supplementary material available online at
http://dev.biologists.org/lookup/suppl/doi:10.1242/dev.070284/-/DC1

References

Ambler, C. A. and Maatta, A. (2009). Epidermal stem cells: location, potential and contribution to cancer. *J. Pathol.* **217**, 206-216.
Ansell, D. M., Kloepper, J. E., Thomason, H. A., Paus, R. and Hardman, M. J. (2011). Exploring the 'hair growth-wound healing connection': anagen phase promotes wound re-epithelization. *J. Invest. Dermatol.* **131**, 512-528.
Blanpain, C. and Fuchs, E. (2009). Epidermal homeostasis: a balancing act of stem cells in the skin. *Nat. Rev. Mol. Cell Biol.* **10**, 207-217.
Blanpain, C., Lowry, W. E., Geoghegan, A., Polak, L. and Fuchs, E. (2004). Self-renewal, multipotency, and the existence of two cell populations within an epithelial stem cell niche. *Cell* **118**, 635-648.
Botchkarev, V. A., Botchkareva, N. V., Roth, W., Nakamura, M., Chen, L.-H., Herzog, W., Lindner, G., McMahon, J. A., Peters, C., Lauster, R. et al. (1999a). Noggin is a mesenchymally-derived stimulator of hair follicle induction. *Nature Cell Biol.* **1**, 158-164.
Botchkarev, V. A., Peters, E. M., Botchkareva, N. V., Maurer, M. and Paus, R. (1999b). Hair cycle-dependent changes in adrenergic skin innervation, and hair growth modulation by adrenergic drugs. *J. Invest. Dermatol.* **113**, 878-887.
Botchkareva, N. V., Botchkarev, V. A., Welker, P., Airaksinen, M., Roth, W., Suvanto, P., Muller-Rover, S., Hadshiew, I. M., Peters, C. and Paus, R. (2000). New roles for glial cell line-derived neurotrophic factor and neurturin: involvement in hair cycle control. *Am. J. Pathol.* **156**, 1041-1053.
Brownell, I., Guevara, E., Bai, C. B., Loomis, C. A. and Joyner, A. L. (2011). Nerve-derived sonic hedgehog defines a niche for hair follicle stem cells capable of becoming epidermal stem cells. *Cell Stem Cell* **8**, 552-565.
Cartharius, K., Frech, K., Grote, K., Klocke, B., Haltmeier, M., Klingenhoff, A., Frisch, M., Bayerlein, M. and Werner, T. (2005). MatInspector and beyond: promoter analysis based on transcription factor binding sites. *Bioinformatics* **21**, 2933-2942.
Chmielowiec, J., Borowiak, M., Morkel, M., Stradal, T., Munz, B., Werner, S., Wehland, J., Birchmeier, C. and Birchmeier, W. (2007). c-Met is essential for wound healing in the skin. *J. Cell Biol.* **177**, 151-162.
Chou, S. J., Perez-Garcia, C. G., Kroll, T. T. and O'Leary, D. D. (2009). Lhx2 specifies regional fate in Emx1 lineage of telencephalic progenitors generating cerebral cortex. *Nat. Neurosci.* **12**, 1381-1389.
Cotsarelis, G. (2006). Epithelial stem cells: a folliculocentric view. *J. Invest. Dermatol.* **126**, 1459-1468.
Cotsarelis, G., Sun, T. T. and Lavker, R. M. (1990). Label-retaining cells reside in the bulge area of pilosebaceous unit: implications for follicular stem cells, hair cycle, and skin carcinogenesis. *Cell* **61**, 1329-1337.
Dahl, L., Richter, K., Hagglund, A. C. and Carlsson, L. (2008). Lhx2 expression promotes self-renewal of a distinct multipotential hematopoietic progenitor cell in embryonic stem cell-derived embryoid bodies. *PLoS One* **3**, e2025.
DasGupta, R. and Fuchs, E. (1999). Multiple roles for activated LEF/TCF transcription complexes during hair follicle development and differentiation. *Development* **126**, 4557-4568.
Driskell, R. R., Clavel, C., Rendl, M. and Watt, F. M. (2011). Hair follicle dermal papilla cells at a glance. *J. Cell Sci.* **124**, 1179-1182.
Frye, M., Fisher, A. G. and Watt, F. M. (2007). Epidermal stem cells are defined by global histone modifications that are altered by Myc-induced differentiation. *PLoS One* **2**, e763.
Fuchs, E. (2007). Scratching the surface of skin development. *Nature.* **445**, 834-842.
Garza, L. A., Yang, C. C., Zhao, T., Blatt, H. B., Lee, M., He, H., Stanton, D. C., Carrasco, L., Spiegel, J. H., Tobias, J. W. et al. (2011). Bald scalp in men with androgenetic alopecia retains hair follicle stem cells but lacks CD200-rich and CD34-positive hair follicle progenitor cells. *J. Clin. Invest.* **121**, 613-622.

Ghazizadeh, S. and Taichman, L. B. (2001). Multiple classes of stem cells in cutaneous epithelium: a lineage analysis of adult mouse skin. *EMBO J* **20**, 1215-1222.
Gurtner, G. C., Werner, S., Barrandon, Y. and Longaker, M. T. (2008). Wound repair and regeneration. *Nature* **453**, 314-321.
Hirota, J. and Mombaerts, P. (2004). The LIM-homeodomain protein Lhx2 is required for complete development of mouse olfactory sensory neurons. *Proc. Natl. Acad. Sci. USA* **101**, 8751-8755.
Hobert, O. and Westphal, H. (2000). Functions of LIM-homeobox genes. *Trends Genet.* **16**, 75-83.
Horsley, V., Aliprantis, A. O., Polak, L., Glimcher, L. H. and Fuchs, E. (2008). NFATc1 balances quiescence and proliferation of skin stem cells. *Cell* **132**, 299-310.
Hsu, Y. C., Pasolli, H. A. and Fuchs, E. (2011). Dynamics between stem cells, niche, and progeny in the hair follicle. *Cell* **144**, 92-105.
Ito, M. and Cotsarelis, G. (2008). Is the hair follicle necessary for normal wound healing? *J. Invest. Dermatol* **128**, 1059-1061.
Ito, M., Liu, Y., Yang, Z., Nguyen, J., Liang, F., Morris, R. J. and Cotsarelis, G. (2005). Stem cells in the hair follicle bulge contribute to wound repair but not to homeostasis of the epidermis. *Nat. Med.* **11**, 1351-1354.
Ito, M., Yang, Z., Andl, T., Cui, C., Kim, N., Millar, S. E. and Cotsarelis, G. (2007). Wnt-dependent de novo hair follicle regeneration in adult mouse skin after wounding. *Nature* **447**, 316-320.
Jaks, V., Barker, N., Kasper, M., van Es, J. H., Snippert, H. J., Clevers, H. and Toftgard, R. (2008). Lgr5 marks cycling, yet long-lived, hair follicle stem cells. *Nat. Genet.* **40**, 1291-1299.
Jensen, K. B., Collins, C. A., Nascimento, E., Tan, D. W., Frye, M., Itami, S. and Watt, F. M. (2009). Lrig1 expression defines a distinct multipotent stem cell population in mammalian epidermis. *Cell Stem Cell* **4**, 427-439.
Jensen, U. B., Yan, X., Triel, C., Woo, S. H., Christensen, R. and Owens, D. M. (2008). A distinct population of clonogenic and multipotent murine follicular keratinocytes residing in the upper isthmus. *J. Cell Sci.* **121**, 609-617.
Kanai, Y. and Koopman, P. (1999). Structural and functional characterization of the mouse Sox9 promoter: implications for campomelic dysplasia. *Hum. Mol. Genet.* **8**, 691-696.
Kasper, M., Jaks, V., Are, A., Bergström, A., Schwäger, A., Barker, N. and Toftgård, R. (2011). Wounding enhances epidermal tumorigenesis by recruiting hair follicle keratinocytes. *Proc. Natl. Acad. Sci. USA* **108**, 4099-4104.
Kloepper, J. E., Tiede, S., Brinckmann, J., Reinhardt, D. P., Meyer, W., Faessler, R. and Paus, R. (2008). Immunophenotyping of the human bulge region: the quest to define useful in situ markers for human epithelial hair follicle stem cells and their niche. *Exp. Dermatol.* **17**, 592-609.
Kumin, A., Schafer, M., Epp, N., Bugnon, P., Born-Berclaz, C., Oxenius, A., Klippel, A., Bloch, W. and Werner, S. (2007). Peroxiredoxin 6 is required for blood vessel integrity in wounded skin. *J. Cell Biol.* **179**, 747-760.
Langton, A. K., Herrick, S. E. and Headon, D. J. (2008). An extended epidermal response heals cutaneous wounds in the absence of a hair follicle stem cell contribution. *J. Invest. Dermatol.* **128**, 1311-1318.
Lau, K., Paus, R., Tiede, S., Day, P. and Bayat, A. (2009). Exploring the role of stem cells in cutaneous wound healing. *Exp. Dermatol.* **18**, 921-933.
Levy, V., Lindon, C., Harfe, B. D. and Morgan, B. A. (2005). Distinct stem cell populations regenerate the follicle and interfollicular epidermis. *Dev. Cell* **9**, 855-861.
Levy, V., Lindon, C., Zheng, Y., Harfe, B. D. and Morgan, B. A. (2007). Epidermal stem cells arise from the hair follicle after wounding. *FASEB J.* **21**, 1358-1366.
Li, L. and Clevers, H. (2010). Coexistence of quiescent and active adult stem cells in mammals. *Science* **327**, 542-545.
Lu, Z., Hasse, S., Bodo, E., Rose, C., Funk, W. and Paus, R. (2007). Towards the development of a simplified long-term organ culture method for human scalp skin and its appendages under serum-free conditions. *Exp. Dermatol.* **16**, 37-49.
Mardaryev, A. N., Ahmed, M. I., Vlahov, N. V., Fessing, M. Y., Gill, J. H., Sharov, A. A. and Botchkareva, N. V. (2010). Micro-RNA-31 controls hair cycle-associated changes in gene expression programs of the skin and hair follicle. *FASEB J.* **24**, 3869-3881.
Merrill, B. J., Gat, U., DasGupta, R. and Fuchs, E. (2001). Tcf3 and Lef1 regulate lineage differentiation of multipotent stem cells in skin. *Genes Dev.* **15**, 1688-1705.
Moll, I., Houdek, P., Schmidt, H. and Moll, R. (1998). Characterization of epidermal wound healing in a human skin organ culture model: acceleration by transplanted keratinocytes. *J. Invest. Dermatol.* **111**, 251-258.
Morris, R. J., Liu, Y., Marles, L., Yang, Z., Trempus, C., Li, S., Lin, J. S., Sawicki, J. A. and Cotsarelis, G. (2004). Capturing and profiling adult hair follicle stem cells. *Nat. Biotechnol.* **22**, 411-417.
Muller-Rover, S., Handjiski, B., van der Veen, C., Eichmuller, S., Foitzik, K., McKay, I. A., Stenn, K. S. and Paus, R. (2001). A comprehensive guide for the accurate classification of murine hair follicles in distinct hair cycle stages. *J. Invest. Dermatol.* **117**, 3-15.
Nguyen, H., Rendl, M. and Fuchs, E. (2006). Tcf3 governs stem cell features and represses cell fate determination in skin. *Cell* **127**, 171-183.
Nguyen, H., Merrill, B. J., Polak, L., Nikolova, M., Rendl, M., Shaver, T. M., Pasolli, H. A. and Fuchs, E. (2009). Tcf3 and Tcf4 are essential for long-term homeostasis of skin epithelia. *Nat. Genet.* **41**, 1068-1075.
Nowak, D. E., Tian, B. and Brasier, A. R. (2005). Two-step cross-linking method for identification of NF-kappaB gene network by chromatin immunoprecipitation. *Biotechniques* **39**, 715-725.
Nowak, J. A., Polak, L., Pasolli, H. A. and Fuchs, E. (2008). Hair follicle stem cells are specified and function in early skin morphogenesis. *Cell Stem Cell* **3**, 33-43.
Philpott, M. P., Green, M. R. and Kealey, T. (1990). Human hair growth in vitro. *J. Cell Sci.* **97**, 463-471.
Porter, F. D., Drago, J., Xu, Y., Cheema, S. S., Wassif, C., Huang, S. P., Lee, E., Grinberg, A., Massalas, J. S., Bodine, D. et al. (1997). Lhx2, a LIM homeobox gene, is required for eye, forebrain, and definitive erythrocyte development. *Development* **124**, 2935-2944.
Rhee, H., Polak, L. and Fuchs, E. (2006). Lhx2 maintains stem cell character in hair follicles. *Science* **312**, 1946-1949.
Romagosa, Y., Hu, S. and Kirsner, R. S. (2008). Wound healing without hair. *J. Invest. Dermatol.* **128**, 1058.
Schafer, M. and Werner, S. (2007). Transcriptional control of wound repair. *Annu. Rev. Cell Dev. Biol.* **23**, 69-92.
Schmidt-Ullrich, R. and Paus, R. (2005). Molecular principles of hair follicle induction and morphogenesis. *BioEssays* **27**, 247-261.
Sharov, A. A., Weiner, L., Sharova, T. Y., Siebenhaar, F., Atoyan, R., McNamara, C. A., Funa, K., Gilchrest, B. A., Brissette, J. L. and Botchkarev, V. A. (2003). Noggin overexpression inhibits eyelid opening by altering epidermal apoptosis and differentiation. *EMBO J.* **22**, 2992-3003.
Sharov, A. A., Fessing, M., Atoyan, R., Sharova, T. Y., Haskell-Luevano, C., Weiner, L., Funa, K., Brissette, J. L., Gilchrest, B. A. and Botchkarev, V. A. (2005). Bone morphogenetic protein (BMP) signaling controls hair pigmentation by means of cross-talk with the melanocortin receptor-1 pathway. *Proc. Natl. Acad. Sci. USA* **102**, 93-98.
Sharov, A. A., Sharova, T. Y., Mardaryev, A. N., Tommasi di Vignano, A., Atoyan, R., Weiner, L., Yang, S., Brissette, J. L., Dotto, G. P. and Botchkarev, V. A. (2006). BMP signaling regulates size of the hair follicles and modulates the expression of cell cycle-associated genes.. *Proc. Natl. Acad. Sci. USA* **103**, 18166-18171.
Snippert, H. J., Haegebarth, A., Kasper, M., Jaks, V., van Es, J. H., Barker, N., van de Wetering, M., van den Born, M., Begthel, H., Vries, R. G. et al. (2010). Lgr6 marks stem cells in the hair follicle that generate all cell lineages of the skin. *Science* **327**, 1385-1389.
Taylor, G., Lehrer, M. S., Jensen, P. J., Sun, T. T. and Lavker, R. M. (2000). Involvement of follicular stem cells in forming not only the follicle but also the epidermis. *Cell* **102**, 451-461.
Tetreault, N., Champagne, M. P. and Bernier, G. (2009). The LIM homeobox transcription factor Lhx2 is required to specify the retina field and synergistically cooperates with Pax6 for Six6 trans-activation. *Dev. Biol.* **327**, 541-550.
Tiede, S. and Paus, R. (2006). Lhx2-decisive role in epithelial stem cell maintenance, or just the 'tip of the iceberg'? *BioEssays* **28**, 1157-1160.
Tornqvist, G., Sandberg, A., Hagglund, A. C. and Carlsson, L. (2010). Cyclic expression of lhx2 regulates hair formation. *PLoS Genet.* **6**, e1000904.
Trempus, C. S., Morris, R. J., Ehinger, M., Elmore, A., Bortner, C. D., Ito, M., Cotsarelis, G., Nijhof, J. G., Peckham, J., Flagler, N. et al. (2007). CD34 expression by hair follicle stem cells is required for skin tumor development in mice. *Cancer Res.* **67**, 4173-4181.
Tumbar, T., Guasch, G., Greco, V., Blanpain, C., Lowry, W. E., Rendl, M. and Fuchs, E. (2003). Defining the epithelial stem cell niche in skin. *Science* **303**, 359-363.
Watt, F. M. and Jensen, K. B. (2009). Epidermal stem cell diversity and quiescence. *EMBO Mol. Med.* **1**, 260-267.
Xu, X., Mannik, J., Kudryavtseva, E., Lin, K. K., Flanagan, L. A., Spencer, J., Soto, A., Wang, N., Lu, Z., Yu, Z. et al. (2007). Co-factors of LIM domains (Clims/Ldb/Nli) regulate corneal homeostasis and maintenance of hair follicle stem cells. *Dev. Biol.* **312**, 484-500.
Yun, S., Saijoh, Y., Hirokawa, K. E., Kopinke, D., Murtaugh, L. C., Monuki, E. S. and Levine, E. M. (2009). Lhx2 links the intrinsic and extrinsic factors that control optic cup formation. *Development* **136**, 3895-3906.